**Cover Page**:

**ALPHA FOUNDATION FOR THE IMPROVEMENT OF MINE SAFETY AND HEALTH**

**Final Technical Report**

**Project Title:** Investigation the Impact of Rock Rubble on Methane-Air Explosions: High-speed Turbulent Deflagrations and Transition to Detonations

**Grant Number:** AFSTI14FO69

**Organization:** Colorado School of Mines

**Principal Investigator:** Gregory Bogin Jr.

**Contact Information :** email **:** gbogin@mines.edu, phone : 303-273-3655

**Period of Performance:** 9/1/2018 – 12/31/2022

**Acknowledgement/Disclaimer:** Final Report must include the following disclaimer language: "This study was sponsored by the Alpha Foundation for the Improvement of Mine Safety and Health, Inc. (ALPHA FOUNDATION). The views, opinions and recommendations expressed herein are solely those of the authors and do not imply any endorsement by the ALPHA FOUNDATION, its Directors and staff."

Contents

# 1.0 Executive Summary

The tragic 2010 explosion at the Upper Big Branch Mine demonstrated that methane and coal dust explosions are still a substantial hazard in modern underground coal mines. The propagation mechanics of coal dust and gas explosions through mine workings are not fully understood. Flame propagation is believed to be accelerated by turbulence created by obstructions, such as rock rubble and equipment. The acceleration caused by such obstructions has the potential to accelerate flame speeds to the point of transition from a deflagration to a detonation. Detonations are suspected to have occurred in the mine explosions at Blacksville no. 1 (1992) and Sago (2006) with turbulence from obstructions potentially contributing to flame speeds reaching the deflagration to detonation transition (DDT) [1], [2]. Characterizing the impact of rock rubble on flame propagation velocities and explosion overpressures will substantially improve the industry's understanding of flame propagation through mine workings, over equipment and rubble, that can lead to detonations.

This research took a multidisciplinary approach to investigating the problem, with the general objectives of establishing a research facility capable of studying gas explosions relevant to mining industry and conducting an investigation into the impact mine workings and gob characteristics on the severity of gas explosions. One of the specific aims of this research is to uniquely leverage the synergistic relationship between experimental work and numerical modeling to produce a robust three-dimensional full-scale model capble of accurately predicting gas explosions in an underground coal mine. The objective of the experimental work is to characterize the impact of gob characteristics on the flame propagation velocities and overpressures. The parameters investigated are gas concentrations, ignition location, and rock rubble obstruction. There are two major objectives with the experimental work. The first is to investigate and characterize the phenomena, in order to improve the understanding of what factors increase the immediate damage potential of an explosion. The impact of these variables on the sustained acceleration of the flame front is of particular interest because a more rapidly accelerating flame front reduces the run-up distance required for an explosion to reach DDT. The second objective of the experimental work is to provide a large relevant data set to the numerical modeling portion of the project. The numerical modeling portion consists of the development of three primary models; a cylindrical a 2D/3D cylindrical reactor gas explosion model, a 3D full-scale longwall ventilation model, and a 3D full-scale longwall explosion model. The completed 3D full-scale longwall explosion model is capable of simulating a gas explosion on an active longwall face, as well as in the gob area near the shields; which allows various ignition and explosion scenarios to be investigated.

The Gas Explosion Research Facility (GERF) was designed and constructed to both meet the needs of this research and to provide a key public research capability otherwise missing in the Western Hemisphere. The GERF successfully carried out the experimental work required for this project, providing both a high quality characterization of the phenomena, and the necessary data for developing and validating the 2D/3D cylindrical reactor gas explosion model. The 3D full-scale longwall explosion model is the result of an integration of the 3D cylindrical gas explosion model and the 3D full-scale longwall ventilation model, producing a model which successfully simulated methane-air ignition and explosion overpressures in an active longwall face area. The benefits to mining safety are twofold. First, the experimental characterization efforts quantitatively and qualitatively improves the understanding of gas explosions and factors that can increase the destructive potential. The second implication is that through pioneering the application of CFD modeling to gas explosions, this work paves the way for the adoption of a powerful new toolset.

# 2.0 Problem Statement and Objectives

The impact of rock rubble obstructions on the acceleration of flame propagation velocities is a poorly understood fluid mechanics and combustion phenomenon where the turbulence from the obstruction increases transport, combustion reaction rates, and stretching of the flame, resulting in heightened velocities and overpressures that can reach the deflagration-to-detonation transition (DDT), increasing the destructive potential of an explosion in an underground mine. This research sought to quantify the impact of rock rubble obstructions on flame propagation, gain further insights into the phenomena, and then apply these insights to develop and validate improved CFD models and generalize the results into safety recommendations for the mining industry. Previously, experimental and preliminary numerical work had been conducted at Colorado School of Mines using smaller scale reactors up to 71 cm (28 in.) in diameter and 6.1 m (20ft) in length. The current project objective is to experimentally measure the impact of rock rubble obstructions and methane concentrations on flame propagation velocities in a large-scale reactor 71 cm (28 in) in diameter and 30.48 m (100 ft) in length and use the measured results to develop, refine, and validate three-dimensional computational fluid dynamics models of gas explosions in underground coal mines. Once the 2D/3D cylindrical reactor gas explosion model was calibrated and validated, it was integrated with the 3D full-scale longwall ventilation model to develop the 3D full-scale longwall explosion model which simulated methane-air ignition  in an EGZ occurring at the shear drum near te coal face. This coupling of experimental and numerical efforts provided a unique opportunity to build on the synergies of these tools. The gas explosion research facility (GERF) was designed to house the new large-scale explosion reactor and provide a key public research facility for researchers in North America.

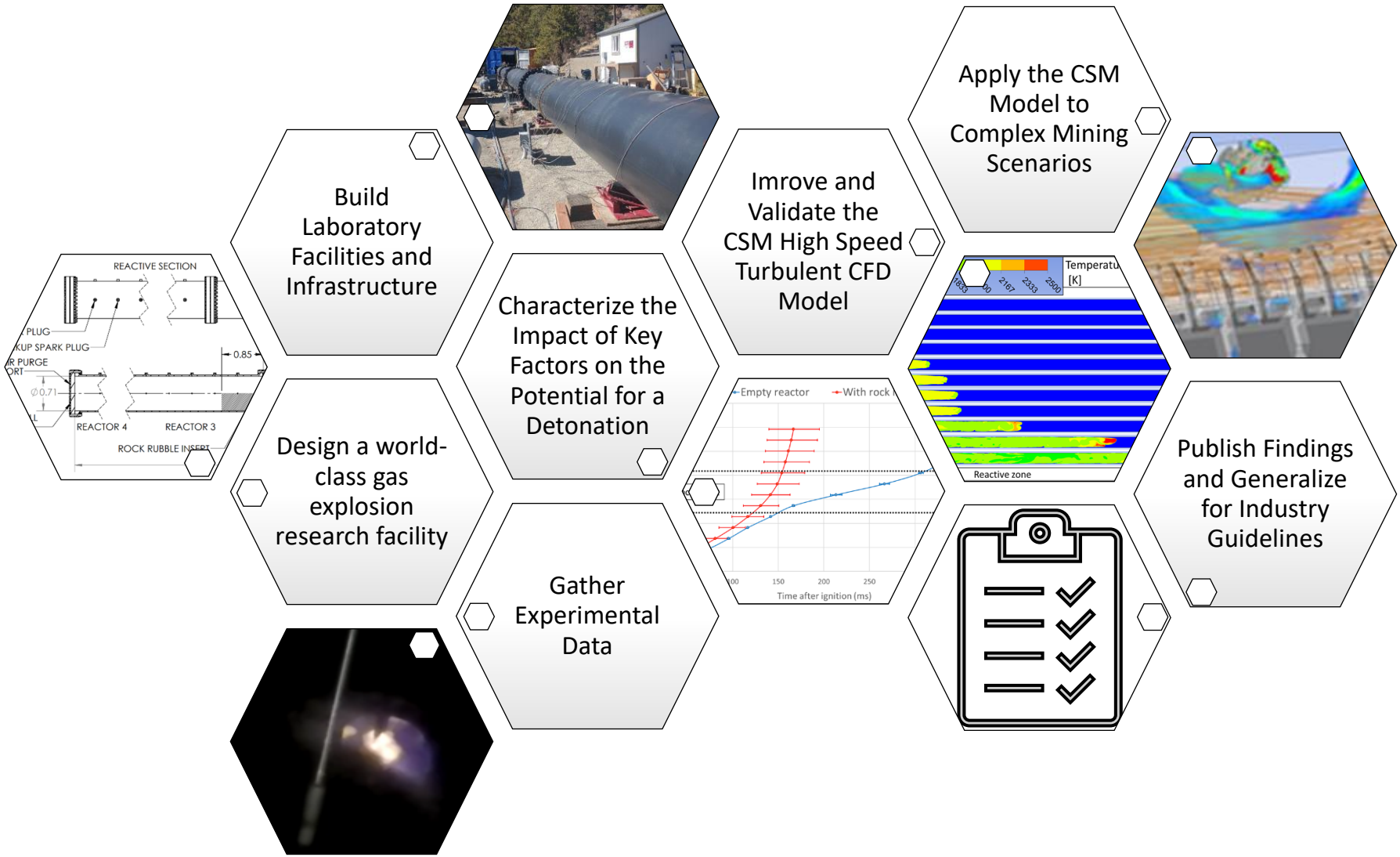


*Figure 1: Project Structure*

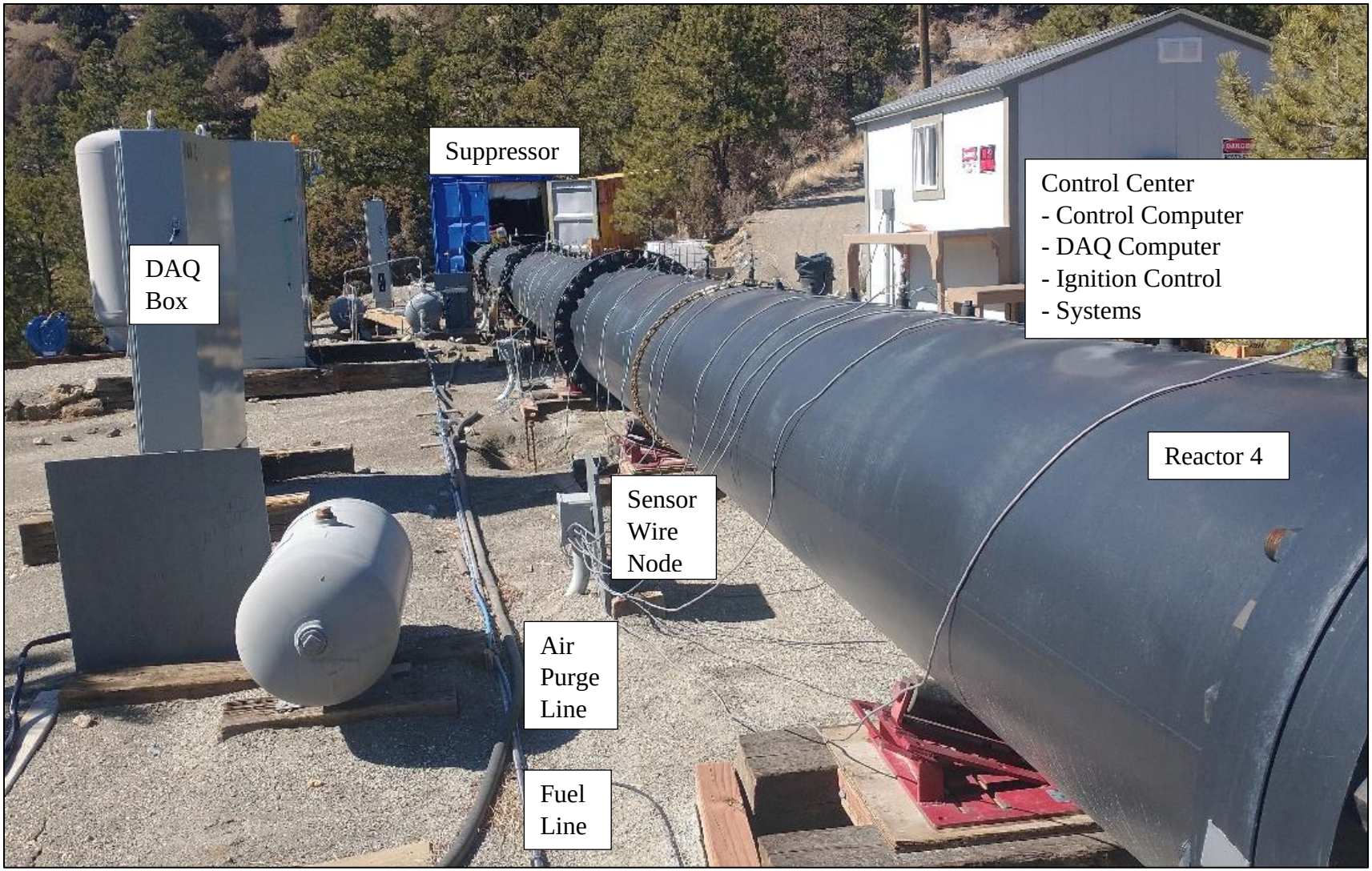


*Figure 2: The explosion reactor at the GERF.*
*DAQ stands for Data Acquisition.*

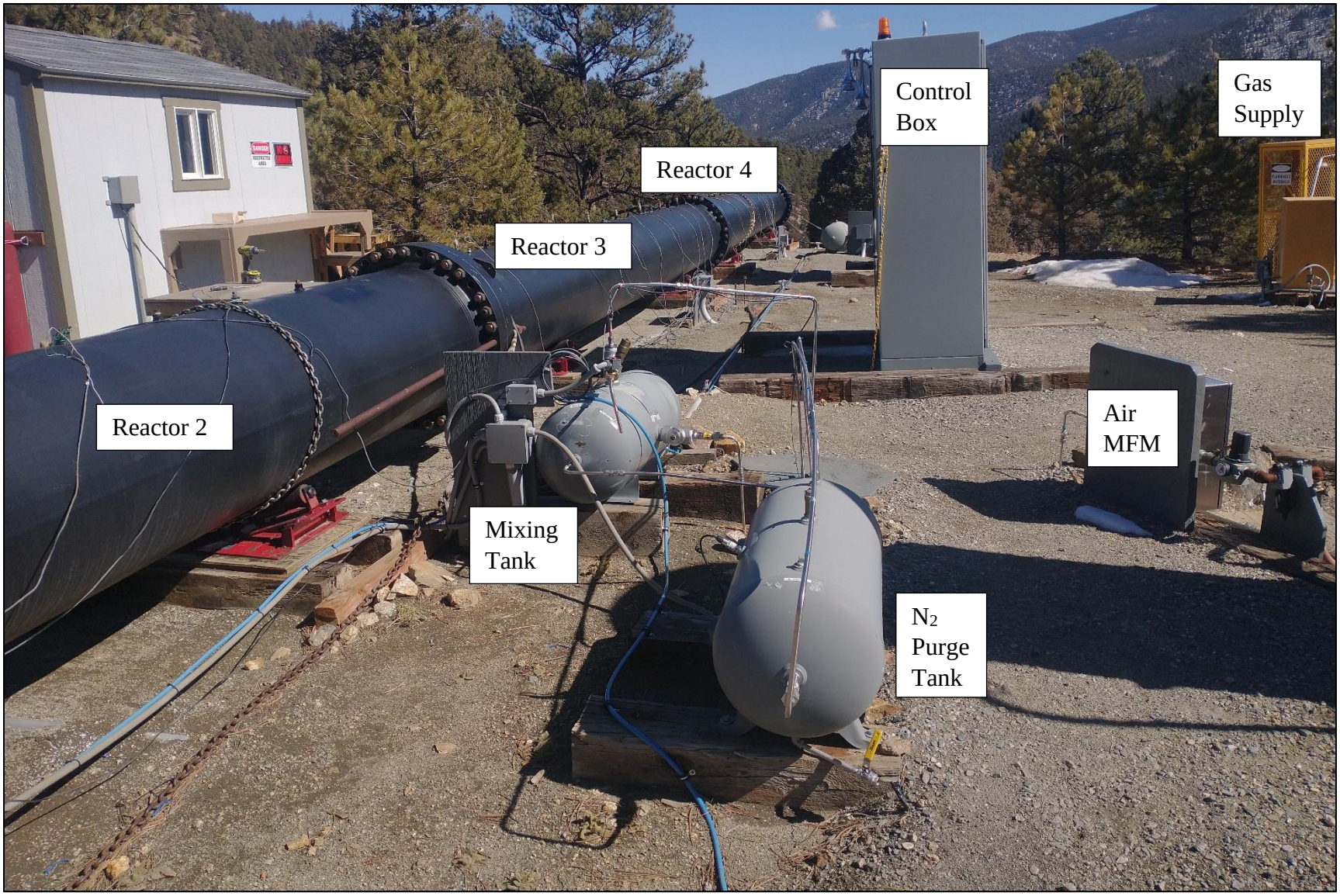


*Figure 3: The gas mixing and control system at the GERF.*

## Proposed Research

One of the main findings of the previous work (AFSTI14) was the initial development of a simplified full-scale model which predicted an ignition of an EGZ located near the shields at the tail-gate corner of the longwall face resulted in explosion velocities of 400 – 600 m/s (1312 – 1970 ft/s) and overpressures reaching ranging from 500 – 1500 kPa (72.5 – 218 psig); the propagation velocities and overpressures from the earlier model was severely over predicted during the earlier simulation times of the explosion event; however, it showed promised that a three-dimension simulation of a methane-air explosion in a longwall coal mine was possible. The predictions from this preliminary work are similar to the velocities and overpressures predicted during the Upper Big Branch explosion in 2010; where investigators determined explosion pressures of 170 kPa (25 psig) and reflected pressure waves of 720 kPa (104 psig), with flames traveling upwards of 450 m/s (1480 ft/s) [3]. While there are CFD models being developed by several researchers (including here at Mines) for predicting methane gas explosions and the resulting devastation that can occur in longwall coal mines, there is still a need for an experimental facility which can provide data which can be used to assist in the development of these models and provide crucial validation at these larger scales. One of the focus areas for this proposed work is to extend the current Mines' large-scale Gas Explosion Research Facility (GERF) to further investigate the high-speed turbulent deflagration-to-detonation transition (DDT) regime where explosion pressures and propagation velocities of the magnitude predicted in UBB can occur. The data obtained from this new explosion reactor provides the necessary data to further validate the 2D/3D cylindrical reactor gas explosion model which is integrated in to 3D full-scale longwall ventilation model resulting in the 3D full-scale longwall explosion model which is capable of simulating methane-air explosions in an underground longwall coal mine. The data obtained from the GERF can also provide crucial information in the detonation regime for validation of higher-fidelity models developed by our collaborators at the University of Maryland (UMD) and the Naval Research Laboratory (NRL). Researchers at UMD and NRL have jointly developed more advanced CFD deflagration and detonation models for methane-air explosions and interaction with rock rubble. Expanding the scaled explosion test facilities at the Colorado School of Mines will not only provide necessary data for the calibration and validation of these advanced explosion models but is also crucial to developing new insights into complex explosion dynamics which will lead to new mitigation and prevention strategies for explosions in longwall coal mines.

## Problem Addressed and Proposed Effort

The impact of rock rubble on a methane-air gas explosion in a longwall coal mine is not fully understood. The potential of the rock rubble to accelerate the flame propagation velocities of a high-speed deflagration and transition to detonation while producing significantly higher explosion overpressures pose a serious hazard to mine workers and cause severe structural damage to the mine. The motivation of increasing mine workers' safety and reducing the risk of structural damage led to the need for a gas explosion research facility that is capable of providing crucial experiments while in parallel developing a full-scale three-dimensional fully coupled combustion and ventilation model of a longwall coal mine to assist in prevention and mitigation strategies,

Understanding the impact of common mine obstacles (e.g. gob, rock rubble, shields, pillars, face equipment, etc.…) on flame propagation will help engineers and researchers recognize situations that could cause the transition of a high-speed turbulent deflagration flame to a detonation with a shorter run-up length. This is crucial to developing mitigation strategies for explosions that can occur in longwall coal mines and will be applicable to other industries as well. This work aimed to acquire high-speed imaging, velocities, and pressure measurements during the run-up to the DDT. Characterizing and quantifying how an obstruction impacts this will be crucial to developing accurate combustion models. The end goal is to experimentally investigate the run-up towards the DDT in a variety of situations and use the resulting experimental data to develop the first full-scale CFD model that can reliably simulate gas explosions in mining situations.

## Research Objective

The overall objective of the proposed research is to develop a world-class explosion test facility capable of investigating the essential characteristics of turbulent high-speed deflagrations and transition to detonations as it relates to explosions that can occur in longwall coal mines. The CSM Gas Explosion Research Facility (GERF) will provide high-quality data and informative results which can be used by researchers to assist in the implementation of transformative mitigation and prevention strategies for gas explosions. Additionally, the insights obtained will be used to provide a comprehensive 3D combustion model coupled with a full-scale CFD model of a longwall coal mine. This inclusive model will be capable of predicting the severity of a methane gas explosion

with respect to propagation velocities and overpressures for various ventilation designs. The specific aims are listed below.

*Enhance our understanding of the impact of rock rubble (i.e. the gob) on flame behavior in both the high-speed deflagration and transition of deflagration to detonation regimes. The high-speed deflagration and interaction with various rock pile geometries and materials will be a continuation of the short-term proposal (AFSTI14) and would allow further improvement of the combustion CFD model developed at Mines which has been successful in capturing the impact of rock rubble on high-speed deflagration of methane flames in cylindrical reactors ranging in scales of 1/50th to 1/8th relative to full size coal mine workings. The proposed work is to extend the knowledge gained in the high-speed deflagration regime to the DDT regime which will allow collaboration with University of Maryland and the Naval Research Laboratory and provide valuable data that can be used as additional validation for the high-fidelity combustion modeling developed at the respective institutions.*

## Expected Research Outcomes

The design and build of a large-scale (12K Liters/427 cu.ft) cylindrical explosion vessel to provide additional insight into the complex interaction of high-speed turbulent deflagrations and detonations with and without a simulated gob (i.e. rock rubble). Data is used to validate and extend CSM's high-speed deflagration combustion model and full-scale three-dimension longwall gas explosion model; and provide data in the DDT regime and further validation for collaborating researchers at UMD and NRL. The validated CSM combustion CFD models are calibrated and validated using the explosion reactor prior to integration with the CSM's full-scale CFD ventilation model of a longwall coal mine, allowing researchers to study the impact of mine explosions and identify conditions that must be met to prevent such explosions through mine layout and ventilation system design, early detection and appropriate emergency response.

# 3.0 Research Approach

The research supported by AFSTI14FO69 consisted of three primary components: the large-scale reactor at the GERF, a secondary small-scale test reactor, and the modeling efforts. The small-scale reactor was used to rapidly test a variety of scenarios at low cost without the time, logistics, and weather constraints of the large-scale reactor. The large-scale reactor at the GERF conducted a variety of experiments to capture the impact of key parameter, such as rock rubble obstructions and methane concentrations on the flame front velocity and explosion overpressures. Results from the large-scale reactor were used to validate combustion CFD models of the same geometry. This validation process is used to improve the accuracy of methane-air gas explosion scenarios in a longwall coal mine using the fully coupled combustion longwall mine ventilation model. The combination of large-scale experimental work and the refinement of CFD modeling in a single research group allowed for closer integration of the work, producing a higher quality modelling effort using experimental validation. This allowed for the development of reliable numerical models of situations, such as an explosion on an active longwall face, which would be costly and requires significant safety protocols to investigate experimentally.

Sections 3 and 4 are arranged as follows. Section 3 begins with a discussion of the objectives and an overview of the research approach. The objectives proposed are presented below, with a brief description of the research approach. The objectives are then used to determine the experimental approach. The key independent and dependent variables are determined and used to develop the requirements and specifications of the GERF. Following the discussion of the facilities and equipment, the specific objectives and the experimental or numerical approach to the objective are presented individually. The findings are presented in Section 4. Section 3 and 4 are arranged with matching headings, and the subheading includes the task numbers present in the following objectives.

**Provide a research facility capable of studying gas explosions relevant to the Mining Industry.**

1. ***Investigate the impact of gob characteristics on the severity of large-scale methane-air gas explosions related to overpressures and flame propagation velocities.***

    a. ***Design, fabricate, and extend existing scaled reactors***

Design, build, and instrument a new large-scale explosion reactor and the necessary support systems and facility to conduct the experiments.

***b. Investigate the impact of methane concentrations under rich, stoichiometric and lean air-fuel ratios on flame propagation velocities and explosion overpressures,***

Conduct a parametric analysis of methane concentrations, methane-air explosive volumes, on explosion dynamics; this is done by altering reactor length, methane volumetric concentrations, and methane-air mixture pressures.

***c. Investigating the impact of ignition energy and location on flame propagation velocities and overpressures***

Conduct two sets of experiments. One with an altered ignition energy and one with a varied ignition location along the length of the explosion reactor.

***d. Investigate the impact of rock rubble geometry (e.g. length, height)) and location relative to ignition source on flame acceleration and overpressures in the high-speed deflagration regime. High-speed imaging will also be used as additional insights into the interaction of the flame and rock pile for additional validation of the CFD combustion models.***

Conduct two sets of experiments, one with varying rock rubble location relative to ignition location and the other with varying the length of the rock rubble section within the reactive methane-air mixture

**2. Provide a fully integrated 3D explosion model of a Longwall Coal mine which utilizes combustion models that have been validated in the high-speed deflagration and DDT regime.**

***1. Continue development, improvement, and validation of the CSM high-speed turbulent deflagration combustion model using the new extended large-scale explosion reactor.***

*a. Initial modeling of the small and large-scale reactor using 2D models to investigate the relative impact of ignition location, and rock rubble geometry.*

Develop a 2D reactor model in parallel with experimental work and use the experimental results to validate and improve the 2D model. Use the faster solve times of the 2D model to explore the impact of various numerical approaches.

b. *Information obtained from the 2D model will be used in the 3D models recently developed for the smaller-scale and will be used to validate the 3D models for the large-scale reactor for select cases to reduce computational effort.*

Use insights from the more rapidly iterated 2D results and experimental results to improve the 3D CFD model of explosions in the flame reactor.

2. ***Improve the full mine scale CFD model initially developed in short-term Alpha Foundation proposal (AFSTI14) with incorporation of the newly acquired data used to improve the combustion model accuracy.***

   a. *Various mine ventilation scenarios currently under investigation will be used in the models to predict the location of the EGZs and vary the ignition location. The validated 3D CFD combustion models of the explosion reactor will be incorporated into the Full-scale Longwall coal model.*

A full scale CFD model of a methane explosion on an active longwall face was developed, using the improved CSM high-speed turbulent deflagration combustion model. This process was broken down into two parts. First, a ventilation model of the mine simulating moving equipment was developed and refined, to provide initial conditions, including methane concentrations. This was utilized in a high-fidelity model of an ignition and explosion on the active face.

3. ***Investigate the impact of rock rubble on the acceleration and transition to Detonation and providing data to researchers at UMD and NRL for further validation of DDT models.***

   a. *Various rock rubble lengths and orientations will be investigated with input from the collaborators at UMD and NRL to provide the key conditions used to validate their high-fidelity DDT models.*

Experiments with varied rock rubble length and reactor configurations were conducted to measure the impact of the obstruction in a variety of configurations and characterize behavior beyond the obstruction. Experiments with a long (75ft) reactive zone were utilized to safely approach the DDT.

4. ***Increase understanding of the methane gas explosions and their complex interaction with obstacles, with the goal of developing recommendations and practical guidelines for explosion prevention in the coal mines.***

The experimental and numerical work in this research highlight the impact of key factors, such as obstructions reducing the run-up distance and transient disruptions in ventilation creating conditions where an ignition may occur. This research experimentally and numerically identifies situations where ignitions become possible and the requirements to reach detonation may be reduced, demonstrating specific potential hazards in underground coal mines.

3. **Provide best practice recommendations to the mining industry for the prevention of methane gas explosions and potential of transitioning to detonations causing catastrophic damage.**

The research identified situations where ignitions can develop despite otherwise effective ventilation and geometry can reduce the run-up distance required for a deflagration to hit the DDT. These findings are generalized into preliminary safety recommendations and areas of interest for future research.

## Objective 1: Investigate the impact of gob characteristics on the severity of large-scale methane-air gas explosions related to overpressures and flame propagation velocities.

The primary motivation of the experimental portion of the proposed research is to quantify the impact of a set of key variables that contribute to the destructive potential of a gas explosion and improve scientific understanding of the mechanisms. In addition to directly measuring and quantifying the phenomena, the data produced by the experimental work was used for validating and fine tuning the numerical modeling portion of the project. The major experimental variables of interest are listed in Table 1. This defined the independent variables for the experimental work. The dependent variables measured in the experiments were selected to quantify changes in the

destructive potential of a gas explosion and to provide a reliable point of comparison for the numerical modeling effort. The flame front propagation velocity and the overpressure fulfill both requirements well and can be measured with relative ease. The pressure is directly measured, and the flame front velocity is calculated from direct ion sensor measurements. The arrival time of the flame front is measured by ion sensors and the velocity of the flame front is then calculated using the detection times and sensor locations. The overpressure is measured with a variety of pressure sensors mounted in the reactor. The flame propagation velocity and the overpressure are an excellent proxy for the destructive potential of an explosion and is a direct measure of how close the flame front speed got to the DDT.

*Table 1: Major Experimental Variables*

| **Independent Variables** | **Dependent Variable** | **Summary of Interest** | **Objective** |
|---|---|---|---|
| Fuel/Air Ratio | Flame Front Velocity, Pressure | Determine the impact of fuel concentration (% volume) on the flame front velocity | 1.b |
| Ignition Energy | Flame Front Velocity, Pressure | Test the impact of changes in the ignition energy on the explosion | 1.c |
| Ignition Location | Flame Front Velocity, Pressure | Measure how flame front behavior varies when the ignition point moves along the length of the reactor. | 1.c |
| Rock Rubble Location | Flame Front Velocity, Pressure | Show if the acceleration from a single rock rubble obstruction is persistent down the reactor length. | 1.d |
| Rock Rubble Geometry | Flame Front Velocity, Pressure | Show the impact of rock rubble geometry variations on the flame front velocity. | 1.d |
| Reactor Length | Flame Front Velocity, Pressure | Demonstrate scaling and allow experiments to start at a smaller scale, reducing the energy in initial experiments. | 1.d, 2.3.a |
| Reactor Pressure | Flame Front Velocity, Pressure | Environmental variable (altitude and sea-level) | 1.b |

Experiments were conducted in a large scale reactor with a 0.71 m (28 in) diameter. This reactor was designed to provide various length configurations with and without a rock rubble obstruction in the reactor. Methane volumetric gas concentrations of 7.5 %, 9.5 %, and 11.5 %. The reactive zone lengths available were 7.62 m (25 ft), 15.24 m (50 ft), and 22.86 m (75 ft) with overall reactor

lengths between 15.24 m (50 ft) and 30.48 m (100 ft). Experiments with 30.48 m (100 ft) reactive zones were originally considered. However, the lack of an empty reactor section at the open end increased the potential fire hazard since it increased the possibility of the deflagration escaping the confinement of the suppressor. This risk was not considered acceptable during the 2022 wildfire season, though longer reactive zones may be revisited in the future.

## Objective 1.a: Design, Fabricate, and Extend Existing Scaled Reactors

The experimental work required the construction of a new lab, the Gas Explosion Research Facility (GERF) at the Edgar Mine in Idaho Springs. The Edgar Mine is a satellite facility of Colorado School of Mines, managed by the Mining Department. It is used for classes and research by a variety of academic departments at the Colorado School of Mines, partner universities, industry, and government. With this diverse array of partners, academic and continuing education classes, and research projects, the Edgar Mine has the infrastructure and facilities to support a variety of activities. The GERF was designed to be a world class research facility capable of hosting this research as well as future projects. As of this report, the GERF is operational and available for additional projects. Building the GERF and having its unique capabilities available for academic use in North America was one of the objectives of the grant.

The experimental work conducted at the GERF focused on the impact of independent parameters on the flame propagation velocity. The primary parameters of interest are the addition of a rock rubble obstruction and secondarily varying the rock rubble geometry. Several additional variables of interest are discussed in the following section. The flame front velocity and the overpressure were used as the primary dependent variable measured. This was done for two reasons. First, it is an excellent indication of changes in the distance required to hit the detonation/deflagration threshold and to the destructive potential of an ignition. Second, measuring the flame front velocity is highly amenable to the use of ion sensors, which provide a very robust sensor system with numerous sample locations. While other measurements were taken, the use of ion sensors to measure the arrival time of the flame front and, by extension, velocity of the flame front provided an extremely robust research methodology which closely linked the physical measurement to the quantifiable hazard of interest.

The centerpiece is the explosion reactor, which was designed to provide a high level of flexibility in experimental setup, ranging from withstanding high pressures to allowing the insertion of rock

rubble and gas barriers. A 30.48 m (100 ft) long explosion reactor was designed in 7.62 m (25 ft) sections to allow for flexible configurations and easy loading of obstructions or instrumentation. The requirements and specification for the reactor and associated facility capabilities are listed in Table 2. The design elements of the GERF are support the experimental objectives and how these specifications and features discussed in detail in the remainder of this section.

*Table 2: Reactor specifications and requirements*

| | **Requirement** | **Specification** |
|---|---|---|
| **Structural** | Detonation Pressure | 1.66 MPa (241 psig) for Methane/Air |
| | Reflected Shockwaves | 4.4 MPa (638 psig) without yield for shockwaves |
| | Recoil | Absorb recoil force dynamically |
| | Anchor points | Prevent excessive movement during experiments |
| **Dimensions** | Length | 30.48 m (100 ft) |
| | Internal Diameter | 0.71 m (28 in) |
| | Individual Sections Length | 7.62 m (25 ft) |
| **Mechanical** | Joint Configuration | 36 hole ANSI pattern |
| | Joint Misalignment | Tolerate slight misalignment |
| | Separation | Sections must be separable to gain access during normal site work. This can be done with a cordless impact driver and a 2.7 t (6000 lb.) hand operated cable puller. Separations of 0.91 m (3 ft) can be achieved. |
| | Support | Fully supported to allow separation and a means of adjustment to allow for alignment even if settling occurs. This is done with large industrial rollers, which are shimmed as necessary. |
| | Clamping | Joints must be able to apply a clamping force capable of retaining a gas barrier at any reactor joint. This is accomplished with a rubber ring that distributes force even with a small misalignment. |
| **Utility** | Sensor Ports | Top and side ½" NPT ports allow for the customization of sensor location, vents, and other features as necessary. |
| | Wire passthroughs into reactor for control | Passthroughs are available for use in the 1.27 cm (½") NPT ports |
| | Mounting Instruments | Instrument mounts can be attached to a clamped ring at reactor joints or with a large magnet for other locations. |

| | | |
|---|---|---|
| **Configuration Changes** | Change Reactor Length | The overall length of the reactor can be changed by moving the blind location (closed end) |
| | Change Reactive Zone Length or Separate Gas Zones | The reactive zone length can be changed by changing the gas barrier or adding an additional barrier. |
| | Insert obstructions and/or instruments | When reactor sections are separated, equipment and obstructions can be hand loaded into the reactor. |
| | Move Sensors | Sensors can be moved by changing what ½" NPT port the sensor is located in. |
| | Move Ignition Point | The modular ignition system can be installed on any ½" NPT port and control wires run back to a safe location for the crew conducting the experiment. |
| **Operations** | Reload | A reload is conducted by breaking the reactor section where the gas barrier is clamped and replacing the gas barrier. Other instrumentation may be inspected or serviced while this occurs. |
| | Ion Sensor Inspections and general maintenance | While the ion sensor system is extremely robust and damage tolerant, the sensors protrude into the path of explosions and require inspection and replacement on occasion. |

The primary systems supporting the reactor are shown in Figure 4.


*Figure 4: GERF Systems*

**GERF Site Overview**

The GERF is located on an access road above the main facilities at the Edgar Mine. An out of the way natural flat spot on the ridge was selected with road access. This maintains a separation between the various facilities at the Edgar Mine and allows for simultaneous operations at the Edgar Mine, the Explosives Research Lab, and the GERF. A level pad was created with fill and provides a large work area with space for infrastructure, storage, and parking. A compressor, water tank, generator, and control center are all present on site at the GERF. The compressor is used to supply air during experiments, and the generator provides backup AC power in situations where the battery system doesn't provide adequate output or endurance. The access road was rerouted to allow for the Conex suppressor to be aligned with the road and lengthened as necessary. Road access to the GERF is gravel and accessible by most 4wd vehicles, mine equipment, and many heavy trucks, such as dump trucks and smaller cranes (for moving reactor sections). The road, generator, and compressor are shown in Figure 6. The preliminary sit survey and layout are presented in Figure 7. The finished GERF facility is shown in Figure 8. A building on (Figure 9) is used on site as a control center, workspace, storage, and shelter.


*Figure 5: GERF Site Features*

*Figure 6: Compressor and generator on GERF site (left) and the access road (right).*

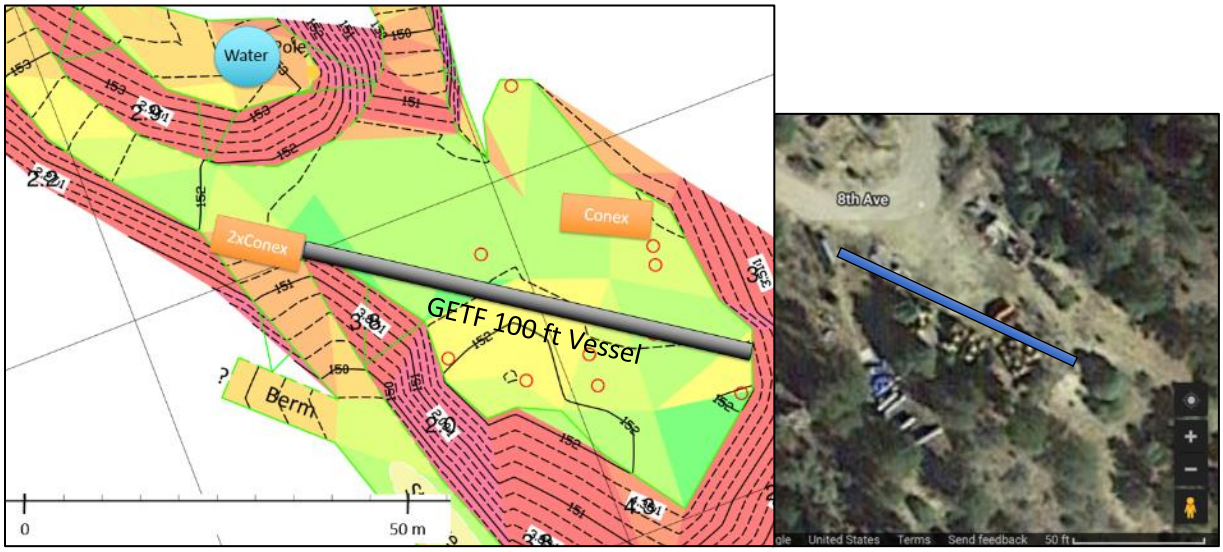


*Figure 7: Preliminary survey of the site (left) and an aerial view of the location prior to pad construction (right).*

*Figure 8: Pictures of the finished GERF site.*

*Figure 9: The GERF Control Center, which houses all controls, DAQ monitoring, ignition control system, and video surveillance of the site during experimental testing*

**Reactor Design**

The flame reactor is a heavy cylindrical pipe which will have one end closed using a blind flange and the other end open to atmosphere. High strength pipe material (API 5Lx65) is used with a 2.54 cm (1 in) wall thickness. The pipe can handle up ~300 bar (4350 psig) steady-state pressure (based on circumferential stress calculations), welded neck raised flanges (WNRF) are used due their ability to handle shocks and significant stresses compared to other type of available flanges. The flanges chosen are 300 series flanges and can handle pressures greater than 50 bar (725 psig). The material specifications for the pipe used to make the flame reactors are presented below in Table 3; along with the safety factors based on circumferential stress (hoop stress) calculations for a cylindrical pipe using a methane-air detonation pressure of 1.66 MPa (241 psig) and 4.4 MPa (638 psig) (based on reflected shocks). It is clear from safety factors of greater than 7 (deformation due to reflected shock during detonation) that the flame reactor is more than capable of handling deflagration explosions as well as detonations. A CAD drawing and detail schematics of the flame reactor sections that was presented for bid is shown in Figure 12. The cylindrical pressure vessel being used as the flame reactor was fabricated by a professional vessel company (Gerard Tank & Steel) to ensure the integrity of fabrication/welding (submerged arc welding commonly used for structural and vessel construction). A photograph of the reactor in the 30.48 m (100 ft) configuration is shown in Figure 11. Gases are confined within the reactor with relatively low strength plastic sheet gas barriers.

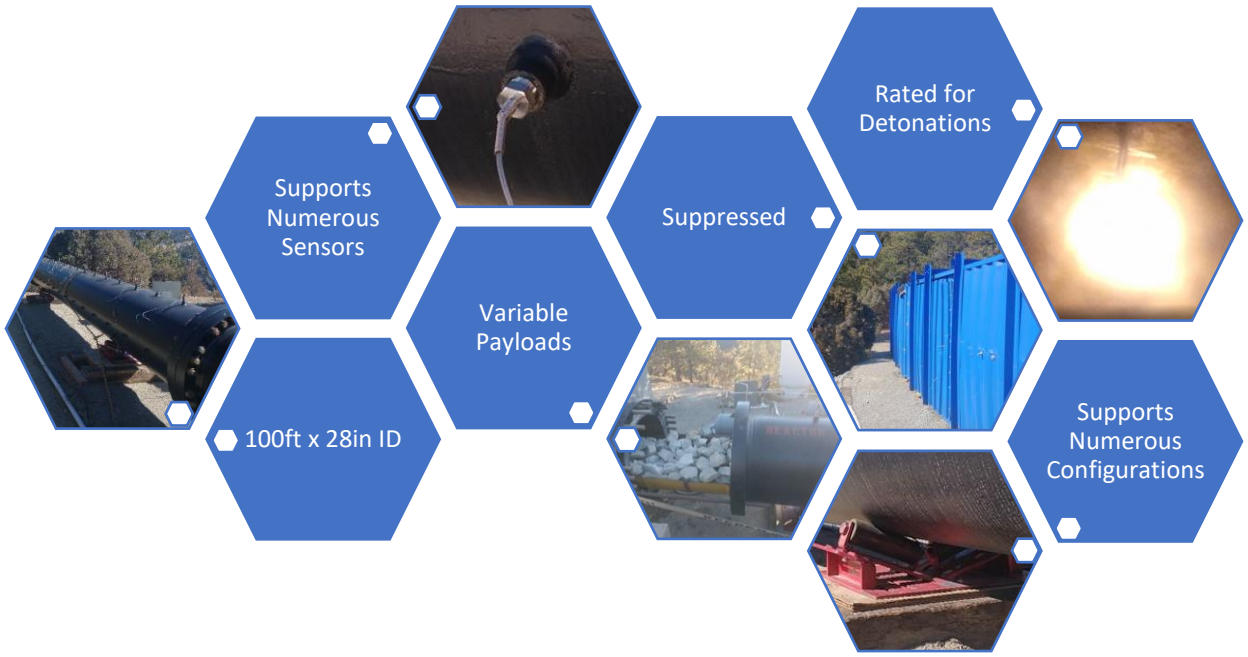


*Figure 10: GERF Reactor Features*

*Table 3. Specification for API 5L x65 standard carbon steel line pipe*

| **Min. Yield strength** | **Max. Yield strength** | **Min. Tensile strength** | **Max. Tensile strength** |
|---|---|---|---|
| 448 MPa (65,000psi) | ≥ 600 MPa (87,000 psi) | 531 MPa (77,000 psi) | ≥ 760 MPa (110,000 psi) |
| Hoop stress (1.66 MPa (241 psi)) | | | Hoop stress (1.66 MPa (241 psi)) |
| 24.8 MPa (3,600 psi) | | | 24.8 MPa (3,600 psi) |
| SF for deformation | | | SF for rupture |
| ~18 | | | ~30 |
| Hoop stress (4.4 MPa (640 psi)) | | | Hoop stress (4.4 MPa (640 psi)) |
| 65.8 MPa (9,544 psi) | | | 65.8 MPa (9,544 psi) |
| SF for deformation | | | SF for rupture |
| ~7 | | | ~11 |

*Figure 11: The 30.48 m (100 ft) flame reactor at the GERF.*

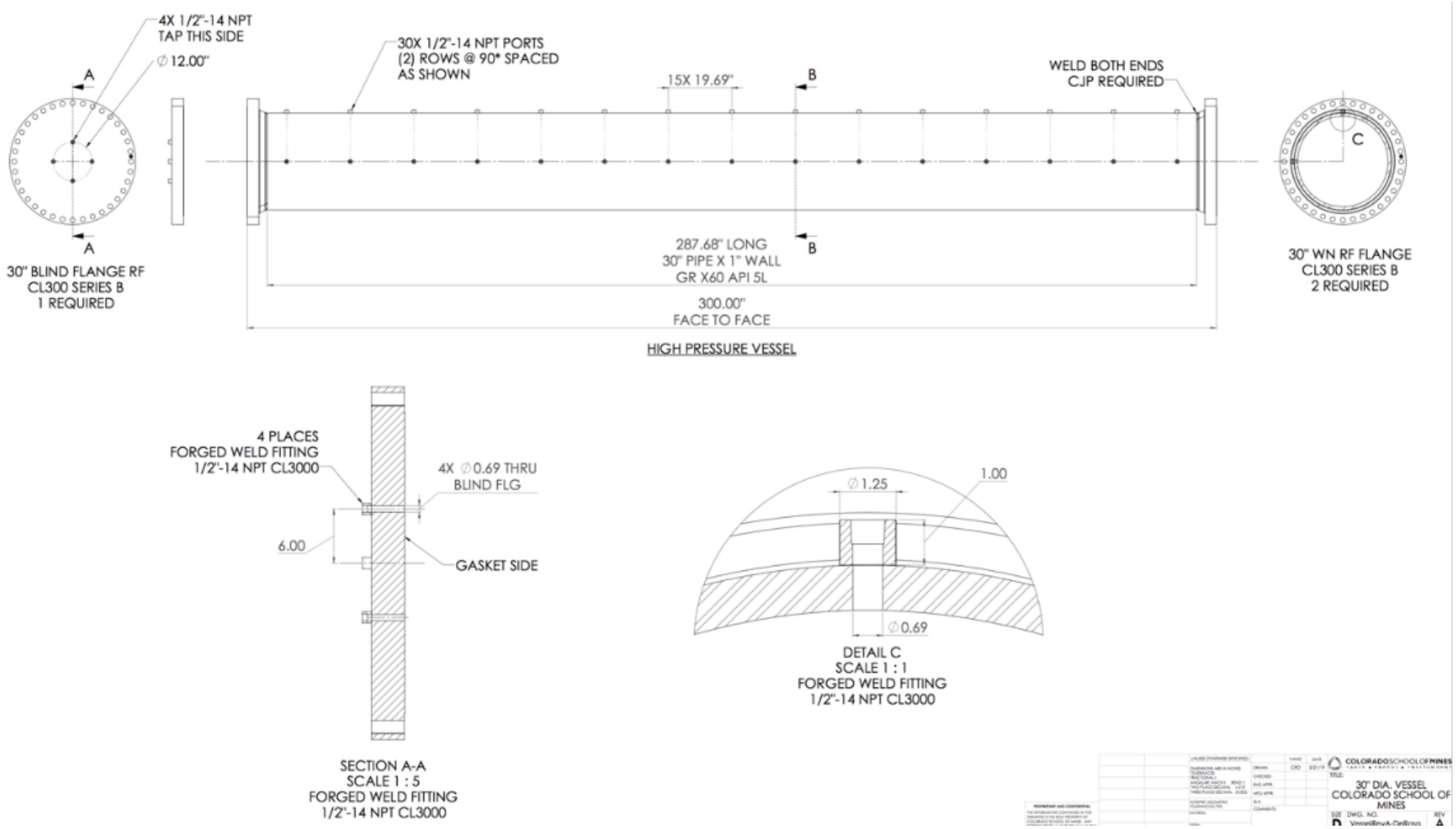


*Figure 12: Schematic of GERF Reactor Section*

A large number of potential design and configuration variables are present in the reactor design. This was simplified down into the independent variables for the experiments and variables in reactor configuration of a primary logistical nature. The major variables are listed in *Table 4*. Independent variables dependent on the reactor configuration are denoted with the following label in the table: "*[Reactor Configuration]*." A general overview of the reactor configuration can be found in *Figure 16*. The selected experimental variables and the associated research objectives are listed in *Table 5*. Note that several independent variables, such as the ignition location, do not depend on the reactor configuration, though there may be some constraints imposed, such as the maximum safe fuel percentage or what NPT ports are available.

*Table 4: Large Scale Reactor Configurations Options*

| | **Reactor Configuration Option** | **Description** |
|---|---|---|
| Independent Variables | Overall Reactor Length *[Reactor Configuration]* | Major experimental variable and heavily influences the maximum flame front velocity. Determines the blind location. |
| | Reactive Zone Length *[Reactor Configuration]* | Major experimental variable and heavily influences the maximum flame front velocity. Determines the blind location. |
| | Air Section Length *[Reactor Configuration]* | The air-filled reactor section has two impacts. First, it causes higher more resistance to the gas being expelled from the reactor, increasing the pressure relative to a reactor with the same reactive zone length and no air-filled section. This slows the flame front propagation in the reactor. Second, it decreases or prevents the deflagration from exiting the open end of the reactor, reducing the fire hazard. |
| | Fuel concentration (%volume) | The fuel concentration determines the potential energy of the reactor, influences the reaction characteristics, and the potential for the deflagration to continue into the air in an air zone or the suppressor. This is both an experimental variable and a safety consideration. |
| | Rock Rubble *[Reactor Configuration]* | Obstructions cause turbulence, which can accelerate the flame front velocity, potentially reducing the runup length required to reach the DDT. |

| | | |
|---|---|---|
| | Location<br>*[Reactor Configuration]* | The location of the rock rubble alters the point in the explosion where a large and likely sustained acceleration in the flame propagation velocity occurs, impacting the effective runup length required to hit the DDT. |
| | Geometry<br>*[Reactor Configuration]* | The geometry (length, height, shape, etc.) impact of blockage ratio and the overall obstructed length. This will impact the magnitude of the acceleration, making it an important factor in the magnitude of acceleration that occurs from an obstruction in the reactor. |
| | Ignition Energy | The ignition energy of the spark influences the nature of the resulting explosion. |
| | Ignition location | The ignition location alters the run-up length and the potential pressures in front of the flame front, changing the explosion dynamics. |
| Logistics Options | Blind Location | The blind can be moved to accommodate various overall reactor length and reactive zone requirements. Wiring and gas plumbing are in place for the blind to be positioned at the end of a reactor with an overall length of 15.24 m (50 ft), 22.86 m (75 ft), and 30.48 m (100 ft). |
| | Fill location | Determined by the blind location when the reactor is configured for normal operations. The system can support nonstandard configurations with fill locations into separate reactive zones. |
| | Vent Location | Can be moved to keep the vent located just upstream of the gas barrier when a reactor configuration change moves the gas barrier location. |
| | Gas Barrier | The gas barrier can be clamped between any two reactor sections or over the open end of reactor 1. It is used to contain the explosive atmosphere within the reactive sections with a minimal strength to minimize the backpressure during experiments. It is possible to equip the reactor with multiple gas barriers if varied reactive zones are required. |
| | Pressure Sensor Locations | Pressure sensors are typically positioned on each side of the gas barrier, so that the barrier burst can be detected. |

| | | |
|---|---|---|
| | Ion Sensor Location | The ion sensor system is designed to allow flexible placement so sensor density cyan be increased in regions of interest. This is primarily done in the final reactor section in order to better characterize the flame front velocity near its highest point. |
| | Camera location | Cameras, along with other supplemental sensors can be positioned inside the reactor as required for different objectives. |
| | Barrier Strength | The strength of the gas barrier can be varied as desired to allow for higher experimental pressures (simulating sea level) or to accommodate other needs, such as a higher pressure (higher speed) fill rate. Barrier strength will influence the magnitude of a transient back pressure, so experiments of the same set should use the same barrier strength where possible. |

*Figure 13: The reactor is supported on rollers, to allow for configuration changes and access to the reactor sections. The reactor sections can be split at any joint. This process is done during reloads when the barrier is clamped between reactor sections.*

*Figure 14: Reactor view showing top and side NPT ports (left), a thermocouple in an NPT port (middle), and a vent (right).*


*Figure 15: Reactor split for loading a rock rubble insert (left) and the blind with fill and purge ports (right).*

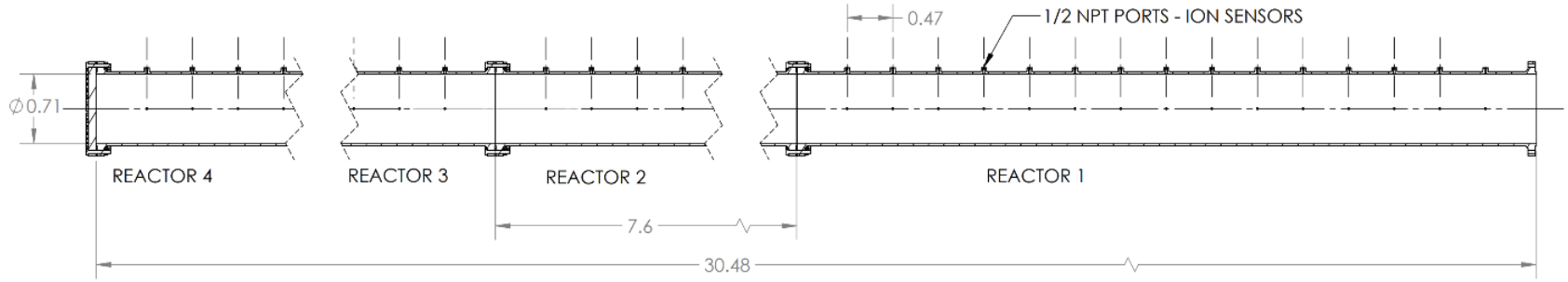


*Figure 16: Full reactor with a total length of 30.48 m (100ft). The reactor is made up of 4 sections 7.62 m (25 ft) sections bolted together at the flanges to allow for acces. In the sketch above, Reactor 1 is represented as a full 7.62 m (25 ft) section while the other 3 sections are abbreviated. The top and east side of the reactor are lined with ½" NPT ports to allow customization of sensor vent and ignition system locations.*

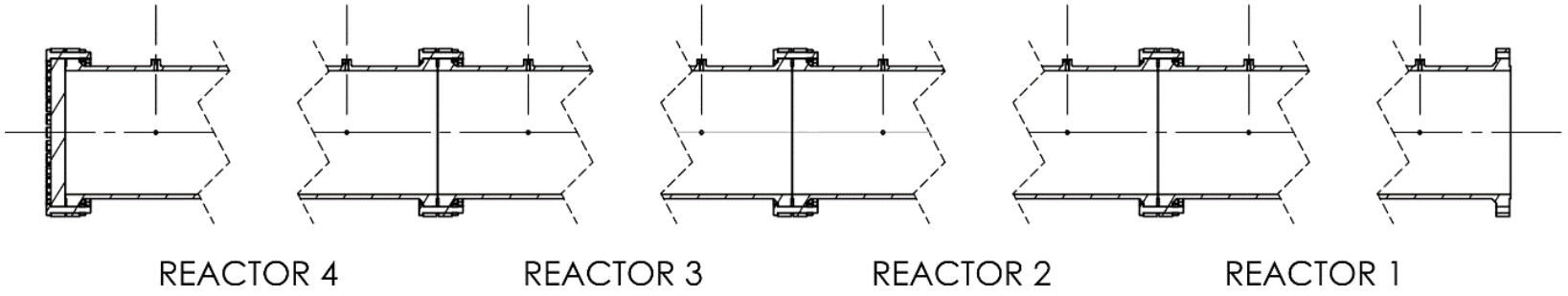


*Figure 17: The reactor joints are shown. The reactor joints are shown above and allow the reactor to be split at any joint for loading or sensor system maintenance.*

*Table 5: Major Experimental Variables*

| **Independent Variables** | **Dependent Variable** | **Summary of Interest** | **Objective** |
|---|---|---|---|
| Fuel/Air Ratio | Flame Front Velocity, Pressure | Determine the impact of fuel concentration (% volume) ratio on the flame front velocity | 1.b |
| Ignition Energy | Flame Front Velocity, Pressure | Test the impact of changes in the ignition energy on the explosion | 1.c |
| Ignition Location | Flame Front Velocity, Pressure | Measure how flame front behavior varies when the ignition point moves along the length of the reactor. | 1.c |
| Rock Rubble Location | Flame Front Velocity, Pressure | Show if the acceleration from a single rock rubble obstruction is persistent down the reactor length. | 1.d |
| Rock Rubble Geometry | Flame Front Velocity, Pressure | Show the impact of rock rubble geometry variations on the flame front velocity. | 1.d |
| Reactor Length | Flame Front Velocity, Pressure | Demonstrate scaling and allow experiments to start at a smaller scale, reducing the energy in initial experiments. | 1.d, 2.3.a |
| Reactor Pressure | Flame Front Velocity, Pressure | Environmental variable (altitude) | 1.c |

*Table 6: Reactor Configurations used in Research*

| Total Length | Reactive Zone | Air Zone | Obstruction | Suppressor | Concentrations Tested % Volume | Figure |
|---|---|---|---|---|---|---|
| 15.24 m (50 ft) | 7.62 m (25 ft) | 7.62 m (25 ft) | Clear | Mist in Conex | 7.5 %, 9.5 %, 11.5 % | Figure 18 |
| | 7.62 m (25 ft) | 7.62 m (25 ft) | 50% x 1.7 m (5.6 ft) | Mist in Conex | 7.5 %, 9.5 %, 11.5 % | Figure 19 |
| | 15.24 m (50 ft) | Not present | Clear | Mist in Conex | 7.5 %, 9.5 %, 11.5 % | Figure 20 |
| | 15.24 m (50 ft) | Not Present | 50% x 1.7 m (5.6 ft) | Mist in Conex | 7.5 %, 11.5 % | Figure 21 |
| 30.48 m (100 ft) | 22.86 m (75 ft) | 7.62 m (25 ft) | Clear | Barrels in Conex | 7.5 % | Figure 22 |
| | 22.86 m (75 ft) | 7.62 m (25 ft) | Clear | Barrels in Conex & Water Slug Insert | 7.5 % | Figure 23 |
| | 22.86 m (75 ft) | 7.62 m (25 ft) | 50% x 1.7 m (5.6 ft) | Barrels in Conex & Water Slug Insert | 7.5 % | Figure 24 |
| | 22.86 m (75 ft) | 7.62 m (25 ft) | 50% x 4 m (13.1 ft) | Barrels in Conex & Water Slug Insert | 7.5 % | Figure 25 |

*Table 7: 6 m (20 ft) pilot reactor previously tested at Mines.*

| Length | Reactive Zone | Air Zone | Obstruction | Suppressor |
|---|---|---|---|---|
| 6 m (20 ft) | 6 m (20 ft) | Not present | Unobstructed | None |
| | 6 m (20 ft) | Not present | Blind End | None |
| | 6 m (20 ft) | Not present | Middle | None |
| | 6 m (20 ft) | Not present | Open End | None |

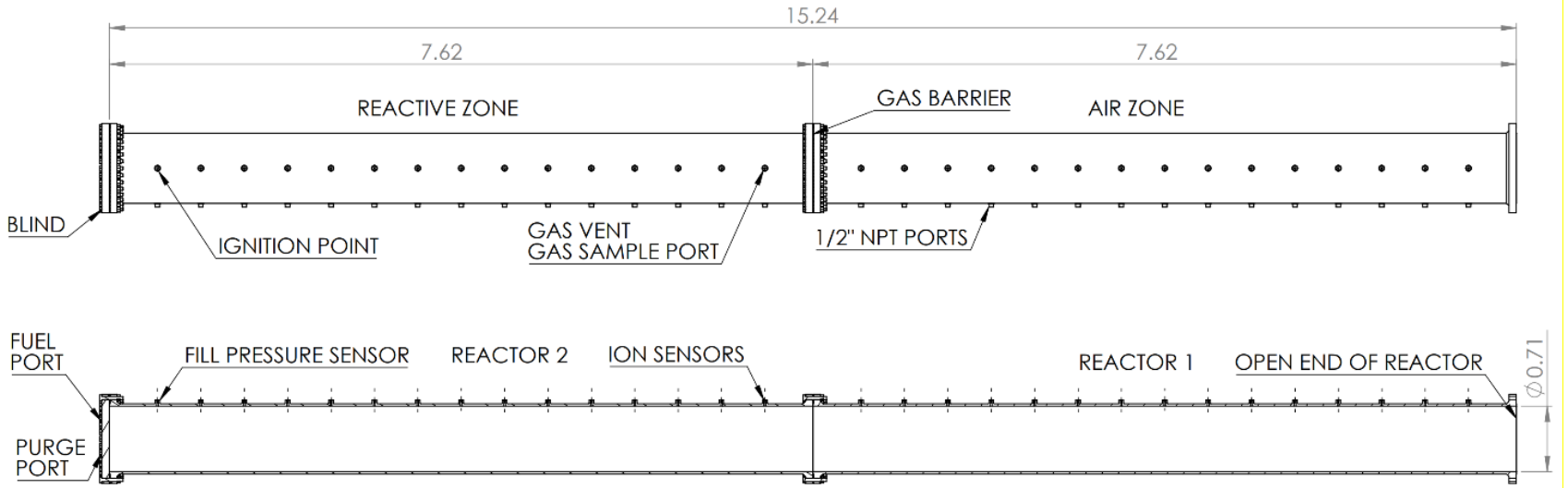


*Figure 18: 15.24 m (50 ft) unobstructed reactor with 7.62 m (25 ft) reactive zone*

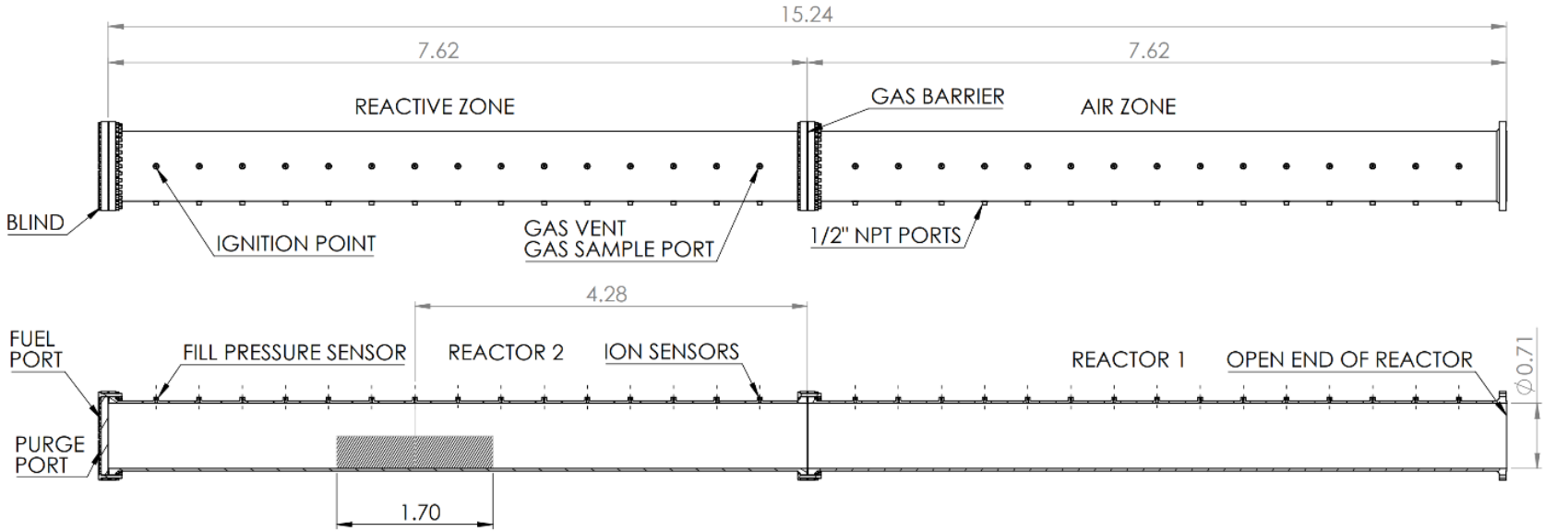


*Figure 19: 15.24 m (50 ft) reactor with 7.62 m (25 ft) reactive zone and a 1.7 m (5.6 ft) 50% rock rubble obstruction*

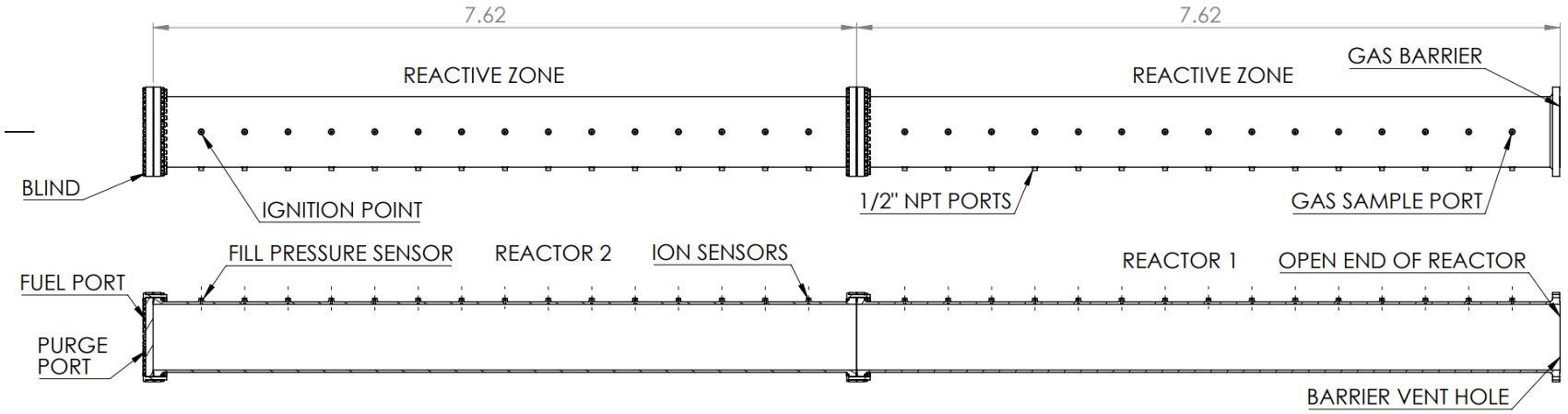


*Figure 20: 15.24 m (50 ft) unobstructed reactor with a 15.24 m (50 ft) reactive zone.*

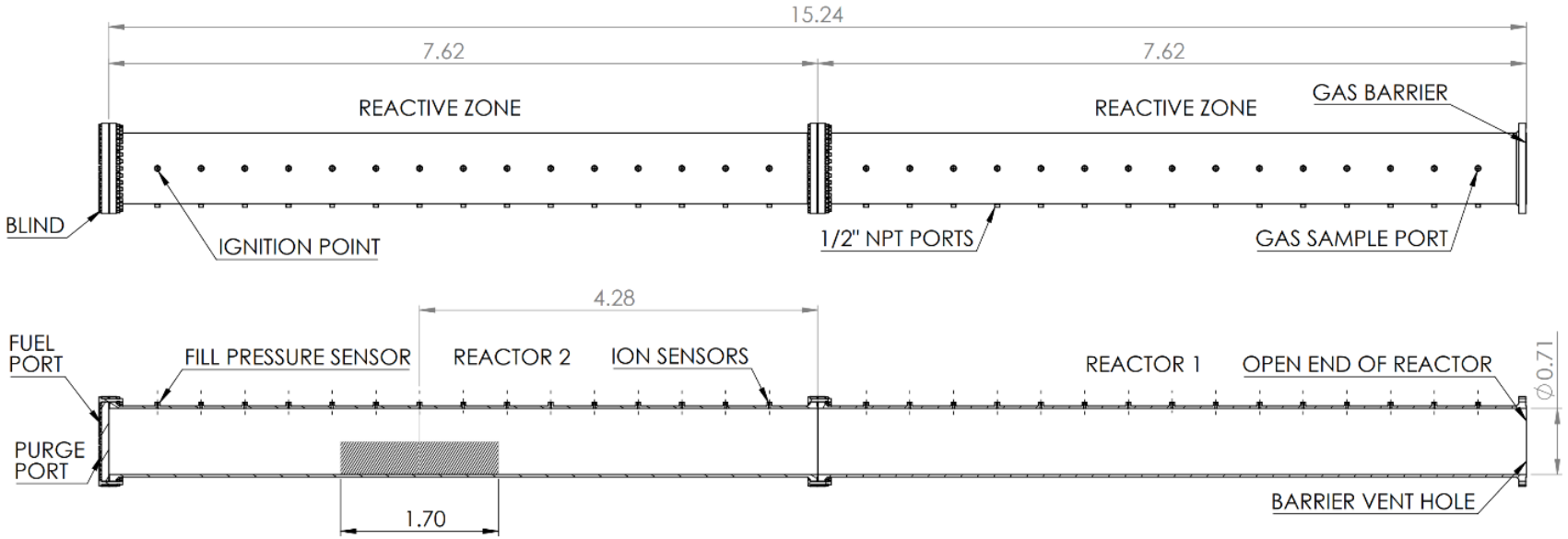


*Figure 21: 15.24 m (50 ft) reactor with a 15.24 m (50 ft) reactive zone and a 1.7 m (5.6 ft) 50% rock rubble obstruction*

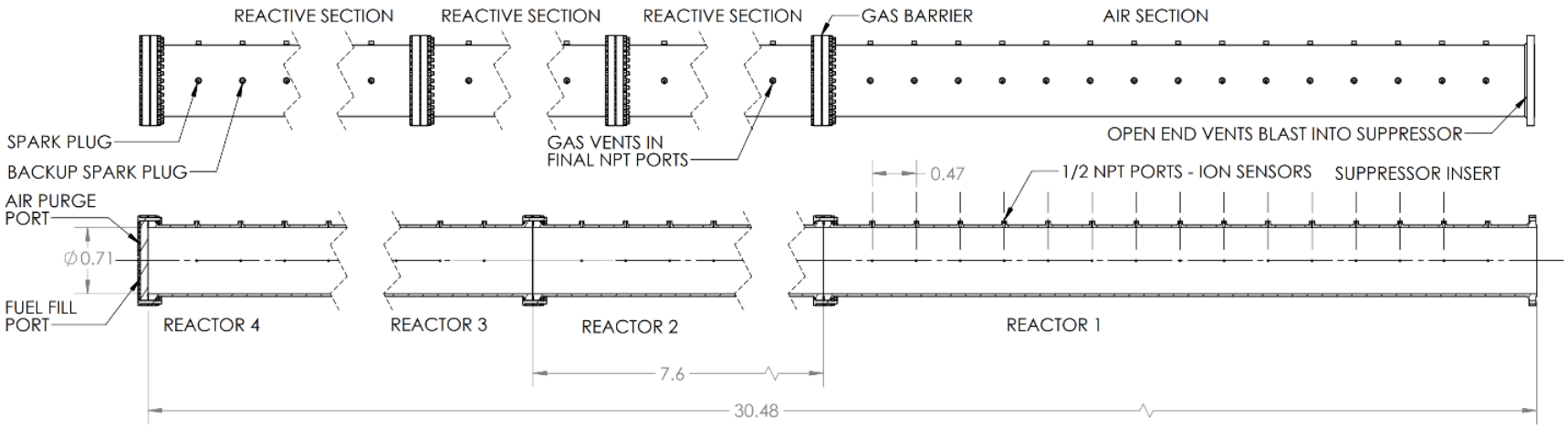


*Figure 22: 30.48 m (100 ft) unobstructed reactor with 22.86 m (75 ft) reactive zone. Using the Conex suppressor with an array of water barrels.*

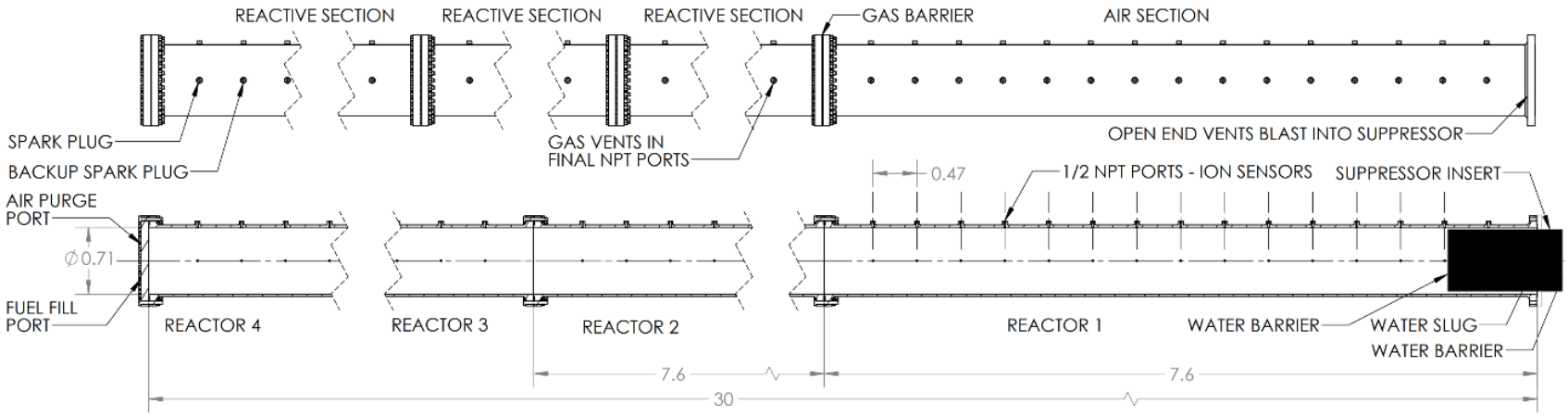


*Figure 23: 30.48 m (100 ft) unobstructed reactor with 22.86 m (75 ft) reactive zone and a water slug insert in the final air filled reactor. Using the Conex suppressor with an array of water barels.*

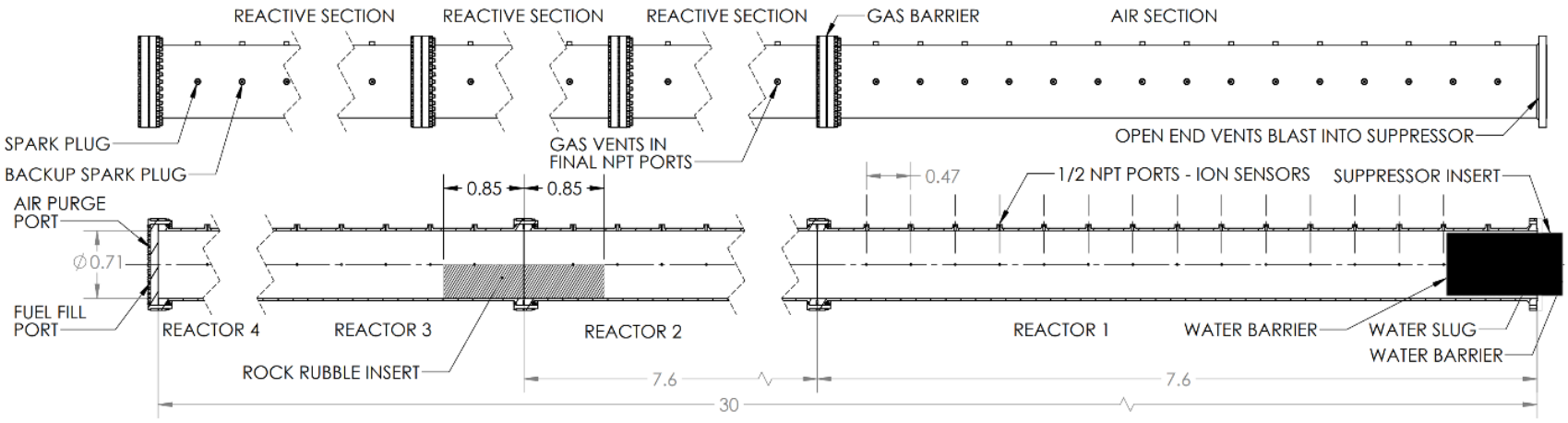


*Figure 24: 30.48 m (100 ft) obstructed reactor with 22.86 m (75 ft) reactive zone and a water slug insert in the final air-filled reactor. Using the Conex suppressor with an array of water barrels. The rock rubble obstruction fills 50% of the reactor with a 1.7 m (5.6 ft) long 50% rock rubble obstruction.*

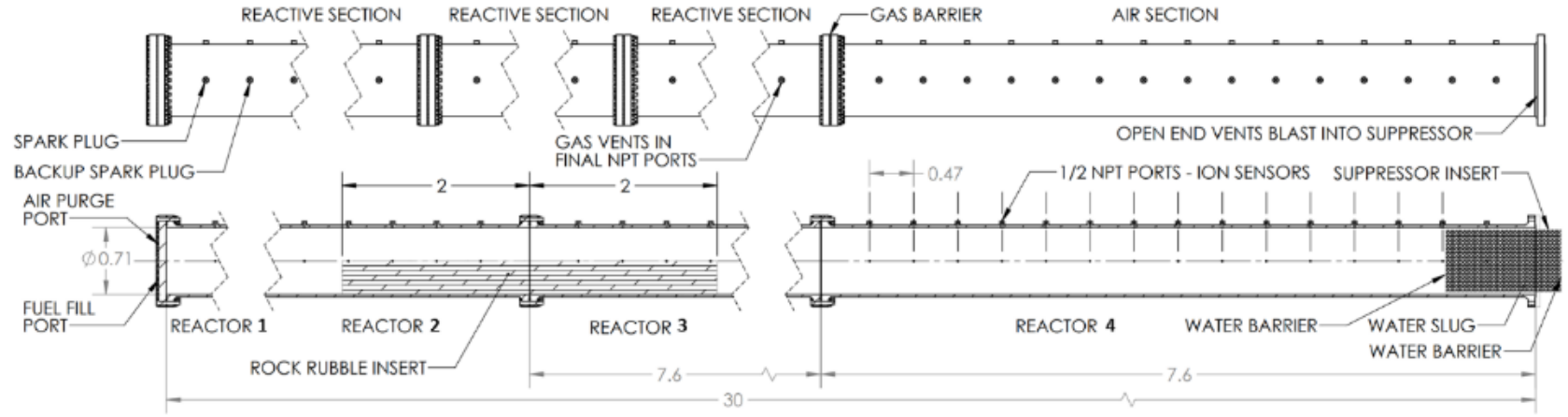


*Figure 25: 30.48 m (100 ft) reactor with 22.86 m (75 ft) reactive zone, extended rock rubble obstruction, and a water slug insert in the final air-filled reactor. Using the Conex suppressor with an array of water barrels. The rock rubble obstruction fills 50% of the reactor with a 4 m (13.1 ft) long 50% rock rubble obstruction.*

Plastic barriers are used to confine the gas within the reactor or to partition the reactor. The gas barrier also determined the maximum gas flow rate in most experiments. The limiting factor for gas flow is the pressure gradient across the vent ports. The stronger barrier allowed an increase in gas pressure and an overall increase in total flow; reducing the gas flow time from apprimately 4 hours to 1.5 – 2 hours. In total, five configurations of gas barriers are used. These are summarized in Table 8. Early experiments used foil barriers and a multilayer barrier made with three layers of 0.15 mm (6 mil) plastic sheeting available from big box home improvement stores for use as a moisture barrier. This configuration was relatively weak, limiting gas flow rates when the barrier did not include a low pressure drop vent hole. These configurations were used in initial tests of 15.24 m (50 ft) reactor variants. For 15.24 m (50 ft) experiments with a 15.24 m (50 ft) reactive zone, the barrier was clamped over the end of reactor one. In this configuration, a vent hole was present in the barrier. In other configurations, which filled the final reactor section (Reactor 1) with air, the barrier needed to be gas tight, to prevent unwanted and unanticipated buildup of combustible gases. Therefore, all venting was done through side ports, which required a higher reactor pressure to achieve the same fill rate.

The weak foil and multilayer barriers limited the safe fill rate of the reactor to the point of being impractical for most experiments. This led to the switch to the 0.18 mm (7 mil) high strength barrier. The burst strength was experimentally tested, with the high strength barrier withstanding approximately 68.95 kPa (10 psig) of air pressure in the reactor. The higher strength barrier allowed for the use of a varied reactor pressures, including the option to match sea level pressure, if desired. With a safety factor of 2, fills could be conducted with a reactor pressure of 34.5 kPa (5 psig), resulting in more practical fill times. Reactor sections are not perfectly aligned due to a variety of geotechnical causes. This causes an uneven clamping force and has the potential to cause a small gap. Reactor sections are aligned manually using a lifting airbag and plywood shims under the rollers. The reactor joints without a gas barrier use a graphite seal, which is sufficient to handle a minor misalignment. The joint with the gas barrier on the 15.24 m (50 ft) reactor uses a rubber ring to ensure that the entire barrier receives adequate clamp force. This clamp ring has a thin sheet steel backer to hold the rubber in place, as well as the wiring in the barrier break sensor. The clamp ring and barrier are shown in Figure 26. It should be noted that the barrier strength does influence flame front propagation velocity. These findings are discussed in the results section.

*Table 8: List of barrier configurations*

| Barrier | Location | Mount | Material | Press | Vent | Used With |
|---|---|---|---|---|---|---|
| Foil | Reactor Joint | Clamped between flanges | aluminum foil sheet | ~27.6 kPa (4 psi) | No | 15.24 m (50 ft) (7.62 m (25 ft) reactive) initial tests |
| Multi layer | Reactor Joint | Clamped between flanges | 3 Layers, 0.15 mm (6 mil) plastic | ~20.7 kPa (3 psi) | No | 15.24 m (50 ft) (7.62 m (25 ft) reactive) initial tests |
| Multi layer | Reactor End | Clamped with flange ring | 3 Layers, 0.15 mm (6 mil) plastic | ~20.7 kPa (3 psi) | Yes ½” | 15.24 m (50 ft) (15.24 m (50 ft) reactive) |
| Single Layer | Reactor Joint | Clamped between flanges | 0.18 mm (7 mil) 207 MPa (30,000 psi) plastic | ~68.9 kPa (10 psi) | No | 15.24 m (50 ft) (7.62 m (25 ft) reactive) |
| Single Layer | Reactor Joint | Rubber faced clamp ring and burst sensor | 0.18 mm (7 mil) 207 MPa (30,000 psi) plastic | ~68.9 kPa (10 psi) | No | 30.48 m (100 ft) (22.86 m (75 ft) reactive) |

*Figure 26: gas barrier seen from inside the reactor (left), gas barrier clamp with a closed reactor (center), and the gas barrier and clamp ring being installed (right).*

**Control and Gas System**

The GERF uses a National Instruments (NI) compact Data Acquisition (cDAQ) and control system. The heart of the system is a NI cDAQ 9132. The 9132 combines an embedded Windows computer with 4 slots for I/O modules. The operator connects to the 9132 by remote login over ethernet. The embedded windows system is used to run a LabVIEW executable with the control software. The LabVIEW virtual instrument running on the 9132 controls the solenoid valves and mass flow controllers in the gas system. This architecture only requires that the operator have an ethernet connection to the control and DAQ systems, allowing for remote operation in the future. The primary control board and the 9132 are shown in Figure 27. The NI control system has some distinct advantages in terms of reliability and safety. NI hardware is ruggedized compared to most normal computer hardware and generally fails gracefully. Control channels have internal breakers, which can be reset remotely with the device. The wiring system is configured with individual fuses on every channel.

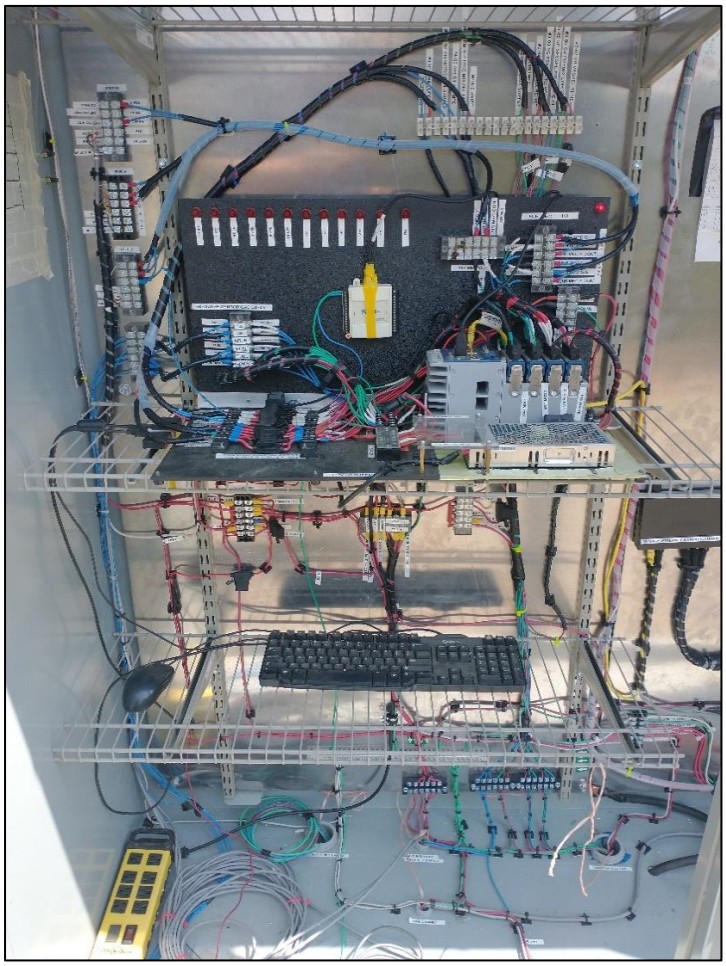

*Figure 27: GERF gas control system using a 9132 embedded system running LabVIEW.*

*Figure 28: Gas supply and mixing tank.*

*Figure 29: Fuel delivery system. Fuel distribution rail with hookups for the blind at the 15.24 m (50 ft), 22.86 m (75 ft), and 30.48 m (100 ft) positions (left). Premix hoses running from the fuel distribution rail to the blind (center). The premix tank, where fuel and air are mixed prior to entry into the fuel distribution rail (right).*

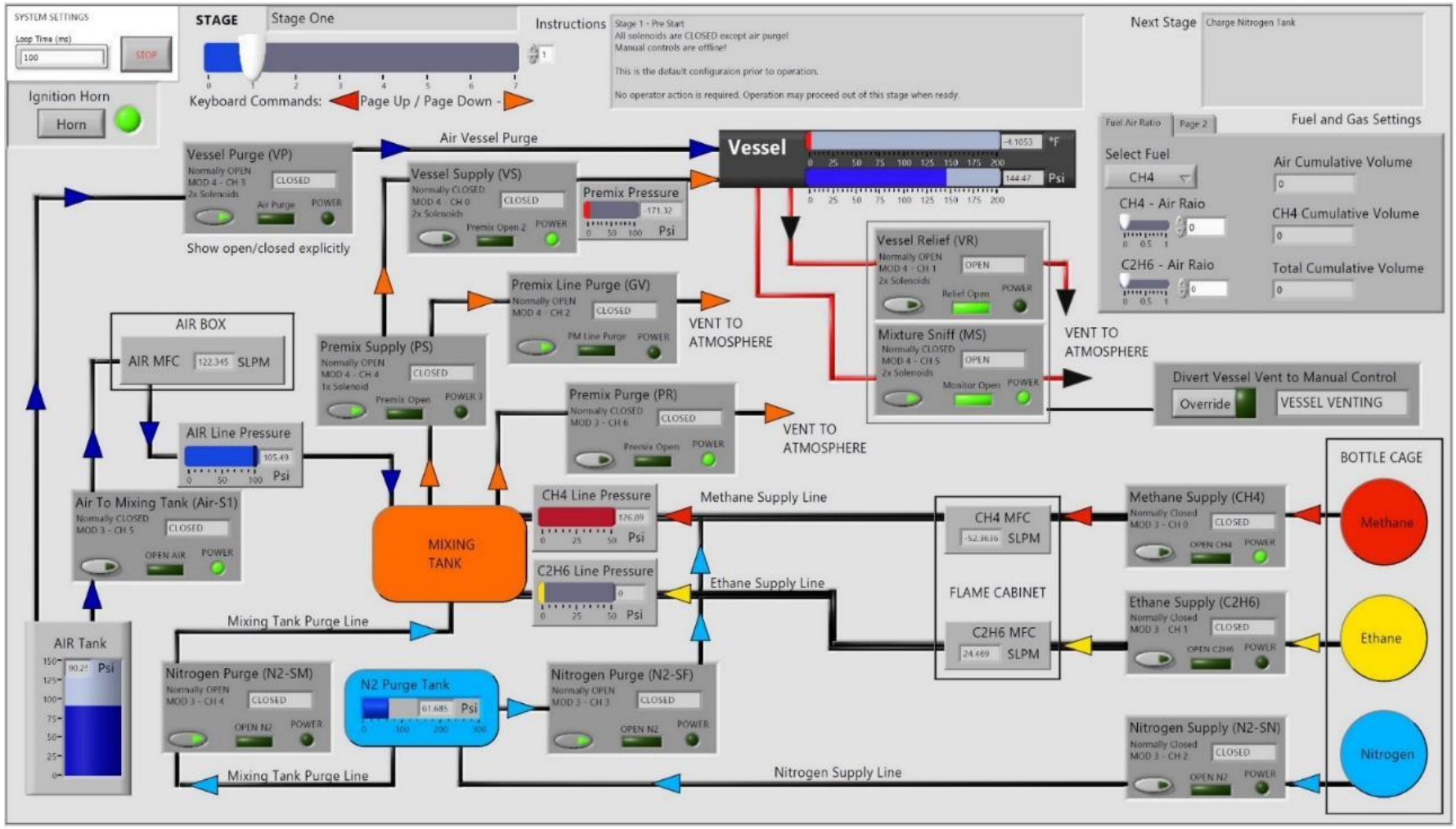


*Figure 30: GERF gas system control program written in LabVIEW. This software allows the operator to directly control the gas flow system by remotely logging into the 9132 cDAQ Chassis from the air gapped local network at the GERF.*


*Figure 31: Operator's station in the Control Center. On the monitor to the left of the image, while to the right is video monitor of the testing site to ensure safe testing*

**Sensor Systems**

The GERF system primarily uses ion sensors to detect the flame front arrival time and pressure sensors. Secondarily, the GERF has infrastructure installed for UV sensors, a variety of thermocouples, and custom sensors, such as the barrier break sensor. The ion sensors are the most numerous in the GERF provide the bulk of the data on the flame front position. Ion sensors are installed in NPT ports across all 4 reactor sections. The ion sensors used in the GERF are an extremely robust design that can be deployed in large numbers for redundancy. The ion sensors have been tested after taking substantial damage and proven to still be in working order. The ion sensor diagram is shown in Figure 33. The ion sensors are an open circuit with an air gap between the electrodes inside the explosion reactor. A battery bank provides a voltage differential across the electrode gap. Every ion sensor has a switch that allows the system to be deenergized when not in use. The data acquisition system measures the voltage differential across a resister in the open circuit. In normal conditions, there is no current and therefore no voltage differential across

the resister. When the flame front passes through the electrode gap, hydronium ions present in the flame front act as a capacitor, briefly closing the DC circuit. When this occurs, a voltage differential can be measured across the resister. This voltage peak indicates that the flame front has passed the ion sensor.

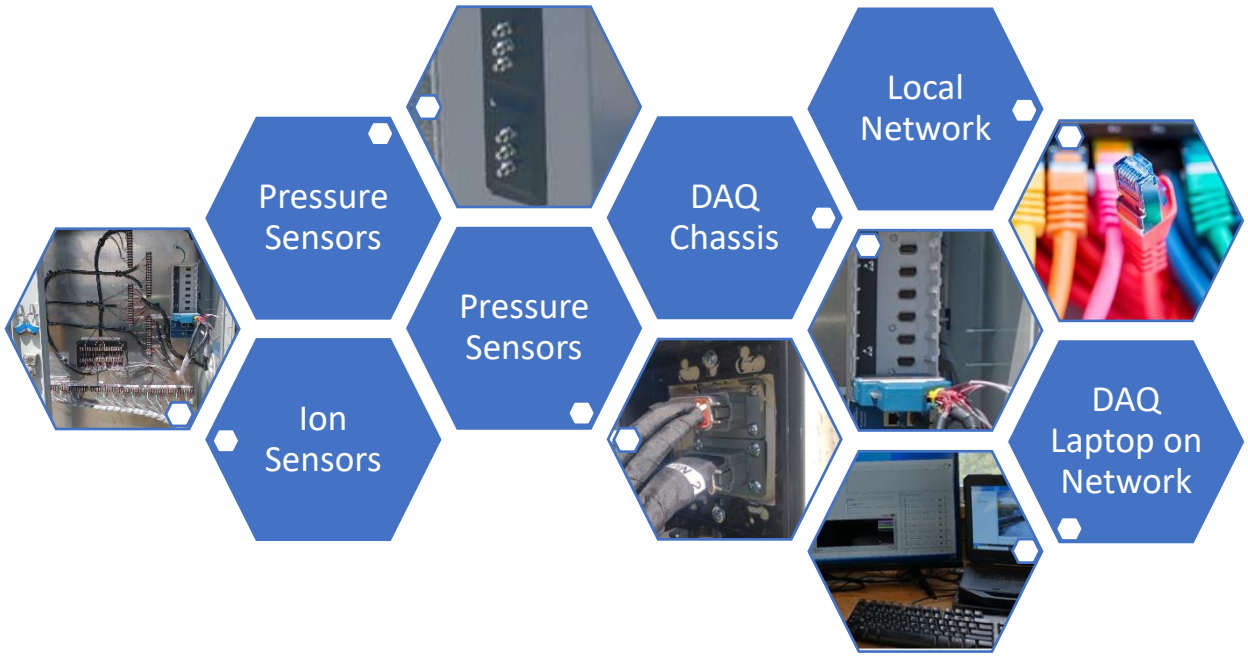


*Figure 32: GERF Sensor Systems*

The ion sensors are placed in the ½" NPT ports along the top of the reactor. These ports are spaced at 0.38 m (15 in) intervals in the explosion reactor. Ion sensors are typically installed in every other port. On experiments with a higher expected flame speed, the ion sensors density is increased to a sensor in every port at the open end of the reactor. Individual ion sensors are configured as shown in Figure 33. Each sensor has its own battery pack and resister to minimize the potential for noise between system components. Battery packs and resisters are housed in the DAQ cabinets for safety and weatherproofing. The electrodes are connected to the battery packs and resistors by shielded cables to minimize the potential for noise. Figure 36 shows a junction box and ion sensor cables. Sensor cables from each 7.62 m (25 ft) Reactor section are collected in a junction box and fed into one of two DAQ cabinets. Each DAQ cabinet is equipped with a NI cDAQ-9189 cDAQ Chassis. The cDAQ-9189 chassis support 8 DAQ modules and are connected to the onsite Ethernet network

for remote data acquisition. This gives the sensor system immense flexibility for future instrumentation changes and upgrades.

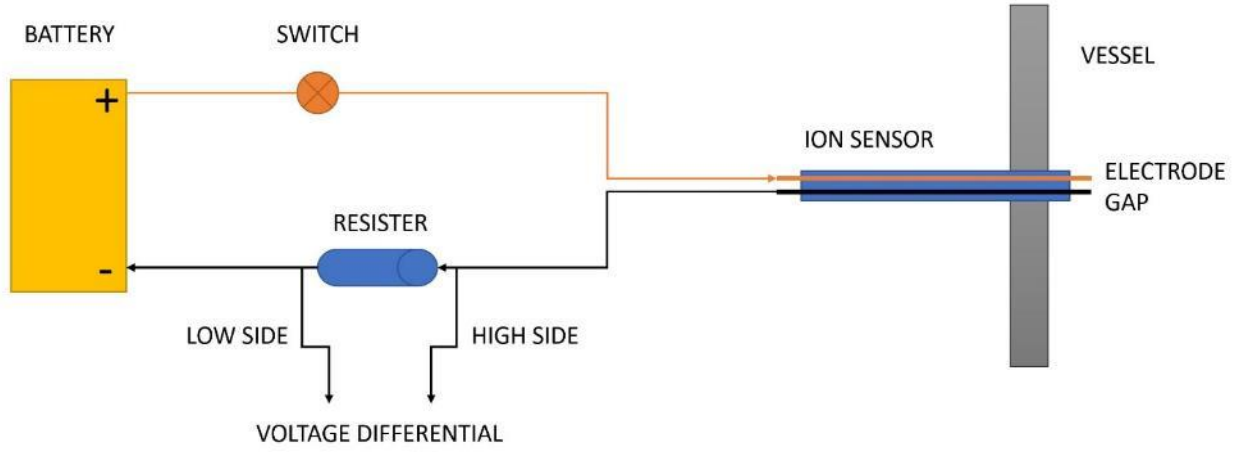


*Figure 33: Ion sensor diagram*

The DAQ cabinet interior is shown in Figure 34. The power packs are made up of nine 9 V batteries for a nominal voltage of 81 V per channel. The cDAQ-9189 shown is equipped with a NI 9220 analog module for a total of 16 channels. In addition, one of the DAQ cabinets is equipped with additional DAQ modules to support the UV sensors, pressure sensors, and the barrier break sensor. In total, the pair of cDAQ-9189 chassis support 16 DAQ modules. The sensors are connected to the cabinets by shielded 4 conductor wires. Two of the conductors are reserved for future sensors, and the other two connect to the electrodes on the respective ion sensor. The DAQ cabinets have Ethernet and 24 V power connections to the control cabinet and Control Center. The data acquisition is done via a LabVIEW VI developed specifically for this project. The DAQ VI is run on the project laptop remotely. To ease the difficulty of changing configurations and allow further expansion of sensor system capabilities, the DAQ cabinet is equipped with a variety of quick disconnect wiring harnesses and other features.

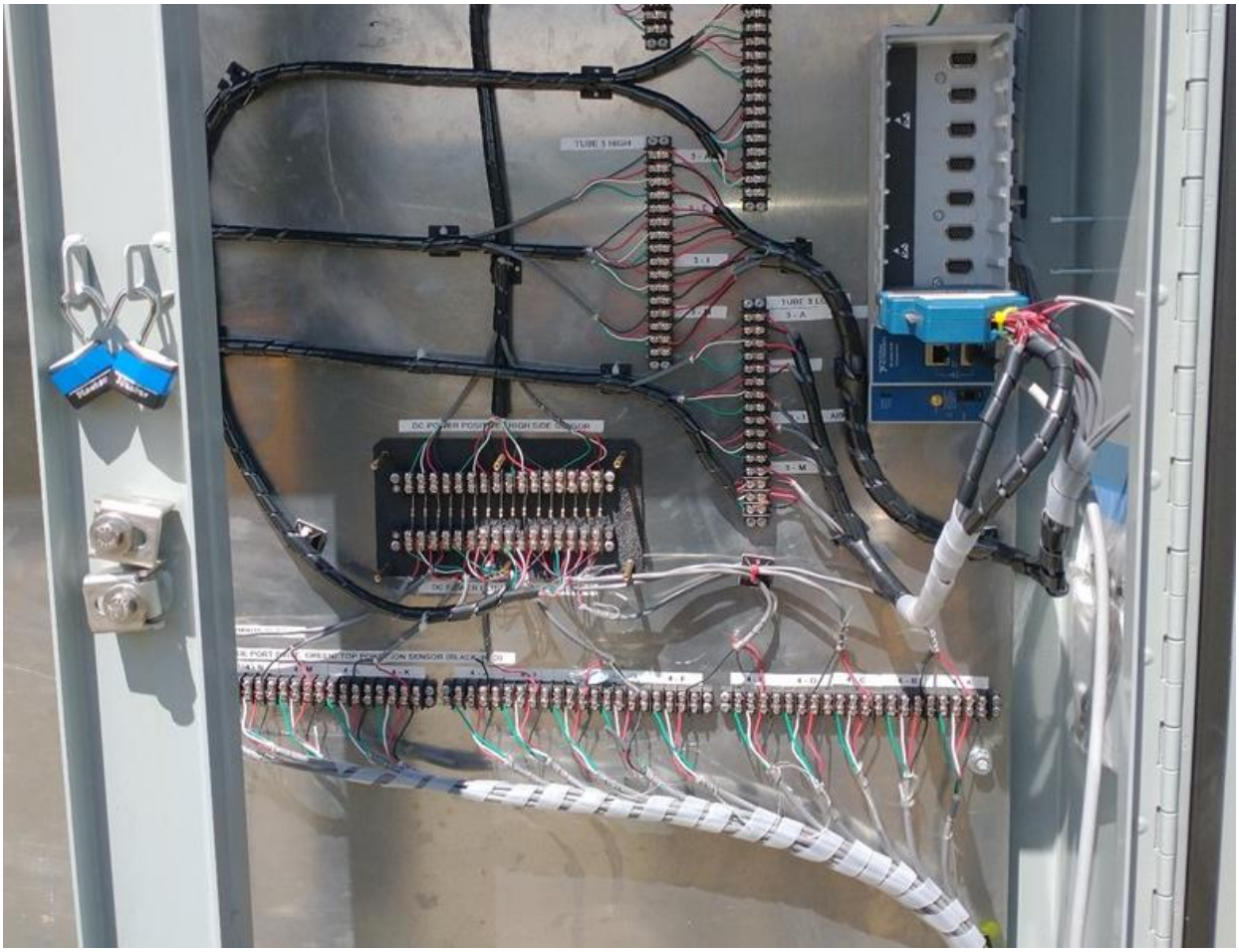

*Figure 34: Ion sensor wiring, resisters, and cDAQ-9189 chassis. The cDAQ-9189 is connected to the local network by ethernet, allowing for operation from the Control Center.*

The DAQ VI reads the ion sensor resister voltage for a specified time period. The DAQ VI is triggered immediately prior to firing and is typically run for 30 seconds in case there is a delay in ignition. As configured for preliminary testing, the DAQ VI reads 16 analog voltage channels from each 9220-module set to 30,000 samples/s per channel. This sample rate has proven to be more than adequate to capture the flame front arrival time in a 30.48 m (100ft) reactor with a 22.86 m (75 ft) reactive zone. The hardware sample rate can be increased if necessary for future sensor configurations. The VI outputs a time stamped data file for each analog voltage channel.

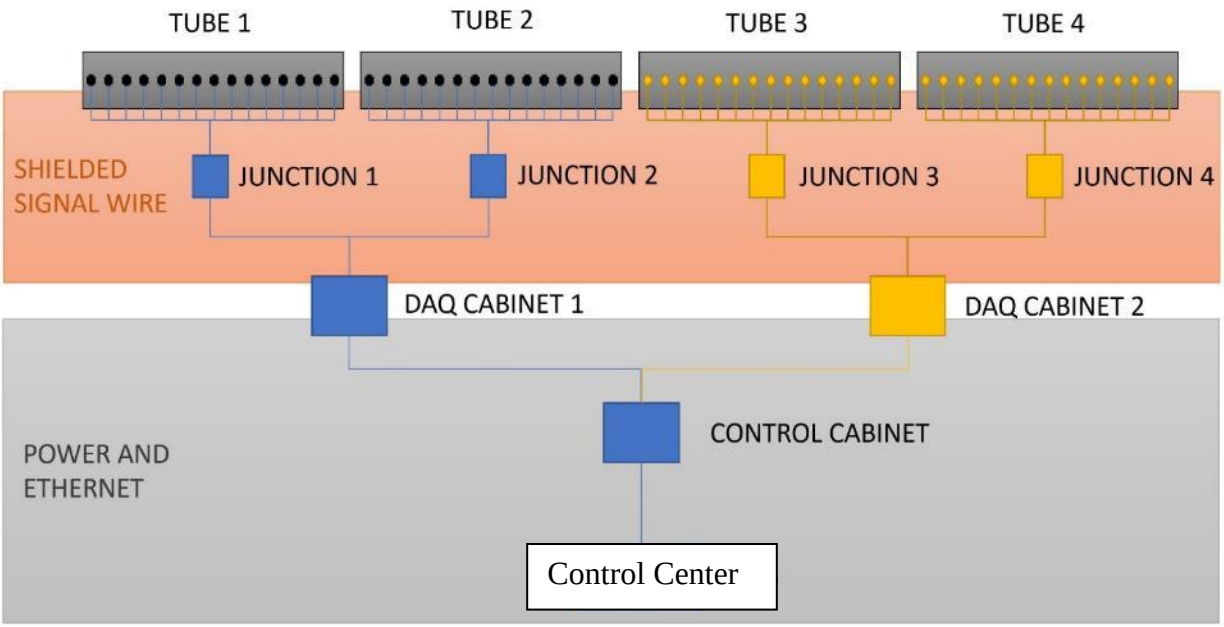


*Figure 35: Ion sensor wiring, separated by DAQ cabinets.*

*Figure 36: External portion of ion sensors.*

*Figure 37: Flame front making contact with an ion sensor during an explosion.*

Figure 38 shows a typical ion sensor signal. This plot represents three ion sensor signals. “R2” represents the reactor number. In this case, the ion sensors are located in reactor 2. The sensor locations within reactor 2 are Port A, Port C, and Port E. As soon as the flame get in contact with the ion sensor electrodes, a voltage drop is recorded. The flame front is being identified with three different methods (i) by the mean of the minimum and maximum of the peak, (ii) by the peak, and (iii) by the midpoint of the gradient for each sensor signal.

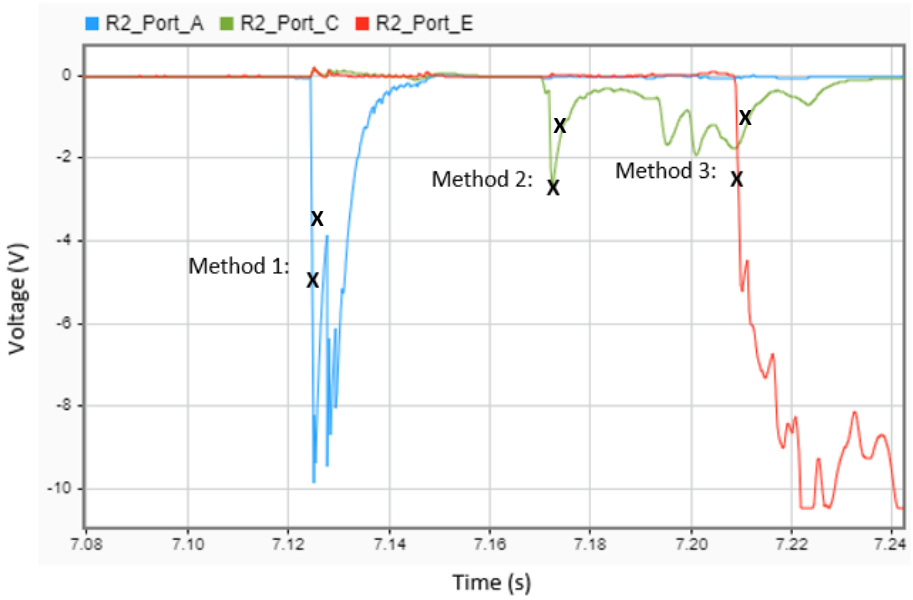


*Figure 38: V-t plot of the ion sensor signal recorded in MATLAB - Signal Analyzer. The sample rate is set to 30,000 samples/s.*

A comparison of two methods to identify the flame front velocity is shown in Figure 39. Due to the steep gradients of the peaks, the impact on the velocity between two methodologies is within ± 5 %. The averaged standard deviation for this comparison was ± 4.2 m/s (13.8 ft/s). The maximum flame front velocity for both methodologies was 227.8 m/s (747 ft/s).

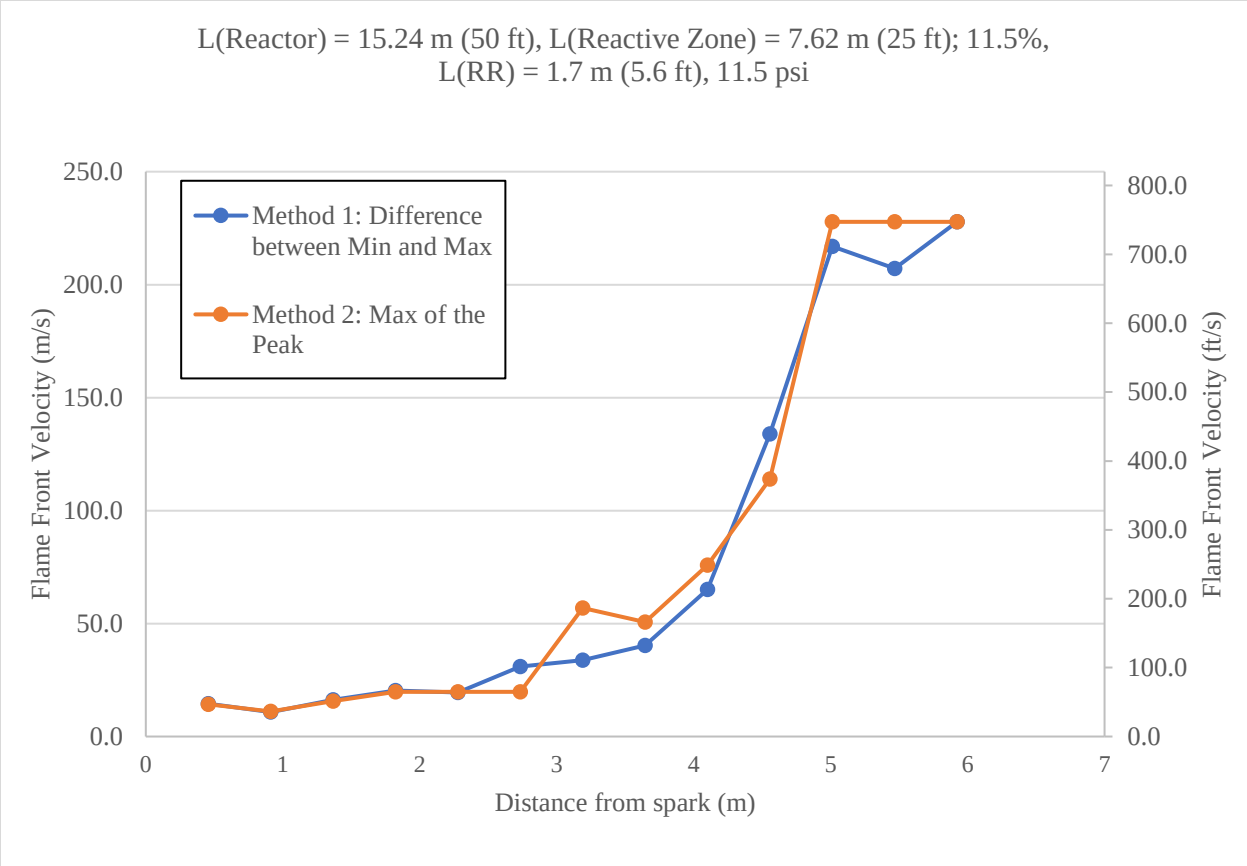


*Figure 39: Methodology comparison of an experiment with a methane concentration of 11.5%.*

The UV sensors as shown in Figure 41 provide a secondary independent source to measure the flame propagation velocity. UV sensors, such as the example shown in Figure 41, are installed along the side ports of the reactor to detect UV radiation emitted by the combustion flame. The sensor powered by a Honeywell burner control (relay module) and its initial signal processing is run on a Honeywell amplifier Figure 42. In general, the UV sensor has a quartz tube filled with gas. The gas is an insulator between two electrodes inside the quartz tube. When the UV sensor gets struck by UV radiation, the gas ionizes, causing current flow between the energized electrodes. A series of resistors is wired in parallel to the UV sensors with a 1:10 ratio. The voltage drop across one resistor is recorded with a DAQ module. Figure 40 represents the sensor system for each UV sensor.

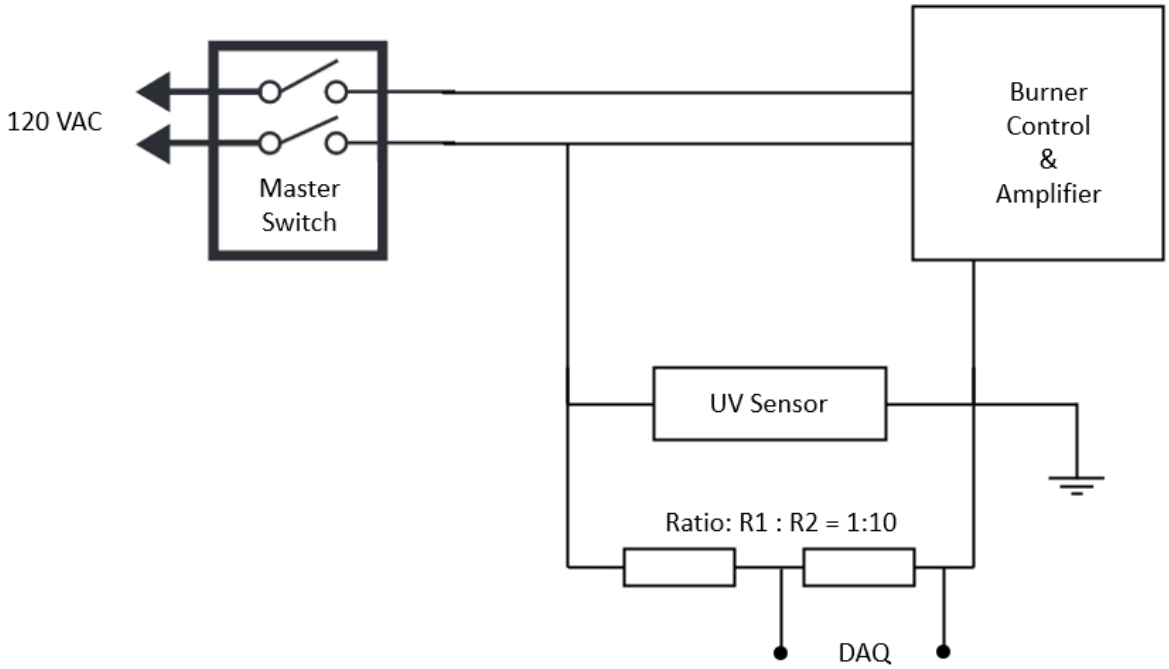


*Figure 40: Sensor system configuration for UV sensor setup including a HONEYWELL Burner Control, a HONEYWELL Amplifier and a HONEYWELL UV Sensor. The system is powered with 120 VAC. The burner control is a relay module. The module energizes the electrodes in the UV sensor continuously with high voltage. A series of resistors (Ratio 1:10) is wired in parallel to the sensor to measure and record the voltage drop with a DAQ module.*

*Figure 41: Honeywell C7027A1023 Flame Sensor – Ultraviolet Flame Detector with ½"npt female threads*


*Figure 42: Left: HONEYWELL RM7890A1015 Burner Control. Right: HONEYWELL R7849A1013 Flame Amplifier*

Figure 43 shows a UV sensor signal from an experiment with 11.5 vol.% methane in the 15.24 m (50 ft) reactor. Due to a sharp voltage signal, the above-mentioned methods for the flame front propagation velocity evaluation can be used.

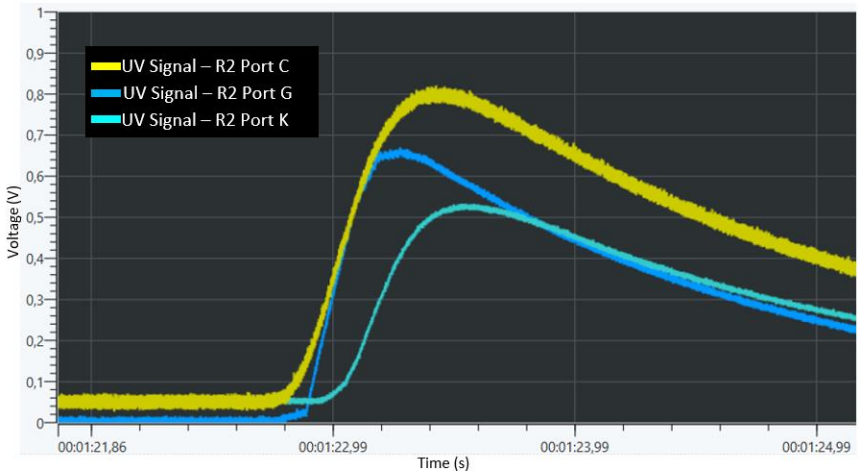


Figure 43: V-t plot of the UV sensor signal recorded in NI – DAQ Express. The sample rate is 8,000 samples/s. Experiment setup: L(Reactor) = 15.24 m/s (50 ft), L(Reactive zone) = 7.62 m (25 ft); methane concentration = 11.5 vol.%, no obstacles and no water barrel. p = 82.7 kPa (12 psia). T = 16 °C.

Figure *44* shows the difference in the flame front propagation velocity processed with the two different sensor technologies. In addition, the three different methods to process the signal data were used for the UV data. The offset between the velocities measured from the UV sensor data can be improved by working on the system's electrical circuit to increase the response rate.

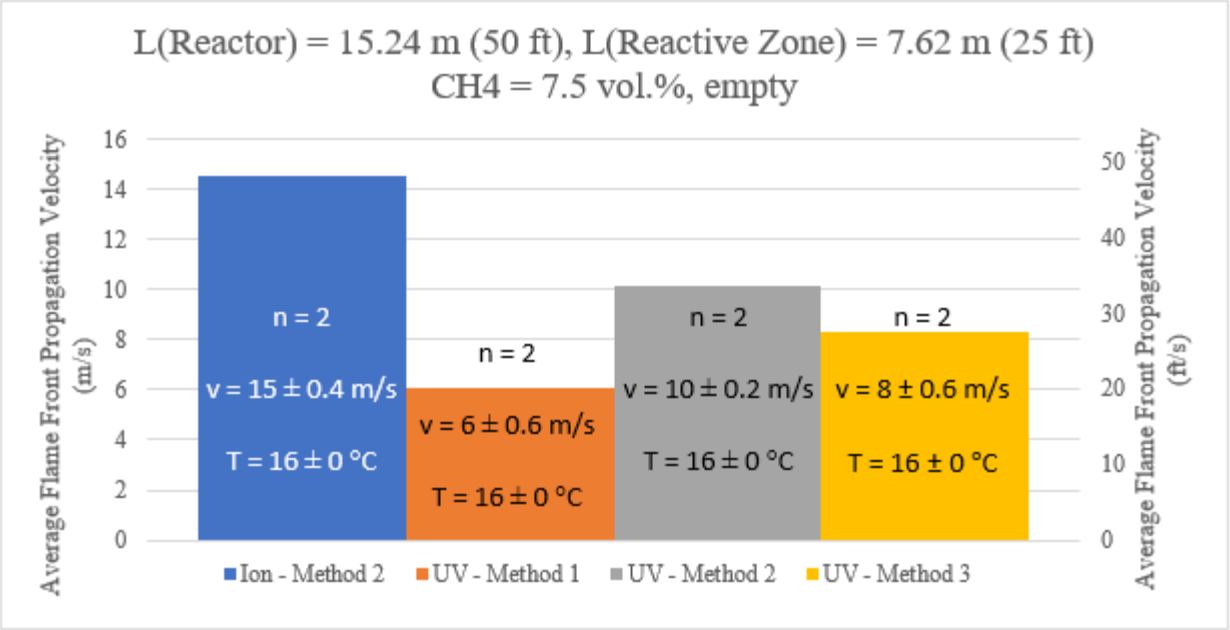


Figure 44: A comparison of the average flame front propagation velocity between Port G and Port K (spacing between ports = 1.83 m (6 ft) in reactor 2 measured with ion sensor and UV sensor signal. L(Reactor) = 15.24 m/s (50 ft), L(Reactive zone) = 7.62 m (25 ft); methane concentration = 11.5 vol.%, no obstacles and no water barrel. p = 82.7 kPa (12 psia). T = 16 °C

**Gas Explosion Research Facility Operations**

The operation of the GERF can be broadly generalized as five general phases: Load, prep, gas flow, ignition, and cleanup. The steps are listed in greater detail below. In general, the GERF is operated by a three-person crew. However, it can be safely and efficiently operated by an experienced two-person crew. The GERF operating steps are summarized below in Figure 45. A generalized list of operating steps is presented below. GERF operations can be summarized as cyclical with five major steps; load, prep, gas flow, explosion, and cleanup. A sixth step, facilities buildout, is often present when the GERF is building out long term capabilities or preparing for a new set of experiments. The GERF and the Edgar Mine provide ample workspace for customizing infrastructure and equipment as needed.


*Figure 45: Simplified GERF Operation Cycle*

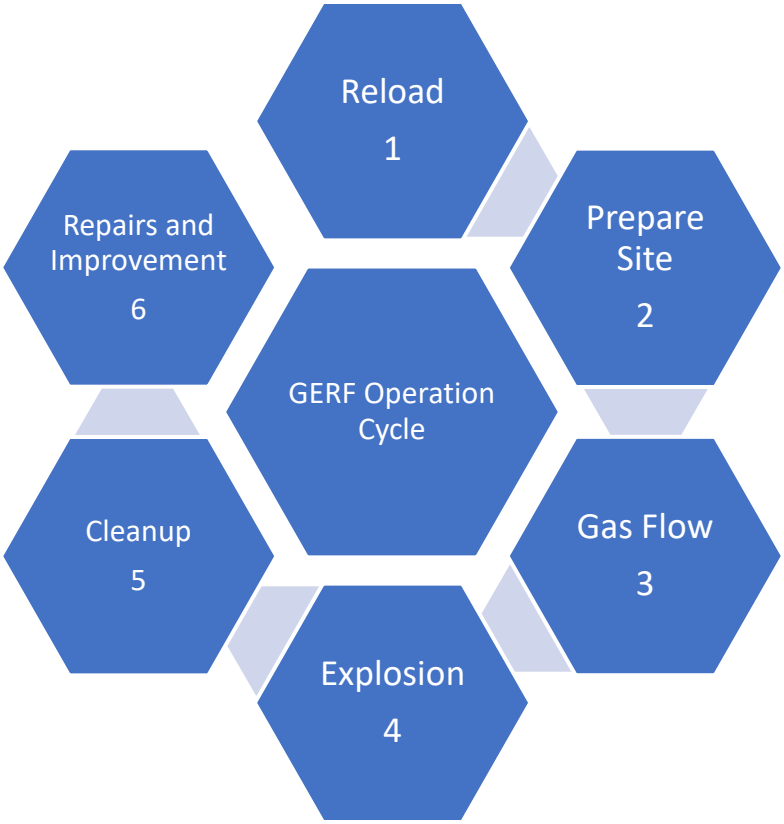


1. Load
    a. Split reactor
    b. Insert a new gas barrier and barrier break sensor between the inert 1st reactor and the reactive zone
    c. Install instrumentation (such as PCB pressure sensor) and route wiring
    d. Close reactor
2. Prep
    a. Set up ignition box
    b. Hook up gas bottles
    c. Fill and install water suppressor section
    d. Fill and position water barrels
    e. Set up gas meters at reactor vents
    f. Inspect system, test as necessary
    g. Install any cameras
    h. Inspect and power up ion sensors and pressure sensor amp

3. Gas Flow
    a. Pre-operation inspection
    b. Set up exclusion zones near suppressor
    c. Final confirmation of experimental start
    d. Charge nitrogen purge tank
    e. Air flush of fuel lines
    f. Start fuel flow
        i. Fuel and air are mixed and routed into the reactor, often takes 3 flows
    g. Record mass flow controller readings
    h. Stop flow at approximately 3 reactor volumes of gas once gas meters verify that vented gas has the targeted fuel percentage.
    i. Cease flow and purge fuel lines
    j. Pause all flow and prepare for ignition
4. Explosion
    a. Verify that site is clear, crew is ready
    b. Arm ignition system
    c. Start DAQ system recording
    d. Fire!
    e. Air purge of the reactor
    f. Sound all clear and open exclusion zones
5. Cleanup
    a. Replace and organize suppressor parts
    b. Fire watch
    c. Put tools/gas meters/etc. away
    d. Inspect systems for damage
    e. Turn off systems and sensor

**Safety**

The GERF is designed to protect operator and community safety. The system design incorporates multiple layers of fail safes on top of a robust operating procedures and crew training. Large scale explosion experiments present numerous potential hazards that must be properly mitigated to allow

for safe operation in addition to the usual industrial, construction, and logistics concerns associated with operating such a facility. The major hazards identified with the GERF are flammable gasses, gas leaks, gas buildup, ignitions, fire, explosion, pressure wave, fireball, flying debris, combustion gases, and potential progressive damage inflicted by experiments. The GERF's systems were designed to provide large safety factors and robust systems design that minimizes the hazard associated with potential failure modes.

The reactor is engineered to provide a safety factor well in excess of the anticipated and measured vessel pressures. A robust recoil management system with redundant anchor points secures the reactor in place while allowing for movement and the safe absorption of energy. The reactor open end of the reactor is vented into a suppressor system that prevents access to the area impacted by the blast exiting the reactor, contains any flames or fireball, and catches any debris or rocks expelled from the reactor. The hazard potential of gas leaks is minimized by the above ground infrastructure and outdoor site. The layout of the site and gas lines facilitates easy line inspection and maintenance, while the site contour minimizes the potential for the buildup of explosive or flammable gases near fuel bottle storage, gas lines, or the reactor.

The fuel system is designed for safety and incorporates a variety of specialized design and operations procedures to further prevent hazardous conditions from developing, even in the event of failures or damage. The fuel supply and control system is designed to default to a safe state. Gas flow is controlled by normally open and normally closed solenoid valves. A power failure will result in a default valve configuration that purges the fuel lines and mixing tank with nitrogen and dilutes and purges the reactor with air. An emergency stop is also incorporated into the control system that will trigger the system purge, regardless of the state of the cDAQ control system, software, or networking. Prior to firing, the fuel system is flushed with a nitrogen purge to add an additional barrier to the potential of a fire propagating up the fuel lines.

In addition to the active and automatic safety features, the reactor, fuel, and control systems incorporate a variety of passive safety features. The pressure ratings on tubing, fittings, and the mixing tank are all rated for substantially higher pressure than an ignition in the lines has the potential to cause. Flashback arrestors are present at vents and fuel/purge ports into the reactor and at the primary reactor vents. The reactor vents are equipped with flashback arrestors to prevent external ignition sources from igniting the gas inside the reactor during the fill process. Reactor

vent ports are placed such that vented gasses can't build up in depressions or confined spaces. Where possible, tubing sizes are small enough to prevent flame propagation inside the lines with some of the potential fuels.

The flame reactor fires into a suppressor system to reduce noise, mitigate pressure waves, and contain any flames and expelled debris. The suppressor housing is comprised of two 6 m (20 ft) Conex containers places end to end. The containers are structurally reinforced and lined with insulation to provide a degree of passive suppression in the housing itself. Active and passive suppression systems are used in addition to the steel housing. The active actively controlled water spray system helps disrupt the pressure wave exiting the reactor and help quench any flames exiting the reactor. While the active system is effective and minimize water usage, it introduce a failure point into the system and would become less effective in the event of a premature ignition or a sustained power failure, if operated as the only suppression system. Therefore, the GERF team designed, tested, and adopted a passive water suppression system in addition to the active water suppression system which disrupts the pressure wave, quenches the flame, and utilizes the impact of the pressure wave to disperse water inside the suppressor, further enhancing fire suppression. This passive water suppression system has redundant layers and is robust enough to operate even with the loss of one or more barrels. The suppressor system's performance is documented in Objective 1.a.

The operating procedures of the GERF incorporate robust and well understood administrative controls that further separate personnel from potential hazards and prevent unexpected or unsafe interactions between work tasks. During its operation, there have been zero reportable time lost injuries, no use of emergency services, and no fires or near misses with fire prevention. The GERF coordinated with the Edgar Mine, Clear Creek County police and fire, and Environmental Health and Safety at the Colorado School of Mines.

**Wildfires and Fire Safety**

Recent events in Colorado highlight the increasingly long and hazardous fire seasons in the Rocky Mountain West and the front range of Colorado in particular. The GERF's location at the Edgar Mine on the outskirts of Idaho Springs is in a region that sees intermittent high wildfire risk. In

order to responsibly maintain operations during dry periods, the GERF's systems, suppressor, and operating procedures were designed to provide a large safety factor and redundant layers of fire protection. The system, as configured at the end of 2021 has four separate layers of passive fire protection, in addition to scheduling and planning policies.

In terms of fire protection, the main source of concern is a flame and/or heated particles exiting the reactor. Footage of lower energy experiments conducted during wet conditions showed residuals of the flame was able to extend out of the reactor approximately 1 m (3.28 ft) into the Conex suppressor with stoichiometric or rich fuel/air ratios, passing through an air-filled reactor section, as shown in Figure 46. To further reduce any partial flames and/or hot particles exiting the reactor a redundant passive suppression system in addition toto of an active water spray system. The fire hazard from explosion experiments is mitigated by four passive, redundant suppression layers. The final reactor section is kept air filled to prevent a deflagration from exiting the end of the reactor. After that, there are two layers of passive water suppression that the pressure wave exiting the reactor travels through. These are part of the sound suppression system, provide substantial redundancy, and are effective even if some components were to be damaged and leak prior to an experiment. Both passive water systems were tested separately and were independently capable of preventing flames from exiting the reactor. The final layer of protection is the suppressor housing itself. This structure, made from a pair of reinforced and lined 6 m (20 ft) Conex shipping containers can contain and isolating a deflagration exiting the reactor from the surround environment. There have been no instances of a flame escaping the confinement systems present at the GERF.

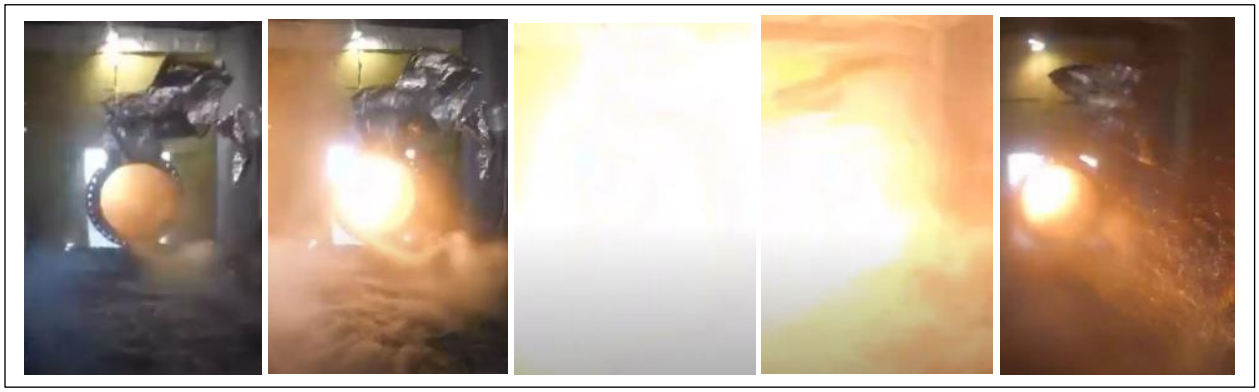

*Figure 46: Footage of a 15.24 m (50 ft) experiment with a 7.62 m (25 ft) reactive section and 7.62 m (25 ft) air section from within the Conex suppressor. This test had a 9.5 % methane*

*atmosphere in Reactor 2 and exited through Reactor 1 before entering the suppressor. To add an additional layer of safety, the large reactive zone experiments conducted during fire season used 7.5 % only, in order to reduce the potential of the deflagration exiting the reactor by running the experiments lean.*

In addition to the passive systems at the reactor exit, experimental work at the GERF is paused when the fire danger presents a substantially elevated risk due to weather conditions. The primary risk factors considered by the GERF are extreme dryness, high winds, and high temperatures. These risks are often, but not always, well represented at the GERF site by local red flag warnings and fire bans. Due to its total enclosure of potential deflagrations, the GERF is able to operate safely during most stage 1 and 2 fire bans. Due to the extreme conditions present when there are local stage 3 fire bans, the GERF will not operate during these conditions (as noted during the report covering Fall 2020 operations). Additionally, the GERF manager and host facility management will evaluate potentially hazardous conditions and may suspend operations for weather events that do not result in a red flag warning or an increase in the published fire ban stage.

**Quantifying 30.48 m (100 ft) Reactor Suppressor Performance and Impact**

Higher energy experiments necessitated the use of an expanded suppression system. Since this system partially obstructs air flow exiting the reactor, its performance and impact on flame front velocities were characterized. In this system, a water slug insert was fitted to the reactor exit at the end of the air-filled section. Expelling this slug increase the disruption of the pressure wave and ensure that the flame was quenched. A side effect of this is that expelling the water slug causes an increase in pressure, resulting in the flame propagating through a higher-pressure gas. The water slug was used in combination with six 208 l (55 gal) water barrels positioned at the reactor exit for high energy experiments. The water slug refers to the 322 l (85gal) barrel filled with water was inserted into the open-end of reactor-4. The water was contained in the water slug by several layers of 6 mm (0.23 in) plastic sheeting clamped to the ends of the barrel. This barrel was in turn bolted into the reactor in the position shown in Figure 48. The 6 external water barrels set in a staggered pattern were placed 0.5 m (19.7 in) away from the reactor open end. The resulting noise level and flame front velocities were compared between tests with and without water slug.

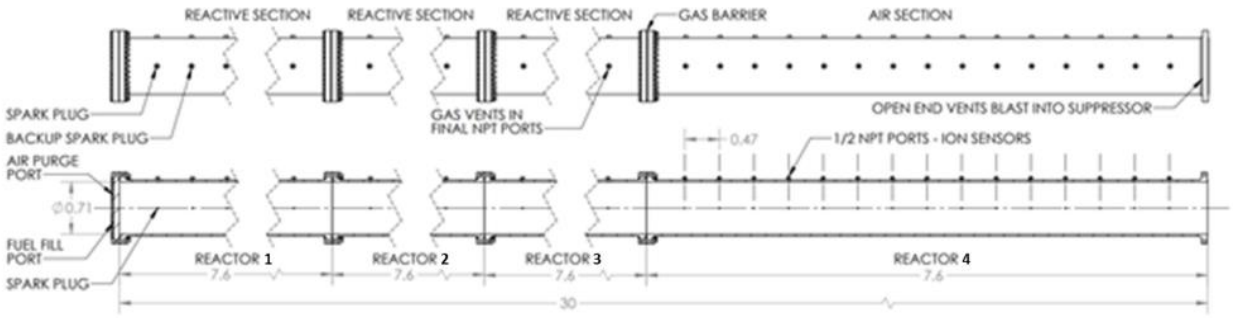


*Figure 47: 30.48 m (100 ft) reactor configuration with a 22.86 m (75 ft) reactive zone, no rock rubble insert, and no water slug.*

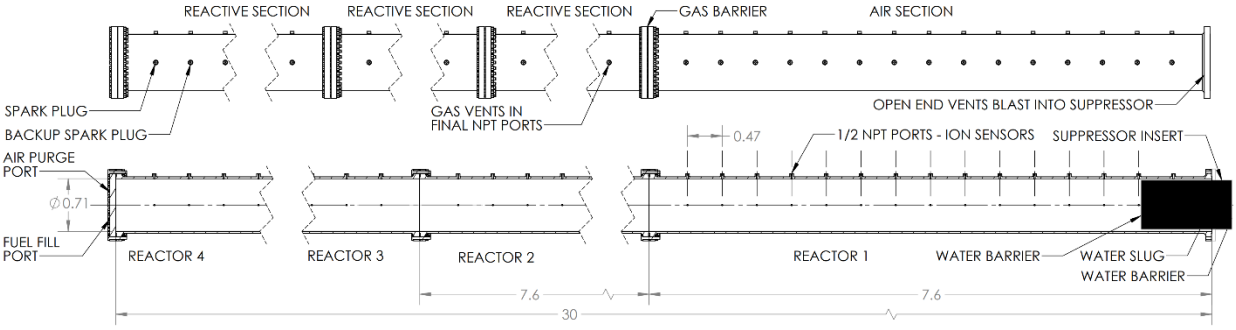


*Figure 48: 30.48 m (100 ft) reactor configuration with a 22.86 m (75 ft) reactive zone, a rock rubble insert, and the water slug.*

A total of four tests, two with and two without the barrier, were conducted to test the performance of the water barrier to suppress the sound from the explosion. Figure 49 shows the comparison of flame front propagation velocity from these tests. Note that in all 30.48 m (100 ft) tests, the six water barrels are positioned in a staggered pattern and the Conex container doors were closed. The result show similar trend during the early stages of the flame propagation, up to 16 m (52.5 ft) away from the closed end. In both cases, the flame propagates more slowly while the gas barrier located 22.86 m (75 ft) away from closed end remained intact and started to accelerate once the gas barrier burst. Prior the barrier opening, the reflected pressure wave hindered the flame propagation, resulting in pressure buildup inside the reactive zone. The gas barrier opening allows for pressure to release, pushing the premixed gas in the reactive zone into the non-reactive zone, and help to accelerate the flame by inducing turbulence. The barrier is a 70.18 mm (7 mil) high

strength plastic sheet with a 207 MPa (30,000 psi) nominal tensile strength and a measured burst pressure of approximately 69 kPa (10 psig) when clamped between reactor sections.

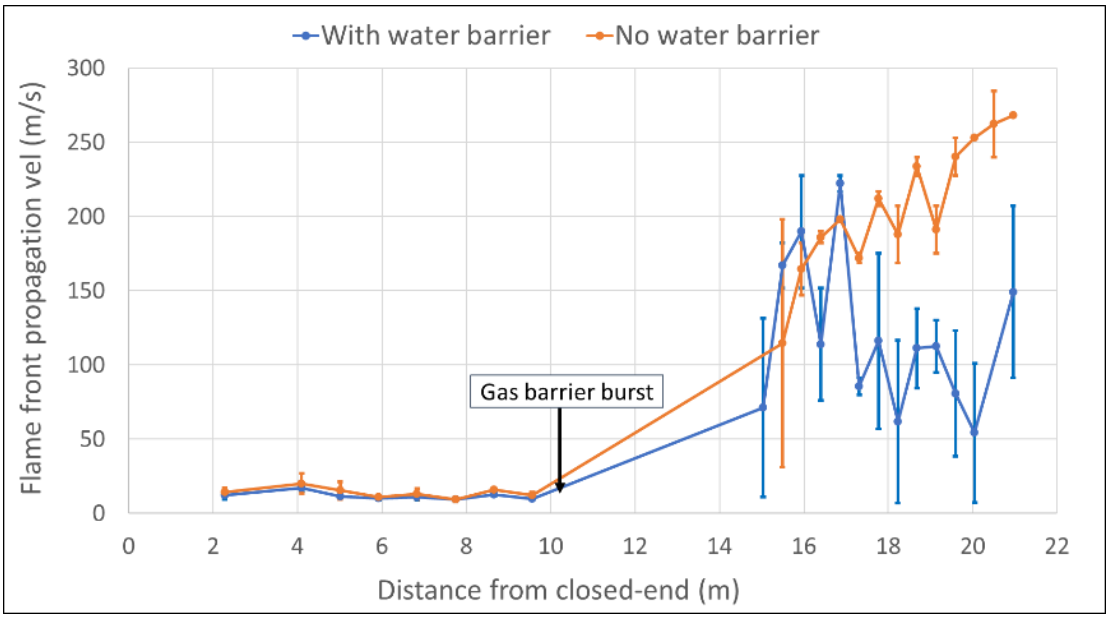


*Figure 49: Experiments measuring the impact of the water slug suppressor on the flame front velocity in a 30.48 m (100 ft) reactor with a 22.86 m (75 ft) reactive zone and no rock rubble obstruction. Note that the water barrier causes a reduction in velocity due to the pressure buildup.*

There is also a notable difference in flame front propagation speed past the 16 m (52.5 ft) distance. In the tests without the water barrier, the flame continues to accelerate up to ~275 m/s (900 ft/s) by the time the flame exiting the reactive zone, ~23 m (75 ft) away from the closed end. In comparison, the tests with the water barrier show a significant deceleration in flame speed due to the additional confinement provided by the water barrier at the open-end of reactor 4. The results show significant reduction on the noise level with the use of water barrier, in addition to the significant reduction on the flame front speed (~40 %) as it propagates closer to the open-end. These results confirmed the effectiveness of the water slug to help suppressed the noise level.

*Table 9: Reduction in noise with and without the water slug present.*

| Setup | LAF max (dB) | LAF peak (dB) |
|---|---|---|
| Without water barrier | 121 | 141 |
| With water barrier | 87 | 101 |

The results show significant reduction in the noise level (~30 %) with the use of water barrier, in addition to the significant reduction on the flame front speed (~40 %) as it propagates closer to the open-end. These results confirmed the effectiveness of the water barrier to help suppressed the noise level. It should be noted that the 7.5 % 22.86 m (75 ft) reactive zone without any obstruction was deemed to be the loudest that should be run without a water slug in order to keep noise levels appropriate and maintain good relations with the host facility and community.

**Gas Barrier Sensing**

Pressure data and flame propagation velocities showed that the high strength barrier does initially inhibit flame propagation by increasing pressure. The barrier is a 0.18 mm (7 mil) high strength plastic sheet with a 207 MPa (30,000 psi) nominal tensile strength and a measured burst pressure of approximately 69 kPa (10 psig) when clamped between reactor sections. This has proven to be enough pressure to noticeably increase pressure and decrease flame propagation until the gas barrier bursts. In order to verify that this was the phenomenon causing the pressure drops and corresponding velocity increases, a barrier clamp was designed and instrumented. This clamp secured the barrier against slight reactor misalignment and passed four wires through behind the barrier. When the barrier ruptured, the wires would be ripped in half soon afterwards, opening a circuit, which would be picked up as a change in voltage by the DAQ system. The clamp ring is shown in Figure 50.

*Figure 50: Barrier clamp ring. This rubber lined ring ensures a solid contact force between the flanges of the reactor. This allows for a slight reactor misalignment without losing clamping force. The clamp ring when new with a fresh rubber seal (left) and fully instrumented (middle). The high strength barrier used with some of the 15.24m (50ft) reactor configurations is shown with a prototype of the sensor system (right).*

**Other Reactors at Colorado School of Mines**

In addition to the large-scale reactor constructed at the GERF, this research had access to several smaller reactors housed on the main campus, as well as the data produced by the initial work with the 6 m (20 ft) long 0.71 m (28 in) diameter reactor produced for the preceding work conducted at Mines under Alpha Foundation grant AFSTI14FO69. This provided three substantial benefits to the overall project. First, the ability to use a smaller reactor to rapidly test potential scenarios of interest allowed for preliminary testing prior to committing the full resources required for testing at a larger scale. Second, the smaller reactors were used as a contingency in case of a disruption that could prevent the use of the GERF, such as inclement weather or extreme fire danger. Third, the smaller reactors produced data sets that allow the comparison of phenomena across a wide range of scales, allowing for the experimental confirmation of the scalability of phenomena. A list of the smaller reactors that have been used in this project or in preceding work is given in Table 10. The 5 cm (1.96 in) and 9.5 cm (3.74 in) reactors are shown in Figure 51. A comparison of the 0.71 m (28 in) diameter large scale reactors is shown in Figure 52. All of the reactors used in this research are equipped with a suite of sensors that includes ion sensors and pressure sensors.

*Table 10: Past and current reactors at Colorado School of Mines.*

| Reactor | Location | Diameter | Length |
|---|---|---|---|
| 5 cm (2 in) | Main Campus Lab | 5 cm (2 in) | 43 cm (17 in) |
| 9.5 cm (3.74 in) | Main Campus Lab | 9.5cm (3.74 in) | 81 cm (2.66 ft) |
| 22.9 cm (9 in) x 7.6 cm (3 in) | Main Campus Lab | 22.9 cm (9 in) x 7.6 cm (3 in) | 1.52 m (5 ft) |
| 6 m (20 ft) | Edgar Mine | 0.71 m (28 in) | 6 m (20 ft) |
| Large Scale | GERF (Edgar Mine) | 0.71 m (28 in) | 30.48 m (100 ft) |

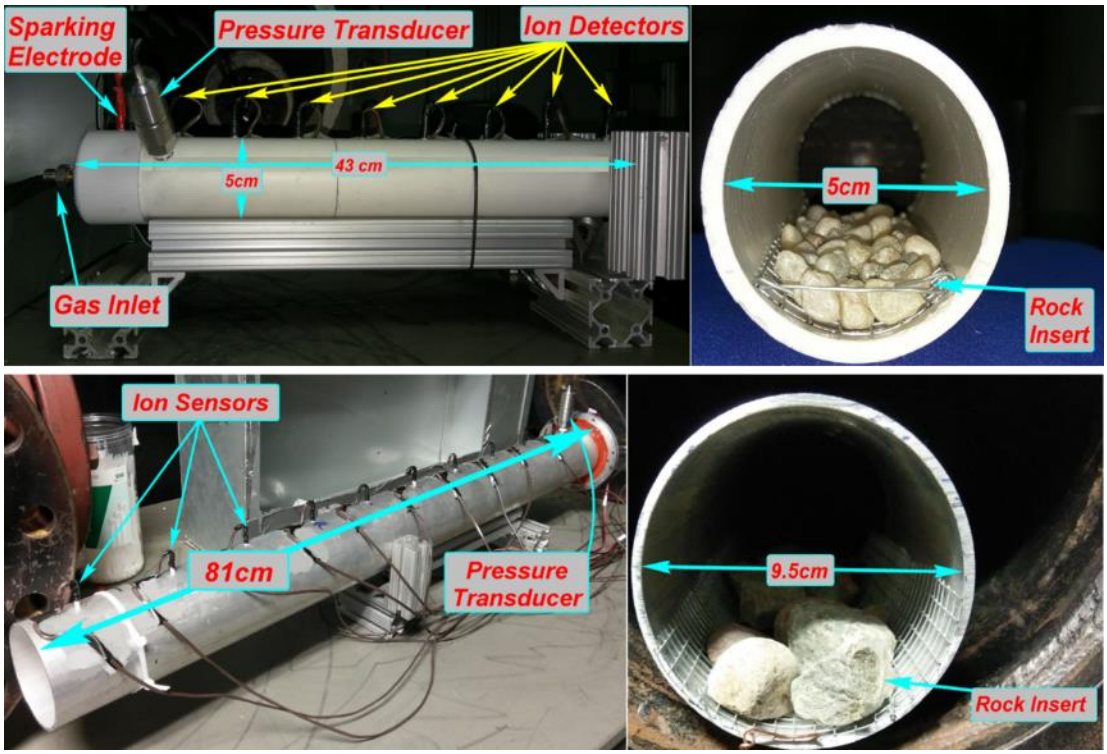


*Figure* 51*: Laboratory scale experimental reactors of diameter 5 cm (1.96 in) (top) and 9.5 cm (3.71 in) (bottom). Experiments are performed at 82 kPa (11.9 psia) and 294 K (70 °F) with stoichiometric methane-air mixtures. Ignition takes place at the closed end, which allows the flame time to accelerate before encountering the rock pile. The rocks used in the 9.5 cm (3.71 in) diameter reactor were on average 1.5 cm (0.6 in) diameter, while the rocks used with the 9.5 cm (3.71 in) diameter reactor were 3 cm (1.18 in).*

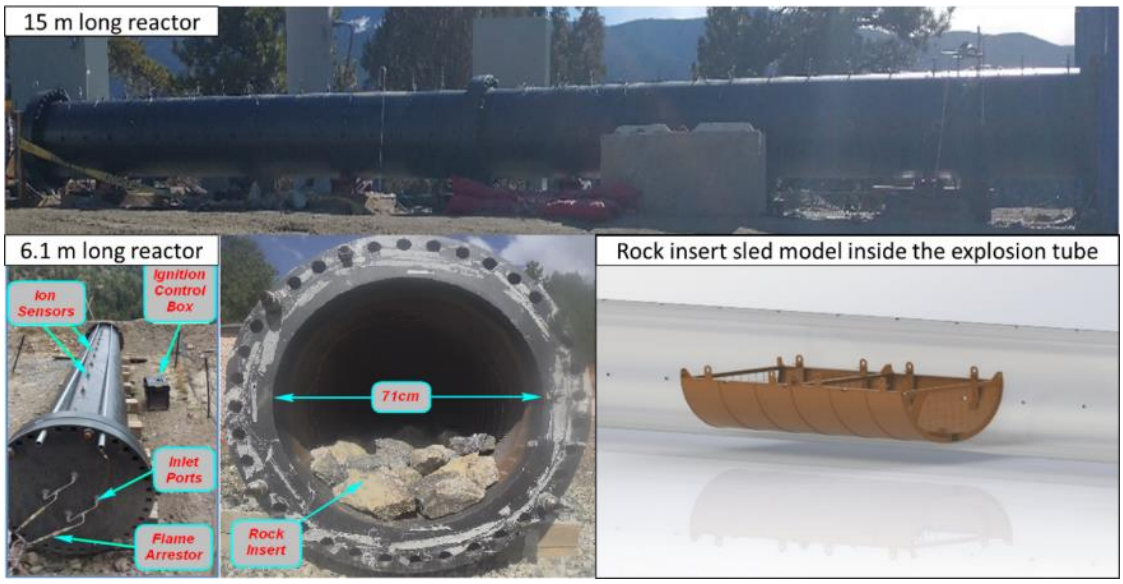


*Figure* 52*: A comparison of the 6 m (20 ft) preliminary large-scale reactor to the 15.24 m (50 ft) of the 30.48 m (100 ft) reactor at the GERF.*

## Objective 1.b: Testing of methane-air across a range of methane concentrations (%vol), and also include various mixtures of other flammable gas species and their relative impact on explosion dynamics.

The fuel concentration (% volume) was tested parametrical with the GERF running experiments at three primary fuel concentrations in the explosive zone: 7.5 %, 9.5 %, and 11.5 %. The experiments were scheduled early in the buildout process and used two 15.24 m (50 ft) reactor configurations: half reactive (7.62 m (25 ft) reactive) or fully reactive (15.24 m (50 ft) reactive). The system configuration is shown in Figure 53. The half reactive configuration contained either with a 7.62 m (25 ft) reactive zone and a 7.62 m (25 ft) air filled section. The fully reactive configuration had a 15.24 m (50 ft) reactive zone. This provides a more efficient experimental workflow, reduces the expenditure of gasses and crew time, and provides a novel data set both for publication and use on other objectives. This configuration was tested with and without rock rubble. Overall, this parametric analysis included four reactor configurations and three fuel/air ratios. The parameters are shown in Table 11.

*Table 11: Parametric Analysis Parameters of Methane Concentration*

| Reactor Length (m (ft)) | Reactive Length (m (ft)) | $CH_4$ | Obstacles | Schematic Figure |
|---|---|---|---|---|
| 15.24 m (50 ft) | 7.62 m (25 ft) | 7.50 % | Unobstructed | Figure 54 |
| 15.24 m (50 ft) | 7.62 m (25 ft) | 9.50 % | Unobstructed | Figure 54 |
| 15.24 m (50 ft) | 7.62 m (25 ft) | 11.50 % | Unobstructed | Figure 54 |
| 15.24 m (50 ft) | 15.24 m (50 ft) | 7.50 % | Unobstructed | Figure 55 |
| 15.24 m (50 ft) | 15.24 m (50 ft) | 9.50 % | Unobstructed | Figure 55 |
| 15.24 m (50 ft) | 15.24 m (50 ft) | 11.50 % | Unobstructed | Figure 55 |
| 15.24 m (50 ft) | 15.24 m (50 ft) | 7.50 % | 50%, 1.7m (5.6 ft) Rock Rubble | Figure 57 |
| 15.24 m (50 ft) | 15.24 m (50 ft) | 9.50 % | 50%, 1.7m (5.6 ft) Rock Rubble | Figure 57 |
| 15.24 m (50 ft) | 15.24 m (50 ft) | 11.50 % | 50%, 1.7m (5.6 ft) Rock Rubble | Figure 57 |
| 15.24 m (50 ft) | 7.62 m (25 ft) | 7.50 % | 50%, 1.7m (5.6 ft) Rock Rubble | Figure 56 |
| 15.24 m (50 ft) | 7.62 m (25 ft) | 9.50 % | 50%, 1.7m (5.6 ft) Rock Rubble | Figure 56 |
| 15.24 m (50 ft) | 7.62 m (25 ft) | 11.50 % | 50%, 1.7m (5.6 ft) Rock Rubble | Figure 56 |

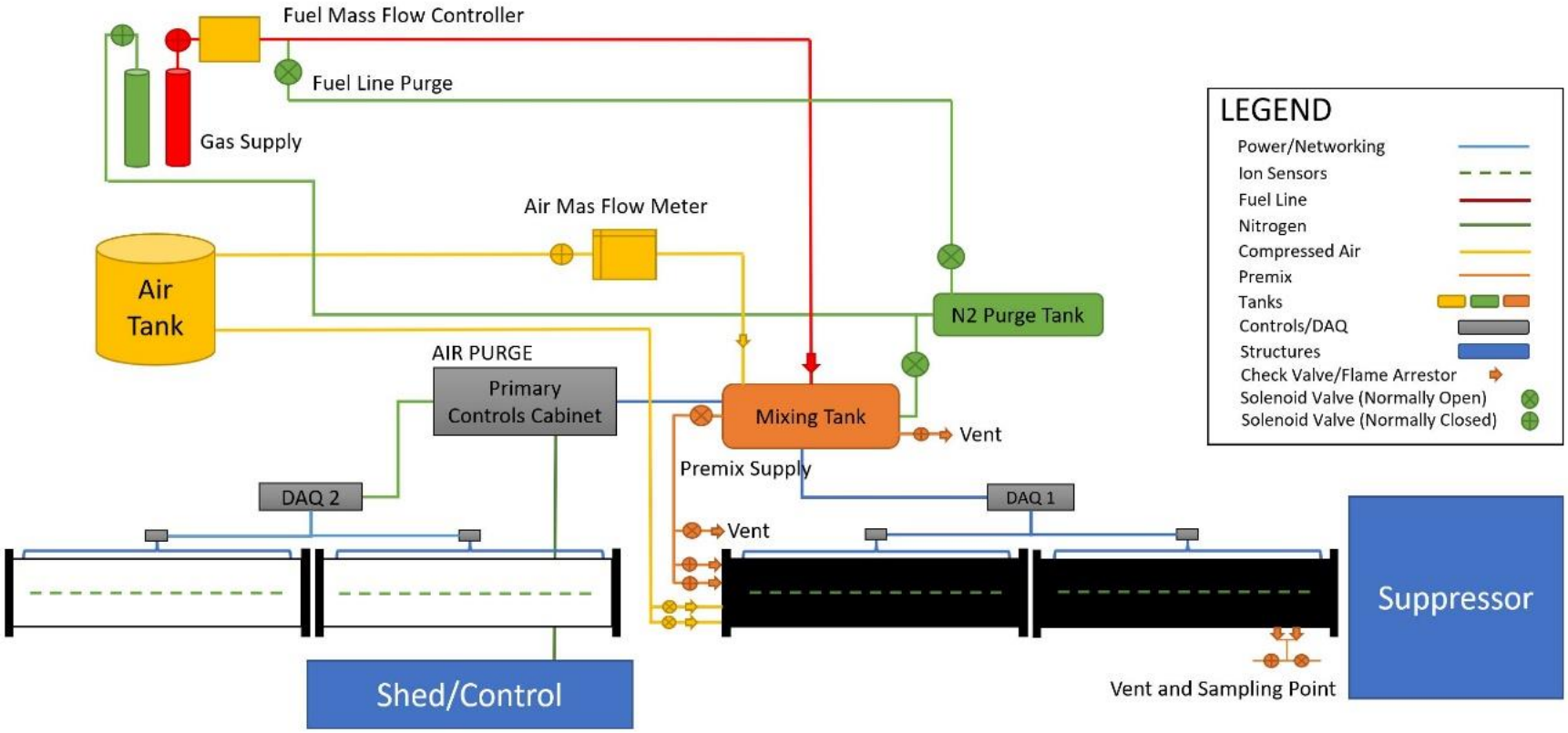


*Figure 53: GERF reactor configuration for parametric experiments using two reactor sections (15.24 m (50 ft) total). The reactor setup was split in half at the 15.24 m (50 ft) joint with the blind and fuel supply moved to this point. The parametric experiments were run in this configuration while the infrastructure for the remaining two reactors was built and tested. Vents were installed next to the barrier for 15.24 m (50 ft) and 7.62 m (25 ft) reactive zones. With the 7.62 m (25 ft) reactive zone, the vent was the primary exit route from the reactor since venting into the air-filled section would result in additional available fuel and alter the results. In the 15.24 m (50 ft) reactive zone, gas was vented through the side vent ports and through a hole in the reactor. This allowed for safe sampling the reactor gas concentrations with a mobile gas meter.*

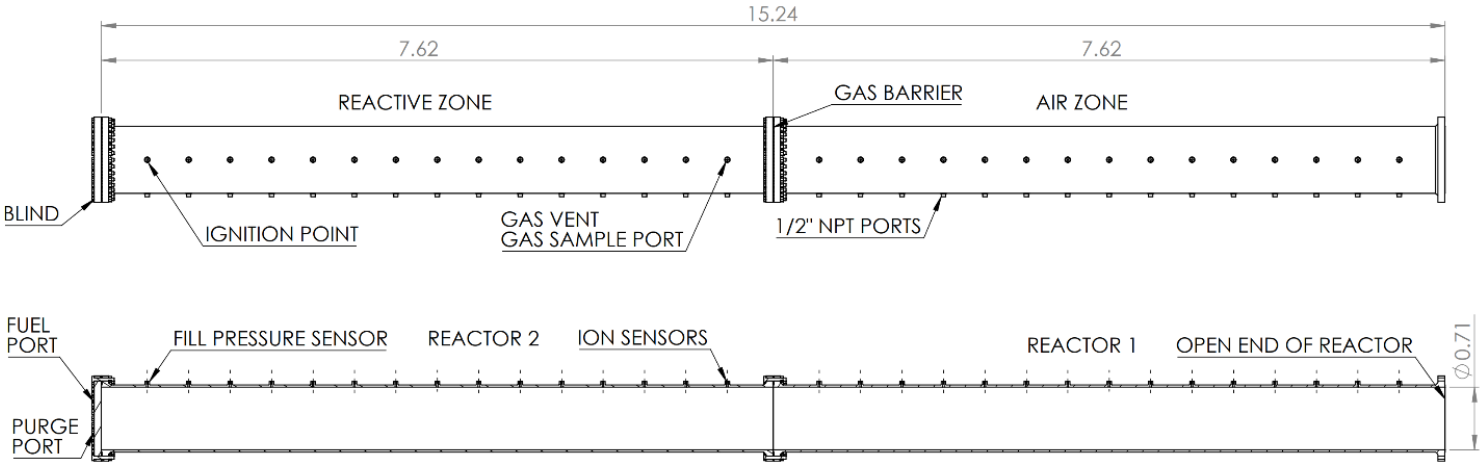


*Figure 54: 15.24 m (50 ft) unobstructed reactor with a 7.62 m (25 ft) reactive zone and a 7.62 m (25 ft) air zone. This configuratation used an ignition point in the first side port next to the blind (closed end). The reactor uses a gas barrier clamped between the two reactor sections, with the venting and gas sample ports placed just to the upstream side of the gas barrier.*

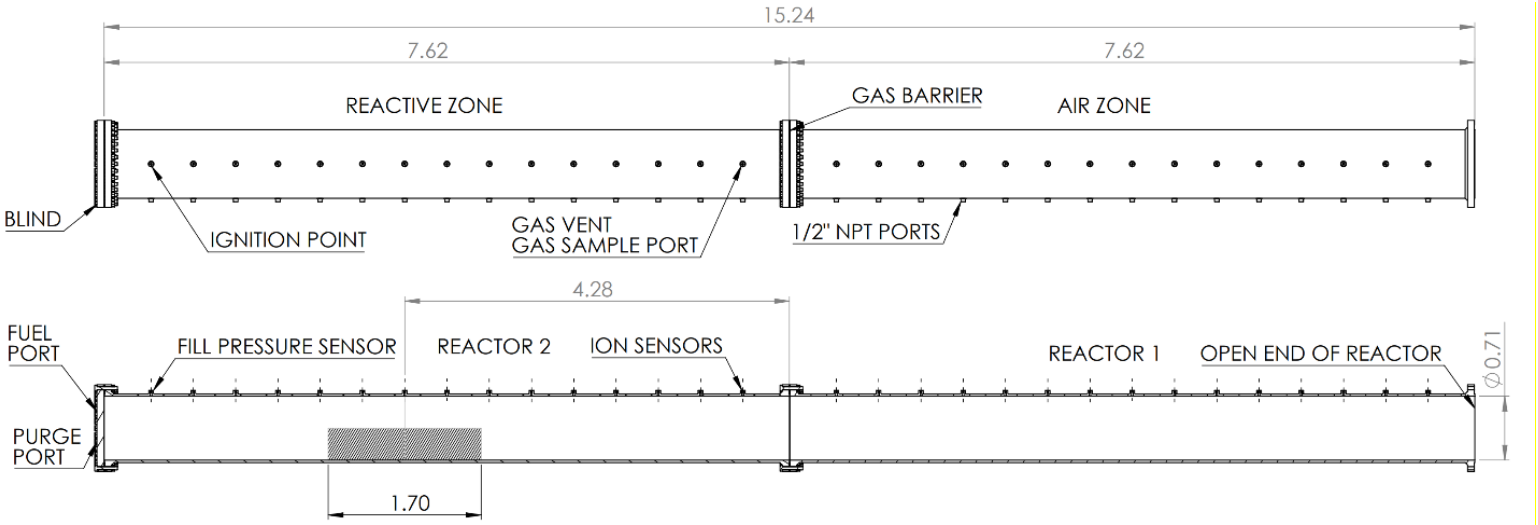


*Figure 55: 15.24 m (50 ft) reactor with a 1.7 m (5.6ft) 50 % rock rubble configuration centered in Reactor 2 one and a 7.62 m (25 ft) air zone. The venting, ignition, and barrierare are identical to Figure 54.*

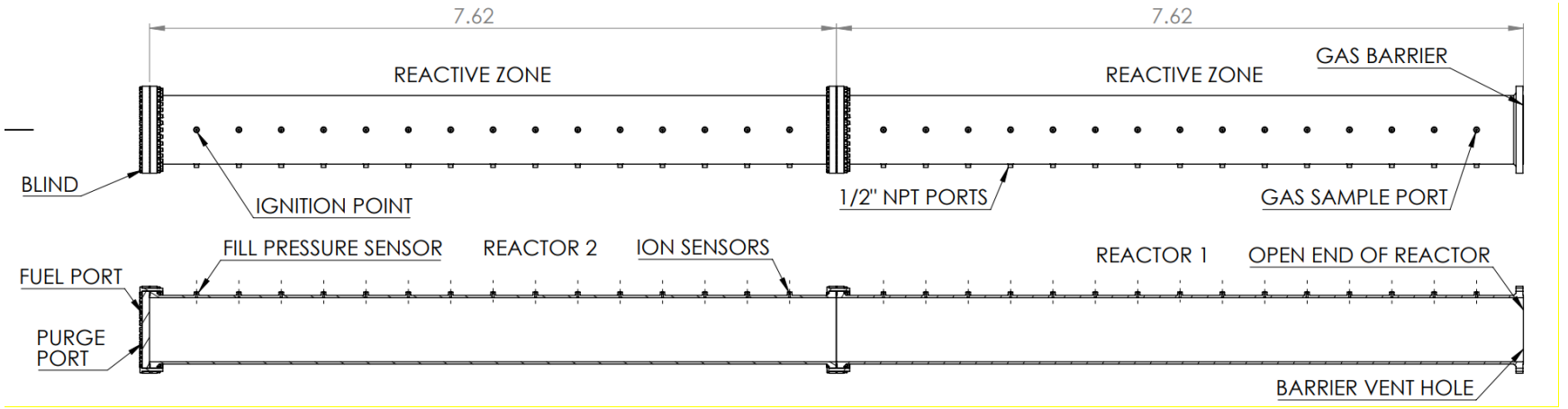


*Figure 56: 15.24 m (50 ft) unobstructed reactor with a 15.24 (50 ft) reactive zone. The gas barrier is clamped to the flange on the exit of Reactor 1. Venting was done through a hole in the barrier, and the vent was relocated next to the barrier for sampling purposes. The ignition was placed next to the blind.*

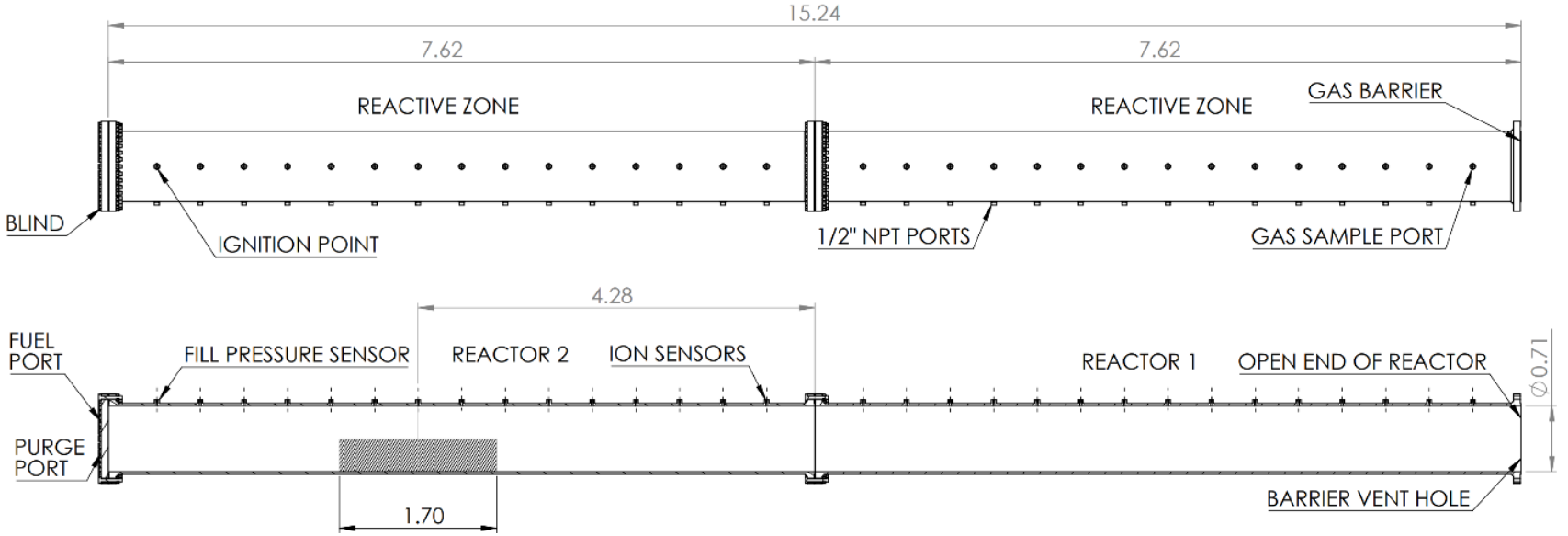


*Figure 57: 15.24 m (50 ft) reactor with a 15.24 (50 ft) reactive zone and a 1.7 m (5.6 ft) 50 % rock rubble obstruction centered in Reactor 2. The ignition and other systems are identical to Figure 56.*

*Figure 58: GERF Reactor in 15.24 m (50 ft) configuration.*

When the barrier was located at the end of the reactor, a relatively weak plastic was clamped across the open end. This barrier configuration was tested with a rupture strength of approximately 21 kPa (3 psi). Venting was accomplished with a 1.3 cm (0.5 in) diameter hole in the barrier material and a vent port. Filling was conducted at a pressure of approximately 6.89 kPa (1 psig), and the pressure was allowed to fall to near the atmospheric of 76 kPa (11 psia) before ignition. When the barrier was located between reactor sections, a 0.18 mm (7 mil) thick plastic barrier with a 206 MPa (30,000 psi) tensile strength material was used. Venting occurred entirely through side ports. The 0.18 mm (7 mil) thick barrier has a tested rupture strength of approximately 55 - 83 kPa (8 – 12 psig). The increased barrier strength accommodated higher fill pressures and compensated for increased pressure drop when venting through side ports equipped with flame arrestors. Atmospheric pressure at the GERF is approximately 76 kPa (11 psia). Fills were conducted at 103 – 110 kPa (15 – 16 psia) absolute, and pressure was vented down to 76 – 83 kPa (11– 12 psia) after filling for ignition. The rock rubble tests repeated the general configuration of the empty reactor tests. The rock rubble experiments covered in the parametric analysis were configured with a 1.7 m (5.6 ft) rubble section filled to the midpoint of the explosion reactor. Further discussion of the rock rubble experiments is in the following sections.

## Objective 1.c: Investigating the impact of ignition energy and location on flame propagation velocities and overpressures.

The reactor and systems designed for both the GERF and the smaller scale reactors housed on the primary mines campus are modular in design intended for use with a variety of configurations. The ignition system of the GERF can be installed on any of the reactor's ports, allowing for a center ignition. The ignition systems used on both reactors allows for the installation of various automotive and industrial components, allowing for a variety of configurations. When this work was proposed, the campus reactor was planned as a contingency for weather or other disruptions. Due to the constraints imposed by COVID and wildfires, it was decided to run the ignition energy and sparkplug location experiments on the smaller secondary reactor on campus so the GERF could operate in parallel.

### Ignition System

In total, three ignition systems with different ignition energies were deployed to investigate the impact on the flame front velocity propagation and changes on the overpressure. The ignition energies used for the experiments are 60 mJ, 132 mJ, and 1200 mJ.

The setup of the ignition system with the lowest ignition energy varies a little bit from the other two system. This system consists of an energy source (12 V Battery), a capacitor, a coil, a switch, a safety lock, a spark plug, and a relay. Current is built up in the capacitor, by activating the spark. After deactivating the switch, the current is discharged through the ignition coil. The coil acts as a step-up transformer to increase the voltage from 12 V to 20,000 V. The high voltage jumps from the positive electrode to the negative electrode of the spark plug creating a spark. The relay, which is connected in parallel to the capacitor, re-energized the coil rapidly over and over again, creating a constant spark with a specific frequency. Figure 59 shows the schematic of the ignition system for the 60 mJ energy with all components. The spark duration of this ignition system is 1 ms.

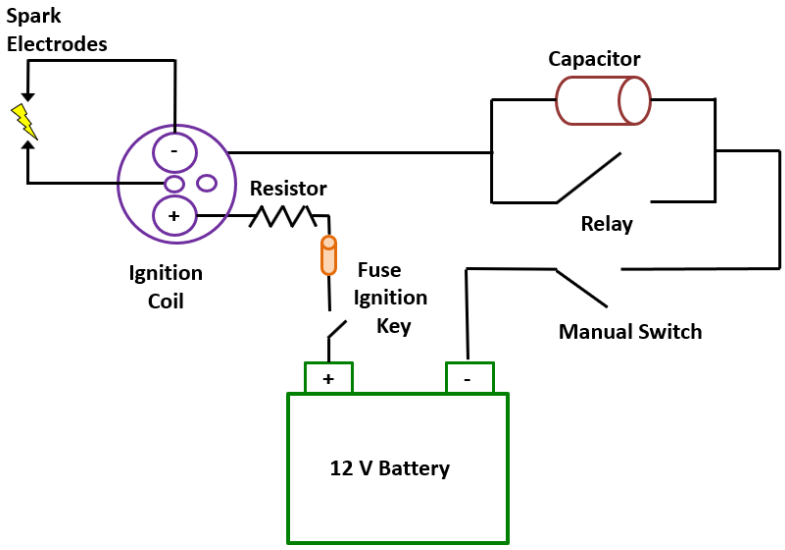


*Figure 59: Schematic of the ignition system with a spark energy of 60 mJ. The system consists of 12 V battery, 1 Ohm resistor, capacitor, coil, relay, ignition key, manual switch, fuse, and spark plug.*

The other two setups use a FAST E6 digital cd ignition box combined with an E-Core ignition coil and an MSD 6AL-2 ignition control module with an MSD ignition coil, and a spark plug Both systems contain a manual switch, an ignition key, and fuses for safety purposes. The frequency of the spark is controlled by an MSD Digital Ignition Tester, which simulates a signal and triggers the box to produce a spark at the spark plug. The purpose of the ignition control module is to create a spark with a higher energy, which is shown in Table 8.

*Table 12: Specification of the ignition systems.*

| **Part** | **Brand** | **Part Description** | **Spark Energy** | **Spark Duration** |
|---|---|---|---|---|
| Ignition Box | FAST | E6 Digital CD | 1,200 mJ | NA |
| Coil | FAST | E92 E-Core | NA | 245 µs |
| Ignition Box | MSD | 6AL-2 | 132 mJ | NA |
| Coil | MSD | Blaster SS | NA | 220 µs |

Figure 60 shows a schematically wire diagram of the ignition system for 135 mJ, and 1,200 mJ spark energies. The system is placed in a plastic container with a transparent cover to allow visualization of the components.

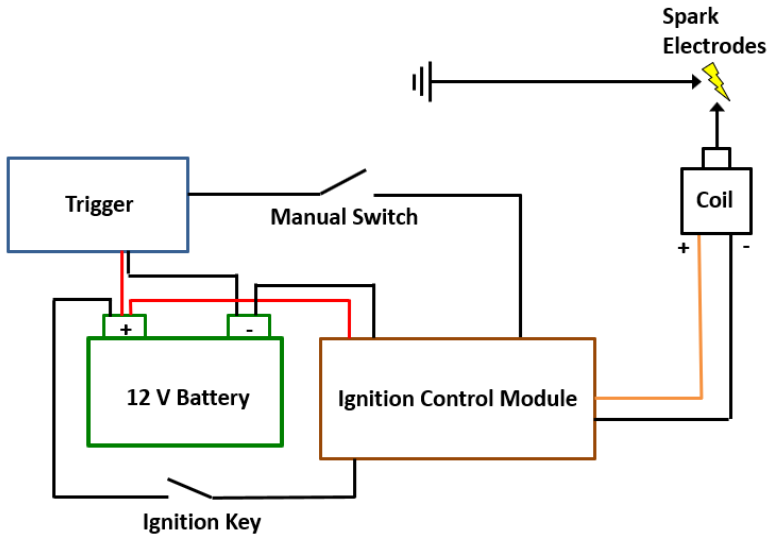


*Figure 60: Setup of the ignition systems for 135 mJ and 1,200 mJ ignition energies. The system consists of 12 V battery, ignition control module, coil, signal trigger, spark plug, manual switch, and ignition key.*

### Ignition location

A set of experiments were conducted with different ignition location: closed-end, and mid-reactor ignition. The variation of the location should show a change in methane flame propagation velocity and overpressure change. The spark electrode was located at the first side port from the inlet, representing closed-end ignition. For the mid-reactor ignition, the electrode was installed 11.5 m (38 ft) from the gas inlet in the reactive zone. All tests were performed without rock rubble and an ignition energy of 60 mJ. Figure 61 shows the two different ignition locations of the 30.48 m (100 ft) reactor.

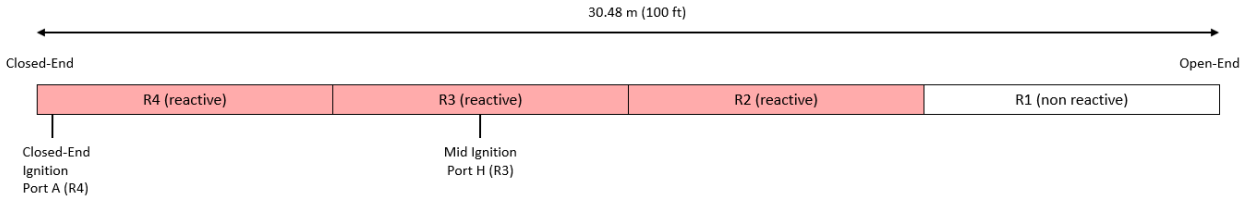


*Figure 61: Schematic of the two different ignition locations in the 30.48 m (100 ft) long reactor.*

## Objective 1.d: Investigate the impact of rock rubble geometry (e.g. length, height, and porosity) and location relative to ignition source on flame acceleration and overpressures in the high-speed deflagration regime. High-speed imaging will also be used as additional insights into the interaction of the flame and rock pile for additional validation of the CFD combustion models.

Rock rubble experiments were run with a variety of conditions, ranging from 7.62 m (25 ft) reactive zones up to 22.86 m (75 ft) reactive zones. The 7.62 m (25 ft) reactive zones were sequenced relatively early in the project to produce early rock rubble data for use in the 2D and 3D reactor models. In order to achieve higher flame propagation velocities and approach the DDT, rock rubble experiments were repeated at larger sizes as the GERF buildout progressed. The experiments designed to approach the DDT with a 22.86 m (75 ft) reactive zone and an altered rock rubble obstruction are discussed in Objective 2.3.

The rock rubble consisted of hand sorted waste rock procured from the Edgar Mine. The rock fragments typically had a major dimension of 10 - 15 cm (4 - 6 in). The rock rubble was piled into a 1.7 m (5.6 ft) long open topped steel sled straddling the joint. The ends of the sled were covered with a wire screen to retain rocks during the experiment. The reactor sections were then closed, leaving the obstruction in place in the center of the joint. The rock rubble preparation and the sled are shown in Figure 62. This resulted in the center of the rock rubble being approximately 7.62 m (25 ft) from the gas barrier and 13 m (5 ft) from the blind and ignition point. For the short rock rubble tests, the sled was sufficient to hold most of the rock obstructions in place. The setup of the extended rock ruble experiments with the flame propagation velocities approaching the DDT are presented with Objective 2.3.

*Figure 62: Sorted rock rubble in storage prior to loading (left) and rock rubble loaded into the sled centered on the reactor 2-3 joint (Right).*

*Figure 63: Close up view of rock rubble being loaded into the sled in preparation for an experiment. The rock used is waste rock from the Edgar Mine, with an average length of 10 – 20 cm (4 to 8 inches).*

**Summary of Experimental Setup for 7.62 m (25 ft) Parametric analysis with and without Rock Rubble**

The experiments were designed to parametrically analyze the impact of fuel air ratios and rock rubble on flame propagation. First, a baseline was established for explosions in an empty reactor.

These were conducted with 7.62 m (25 ft) and 15.24 m (50 ft) reactive zones. The 7.62 m (25 ft) empty reactor experiments used two 7.62 m (25 ft) reactor segments, as show in Figure 64. The first reactor section was filled with the explosive mixture and the second section was filled with air. A foil barrier was clamped between the reactor sections to contain the explosive atmosphere. The reactor was vented out a side port to ensure that there was not a gas buildup in the air-filled reactor. Only a few of these tests were conducted to validate the experimental setup and the effectiveness of the suppressor. The second configuration, shown in Figure 65, used a plastic barrier clamped over the open end of the second reactor to contain the explosive atmosphere. Due to the lack of an air-filled reactor to block access or create a location for unwanted gas to accumulate, this configuration was vented through a hole in the barrier, potentially allowing for high fill speeds with a relatively low reactor pressure and a weaker barrier. The need for enhanced sound suppression and fire safety prevented this configuration from being used on larger experiments at a later date.

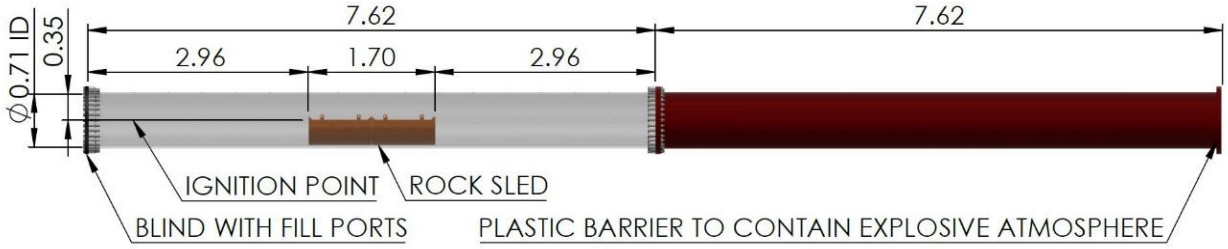


*Figure 64: 15.24 m (50ft) Rock Rubble Experiment. Note that some usages of this reactor configuration do not include the rock rubble sled.*

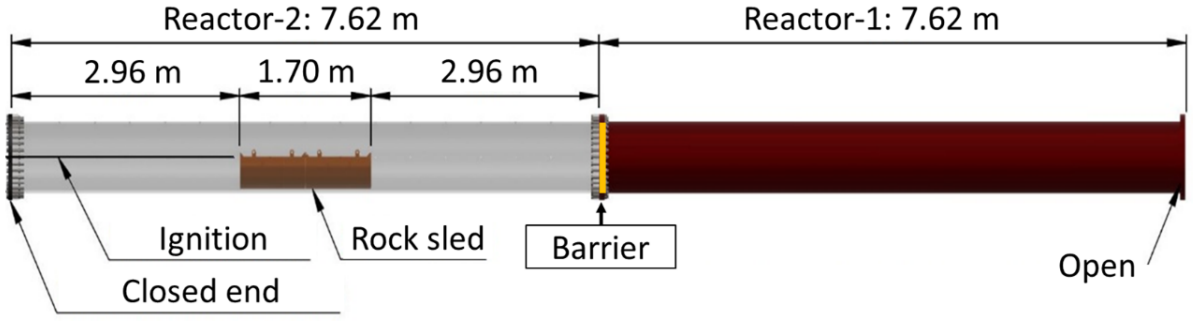


Figure 65: Schematic of 15.24 m (50 ft) reactor with 7.62 m (25 ft) reactive zone and a barrier installed at the reactor 1-2 joint. Note that some usages of this reactor configuration do not include the rock rubble sled.

A set of parametric empty reactor tests were conducted with a 15.24 m (50 ft) reactive zone. In this configuration, the reactor was filled through the blind installed at the 15.24 m (50 ft) split,

between reactors 2 and 3. The reactor was capped with a plastic barrier to retain the explosive atmosphere. It was ventilated through a hole in the barrier and the final side port was used for taking gas readings. To ensure that the gas mixture was uniform and stabilized, the total gas flow was approximately three times the volume of the reactive zone. The gas readings at the far end of the reactor were found to be stable by the time the total fill flow reached three times the reactive zone volume. The 15.24 m (50 ft) configuration is shown in Figure 64. The igniter was mounted in the first side port adjacent to the blind with the spark location in the centerline of the reactor. Experiments were conducted at 7.5, 9.5, and 11.5 %$CH_4$.

The rock rubble tests repeated the general configuration of the empty reactor tests. The rock rubble experiments covered in this paper were configured with a 1.7 m (5.6 ft) rubble section filled to the midpoint of the explosion reactor. The rock rubble configuration is shown in Figure 64. The loaded rock rubble sled is shown in Figure 66. The rock rubble was procured from waste rock at the Edgar Mine's dump. The rock sled was loaded when the pipe sections were separated and then pulled into position using a snatch block and cable puller. The rock rubble sled was positioned approximately in the middle of the first section of the reactor.

*Figure 66: Rock rubble sled loaded into the reactor (left), rock rubble during loading (center), and a model of the sled inside the reactor (right).*

The rock rubble experiments, and the 7.5 % $CH_4$ experiments analyzed in this paper occurred during winter conditions at the Edgar Mine. The weather was cold and clear on both shots with temperatures in the 5–10 ℃ (41 – 50 °F). The winter shots were carried out early to midafternoon to maximize the temperature on the site. The absolute pressure in the reactor was maintained at approximately 81.4 – 82.7 kPa (11.8 – 12 psia), slightly exceeding atmospheric pressure.

*Table 13: Table of Methane (%vol) Concentration Parametric Experiments*

| Reactor Length (m (ft)) | Reactive Length (m (ft)) | $CH_4$ | Obstacles | Ignition location | Number of tests | Water Barrel |
|---|---|---|---|---|---|---|
| 15.24 m (50 ft) | 7.62 m (25 ft) | 7.50% | Empty | closed-end | 2 | no |
| 15.24 m (50 ft) | 7.62 m (25 ft) | 9.50% | Empty | closed-end | 2 | no |
| 15.24 m (50 ft) | 7.62 m (25 ft) | 11.50% | Empty | closed-end | 2 | no |
| 15.24 m (50 ft) | 15.24 m (50 ft) | 7.50% | Empty | closed-end | 4 | no |
| 15.24 m (50 ft) | 15.24 m (50 ft) | 9.50% | Empty | closed-end | 3 | no |
| 15.24 m (50 ft) | 15.24 m (50 ft) | 11.50% | Empty | closed-end | 1 | no |
| 15.24 m (50 ft) | 15.24 m (50 ft) | 7.50% | RR (L=1.7 m (5.6 ft)) | closed-end | 1 | no |
| 15.24 m (50 ft) | 15.24 m (50 ft) | 11.50% | RR (L=1.7 m (5.6 ft)) | closed-end | 1 | no |
| 15.24 m (50 ft) | 7.62 m (25 ft) | 7.50% | RR (L=1.7 m (5.6 ft)) | closed-end | 7 | no |
| 15.24 m (50 ft) | 7.62 m (25 ft) | 9.50% | RR (L=1.7 m (5.6 ft)) | closed-end | 3 | yes |
| 15.24 m (50 ft) | 7.62 m (25 ft) | 11.50% | RR (L=1.7 m (5.6 ft)) | closed-end | 4 | no |
| 30.48 m (100 ft) | 22.86 m (75 ft) | 7.50% | Empty | closed-end | 2 | yes |
| 30.48 m (100 ft) | 22.86 m (75 ft) | 7.50% | Empty | closed-end | 2 | no |
| 30.48 m (100 ft) | 22.86 m (75 ft) | 7.50% | Empty | mid | 1 | yes |
| 30.48 m (100 ft) | 22.86 m (75 ft) | 7.50% | RR (L=1.7 m (5.6 ft)) | closed-end | 2 | yes |
| 30.48 m (100 ft) | 22.86 m (75 ft) | 7.50% | RI (L=4 m (13.1 ft)) | closed-end | 2 | yes |

Two barrier and vent configurations were used. When the barrier was located at the end of the reactor, a relatively weak plastic was clamped across the open end. This barrier configuration was tested with a rupture strength of approximately 21 kPa (3 psig). Venting was accomplished with a 1.3 cm (0.5 in) diameter hole in the barrier material and a 1.3 cm (0.5 in) diameter vent port. Filling was conducted at a gauge pressure of approximately 6.89 kPa (1 psig), and the pressure was allowed to fall to near the atmospheric of 76 kPa (11 psia) before ignition. When the barrier was located between reactor sections, a 0.18 mm (7 mil) thick plastic barrier with a 207 MPa (30,000 psi) tensile strength material was used. Venting occurred entirely through side ports. The 7mil barrier has a tested rupture strength of approximately 55.2 – 82.7 kPa (8 – 12 psig). The increased barrier strength accommodated higher fill pressures and compensated for increased pressure drop when venting through side ports equipped with flame arrestors. Atmospheric pressure at the GERF is approximately 76 kPa (11 psia). Fills were conducted at 103 – 110 kPa (15 – 16 psia), and pressure was vented down to 76 – 83 kPa (11-12 psia) after filling for ignition.

**Experiments with and without Rock Rubble in the 30.48 m (100 ft) Reactor**

Several experiments comparing the impact of the Rock Rubble and quantifying the impact of the suppression system were conducted. These utilized the 71 cm (28 in) diameter, 30.48 m (100 ft) long reactor configuration, with 22.86 m (75 ft) (reactor-1, 2, and 3) reactive zone filled with 7.5 % $CH_4$ premixed methane-air mixtures, while the last ~7.62 m (25 ft) (reactor-4) was designated as non-reactive zone filled with air, as shown in Figure 47. A barrier that can withstand ~100 kPa (~15 psig) was installed between reactor-3 and reactor-4 to separate the reactive zone and the non-reactive zone that was filled with air. All tests were done at ~86 kPa (~12.5 psia) reactor pressure, 4 kPa (0.6 psia) higher than the local atmospheric pressure at ~76 - 82 kPa (~11 – 12 psia), and at temperature of 283 – 295 K (50 – 71 °F) just before the ignition. For every test, the reactor's reactive zone was filled with ~27 $m^3$ (812 $ft^3$) of premixed methane-air mixtures, three time the volume of the reactive zone, from the closed-end, while the air inside the reactor is allowed to bleed through small opening at the port close to the gas barrier at the end of reactor-3. Gas mixtures concentration inside the reactive zone was verified using a handheld gas analyzer connected to a gas vent and compared to the setpoint of the mass flow controllers.

*Table 14: Experiments performed with 30.48 m (100 ft) reactor (22.86 m (75 ft) reactive zone).*

| **Tested parameter** | **Experiment setup** | **$CH_4$-Air mixture** | **Reactive zone length** | **Number of test** |
|---|---|---|---|---|
| Effect of water barrier | With water barrier | 7.5 % $CH_4$ | 22.86 m (75 ft) | 2 |
| | Without water barrier | 7.5 % $CH_4$ | 22.86 m (75 ft) | 2 |
| Effect of rock rubble | With rock rubble | 7.5 % $CH_4$ | 22.86 m (75 ft) | 2 |
| | With extended rock rubble | 7.5 % $CH_4$ | 22.86 m (75 ft) | 2 |
| | Empty reactor | 7.5 % $CH_4$ | 22.86 m (75 ft) | 2 |

## Objective 2: Continue development, improvement and validation of the CSM high-speed turbulent deflagration combustion model using the new extended large-scale explosion reactor.

The end goal of the numerical modeling efforts was to further develop and refine the CSM model using experimental results and then apply the improved modeling methods and to larger scale and complexity situations common to mine safety. For safety purposes and to facilitate experimental work while the buildout was in progress, the GERF started with relatively simple and low energy experiments and progressively increased the reactor length and potential energy as it expanded towards the use of a 22.86 m (75 ft) reactive zone with rock rubble. The numerical work was sequenced similarly with a progressive increase in simulation complexity. The calibration work encompassed 2D reactor models, 3D models, and then models with a rock rubble obstruction. Other physical phenomena, such as the transient impact of the gas barrier on reactor pressure, were also modeled to achieve a better comparison point with experiments. These reactor configurations matched the configurations tested at the GERF and were used to calibrate and validate the CSM model for use on a variety of geometries. The groundbreaking full scale CFD model of an ignition on the active face of a longwall was built with the results of this work.

Conducting methane explosion experiment in a full-scale industrial setting is not practical due to cost and safety concern. In recent years, Computational Fluid Dynamics (CFD) modeling has been used intensively to study the flame behavior and potential impact of explosion in different industrial settings, such as mineral processing plants or refineries. Previous CFD modeling study show that the resulting simulation is highly sensitive on the turbulent model and initialization parameters. Having an intensive database of experimental results with different ignition conditions was required to develop and validate the CFD model starting from laboratory scale, before scaling it up to a full-scale explosion simulation. Comparison of flame speed and flame front location at different time instances between the experiment results and CFD models were used for benchmarking the CFD model accuracy. Once validated, CFD model can be used as a cost-effective method to simulate different ignition condition. The result of this study can provide better understanding on the flame behavior should ignition occurred in a confined space filled with obstacles.

**Objective 2.1.a: Initial modeling of the small and large-scale reactor using 2D models to investigate the relative impact of ignition location, rock rubble geometry, and the addition of other flammable gas species.**

**Objective 2.1.b: Information obtained from the 2D model will be used in the 3D models recently developed for the smaller-scale and will be used to validate the 3D models for the large-scale reactor for select cases to reduce computational effort.**

CFD models of a variety of reactor configuration were developed. The experimental results are then used to assist in the development of the 2D models, which have the advantage of more rapid iteration compared to a 3D model. One important feature of the reactor models is the gas barrier. It is an important part of the reactor design. It contains the explosive atmosphere within the correct volume of the vessel. However, the strength of the barrier does impact the flame propagation rate inside the reactor. To capture this detail in the CFD models, they were designed to were run in two stages. The first stage is when the gas barrier still intact and only the 22.86 m (75 ft) reactive zone was modeled to reduce the computational time. At his stage, the gas barrier is assigned as a wall boundary condition. The second stage is when the gas barrier opened and the whole 30.48 m (100 ft) reactor length was modeled. At this stage, the gas barrier boundary condition is switched from wall to interface. Once the reactive zone is connected to the non-reactive reactor-1, patch function is used to patch the initialization parameter to this non-reactive zone and the open-end is assigned as pressure outlet boundary condition, and the simulation is then resumed.

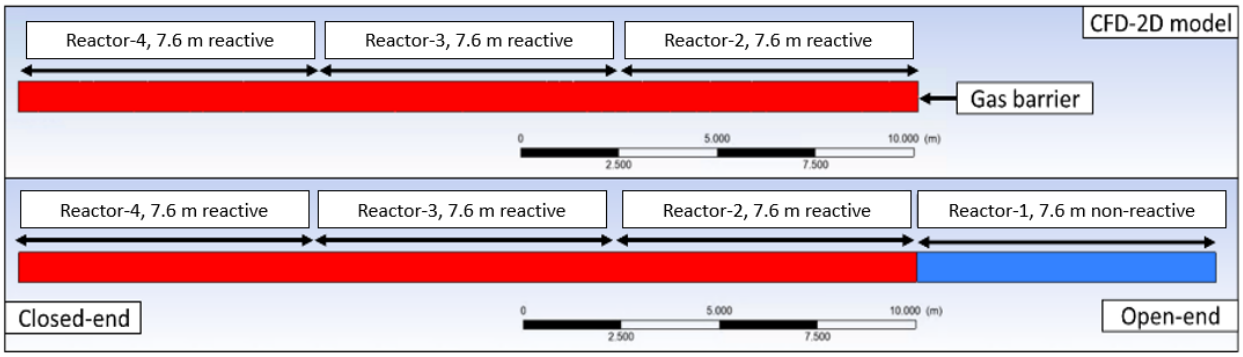


*Figure 67: 2D CFD model geometry of the 30.48 m (100 ft) long, 71 cm (28 in) diameter reactor, when gas barrier still intact (top) and gas barrier opened (bottom).*

The 2D CFD model use 5 mm (0.07 in) uniform base mesh, while the 3D model uses 2 cm (1.06 in) base mesh with 2 level of mesh adaption based on temperature gradient to reduce the number of mesh and computational time required to run the simulation. The use of 2 level of mesh adaption

with 2 cm (1.06 in) base mesh resulted in 5 mm (0.07 in) mesh at the flame front region in the 3D model. For initialization, both the 2D and 3D models were initialized with the same parameters. The kinetic energy and specific dissipation rate values are based on experiment data from previous tests using 6.1 m (15 ft) long, 71 cm (28 in) diameter reactor, which resulted in average flame speed of 40 m/s (131 ft/s) once the flame reached fully turbulent regime. More information on the process of reactor modeling can be found in paper: *Study of Methane Flame Interaction with Obstacles Using* 30.48 m *(100 ft) Long Reactor and CFD Model.* The ANSYS Fluent model settings for the 2D CFD model are given in Table 15.

*Table 15: ANSYS Fluent v 18.2 model settings for 2D CFD model*

| Parameter | Setting |
|---|---|
| **Time** | Transient |
| **Solver** | Pressure based |
| **Turbulent model** | Standard k-ω SST model |
| **Species transport** | volumetric reactions, finite rate chemistry, laminar flame speed theory |
| **Chemical mechanism** | Methane-air 2 step mechanism |
| **Flow density** | Compressible |
| **Solution methods** | PISO scheme with second order discretization |
| **Convergence criteria** | $1 \times 10^{-4}$ for continuity and momentum, $1 \times 10^{-4}$ for turbulence, $1 \times 10^{-5}$ for gas species, and $1 \times 10^{-10}$ for energy |
| **Boundary condition** | Pressure outlet, adiabatic wall |
| **Time step** | 40 µs until 820 ms; 20 µs onward, with 50 iterations per time step |
| **Mesh setting** | 5 mm base mesh, 3 inflation layers at reactor walls |
| **Operating condition and initialization** | Operating pressure: 79,300 Pa (11.5 psia), Temperature: 295 K (71.3 °F)<br>Reactor pressure: 4,000 Pa (0.58 psig)<br>Turbulent kinetic energy: 1.68 $m^2/s^2$<br>Specific dissipation rate: 47.7 $s^{-1}$ |
| **Spark model** | Spark energy: 60 mJ, spark duration: 1 ms, kernel radius: 0.35 cm |

The 2D model took 5 days to simulate 960 ms of combustion event using 4 x 36 cores computational power. Figure 68 shows the flame development inside the reactor at different time instances in 2D CFD model. Similar to the event observed in the physical experiment, the gas

barrier was opened at 820 ms after the ignition occurred. The 2D model predicts 56 kPa (8.1 psig) at 820 ms, just before the gas barrier is opened.

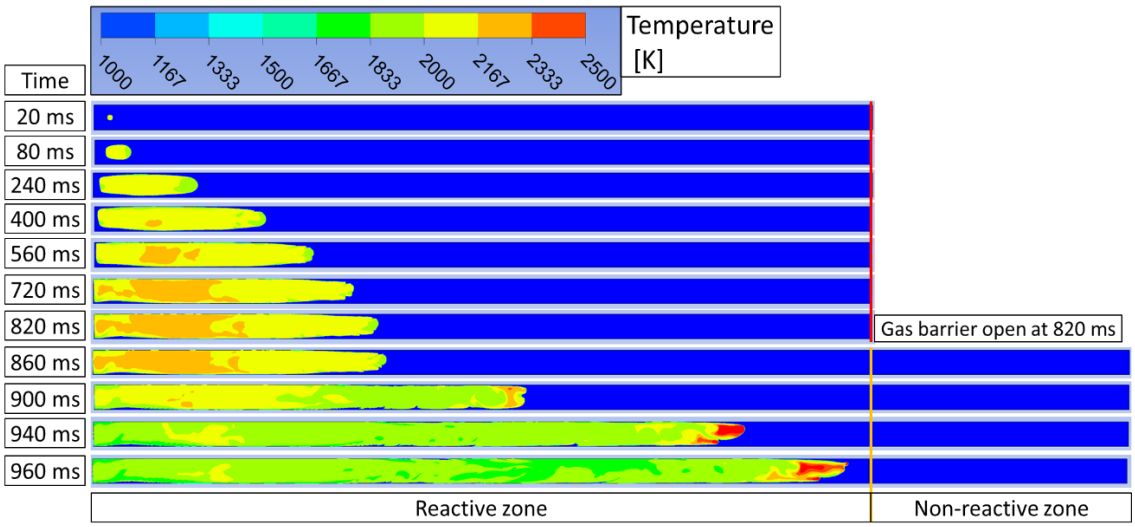


*Figure* 68*: Contour plot of temperature showing the flame propagation inside the reactor at different time instances in 2D model*

The experience and information lessons learned from the quickly iterated 2D modeling were used to accelerate the development of the 3D model. The 3D model was validated against the experimental results in a similar process to the 2D model. The 3D empty reactor model configuration is shown in Figure 69. The ANSYS Fluent configuration for the 3D models is given in Table 16. The 2D CFD model use 5 mm (0.07 in) uniform base mesh, while the 3D model uses 2 cm (0.79 in) base mesh with 2 level of mesh adaption based on temperature gradient to reduce the number of mesh and computational time required to run the simulation. The use of 2 level of mesh adaption with 2 cm (0.79 in) base mesh resulted in 5 mm (0.07 in) mesh at the flame front region in the 3D model. Figure 70 shows the comparison of mesh around the flame front between the 2D and 3D CFD models at 500 ms after ignition.

For initialization, both the 2D and 3D models were initialized with the same parameters. The kinetic energy and specific dissipation rate values are based on experiment data from previous tests using 6.1 m (20 ft) long, 71 cm (28 in) diameter reactor, which resulted in average flame speed of 40 m/s (131 ft/s) once the flame reached fully turbulent regime.

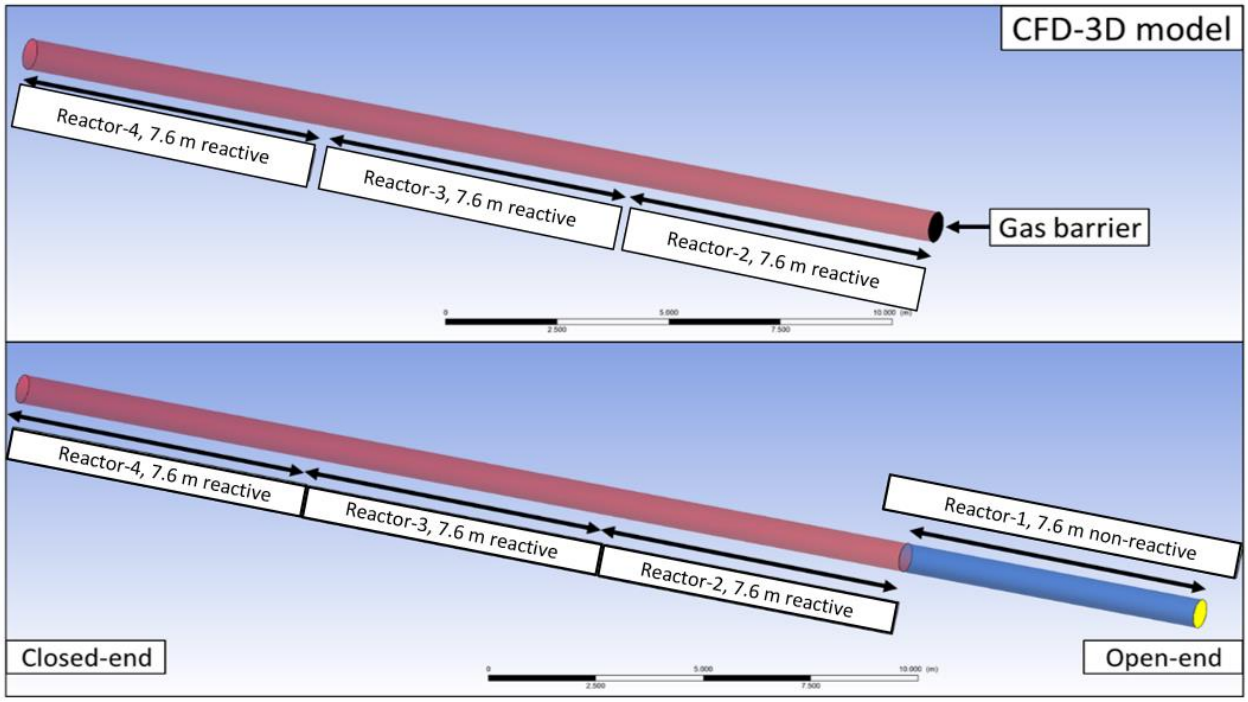


*Figure 69: 3D CFD model geometry of the 30.48 m (100 ft) long, 71 cm (28 in) diameter reactor, when gas barrier still intact (top) and gas barrier opened (bottom)*

Table 16: ANSYS Fluent v 18.2 model settings for 3D CFD model

| Parameter | Setting |
|---|---|
| **Time** | Transient |
| **Solver** | Pressure based |
| **Turbulent model** | Standard k-ω SST model |
| **Species transport** | volumetric reactions, finite rate chemistry, laminar flame speed theory |
| **Chemical mechanism** | Methane-air 2 step mechanism |
| **Flow density** | Compressible |
| **Solution methods** | PISO scheme with second order discretization |
| **Convergence criteria** | $1 \times 10^{-4}$ for continuity and momentum, $1 \times 10^{-4}$ for turbulence, $1 \times 10^{-5}$ for gas species, and $1 \times 10^{-10}$ for energy |
| **Boundary condition** | Pressure outlet, adiabatic wall |
| **Time step** | 40 µs until 820 ms; 20 µs onward, with 50 iterations per time step |

| | |
|---|---|
| **Mesh setting** | 2 cm base mesh with 2 levels mesh adaption based on temperature gradient every time step, 3 inflation layers at reactor walls |
| **Operating condition and initialization** | Operating pressure: 82,700 Pa (12 psia), Temperature: 295 K (71.3 °F)<br>Reactor pressure: 4,000 Pa (0.58 psig)<br>Turbulent kinetic energy: 1.68 $m^2/s^2$<br>Specific dissipation rate: 47.7 $s^{-1}$ |
| **Spark model** | Spark energy: 60 mJ, spark duration: 1 ms, kernel radius: 0.35 cm (0.14 in) |

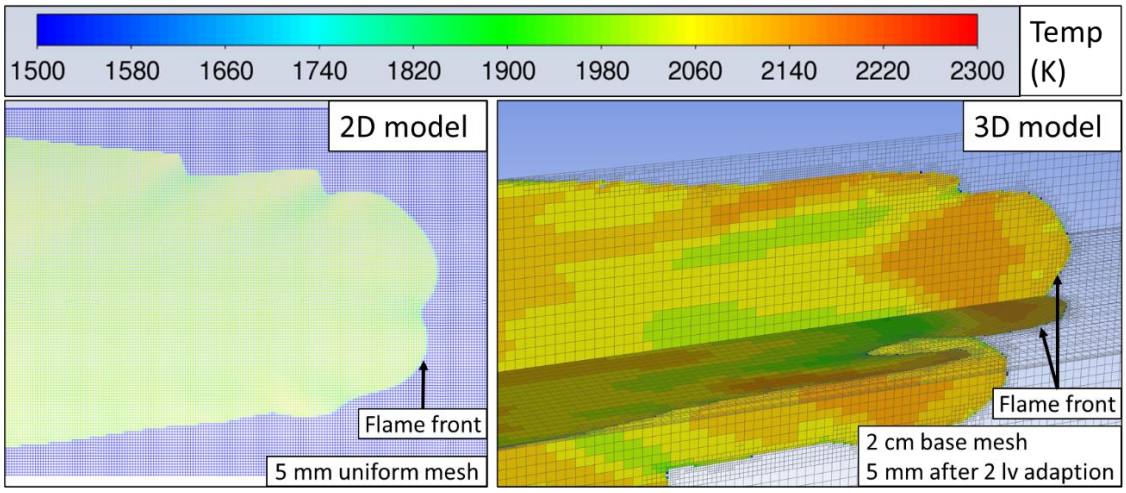


*Figure 70: Comparison of mesh around the flame front in the 2D (left) and 3D (right) CFD model.*

The 3D CFD model took 21 days to simulate 960 ms of combustion event using 4 x 36 cores computational power. Figure 71 shows the flame development inside the reactor at different time instances in 3D CFD model. Similar to the experiments and 2D CFD model, the gas barrier was opened at 820 ms after the ignition occurred. The 3D model predicts 113 kPa (16.4 psig) at 820 ms, just before the gas barrier is opened.

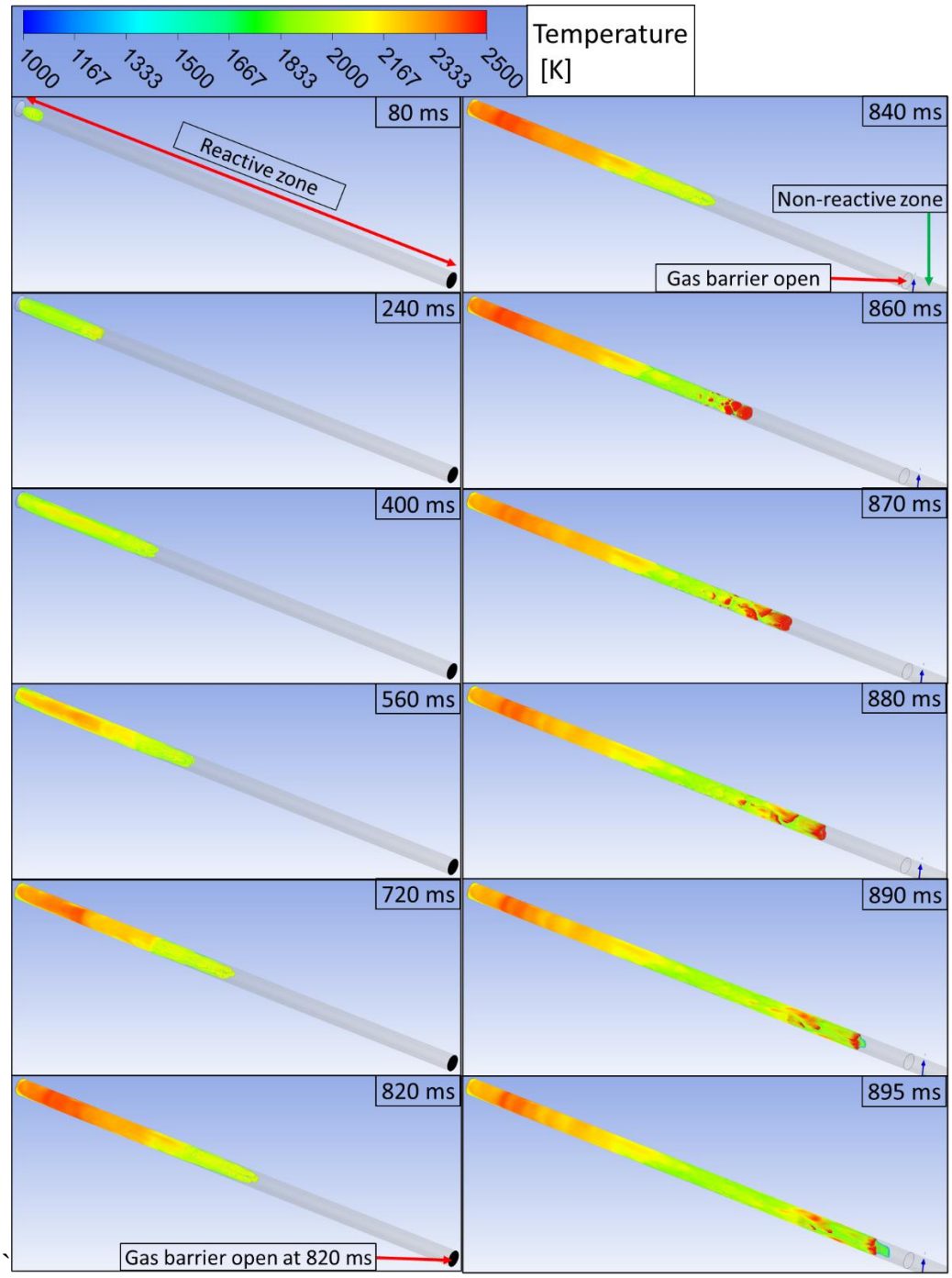


*Figure 71: Volume rending of temperature showing the flame propagation inside the reactor at different time instances in 3D model*

The improved CSM model was intended to provide the foundation for the development of high-quality robust models in mining situations, enabling the development of the full mine scale CFD.

## Objective 2.2: Improve CSM's 3D full-scale longwall explosion model initially developed in short-term Alpha Foundation proposal (AFSTI14) with incorporation of the newly acquired data used to improve the combustion model accuracy.

Longwall face ignitions from accumulated methane gas remain one of the most common causes of methane gas explosions in underground coal mining operations. In 2017, the U.S. Mine Safety and Health Administration (MSHA) mines reported 22 cases of face ignitions during coal cutting and roof bolting operations, in 2018, there were 19 such cases. Fortunately, none of them led to a larger mine explosion. The severity of a methane explosion can be further amplified if it transitions to a coal dust explosion, as was the case in the 2010 Upper Big Branch (UBB) mine disaster, where the resulting flame propagated more than 60 km (37 mi) throughout the mine [4], killing 29 miners and injuring two other miners.

In U.S. longwall operations, point-type sensors methane monitors are usually installed on the body of a longwall shearer and the tailgate drive. To provide a sufficient margin of safety, the U.S. regulation 30 CFR §75.342 (Methane monitors) [5] requires the mine operator to install a methane sensor that will automatically deenergize electric equipment or shut down diesel-powered equipment at the longwall face once the methane concentrations exceed 2.0 %, which is deemed sufficiently below the lower explosive limit of around 5 %. U.S. regulation 30 CFR §75.323 (Actions for excessive methane) [5] also requires measurements with handheld methanometers to be made at least 0.3 m (12 in) from the surrounding roof and rib. If these measurements detect methane in excess of statutory limits, a hazardous condition is deemed to exist. Mine operators must shut down all mining equipment and take steps to improve ventilation to dilute the methane. Despite these requirements, face ignitions continue occur, posing a serious threat to miners and equipment. Changes in ventilation conditions, and sudden outbursts of methane from the coal, roof or floor strata can form explosive mixtures that could be ignited by the shearer cutting actions.

Computational fluid dynamics (CFD) modeling is frequently used to simulate ventilation conditions in longwall mines and to analyze airflow patterns and formation of hazardous gas mixtures, some of which are not detectable using conventional monitoring and ventilation system inspection methods. Full integration of a CFD combustion model into a full-scale longwall ventilation model is difficult due to the computational time and resource requirements. The purpose of this study is to demonstrate the viability of modeling a methane gas explosion in a full-

scale longwall face model and the capability of predicting the impact of an explosion, by reducing the model coverage to only include area of interest and utilizing data interpolation. An improved understanding of possible explosive gas mixture locations inside the longwall face and the potential impact of methane gas explosions will aid in developing more reliable methane monitoring practices and explosion mitigation strategies to improve safety in longwall coal mining operations. For example, excessive methane concentrations are more likely when the shearer is cutting the coal face near the tailgate (TG) corner.

Following the UBB mine explosion in 2010, Davis et al. [6] conducted several studies to simulate the flame propagation that may have occurred during the accident. However, these studies were limited to modeling the flame propagation along the mine entries. To the authors' knowledge, methane explosion modeling in a complex mining environment, such as with the shearer cutting coal in the longwall face and including longwall component such as shields, the shearer with cowls and rotating cutter drums, stage loader, gob plate, etc. has not been published. Therefore, it is the goal of this study to develop a comprehensive CFD longwall mine ventilation and explosion propagation model capable of investigating different methane explosion scenarios and the potential impact on miners and mine infrastructure.

**Objective 2.2.a: Various mine ventilation scenarios will be used in the 3D full-scale longwall ventilation model to predict the location of the EGZs and vary the ignition location. The validated 2D/3D cylindrical reactor gas explosion model will be incorporated into the 3D full-scale longwall ventilation model .**

One of the main challenges in underground longwall coal operations is providing adequate fresh air to dilute the inflow of methane gas from the active coal face to. Methane concentrations must remain below the lower explosive limit, typically around 4.5 % $CH_4$ by volume at standard ambient temperature and pressure [7], [8]. This can be difficult to achieve due to air leakage from the longwall face into the mined-out area or gob and vice versa. Different ventilation systems can significantly change the airflow patterns and movement of gas mixtures in and around the longwall face. In bleeder ventilation common in the U.S., leakage to the gob is intended and common. These leakage flows, along with the natural increase of methane along the face, makes the tailgate corner a critical location for methane monitoring. Depending on the face length, gob characteristics, and immediate roof caving conditions, face-to-gob leakage may amount to more than half of the supplied fresh air from the headgate (HG) in bleeder ventilation [9], [10], [11]. This observation

is also supported by experimental studies by Gangrade et al. [12], [13] that utilized a 1/30$^{th}$ scale physical longwall model to show the airflow interactions between the longwall face and the gob for different gob caving characteristics and ventilation set-ups. Additionally, certain tailgate configurations or tailgate blockages from roof falls may direct face air to flow outby the face at the tailgate corner. In bleeder systems this may entrain methane from behind the shields back into the face area [14], [15], a condition that is suspected to have caused the 2010 Upper Big Branch explosion. In a U-type ventilation pattern, the supplied fresh air leaks into the gob at the headgate and comes back into the face at the tailgate.

With wider longwall panels, more face-to-gob leakage occurs in bleeder systems, and less air reaches the tail end of the face. Since methane continues to emanate along the face, the highest methane concentrations can be expected at or near the tailgate end of the face, as described by [16], [17], [18], [19] Diamond et al., 1999; Kissell, 2006; Thakur, 2006; Schatzel et al., 2006, and Schatzel et al., 2012. Other factors, such as shearer location, cutting direction, and the use of shearer cowls also affect the flow and gas accumulation near the shearer. Without the shearer present, the bulk of the face air flow is concentrated in the area between the shield's hydraulic jacks and coal face [17], [20], [21]. This flow pattern shifts due to blockage by the shearer body. Near the tailgate, this blockage forces the bulk face air flow to move towards the back of the shields, resulting in higher leakage rates into the gob upwind from the shearer. The effect of this flow disturbance is most prominent when the shearer is located at the headgate or tailgate corners of the longwall face. In addition, the shearer cowls that direct the broken coal into the armored face conveyor (AFC) can increase the ignition risk by blocking and diverting the fresh air away from the cutting path and trapping the incoming methane from the coal face between the rotating drums and cowls [17]. The combination of these factors can lead to the formation of explosive methane-air mixtures around the shearer drums, especially when the shearer is cutting the tailgate corner of the longwall face.

To obtain further insight into the complex flow patterns and gas distribution in a longwall operation, several researchers have performed CFD studies modeling airflow patterns and methane distribution inside the longwall face, including [20], [21], [22], [23], [24] and inside the gob [25], [26], [27], [28], [29], [30], [31], [32]. In addition, Gangrade et al. [12], [13] and Pinheiro et al. [33] used a scaled, physical longwall model to observe the flow patterns inside the gob for different

gob characteristics and ventilation scenarios. The results of these studies are useful to identify critical parameters impacting the longwall ventilation, while also identifying explosive gas concentrations in longwall faces. However, to the authors' knowledge, no combustion CFD study has been presented in literature that predict the impact of a methane gas explosion during longwall shearer cutting operations.

Figure 72 shows the development schematic of the CFD model to simulate face ignition scenario at the longwall face.

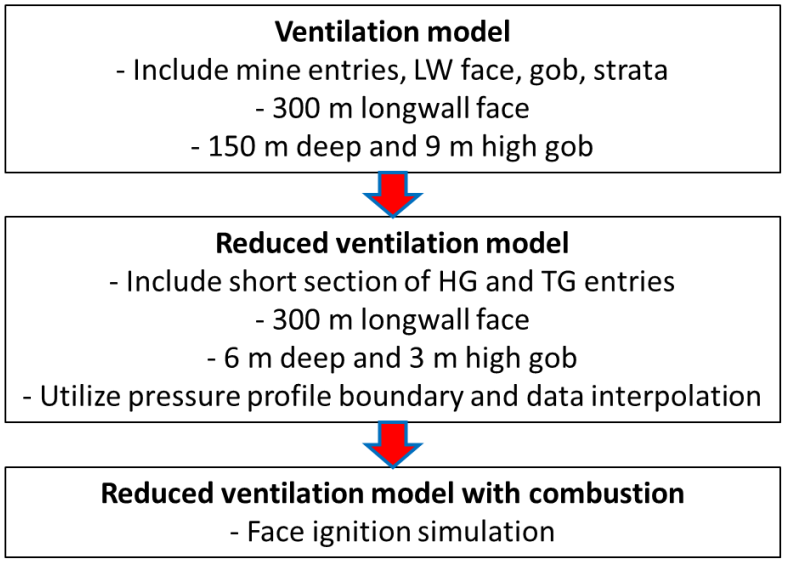


*Figure 72: CFD model development schematic*

**Ventilation Modeling of Longwall**

CFD simulations were performed using the commercial software package ANSYS Fluent (v. 18.2). The longwall bleeder ventilation model, shown in Figure 73 is used as the base ventilation model to simulate the airflow distribution in the longwall face area.

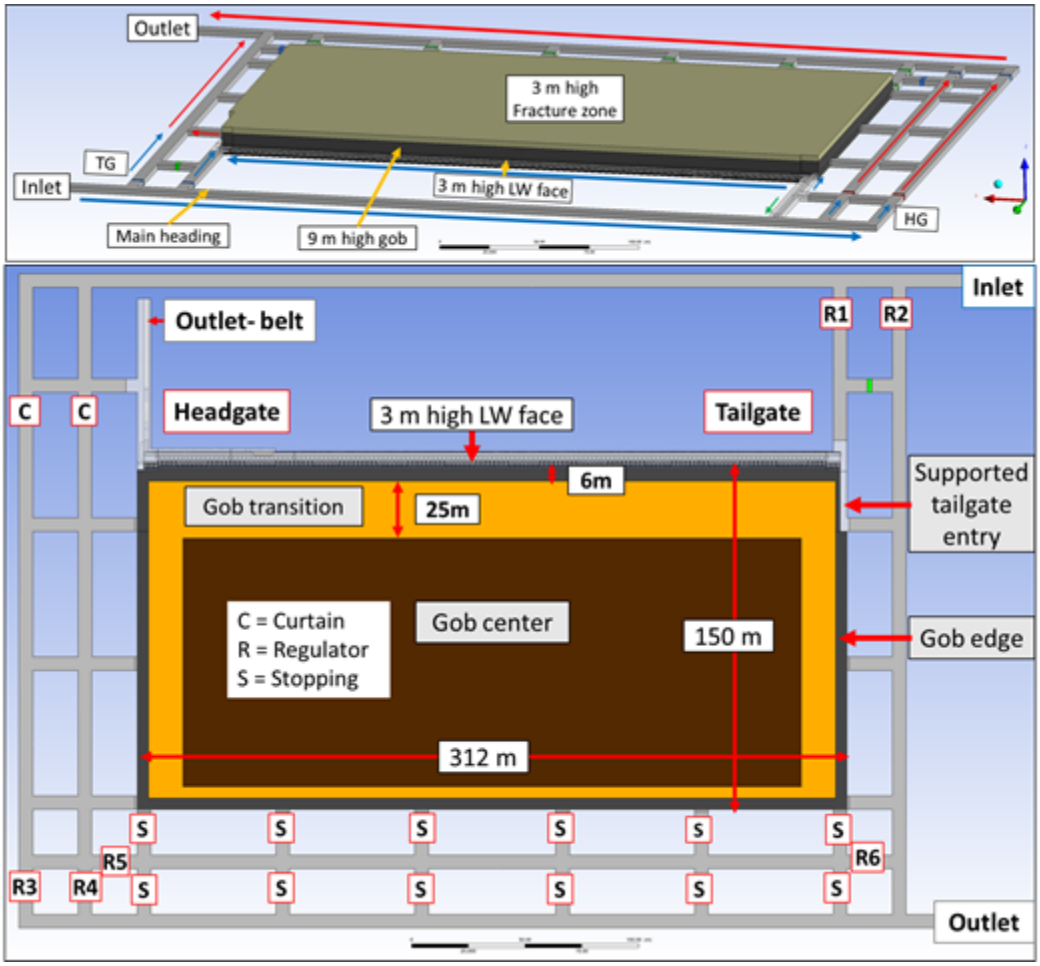


*Figure 73: Longwall bleeder model geometry*

The model panel is 150 m (492 ft) long and 300 m (984 ft) wide and the coal seam is 3 m (9.8 ft) high. The coal chain pillar dimension is 55 m (180 ft) by 20 m (65 ft). The mine entry dimensions are 6 m (19.7 ft) by 3 m (9.8 ft), consisting of two headgate entries, a belt entry and two tailgate entries. The gob and fracture zone heights are 9 m (29.5 ft) and 3 m (9.8 ft), respectively. The gob is further divided into the gob edge, transition zone, and gob center, with different porosity and viscous resistance value assigned to each zone.

The longwall face model includes the operational components typically found in a longwall operation, such as a shearer, stage loader, face conveyor, shield supports, face curtain, gob plate and the headgate and tailgate drives. A detailed view of the longwall face equipment models is shown in Figure 74 and Figure 75. The longwall face is supported by 152 shields. In full scale, each shield is roughly 7 m (23 ft) long, 2 m (6.6 ft) wide and 3 m (9.8 ft) high. Headgate and tailgate shields are slightly longer to accommodate the headgate and tailgate drives. On the backs

of each shield, there is an opening of approximately 0.28 $m^2$ (3 $ft^2$) that allows leakage air to exit and enter the face. The gob is modeled as a porous medium and divided into three zones with different porosities and viscous resistances, calculated as the inverse of permeability, based on findings by Marts et al. [25]. The gob fringe, green color in Figure 73, extends to 6 m (19.7 ft) deep inside the gob and has a 40 % porosity with a viscous resistance of $1.5x10^5$ $m^{-2}$ (permeability value of $6.9x10^{-6}$ $m^2$). The transition zone, blue color, has a 25 % porosity and viscous resistance of $1x10^6$ $m^{-2}$ (permeability value of $1x10^{-6}$ $m^2$) while the fully compacted center of the gob, brown color, has a 14 % porosity and a viscous resistance of about $5.0x10^6$ $m^{-2}$ (permeability value of $2.0x10^{-7}$ $m^2$). Note that the gob permeability can vary significantly for each mine, as reported by Esterhuizen and Karacan ($2.0x10^{-10}$ $m^2$ to $6.0x10^{-10}$ $m^2$) [34], Yuan et al. ($1.2x10^{-10}$ $m^2$ to $3.0x10^{-12}$ $m^2$) [35], and Wachel ($2.0x10^{-5}$ $m^2$ to $2.0x10^{-7}$ $m^2$) [36].

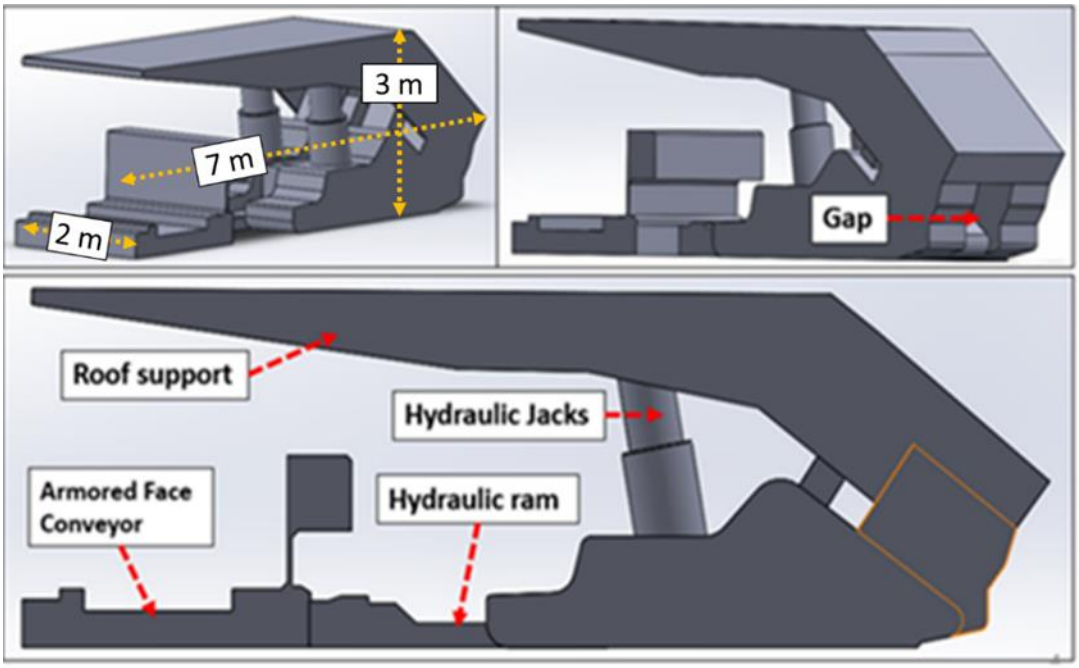


*Figure 74: Geometry of simplified longwall shield model*

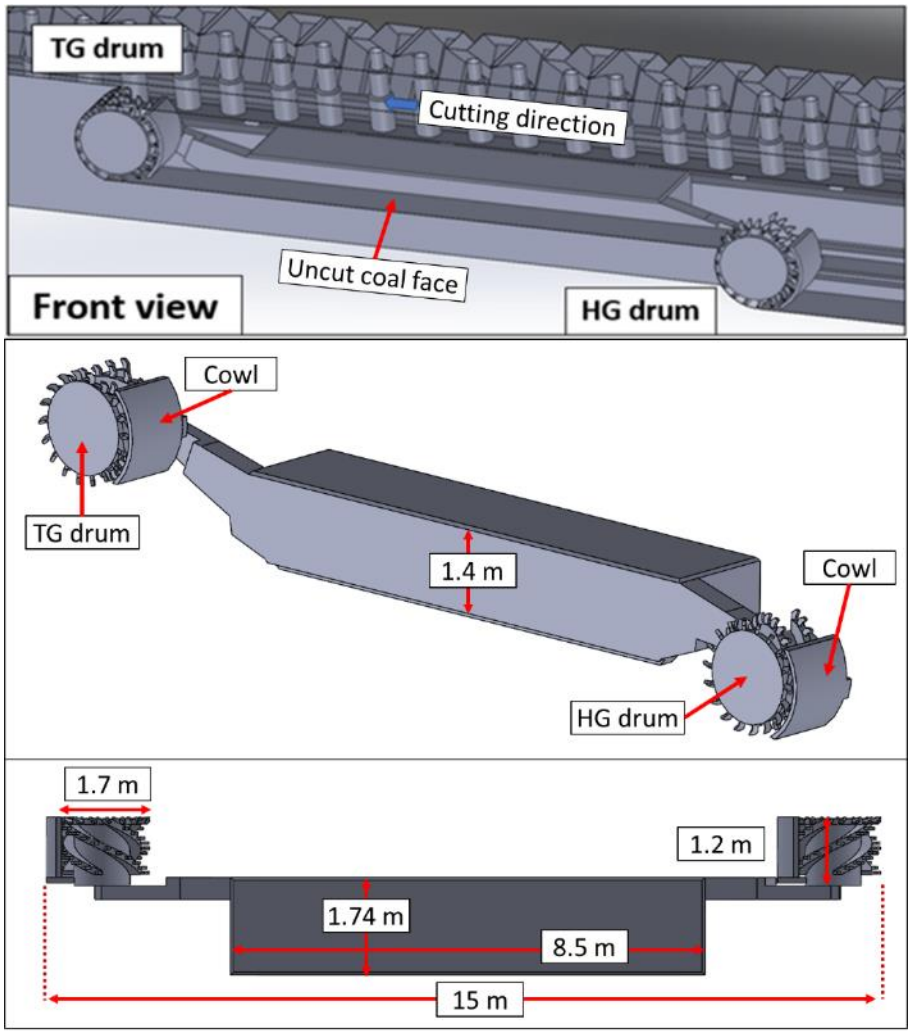


*Figure 75: Geometry of simplified longwall shearer model*

For the chosen bleeder ventilation scenario, it is assumed that the tailgate corner provides a back return, that is, the return air is coursed through the first crosscut inby the tailgate. This is common practice to clear the tailgate corner of methane accumulations. The shearer is located close to tailgate corner, between shield 140 and 146, cutting towards the tailgate. Both shearer drums are rotating at 30 RPM and shearer cowls are used.

The two headgate entries deliver a total of 55 $m^3/s$ (1942 $ft^3/s$) of fresh air to the face, a typical quantity for U.S. longwall operations. Some of that air leaks through the headgate curtains, shown as 'C' in Figure 73, resulting in 41 $m^3/s$ (1448 $ft^3/s$) of air delivered to the face. Inby the headgate, a ventilation curtain extends from the rib of the chain pillar to shield number 3 to help direct the fresh air into the face. Each of the two tailgate entries outby the face is set to supply 4.7 $m^3/s$

(166 $ft^3/s$) of fresh air. Due to the bleeder setup, most of the 41 $m^3/s$ (1448 $ft^3/s$) of face air leaks into the gob, leaving only 16 $m^3/s$ (565 $ft^3/s$) airflow at the tailgate corner. The air flow through the bleeder entries inby the face is controlled with a series of stoppings and bleeder regulators. Regulator R3 (Figure 73) is set to allow 4.7 $m^3/s$ (166 $ft^3/s$) of air to pass through, while R4 and R5 are closed to force air from the headgate entries to sweep the back end of the longwall panel. Regulator R6 is kept fully open.

To simulate ignition and methane flame propagation, researchers reduced the three-dimensional ventilation model to only contain the longwall face, a portion of the gob behind the shields extending up to 6 m (19.7 ft) deep and 3 m (9.8 ft) high, and a portion of the tailgate and tailgate bleeder entries. To maintain computational accuracy, pressure profiles obtained from the full-scale, steady state bleeder model are used as boundary conditions. Mesh sizes between 3 cm (1.18 in) to 30 cm (11.8 in) are used in the steady state fluid flow model: a 3 cm (1.18 in) mesh is used in high turbulence areas around the shearer drums, while a range of 3 - 30 cm (1.18 – 11.8 in0 mesh is used in the bulk flow regions to accurately capture the flow physics. This reduced three-dimensional model has over 31.5 million base cells before integrating the combustion model.

Limiting the model to this smaller section of the mine allows for improved cell allocation by refining the mesh in critical areas where the ignition is simulated. Once the flame expands and travels towards the model boundaries, the model will be expanded into the adjacent zones and data can be interpolated to allow flame propagation into the adjacent zones to potentially simulate the entire longwall mine model.

Table 17 lists the CFD modeling parameters and settings used with ANSYS Fluent v. 18.2 to simulate the ventilation airflow.

*Table 17: ANSYS model setting for ventilation simulation*

| Parameter | Setting |
|---|---|
| **Time** | Steady state |
| **Solver** | Pressure based |
| **Flow density** | Incompressible |
| **Species transport** | Methane – Air mixtures |
| **Turbulent model** | Realizable k-ε with standard wall function |

| | |
|---|---|
| **Solution methods** | SIMPLE scheme with second order discretization for all parameters (pressure, momentum, energy, turbulence, etc.) |
| **Convergence criteria** | $1 \times 10^{-4}$ for continuity and momentum, $1 \times 10^{-3}$ for turbulence, $1 \times 10^{-5}$ for gas species, and $1 \times 10^{-10}$ for energy<br>Grid convergence and iterative convergence was checked using velocity and methane distribution across the longwall face |
| **Boundary condition** | Pressure inlet and Pressure outlet<br>Wall roughness constant: 1; Wall roughness height: 5 cm (1.96 in) for longwall face, 20 cm (7.87 in) for mine entries |
| **Gob and uncut coal model** | Porous medium |

Figure 76 shows the resulting reduced ventilation model, showing a plan view of air flow velocity inside the longwall face, along with a close-up, isometric view of velocity contours around the shearer drums in the tailgate corner area. The longwall bleeder ventilation scheme shown in Figure 76 is used to simulate the gas flow distribution and subsequent ignition of explosive methane-air mixture.

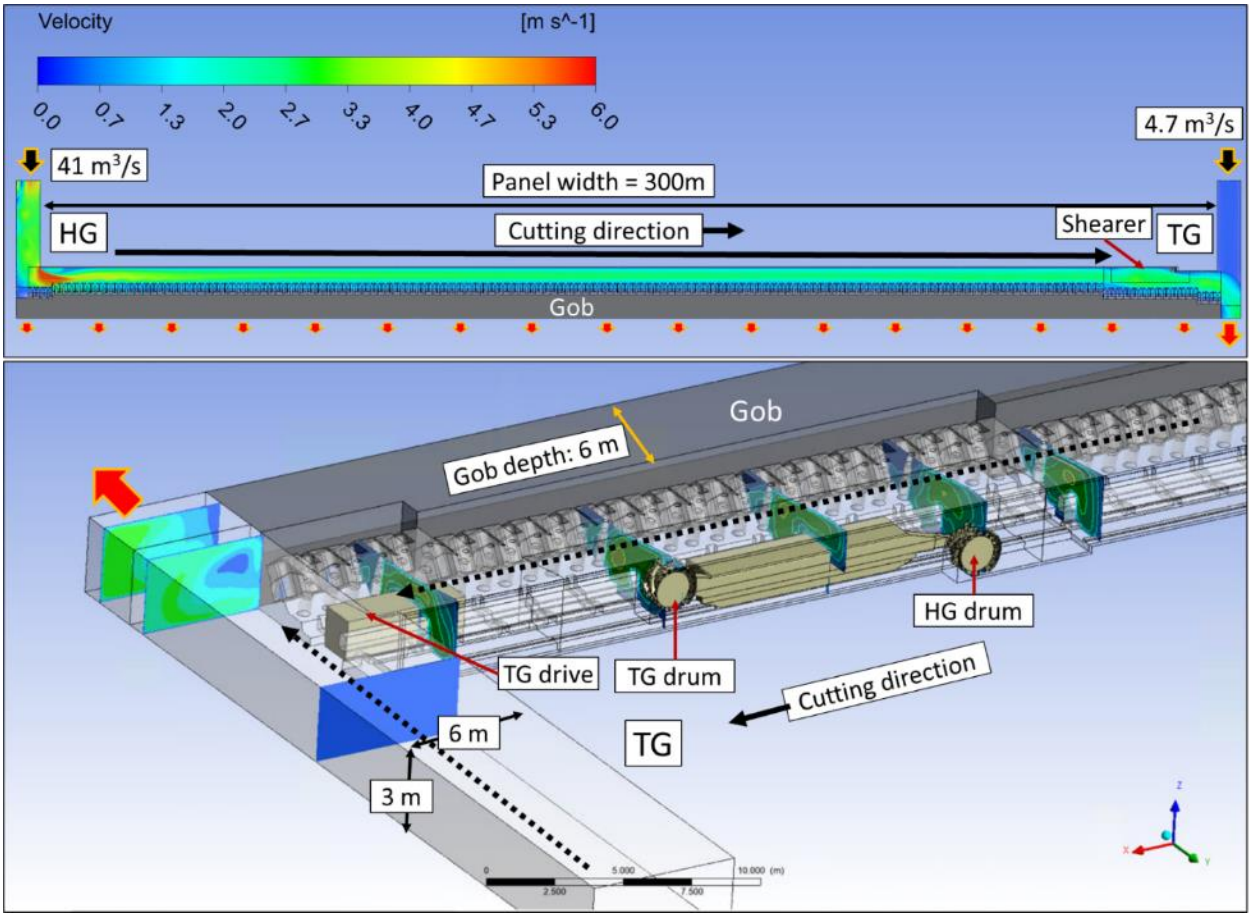


*Figure 76: Steady state volume rendering of velocity inside longwall face from plan view (top) and velocity contour plot showing close-up view of flow around shearer drums*

Figure 77 shows the CFD simulated airflow quantity declining over the length of the longwall face. Significant portions of fresh air leaks into the gob as the air travels across the face from headgate to tailgate. Leakage from the face into the gob increases if the gob fringe behind the shields has a high permeability, i.e., if it caves poorly and is only lightly compacted, or if the immediate roof has not been completely collapsed.

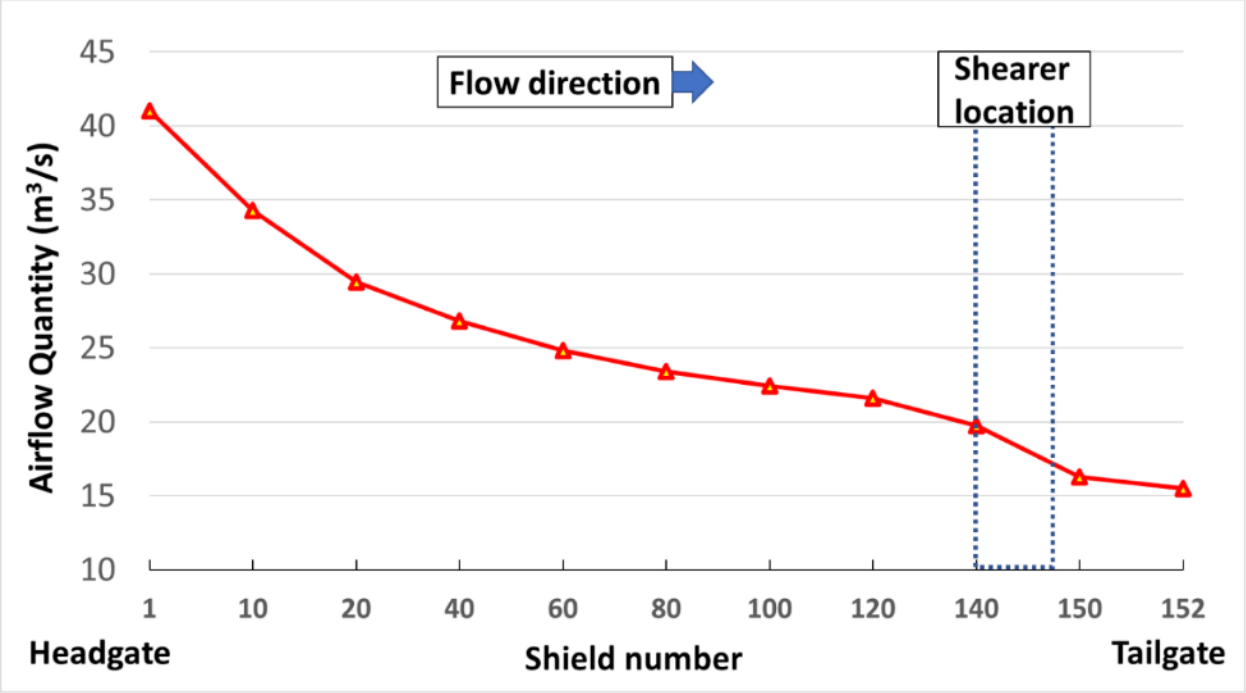


*Figure 77: Simulated airflow quantity along the longwall face*

Out of the 41 $m^3/s$ (1448 $ft^3/s$) of fresh air supplied from the headgate side of the face, only around 16 $m^3/s$ (565 $ft^3/s$) (39 % of the supplied fresh air from headgate side of the face) reached the tailgate corner due to leakage from the face to the gob. This leakage is within the expected range. According to Thakur [10], for a longwall operation with a face width of 300 m (984 ft), about 70 % of supplied fresh air may leak into the gob by the time it reaches the tailgate corner. A study using tracer gas by Krog et al. [11] on a 300 m (984 ft) longwall face reported that only about half the airflow reached the tailgate bleeder entry, while the rest leaks through the gob behind the shields.

For the methane inflow source, this study only considers methane emanating from the uncut coal face around the shearer location. To simulate methane emanating from the coal face, a 20 cm (7.87 in) thick, porous medium is modeled behind the coal face. The source term method is used to supply 0.07 $m^3/s$ (2.47 $ft^3/s$) of pure methane gas, simulating methane flowing from the cleats in the uncut coal around the shearer drums. This amount of methane resulted in a CFD model that predict close to, but still less than 2 % $CH_4$ at the shearer body and TG drive where methane sensors are usually installed in real mine operation. The amount of incoming methane gas is within the expected cumulative longwall face methane emission for 300 m (984 ft) long active face based on study by Schatzel et al. [19]. Figure 78 and Figure 79 show volume rendering of the methane mole

fraction around the shearer for this ventilation scenario, while Figure 80 shows the assumed ignition location at the top of tailgate side cutter drum. The underlying assumption is that this drum cuts into the sandstone roof where cutter bits leave hot, incendive metal smears [37]. The shearer drums are modeled as rotating drums by assigning rotating wall boundary condition with 30 RPM rotational speed, which is discussed in more detail in Juganda [24].

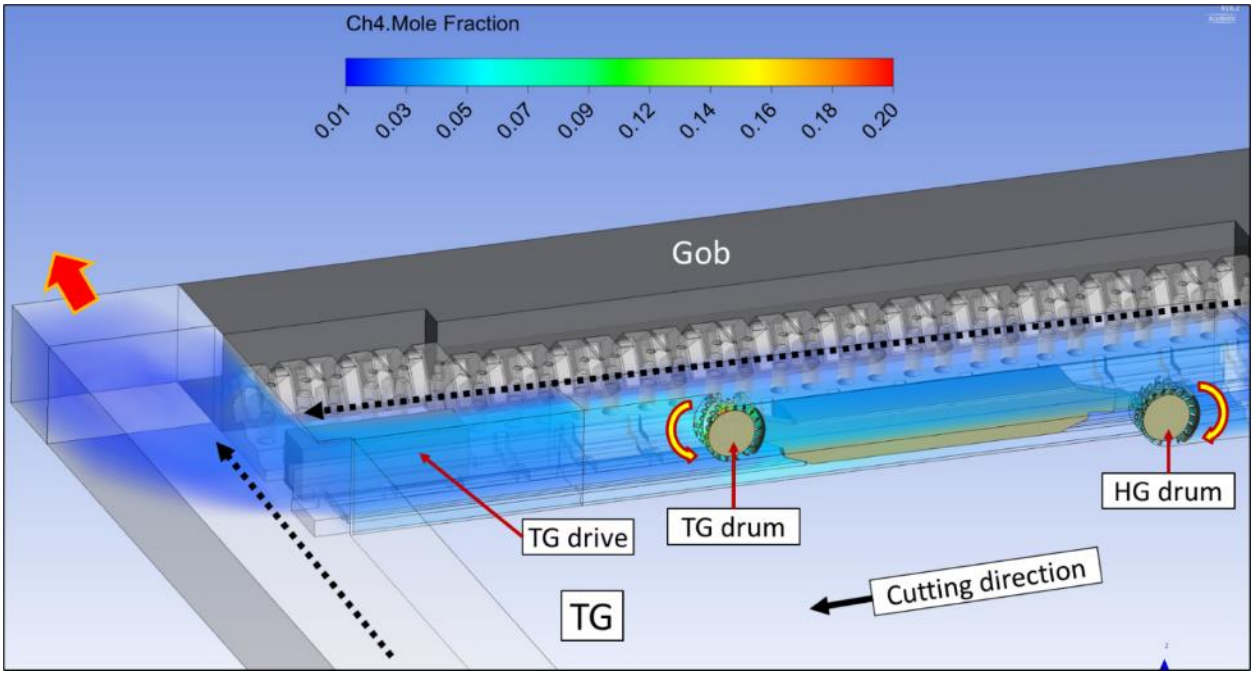


*Figure 78: Steady state volume rendering of methane mole fraction around shearer from front view*

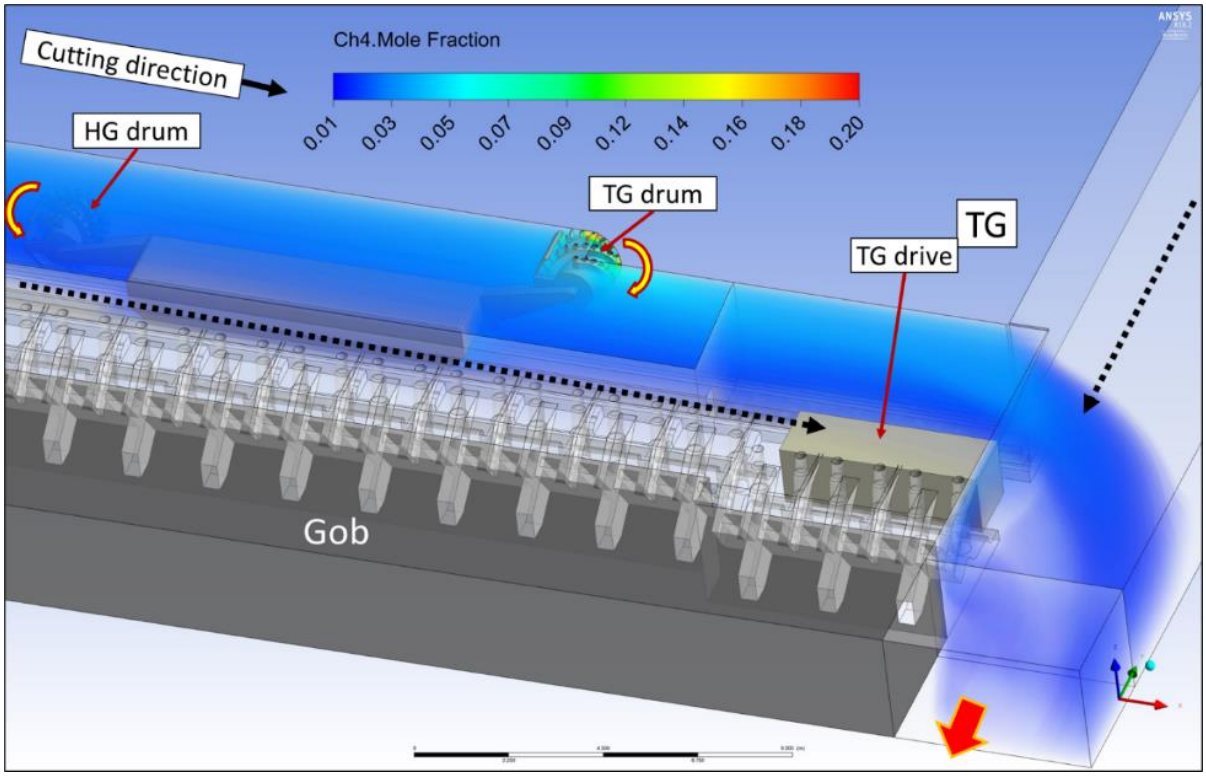


*Figure 79: Steady state volume rendering of methane mole fraction around shearer, viewed from the back side*

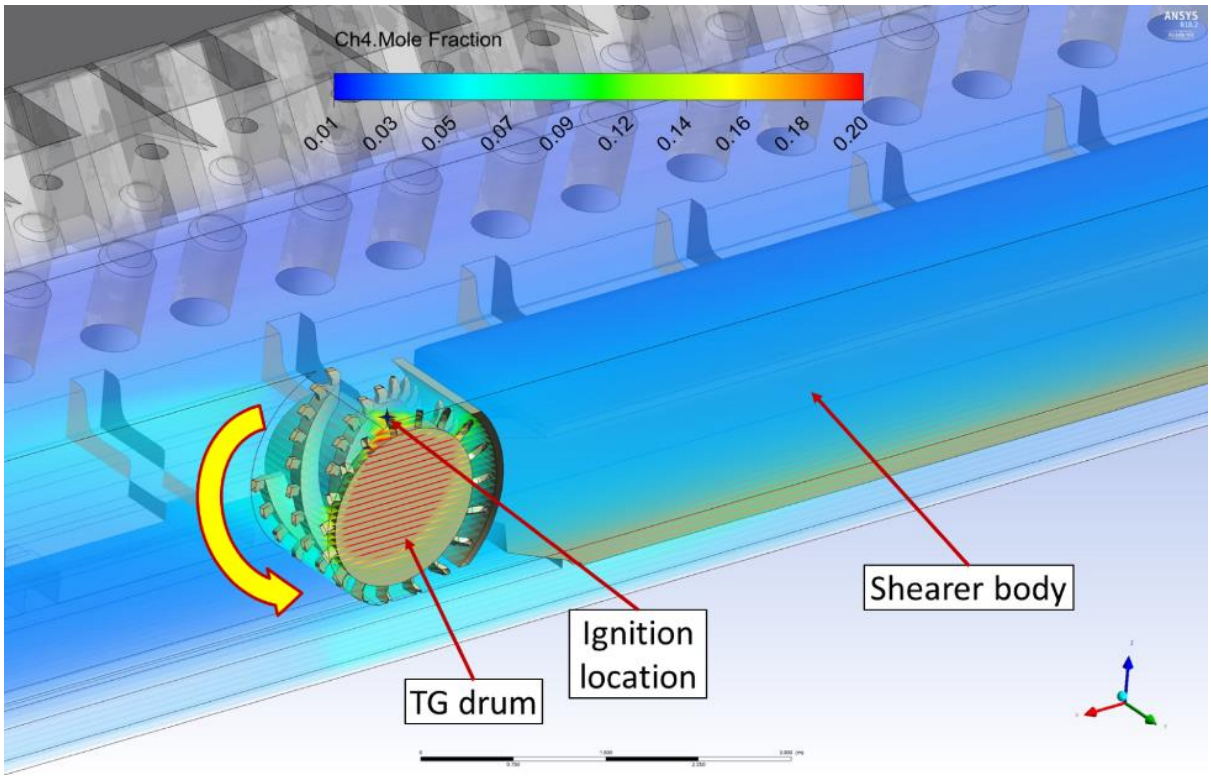


*Figure 80: Steady state volume rendering of methane mole fraction around shearer drums and ignition location*

Figure 80 shows methane accumulations between the tailgate drum and the uncut coal as well as between the tailgate drum and the cowl while the shearer is cutting towards the tailgate. For this scenario, it is assumed an ignition occurs at the coal face, near the roof, while the tailgate drum is cutting the coal face. It should be noted here that the space between the cutter and the cowl is usually filled with coal but when the shearer movement stops, this area quickly clears and will fill with explosive methane-air mixture. Furthermore, the investigation of the Upper Big Branch explosion mine revealed that non-functional dust control sprays on the cutter drum likely contributed the ignition [4].

This ignition location was chosen to represent a possible face ignition scenario during the headgate-to-tailgate cutting scenario. In the model, the shearer drums rotate with a fully developed flow. At the onset of ignition, the drum rotation at 30 RPM (~2.8 m/s (9.2 ft/s) linear velocity) is significantly slower compared to the pressure wave generated during the simulated methane combustion event; thus, the drum rotation is switched off and the drums are treated as stationary to simplify the model during the explosion simulation. Considering the time scale of the explosion, on the order of milliseconds, the continuous movement of the shearer and rotation of the drums does not have a significant impact on the pressure waves generated from the methane ignition. During the first 5 ms, the cutter bits will advance a distance of ~14 mm (0.55 in), less than half the diameter of a cutter pick.

**Integration of the CFD Combustion Model**

Methane combustion modeling is computationally intensive and has more restrictions on mesh size and quality than modeling non-reactive fluid flow. For example, laminar methane-air flames have a flame thickness on the order of 1 mm (0.04 in) and a quenching distance of 2 – 3 mm (0.08 – 0.12 in) for a stoichiometric flame (9.5 % methane by volume) at 300 K (80.3 °F) and 101 kPa (14.65 psia) [38], [38]. For modeling purposes, the mesh size should be less than a millimeter to resolve the chemical reaction zone and not larger than a few millimeters to resolve the temperature and specifies gradients immediately upstream of the reaction zone in order to fully resolve the propagation of the flame front. The fluid flow boundary layers and other key fluid flow features in full-scale ventilation model are much larger than the flame thickness; thus, the base mesh for the fluid flow can be larger than what is required to fully resolve the flame reaction front. Therefore,

mesh adaptation is important to ensure model accuracy under acceptable computational times. To resolve the flame front propagation, the model uses 3 levels of mesh adaption on the temperature gradient resolve the flame front each time step. This method has proved useful when simulating methane combustion in both small and large domains [39], [40].

After steady state simulation of the ventilation conditions, the model settings are changed to simulate a transient combustion event. The model settings for ignition and subsequent methane flame propagation are shown in Table 18 and the two-step methane-air reaction mechanism settings are detailed in Table 19 and Table 20. Reaction parameters 1 and 2 required for the Arrhenius rate equation were taken from Dryer & Glassman [41]. When simulating the combustion event, the model is run as transient to understand the time-varying nature of the methane flame and pressure wave propagation. The turbulent model used for modeling flame interaction with obstacles (i.e. shearer) is a standard k-ω with low Reynolds corrections and shear corrections. The other major change is the change from incompressible to compressible flow which is necessary for accurate simulating methane deflagrations. Finally, it is important to note the changes in time steps as the simulation progresses. A time-step of 10 μs to resolve the reaction kinetics during the early stage of flame expansion, which is then increased to 20 μs and 40 μs after certain time periods as the flame propagate into region with larger base mesh to speed up the simulation time.

*Table 18: ANSYS Fluent v 18.2 model settings for methane combustion*

| Parameter | Setting |
|---|---|
| **Time** | Transient |
| **Solver** | Pressure based |
| **Turbulent model** | Standard k-ω model, with low Reynolds number corrections and shear flow corrections |
| **Species transport** | volumetric reactions, finite rate chemistry, laminar flame speed theory |
| **Chemical mechanism** | Methane-air 2 step mechanism |
| **Flow density** | Compressible |
| **Solution methods** | PISO scheme with first order discretization |
| **Convergence criteria** | $1 \times 10^{-4}$ for continuity and momentum, $1 \times 10^{-3}$ for turbulence, $1 \times 10^{-5}$ for gas species, and $1 \times 10^{-10}$ for energy |
| **Boundary condition** | Pressure inlet and Pressure outlet profile, adiabatic wall |
| **Time step** | 10 μs until 20 ms; 20 μs for 20 – 50 ms; 40 μs onward, with 200 iterations per time step |

| | |
|---|---|
| **Adaptive meshing** | 3 levels refinement based on temperature gradient every time step |

*Table 19: Arrhenius two-steps equation for methane-air two step reaction [41].*

| Reaction | |
|---|---|
| 1 | $CH_4 + 1.5\ O_2 \rightarrow CO + 2\ H_2O$ |
| 2 | $CO + 0.5\ O_2 \rightarrow CO_2$ |
| 3 | $CO_2 \rightarrow CO + 0.5\ O_2$ |

*Table 20: ANSYS Fluent 2-step methane-air chemical mechanism settings. R stands for reactant and P stands for product. Parameter values for reactions 1 and 2 are taken from Dryer and Glassman [41]*

| **Reaction** | **Molecule** | **Reaction Order** | **Path** | *A* **Pre-Exponential Factor (kmol/m$^3$)** | $E_a$ **Activation Energy (J/kg-mol)** | *b* **Temperature Exponent** |
|---|---|---|---|---|---|---|
| **1** | $CH_4$ | 0.7 | R | $5.01 \times 10^{11}$ | $2 \times 10^8$ | 0 |
| **1** | $O_2$ | 0.8 | R | | | |
| **1** | CO | 0 | P | | | |
| **1** | $H_2O$ | 0 | P | | | |
| **2** | CO | 1 | R | $2.24 \times 10^{12}$ | $1.7 \times 10^8$ | 0 |
| **2** | $O_2$ | 0.25 | R | | | |
| **2** | $CO_2$ | 0 | P | | | |
| **2** | $H_2O$ | 0.5 | P | | | |
| **3** | $CO_2$ | 1 | R | $5 \times 10^8$ | $1.7 \times 10^8$ | 0 |
| **3** | CO | 0 | P | | | |
| **3** | $O_2$ | 0 | P | | | |

Ignition was initiated using the ANSYS Fluent Spark Model (v18.2) with the following settings:

- Ignition energy, $E_{ign}$ = 60 mJ
- Ignition energy duration = 1 ms
- Initial kernel radius = 2 cm (0.79 in)
- Laminar kernel expansion

## Objective 2.4: Investigate the impact of rock rubble on the acceleration and transition to Detonation and providing data to researchers at UMD and NRL for further validation of DDT models.

Previous full-scale work with the 6.1 m (20 ft) reactor did not have a long enough runup distance relative to the reactor diameter to result in flame speeds approaching the DDT regime. One of the major benefits of the extended full scale reactor present at the GERF is having sufficient runup distance to achieve flame propagation velocities much closer to DDT. Due to extreme fire safety concerns, the decision was made to separate the reactive sections from the open end of the reactor by an air section and run the longer experiments at a 7.5 % methane concentration. This limited the potential velocity of unobstructed experiments to approximately 265 m/s (870 ft/s). Therefore, an extended rock rubble obstruction in the 22.86 m (75 ft) reactive zone was utilized to produce the higher flame propagation velocities for characterizing the runup to DDT and the impact of altering the rock rubble geometry.

### Objective 2.4.a: Various rock rubble lengths and orientations will be investigated with input from the collaborators at UMD and NRL to provide the key conditions used to validate their high-fidelity DDT models.

The extended rock rubble experiments centered the obstruction on the same point as the shorter rock rubble obstruction experiments conducted with a 23.86 m (75 ft) reactive zone (Section 3.5). The rock extended rubble obstruction was centered approximately 7.62 m (25 ft) from the gas barrier and 13 m (43 ft) from the blind. This again centered the obstruction on the joint between reactors 2 and 3, as shown in Figure 81. The total length of the obstruction was approximately 4 m (13.1 ft), with a blockage ratio of approximately 50 %. The sled used in the shorter rock rubble experiments was used as dam on the downstream end of the rock rubble obstruction to maintain the location and approximate geometry of the obstruction. This resulted in the sled being positioned entirely in reactor 3. Rocks were stacked in the remainder of the specified reactor 3 length and in reactor 2 to produce the 4 m (13.1 ft) obstruction.

This configuration was instrumented with ion sensors, pressure sensors, and the barrier break detection system. The ion sensor deployment largely matched previous configurations, with one small change. In anticipation of higher flame front velocities and to hedge against potential sensor damage from debris blown out of the reactor, the density of ion sensors was increased near the open end of the reactor. This provided a higher fidelity measurement of maximum velocities and

ensured that the sensor system could collect valuable data even if individual sensors were damaged. As discussed in section 3.1, the ion sensor system is extremely robust, with individual sensors able to provide useful data even when damaged. In addition, a pair of PCB pencil probes in axial direction were installed in the reactor, with one upstream and one downstream of the gas barrier. Radial measurements were conducted with two OMEGA pressure transducers, installed upstream and downstream of the gas barrier. The radial pressure sensors measure the absolute pressure, while the axial PCB pencil probes measure overpressure rise of the pressure wave. For comparison, the gauge pressure was converted to absolute pressure, by adding 75.8 kPa (11.7 psia).

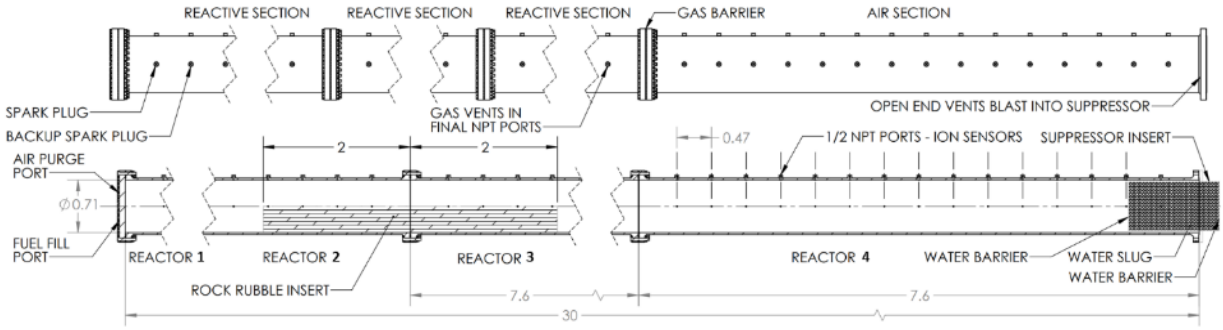


*Figure 81: Reactor configuration for 30.48 m (100 ft) experiment with a 22.86 m (75 ft) reactive zone, a water slug in the air filled section, and the extended rock rubble.*

# 4.0 Research Findings and Accomplishments

The research activities funded under Alpha Foundation grant AFSTI14FO69 produced experimental results that help to further explore and quantify the impact of rock rubble on the acceleration of flame front velocities and increased overpressures that occur during a methane-air gas explosion in a semi-confined space. The results from this study demonstrate that rock rubble obstructions significantly enhances propagation velocities and the probability of a high-speed deflagration explosion reaching the DDT regime, thereby increasing the danger of more damaging detonation. The data from a variety of experiments was used to calibrate, improve, and validate the CSM's 2D/3D cylindrical reactor gas explosion model. The CSM gas explosion model was then used to improve the accuracy and robustness of the CSM's 3D full-scale longwall explosion model which investigated a methane explosion at the face of a longwall coal mine. This improved and experimentally validated 3D full-scale longwall explosion model resulted in an improved understanding of ventilation and explosion dynamics, as a result of methane-gas ignition at the face. The experimental work required the construction of the GERF, which replaces the capabilities lost with the closure of NIOSH's Lake Lynn Lab. The GERF is already producing valuable data and is designed to be adaptable for future research projects. The GERF is now the only publicly accessible largescale (greater than 12K Liters/107 cu. ft.) flame reactor operating in North America (based on published literature), with the potential to assist on variety of related gas explosion projects. As of this report, several research groups have expressed interest in utilizing the GERF.

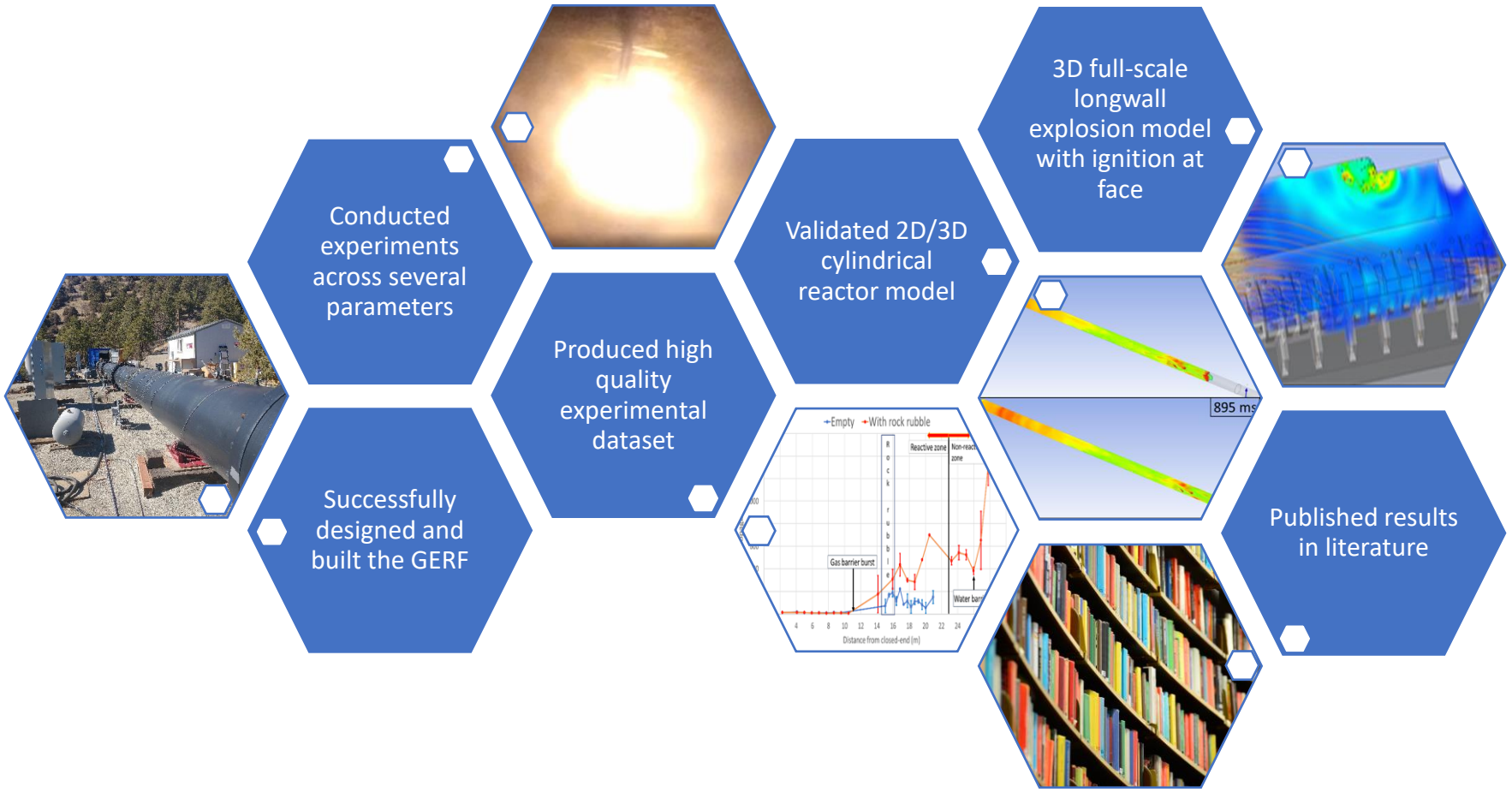
Conducted experiments across several parameters
Successfully designed and built the GERF
Produced high quality experimental dataset
Validated 2D/3D cylindrical reactor model
3D full-scale longwall explosion model with ignition at face
Published results in literature
Empty
With rock rubble
Reactive zone
Gas barrier burst
Distance from closed-end (m)
895 ms

**Objective 1: Investigate the impact of gob characteristics on the severity of large-scale methane-air gas explosions related to overpressures and flame propagation velocities.**

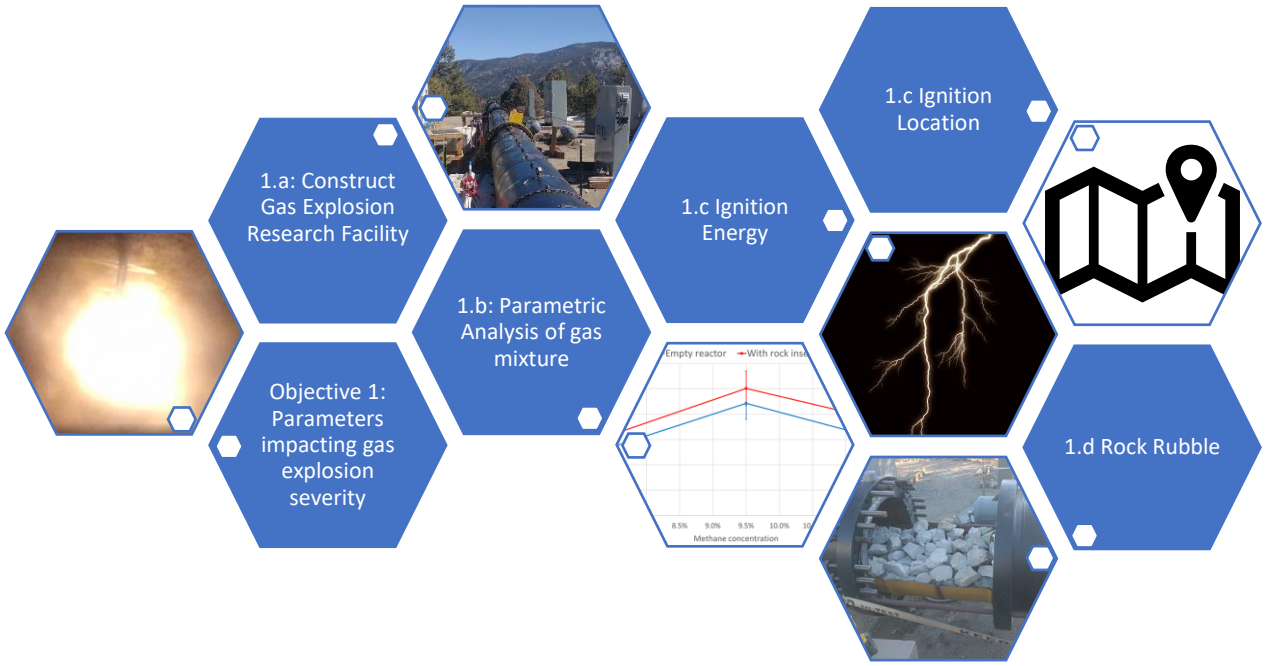


**Objective 1.a: Design, Fabricate, and Extend Existing Scaled Reactors**

The research efforts succeeded in designing the facilities necessary for the experimental work, providing a critical piece of infrastructure missing in the United States. The GERF is the only public operating and publishing large scale flame reactor of its kind in the Western Hemisphere. Other known flame rectors worldwide are listed in Table 21. In addition to successfully completing the research, this fills a key research gap in the U.S, The four major research variables under section 1; fuel concentration, ignition energy, ignition location, and rock rubble were all experimentally investigated and shown to impact the behavior of a gas explosion.

*Table 21: Known gas explosion reactors worldwide. Blank cells are unknown or unclear.*

| Vessel | Location | Status | Dimensions | Open/ closed Ends | Ignition Energy | Reactor Pressure | Deflagration Detonation | Velocity | Gases |
|---|---|---|---|---|---|---|---|---|---|
| Barbara Experimental Mine | Poland | operational | 100-m x 2-m (ID) | | | 1,200 kPa | | | Methane |
| | | operational | 200-m x 11-m² | | | 1,200 kPa | | | Methane |
| | | operational | 400-m x 11-m² | | | 1,200 kPa | | | Methane |
| Kloppersbos | Africa | operational | 200-m x 2-m (ID) | Closed @ 1 | | | | | Methane |
| NIOSH Lake Lynn Laboratory | United States | Closed | 73-m x105-cm (ID) | Closed @ 1 | 1 KJ (non-el blasting cap) | 1.2 - 1.7 MPa (Average), 7 MPa dynamic | Detonation | 1512-1863 m/s | Methane |
| State Key Laboratory of Explosion Science and Technology | China | operational | 29.6-m x 199-mm (ID) | Closed @ 1 | 40 J | 50 -72 kPa | | 370-420 m/s | Dust |
| Bergbau Forschung Versuchs-strecke | Germany | Closed | 130-m x 2.5-m | Closed @ 1 | | | | 500-700 m/s | Gas and Dust |
| Gardner | | unknown | 42-m x 0.6-m | | | 8.1 MPa | Detonation | 2200 m/s | Dust |
| Russian Scientific | Russia | unknown | 100-m x 1.45-m | Closed @ 1 | fused nichrome wire | | Deflagration | 400 m/s | propane-butane-air |
| University of Newcastle | Australia | operational | 30-m x 0.5-m(ID) | Closed @ 1 | 1-10 kJ | 0.45 MPa | Deflagration | 320 m/s | Methane |
| University of Chongqing | China | operational | 99.1-m x 0.70-m | Closed @ 1 | 375 mJ | 1.9 MPa | | 1600 m/s | Natural gas |
| University of Chongqing | China | operational | 66.5-m x 0.50-m | Closed @ 1 | 375 mJ | 1.9 MPa | | 1000 m/s | Natural gas |
| Nanjing Tech University | China | unknown | 8-m x 6-cm(ID | Closed @ 1 | 0-5 J | 1.86 MPa | Detonation | 1990 m/s | Methane |
| University of Beijing | China | unknown | 29.6-m x 0.2-m(ID) | Closed @ 1 | | 70 kPa | Deflagration | 370 m/s | Dust |
| CSM-GERF | United States | operational | 30-m x 0.71-m(ID) | Closed @ 1 or both | 60-1,200 mJ | 720 kPa | Deflagration/ Detonation | ~2000 m/s | Methane & mixture |

## Objective 1.b: Testing of methane-air across a range of methane %vol.-concentrations, and also include various mixtures of other flammable gas species and their relative impact on explosion dynamics

A parametric analysis was done with a 15.24 m (50 ft) reactor. The variables in the analysis were the fuel concentration and the reactive zone length. The experiments were run lean (7.5%), stoichiometric (9.5 %), and rich (11.5 %) with 7.62 m (25 ft) and 15.24 m (50 ft) reactive zones as shown below Figure 82. The experiments with the stoichiometric mixture of methane show in both setups the highest maximum flame speed, as was expected with the ideal chemistry. Figure 84 shows the impact of the water barrel, which was installed at the open-end. The methane concentration was 7.5 %. It can be seen of the water barrel influences the maximum flame front propagation velocity acting as a suppressor. Table 22 presents the list of experiments in this parametric analysis.

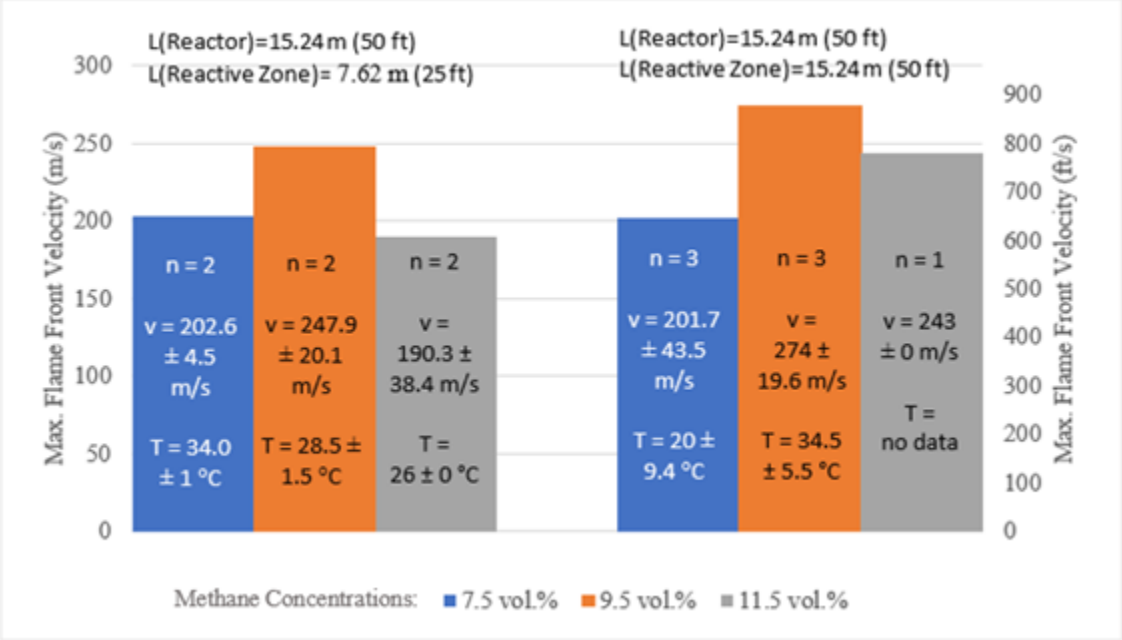


*Figure 82: Bar chart of experiments with different methane concentrations (7.5 vol.%, 9.5 vol.%, and 11.5 vol.%) and varying reaction zones. Ignition location: closed-end; n = number of tests of each condition, v = max average flame front velocity of each condition with the standard deviation. T = average ambient temperature measured on the side at the time of ignition with the standard deviation. Vessel pressure at ignition = 82.73 kPa (~12 psia)*

Figure 83 compares the maximum radial pressure of two different methane concentrations: 7.5 vol.% and 9.5 vol.%. The experiments were conducted in the 15.24 m (50 ft) reactor with a 15.24 m (50 ft) reactive zone with no rock rubble. The pressure was measured in Reactor 1. The pressure wave results in a higher magnitude for the stoichiometric gas mixture. In addition, a pencil probe style pressure sensor was installed 6 m (20 ft) from the open-end of the reactor to measure the axial pressure wave. A mitigation of 15 % of the pressure wave was recorded inside the conex.

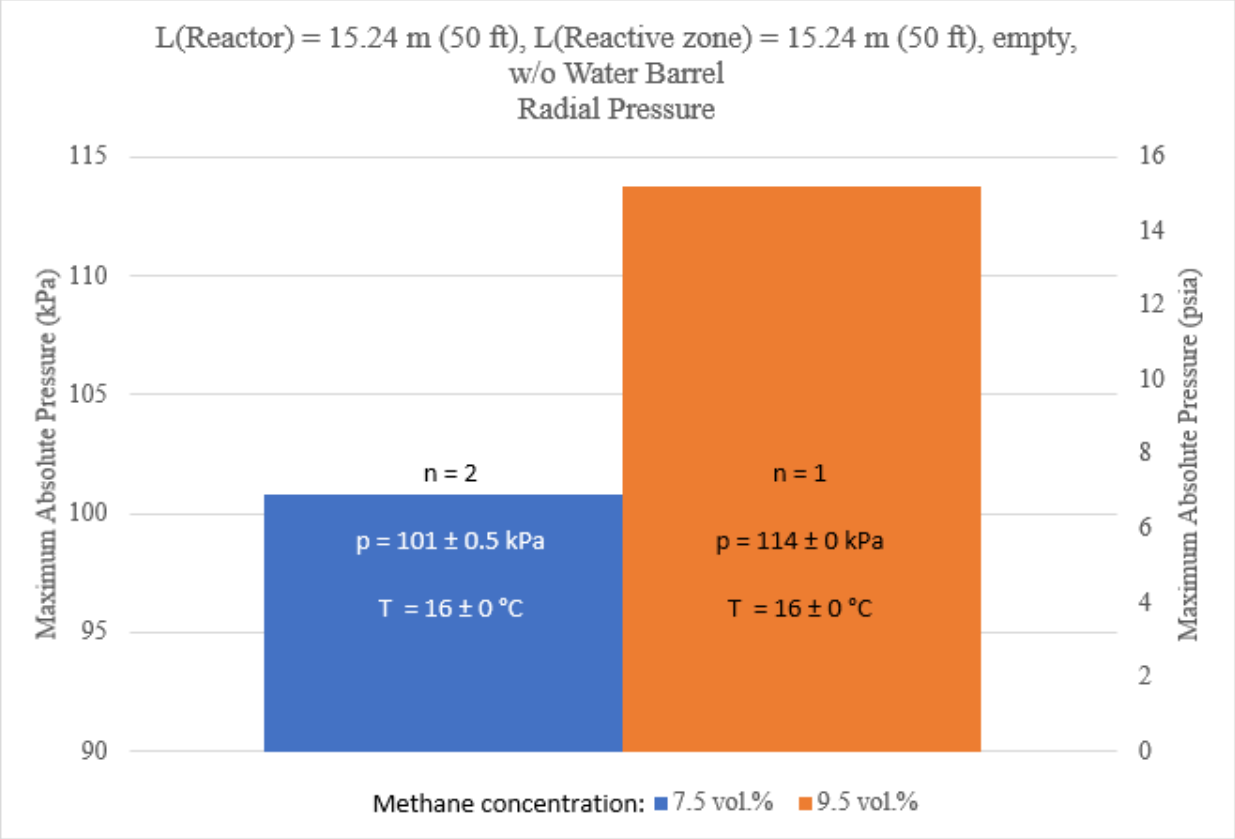


*Figure 83: Maximum radial absolute pressure results; Sensor location = reactive zone; Reactive zone = 22.86 m (75 ft); Methane concentration = 7.5 vol.% and 9.5 vol.%. n = number of tests of each condition, p = max average radial absolute pressure of each condition with the standard deviation; Vessel pressure at ignition = 82.73 kPa (~12 psia)*

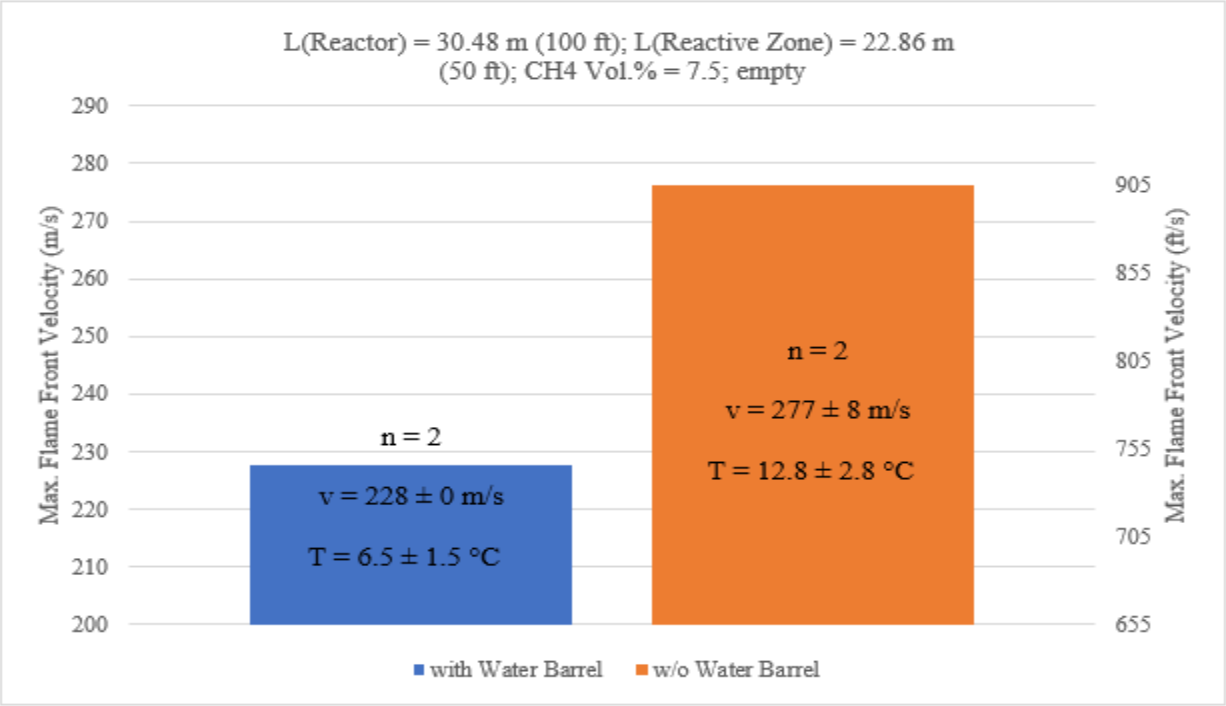


*Figure 84: Impact of water barrel at the open end of the reactor on the max flame front propagation velocity; n = number of tests of each condition, v = max average flame front velocity of each condition with the standard deviation. T = average ambient temperature measured on the side at the time of ignition with the standard deviation. Vessel pressure at ignition = 82.73 kPa (~12 psia)*

*Table 22: Parametric Analysis of methane concentration*

| Reactor Length (m (ft)) | Reactive Zone (m (ft)) | $CH_4$ | Obstacles | Ignition location | Number of tests | Water Barrel |
|---|---|---|---|---|---|---|
| 15.24 m (50 ft) | 7.62 m (25ft) | 7.50 % | Empty | closed end | 2 | no |
| 15.24 m (50 ft) | 7.62 m (25ft) | 9.50 % | Empty | closed end | 2 | no |
| 15.24 m (50 ft) | 7.62 m (25ft) | 11.50 % | Empty | closed end | 2 | no |
| 15.24 m (50 ft) | 15.24 m (50 ft) | 7.50 % | Empty | closed end | 4 | no |
| 15.24 m (50 ft) | 15.24 m (50 ft) | 9.50 % | Empty | closed end | 3 | no |
| 15.24 m (50 ft) | 15.24 m (50 ft) | 11.50 % | Empty | closed end | 1 | no |
| 30.48 m (100 ft) | 22.86 m (75 ft) | 7.50 % | Empty | closed end | 2 | yes |
| 30.48 m (100 ft) | 22.86 m (75 ft) | 7.50 % | Empty | closed end | 2 | no |
| 30.48 m (100 ft) | 22.86 m (75 ft) | 7.50 % | Empty | mid | 1 | yes |

## Objective 1.c: Investigating the impact of ignition energy and location on flame propagation velocities and overpressures

Figure *85* shows the maximum flame velocity for two different ignition locations. The experiments with the closed-end ignition result in a substantially higher flame velocity than the experiments with a mid-reactor ignition. This matches the theoretical expectation of a lower overall flame propagation velocity. This result was expected for two reasons; a reduction in the linear length travelled by a flame front and the pressure buildup on the closed end of the reactor. The relocation of the ignition point to the center of the reactive zone resulted in two flame fronts simultaneously propagating away from the ignition point, with one half of the total run-up distance that was present from an ignition at the blind (closed) end of the reactive zone. As demonstrated by this and other research, a longer run up length for a given reactor results in an increased final flame propagation velocity, all other factors being equal. The flame front propagating towards the blind end is further stymied by the pressure buildup. The impact of pressure buildup is shown in the experiments characterizing the system performance of the GERF, where stronger gas barriers resulted in a transient pressure buildup in front of the flame front. This temporarily retarded flame propagation, until the pressure buildup was sufficient to rupture the gas barrier. As would be theoretically expected, this resulted in a substantially lower maximum propagation velocity than an ignition at the closed end with an otherwise identical reactive zone.

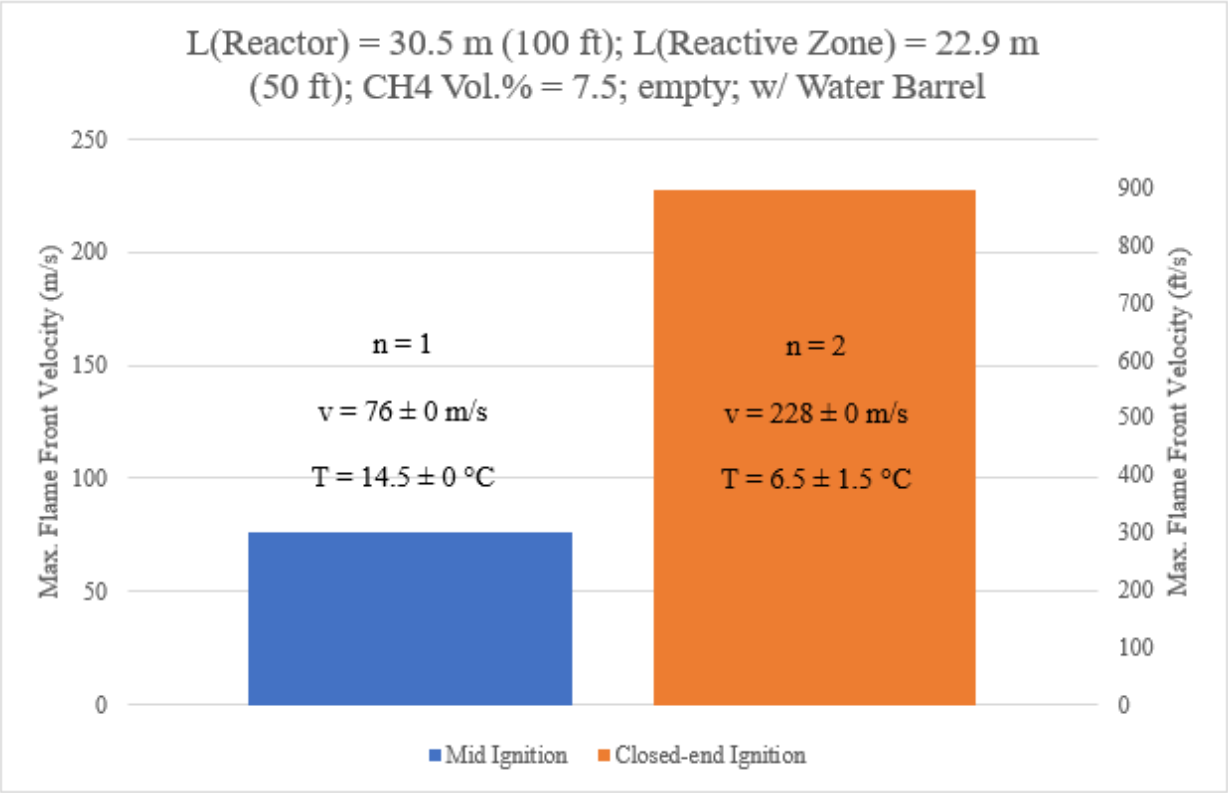


*Figure* 85*: Bar chart of experiments with different ignition locations. Methane concentration is 7.5 %. n = number of tests of each condition, v = max average flame front velocity of each condition with the standard deviation. T = average ambient temperature measured on the side at the time of ignition with the standard deviation. Vessel pressure at ignition = 82.73 kPa (~12 psia)*

Figure 86 demonstrates the increase of the magnitude of the pressure wave comparing two different ignition locations. The bar chart shows the axial absolute pressure recorded for experiments with a methane concentration of 7.5 % and a reactive zone of 22.86 m (75 ft).

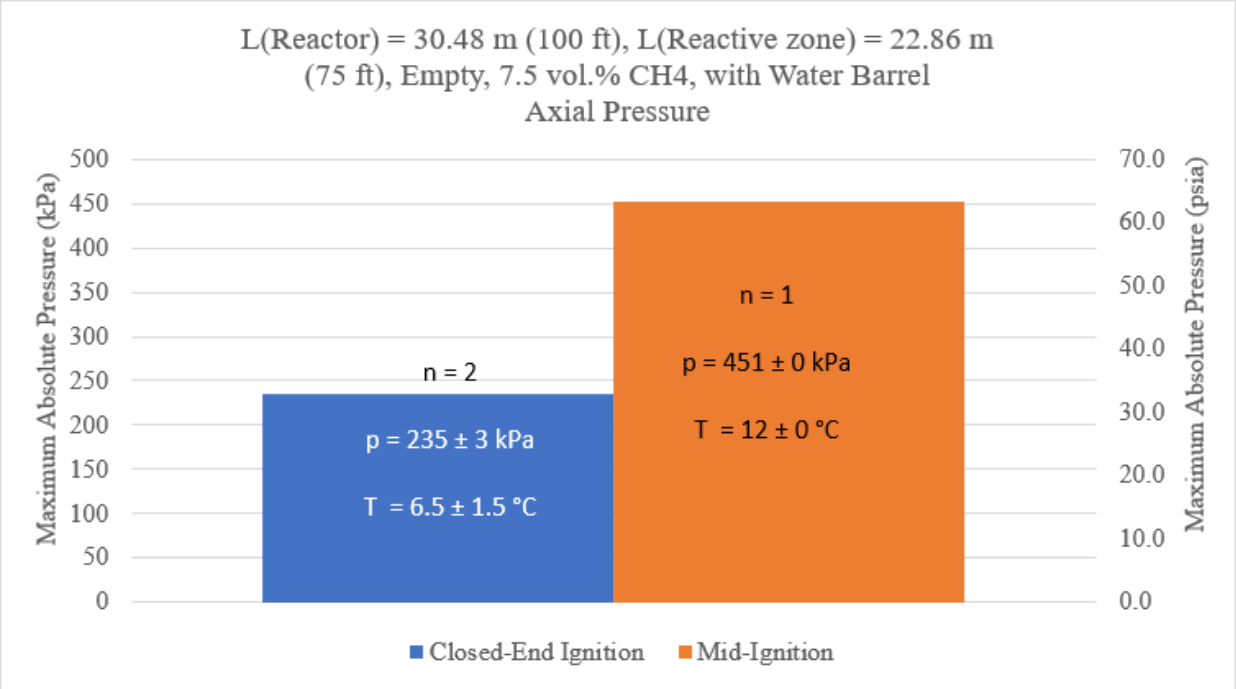


*Figure 86: Maximum axial absolute pressure results; Sensor location = reactive zone; Reactive zone = 22.86 m (75 ft); Methane concentration = 7.5 %. n = number of tests of each condition, p = max average radial absolute pressure of each condition with the standard deviation; Vessel pressure at ignition = 82.73 kPa (~12 psia)*

Experiments testing the impact of the ignition energy were performed with a stoichiometric mixture. Spark ignition energies 60 mJ, 132 mJ, and 1200 mJ were tested in the small-scale reactor. The ignition was located at the closed-end of the reactor and the methane concentration was set to 9.5 Vol%. In total five tests of each data set were conducted.

The results in Figure 87 show an impact on the flame velocity close to the open end of the reactor. For ignition energies of 60 mJ and 132 mJ, the flame velocity decreases, whereas the propagation velocity for the 1,200 mJ still increases. In addition, the decrease of the flame front velocity starts dropping earlier for the experiments with the lowest ignition energy, which happens at about 0.9 m (2.95 ft) from the ignition source. In comparison, the flame speed decreases after about 1.1 m (3.6 ft) from the ignition when using the 132 mJ ignition system.

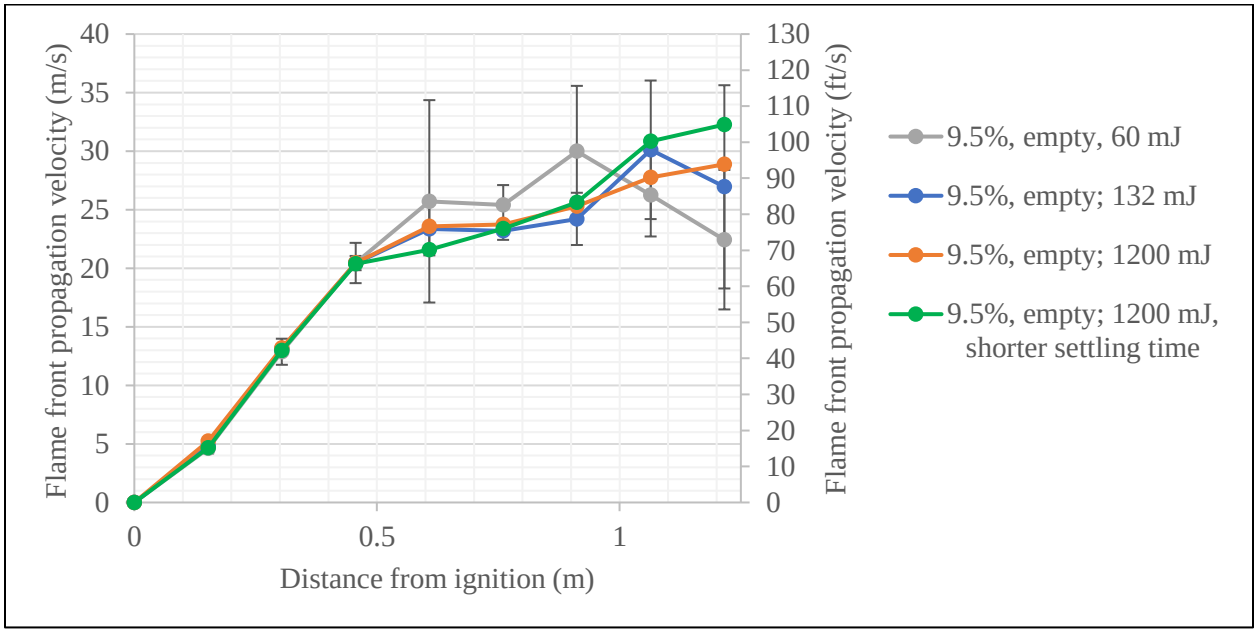


*Figure 87: Comparison of the flame front propagation velocity with different ignition energy in the small-scale reactor. Methane concentration = 9.5 %; Ignition location = Closed-end. Total number of tests: 20.*

## Objective 1.d: Investigate the impact of rock rubble geometry (e.g. length, height, and porosity) and location relative to ignition source on flame acceleration and overpressures in the high-speed deflagration regime. High-speed imaging will also be used as additional insights into the interaction of the flame and rock pile for additional validation of the CFD combustion models

The rock rubble experiments conducted at the GERF demonstrates the ability of rock rubble obstructions reducing the run-up length required for flame propagation velocities to transition from high-speed deflagrations into the DDT regime. The rock rubble experiments produced substantially higher flame propagation velocity compared to an otherwise identical unobstructed reactor. A comparison of otherwise identical obstructed and unobstructed reactors is shown in *Figure* 94. Note that the data is presented in terms of the arrival time at a distance down the reactor from the point of ignition. This effect was consistently observed with all rock rubble configurations tested, with all fuel air ratios that were tested. The longer full-scale reactor experiments also show that the acceleration of the rock rubble is persistent, resulting in an otherwise identical experiment sustaining a higher velocity in the reactor after passing the rock rubble.

This work makes multiple valuable contributions to the literature. It fills two gaps in previous work; it uses non-idealized obstructions in large scale experiments, and it captures a wider range of flame front velocities in the run up to the DDT at a larger scale. This provides experimental proof that rubble and potentially many other internal geometries that cause turbulence can cause flame propagation to accelerate. Thereby reducing the distance required for a deflagration to reach the DDT and turn into a more destructive detonation. Previous work at Mines demonstrated this at a smaller scale. The trend holds at the large scale in, as shown in Figure 88. Furthermore, the results of this research show that the geometry is scalable. The data from this research provides robust experimental evidence that obstruction can alter the requirements for a detonation to occur, confirming the importance of obstructions and internal geometries to explosion safety.

Rock rubble experiments were conducted with all three reactive zone lengths: 7.62 m (25 ft), 15.24 m (50 ft), and 22.86 m (75 ft). The 7.62 m (25 ft), 15.24 m (50 ft), and the 22.86 m (75 ft) experiments are in section (Objective 1.d). Varying rock rubble dimensions and near DDT velocities are presented with Objective 2.3.

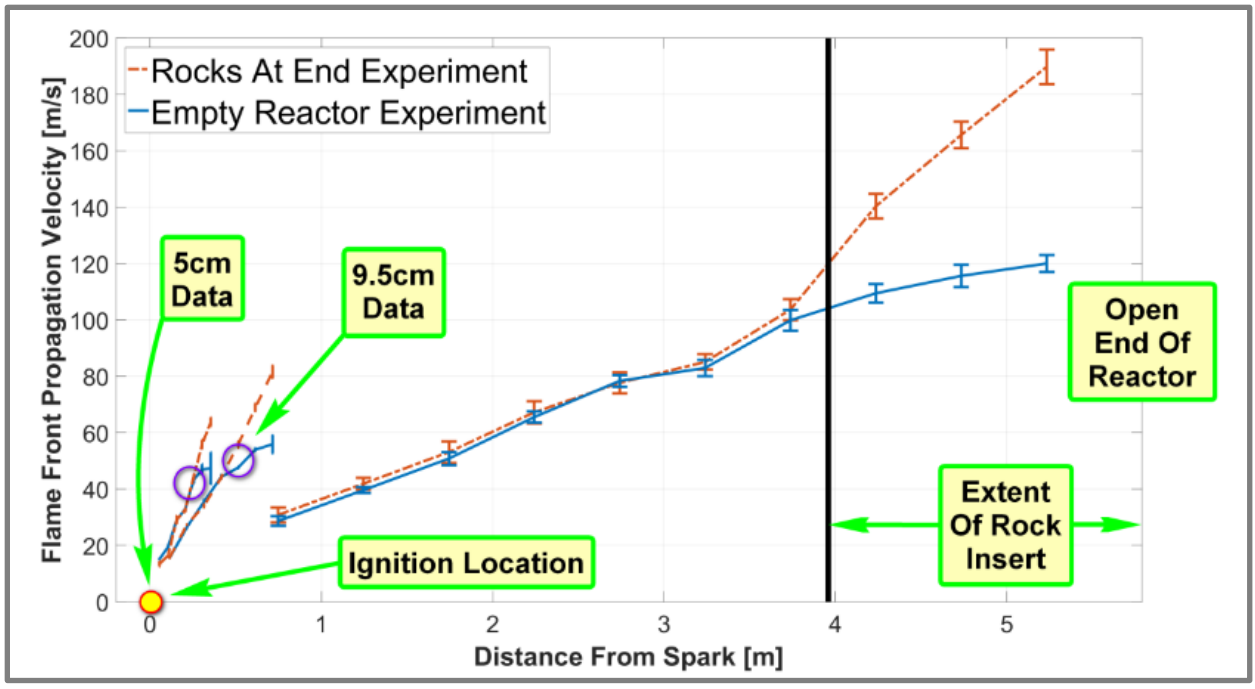


*Figure 88: Comparison of experimental results for the 5 cm (1.97 in), 9.5 cm (3.74 in), and 71 cm (28 in) diameter reactors with stoichiometric methane-air mixtures. The ignition takes place near the closed end of the reactor, and the rock insert was placed at the open end.*

**Rock Rubble in 7.62 m (25 ft) Parametric Experiments**

Figure 89 shows the results of experiments for two different methane concentrations (7.5 % and 11.5 %) and the impact of the rock rubble comparing these concentrations. The results show that the average maximum flame propagation speed is about 1.5 times higher with a lean mixture of methane.

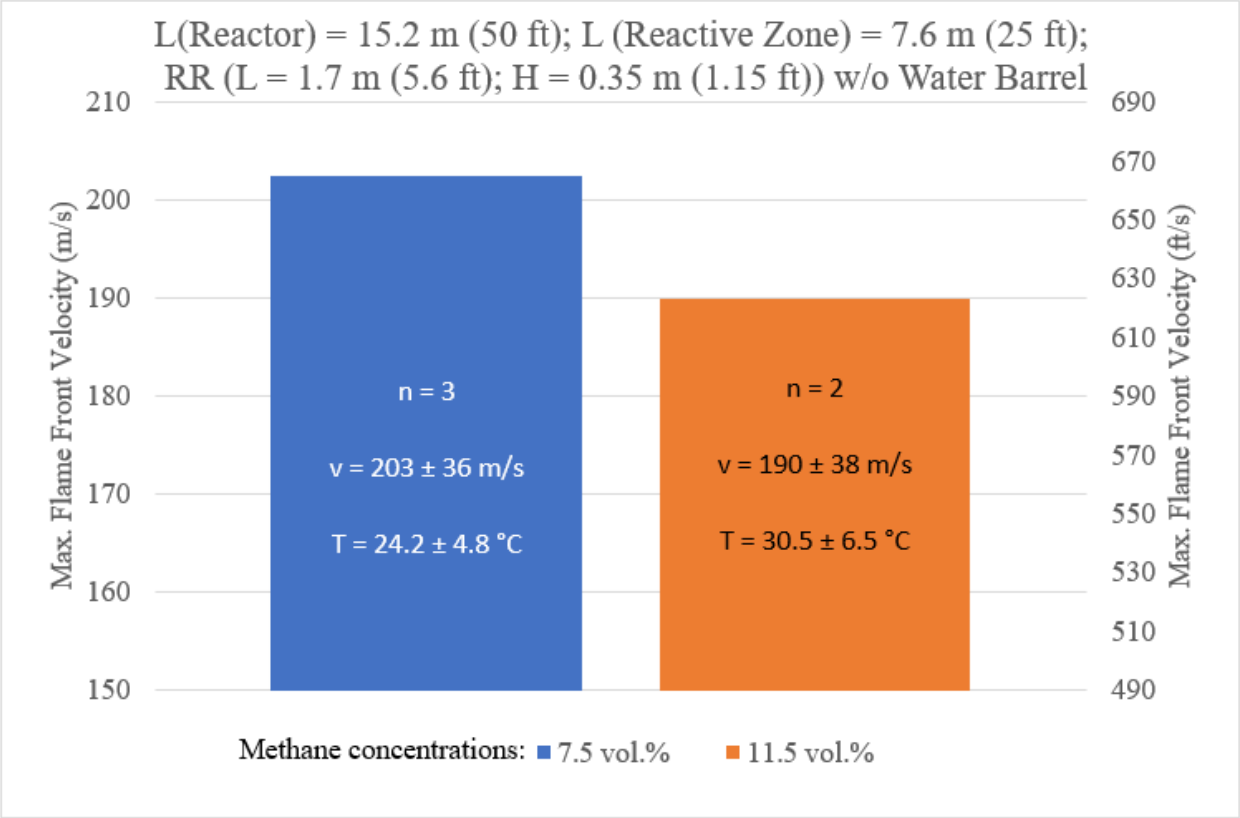


*Figure 89: Impact of the methane concentration (7.5 vol.% and 11.5 vol.%) with rock rubble on the maximum flame propagation velocity. RR = rock rubble test... n = number of tests of each condition, v = max average flame front velocity of each condition with the standard deviation. T = average ambient temperature measured on the side at the time of ignition with the standard deviation. Vessel pressure at ignition = 82.73 kPa (~12 psia)*

*Table 23: Parametric analysis of the impact of rock rubble and methane concentration on the flame front arrival time at the end of the reactive zone in a 15.24 m (50 ft) reactor with a 7.62 m (25 ft) reactive zone.*

| | Time from ignition until 1.6 m (5.2 ft) from the end of reactive zone (ms) | |
|---|---|---|
| Reactor Length | 15.24 m (50 ft), 7.62 m (25 ft) reactive | |
| Setup | Empty residence time (ms) | Rock Rubble insert residence time (ms) |
| 7.50 % $CH_4$ | 512 | 315 |
| 9.50 % $CH_4$ | 337 | 167 |
| 11.50 % $CH_4$ | 300 | 214 |

The results of the 15.24 m (50 ft) experiments with a 7.62 m (25 ft) reactive zone are presented in Figure 90. It was found that both the empty and rock rubble experiments produced a similar distribution of velocities, with the highest velocities occurring at 9.5 % (stoichiometric). High speed camera footage was recorded from the open end of Reactor 1 during some of the 15.24 m (50 ft) rock rubble experiments with a 7.62 m (25 ft) reactive zone. The flame front accelerating across the rock rubble obstruction is shown in Figure 91, Figure 92, and Figure 93. In the figures below, the flame front can be seen before encountering the rock rubble obstruction. Prior to encountering the rock rubble, the flame front behavior was similar to that of the unobstructed reactor experiment. Once the flame front encountered the rock rubble, turbulence developed, leading to an acceleration of the combustion reaction and a sudden increase in the flame front acceleration relative to the unobstructed case. The comparison of flame front arrival times between obstructed and unobstructed 15.24 m (50 ft) experiments with a 7.62 m (25 ft) reactive zone is shown in Figure 93. Note that the plot of the arrival times diverges at the point where the flame front in the obstructed reactor approaches the rock rubble. Larger images of the flame front encountering the rock rubble obstruction are shown in Figure 95. This plot presents the flame front arrival time at specific at ion sensors. The X axis is the arrival time in ms, and the Y axis is sensor location in meters from the ignition point.

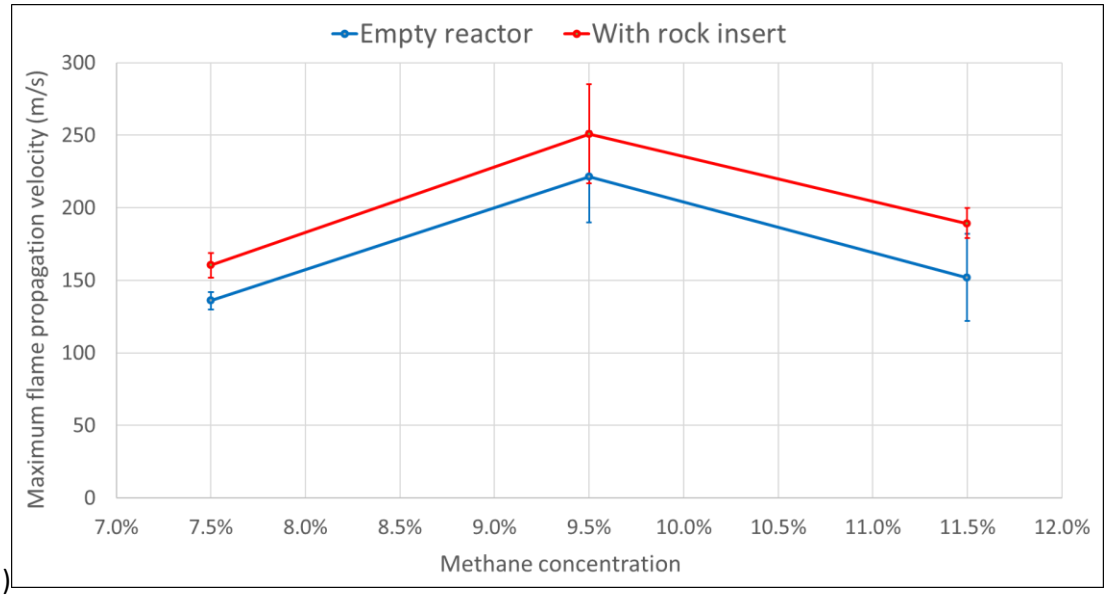


*Figure 90: Parametric analysis of flame front velocities in 15.24 m (50 ft) reactor with a 7.62 m (25 ft) reactive zone.*

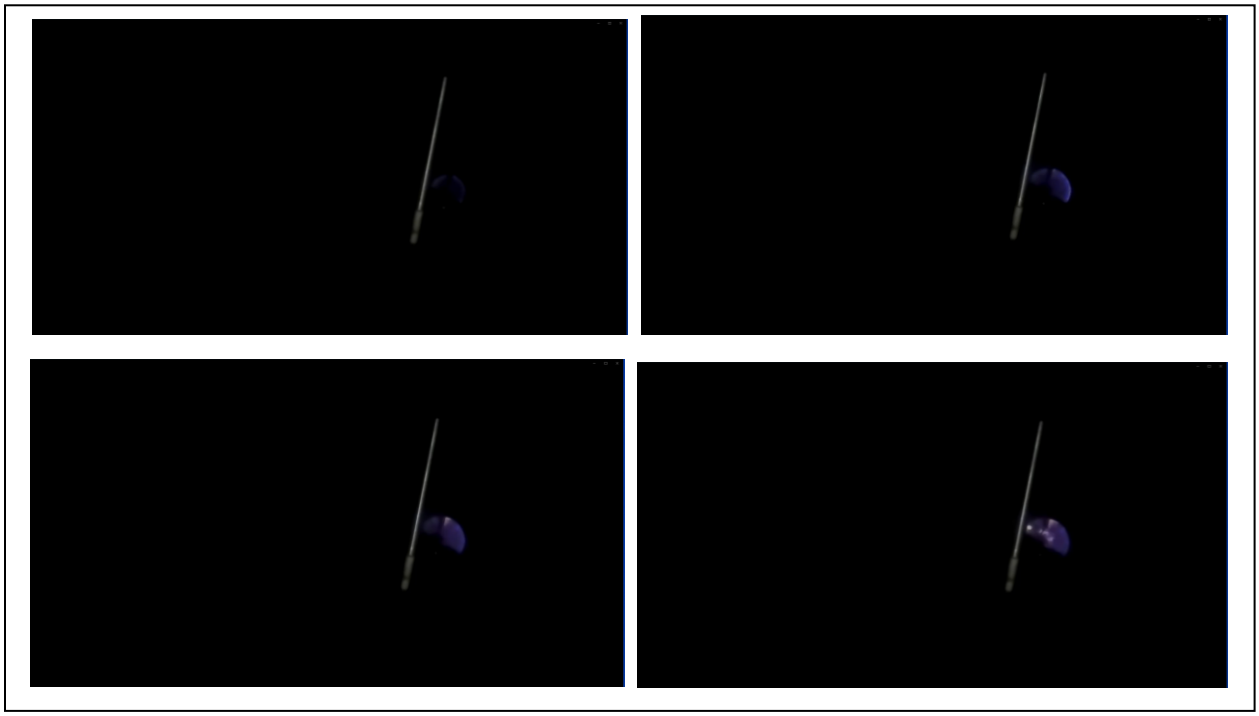

*Figure 91: High speed footage of an ignition in a 15.24 m (50 ft) rock rubble experiment with a 7.62 m (25 ft) reactive zone (5/7/2021). In these frames, the flame front can be seen developing downstream of the rock rubble obstruction. The rock rubble obscures the bottom half of the initial flame and is silhouetted in black. The rod in the foreground is an ion sensor.*

*Figure 92: Footage of the flame front accelerating rapidly when encountering the rock rubble obstruction. This increase flame velocity can be seen in Figure 94 showing the comparison between empty and rock rubble flame front arrival times.*

*Figure 93: Flame front accelerating after crossing the rock rubble.*

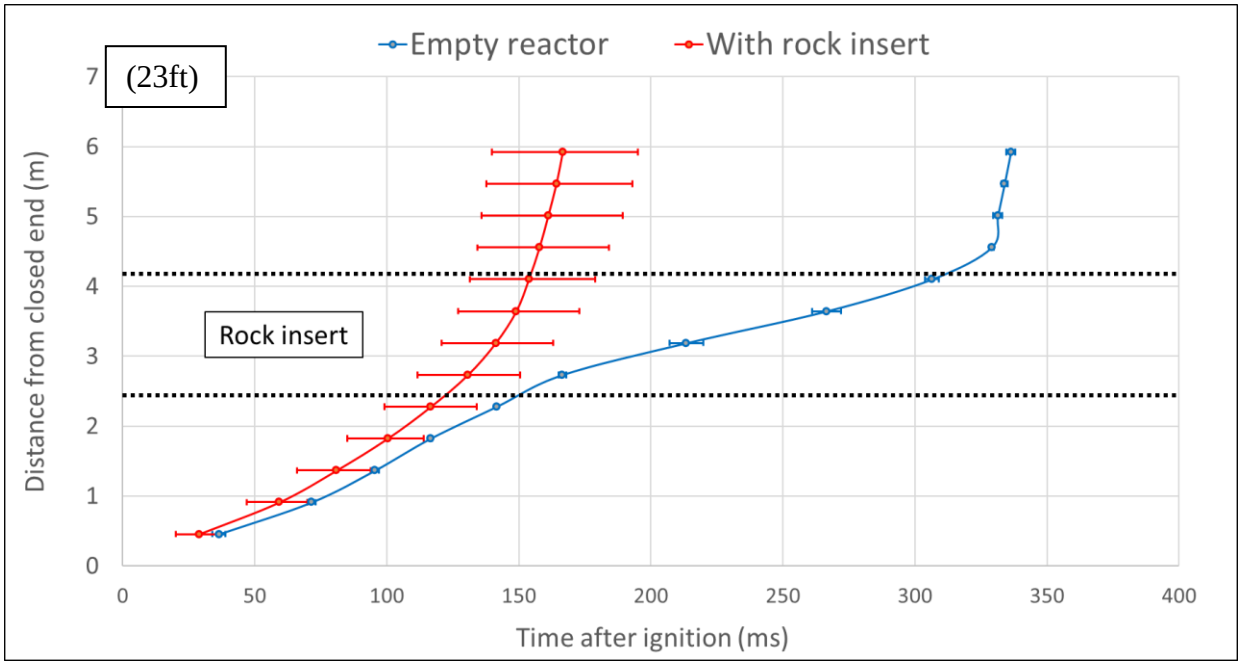


*Figure* 94*: Comparison of the flame front arrival time (x-axis) and the position (y-axis) of a 1.7 m (5.6 ft) rock rubble obstructed reactor and an unobstructed reactor. The experiments were conducted in a 15.24 m (50 ft) with a 7.62 m (25 ft) reactive zone at 9.5 vol.% $CH_4$.*

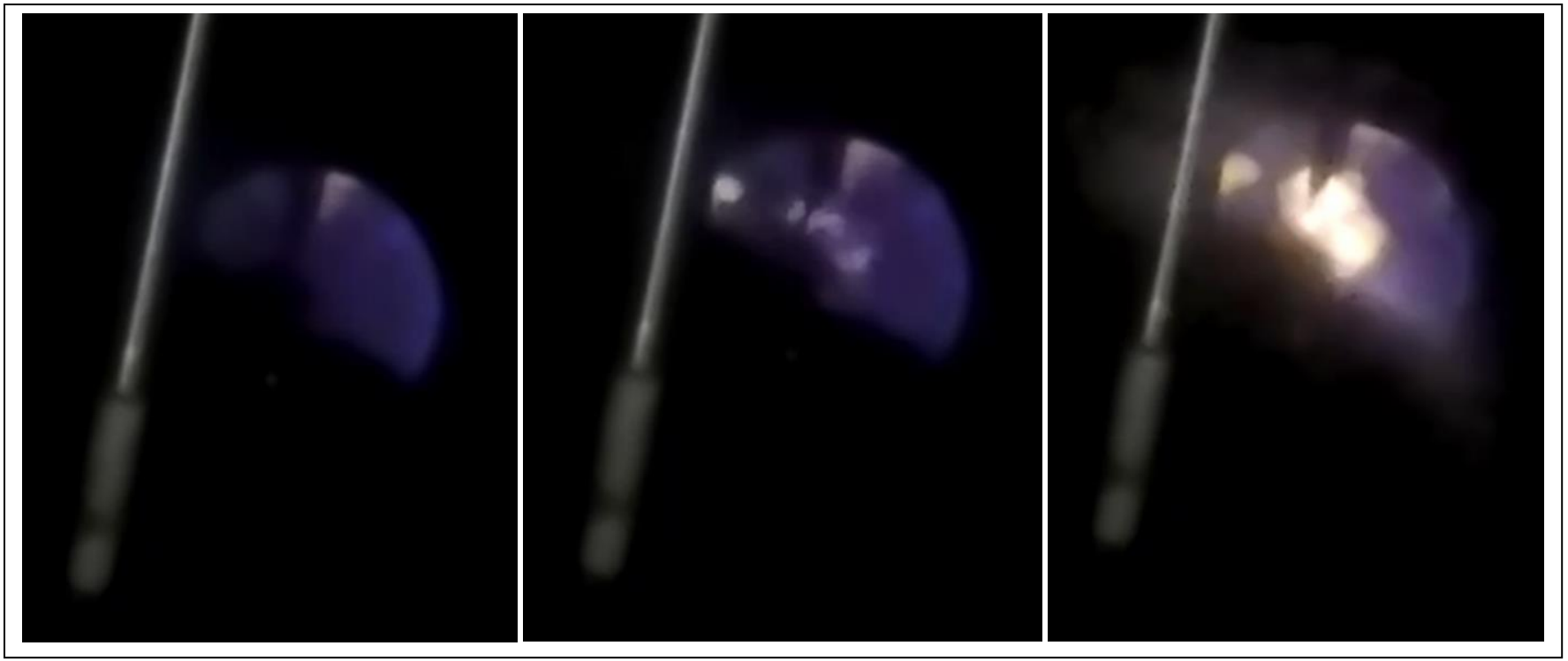

*Figure 95: Turbulence developing as the flame front passes over the rock rubble obstruction and begins rapidly accelerating. The rod in the foreground is an ion sensor.*

The development of turbulence and acceleration of the flame front propagation velocity can be seen in Figure 95. In these images, the flame rock rubble obstruction is in the lower portion of the reactor. The visible flash is the emission of black body radiation from the burning particles and local quenching of the flame as it interacts with the rock rubble pile. The yellow glow is black body radiation emitted from dust particles and unburned fuel producing hot soot particles. Dust particles are picked up when the flame front and leading pressure wave passes through the rock rubble.

**Rock Rubble in 15.24 m (50 ft) Experiments**

Figure 96 illustrates the impact of obstacles on the maximum flame speed. The left set of data shows experiments done without rock rubble, whereas the right data set show experiments conducted with the rock rubble (length = 1.7 m (5. ft)) placed in the middle of the reactor. In this case, the average max flame velocity is higher with the rich methane mixture (11.5 %), whereas in the previous case, the lean mixture (7.5 %) resulted in higher flame velocities. This shows also an impact of the length of the reactive zone. As observed previously, the rock rubble has a significant impact acceleration of the flame for both methane concentrations.

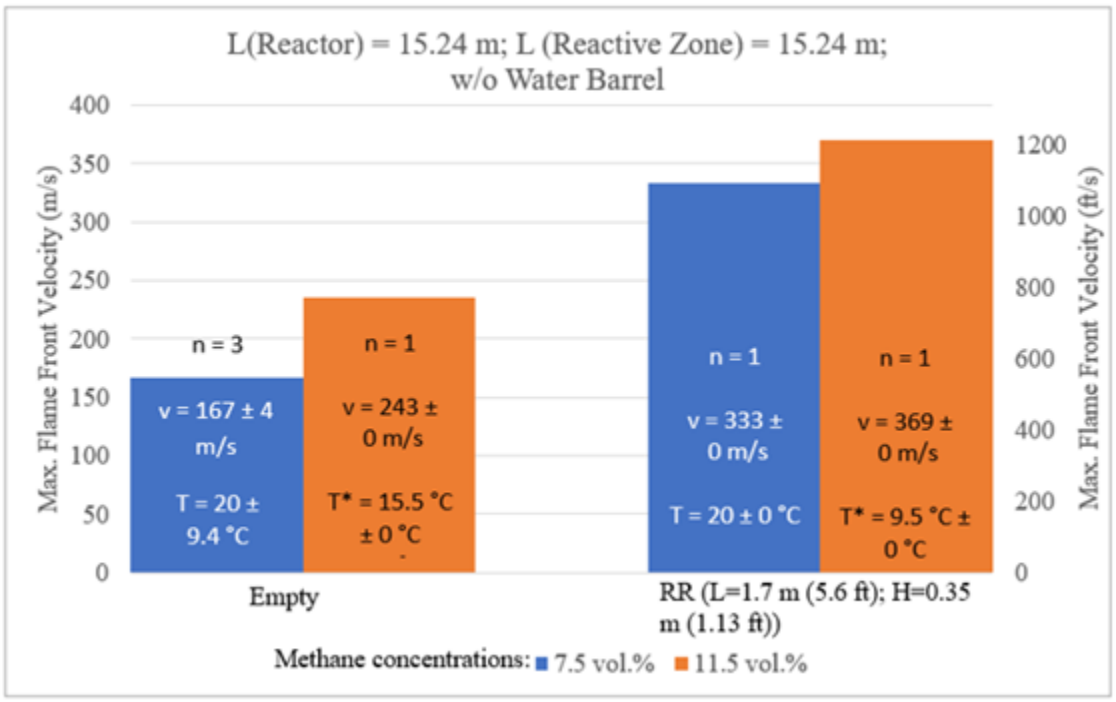


*Figure 96: Impact on the maximum flame propagation velocity for different methane concentrations (7.5 vol.% and 11.5 vol.%), with and without rock rubble. RR = rock rubble test. n = number of tests of each condition, v = max average flame front velocity of each condition with the standard deviation. T = average ambient temperature measured on the side at the time of ignition with the standard deviation. T* = temperature from weather station for Idaho Springs, CO. Vessel pressure at ignition = 82.73 kPa (~12 psia)*

*Table 24: Parametric analysis of the impact of rock rubble and fuel concentration (%volume) on the flame front arrival time at the end of the reactive zone in a 15.24 m (50 ft) reactor with a 15.24 m (50 ft) reactive zone.*

| | Time from ignition until 1.6 m (5.25 ft) from the end of reactive zone (ms) | |
|---|---|---|
| Reactor Length | 15.24 m (50 ft), 15.24 m (50 ft) reactive | |
| Setup | Empty residence times (ms) | Rock Rubble insert residence times (ms) |
| 7.50 % $CH_4$ | 497 | 299 |
| 9.50 % $CH_4$ | 256 | - |
| 11.50 % $CH_4$ | 305 | 205 |

The trend holds with the unobstructed 15.24 m (50 ft) reactor with a 15.24 m (50 ft) reactive zone as shown in Figure 97. The stoichiometric (9.5 %) experiments produced the highest flame front velocities, followed by the fuel rich 11.5 % and finally the 7.5 % experiments. Additionally, a 7.5 % and an 11.5 % rock rubble experiment with a 15.24 m (50 ft) reactive zone and no water suppression were conducted to determine the maximum allowable energy with the light duty suppression system. That was reached with the 11.5 % rock rubble experiment, and the suppression system was reconfigured to the heavy-duty water-based design used for high energy experiments. The parametric work confirmed that stoichiometric was producing the highest velocity experiments and showed that rock rubble followed the same velocity pattern as the unobstructed reactor experiments.

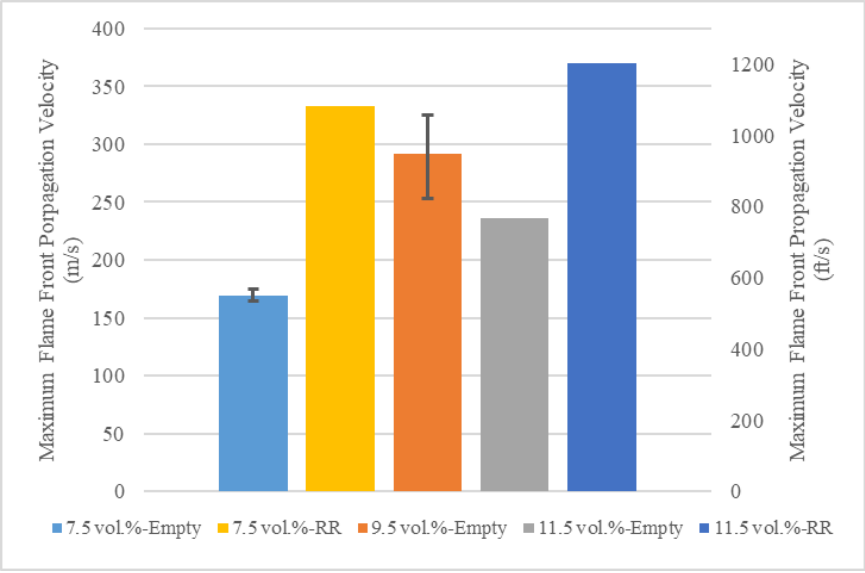


*Figure 97: Parametric Analysis of 15.24 m (50 ft) reactor with a 15.24 m (50 ft) reactive zone.*

**Quantifying the Impact of Rock Rubble in 30.48 m (100ft) Reactor**

Figure 98 compares the maximum flame velocity in the 30.48 m (100 ft) reactor with a 22.86 m (75 ft) reactive zone with different rock rubble setups: empty, 1.7 m (5.6 ft) long rock rubble, and 4 m (13.1 ft) long rock rubble. The height was kept the same. It can be noted how the rock rubble length has a significant impact on the flame inducing more turbulences which enhances the flame.

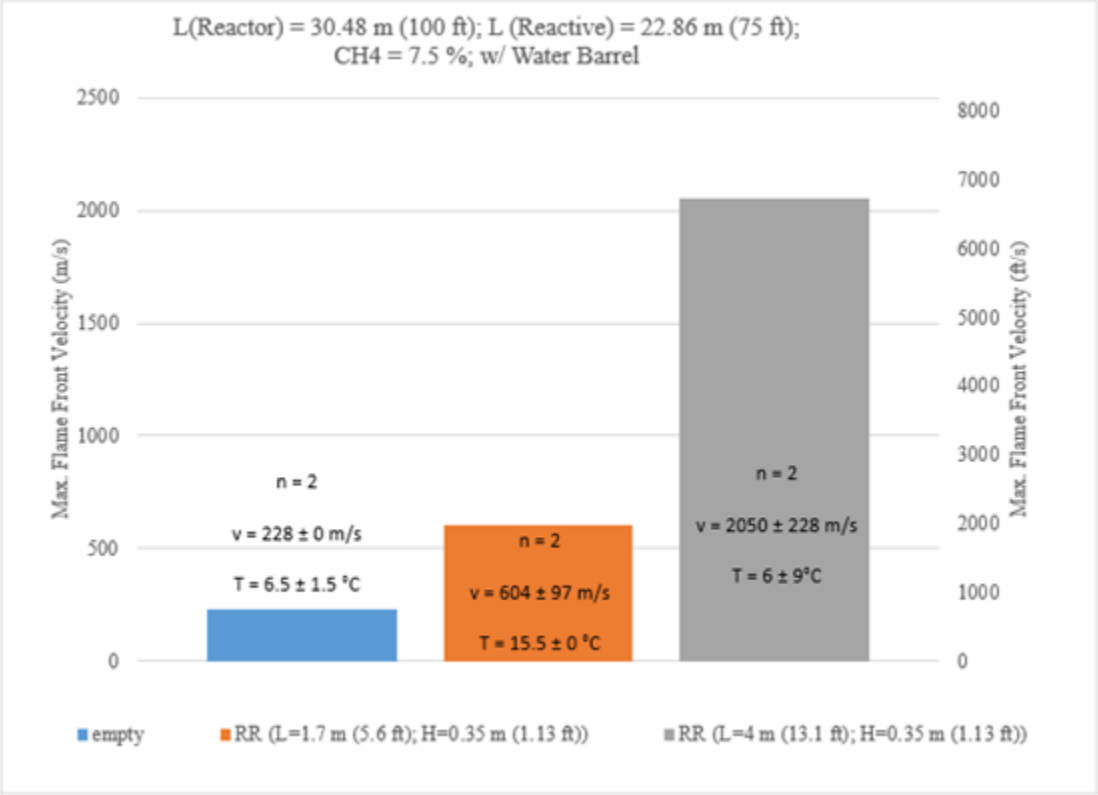


Figure 98: Comparison of maximum flame propagation velocities. n = number of tests of each condition, RR = rock rubble tests, v = maximum average flame front propagation velocity of each condition with the standard deviation. T = average ambient temperature measured on the side at the time of ignition with the standard deviation. *Vessel pressure at ignition = 82.73 kPa (~12 psia)*

Figure 99 demonstrates the magnitude of the pressure wave comparing no rock rubble and two different setups of the rock rubble length. The graph shows the maximum axial absolute pressure recorded for experiments with a methane concentration of 7.5 % and a reactive zone of 22.86 m (75 ft). The results show an increasing trend of pressure with an increase in rock rubble length. The same trend can be observed in Figure 100 and. as expected, the axial pressure measurement

is higher than the radial pressure. In addition, the pressure wave increases after the burst of the gas barrier, resulting in a higher pressure downstream of that barrier.

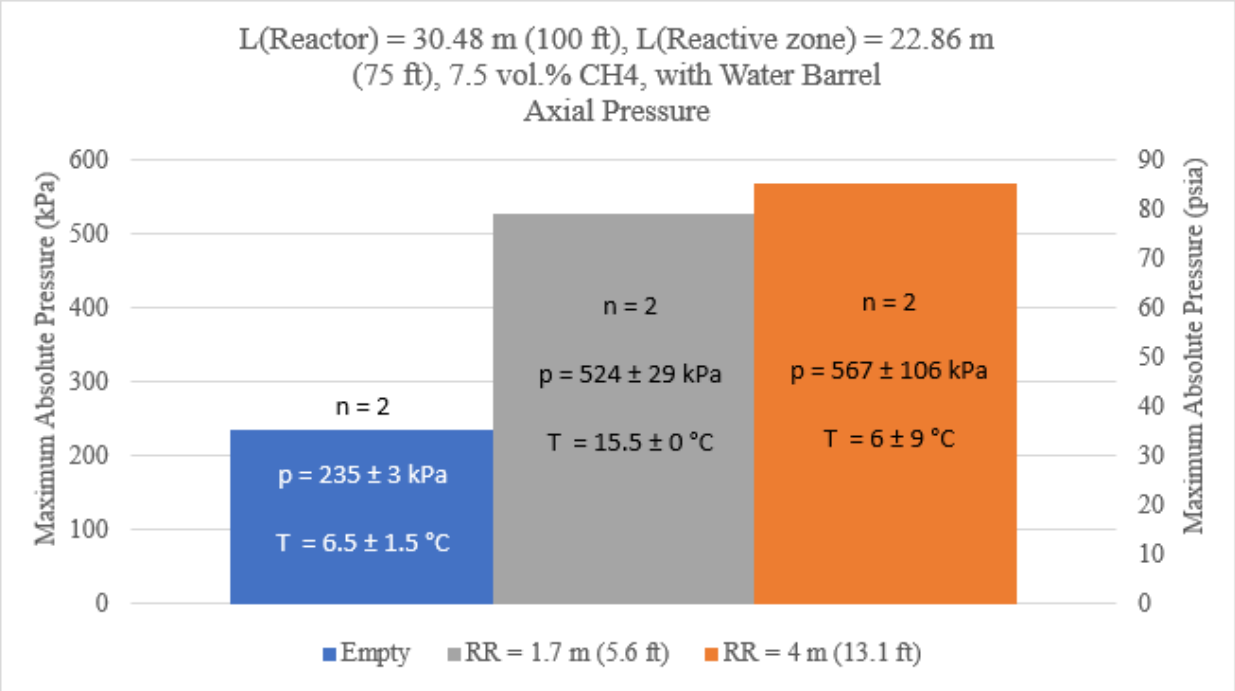


*Figure 99: Maximum axial absolute pressure result comparing an empty reactor and different rock rubble lengths; Measure location = reactive zone; Reactive zone = 22.86 m (75 ft); Methane concentration = 7.5 %. n = number of tests of each condition, p = max average radial absolute pressure of each condition with the standard deviations. Vessel pressure at ignition = 82.73 kPa (~12 psia)*

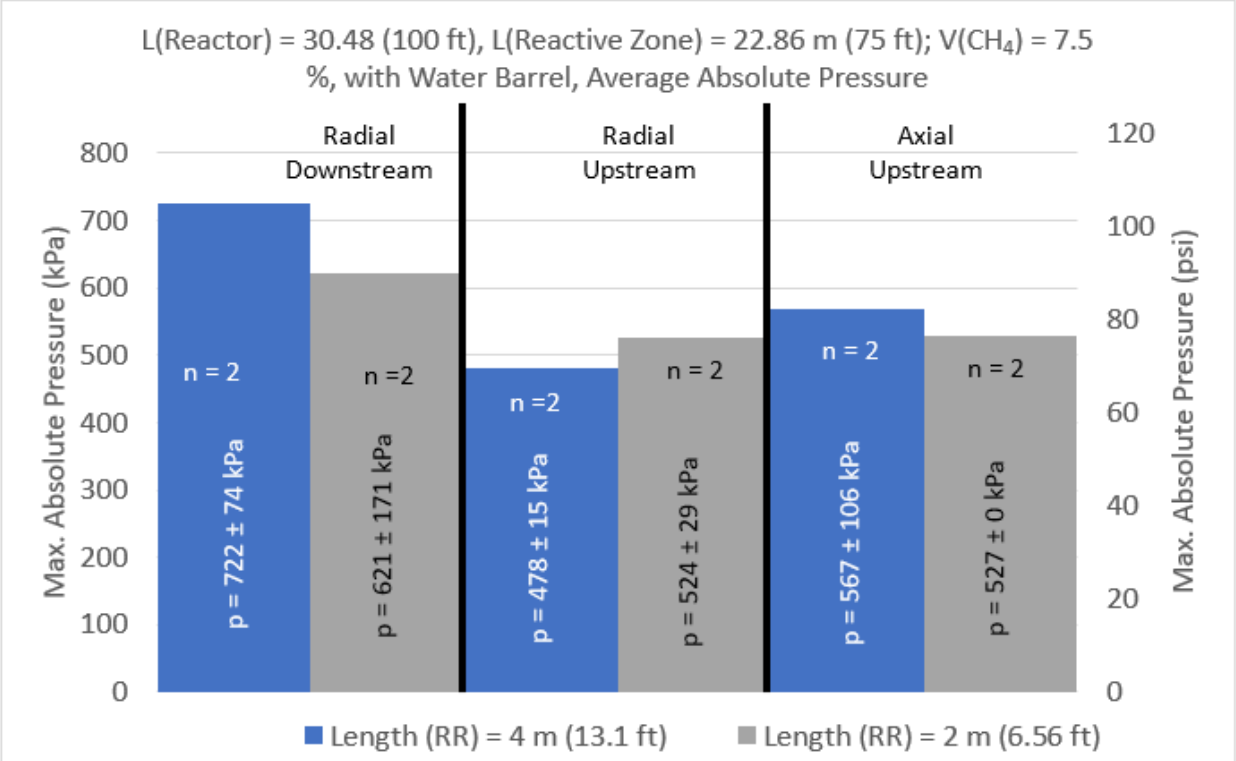


*Figure* 100*: Maximum radial and axial absolute pressure result comparing different rock rubble lengths; Upstream = reactive zone; Downstream = non-reactive zone; Reactive zone = 22.86 m (75 ft); Methane concentration = 7.5 %. n = number of tests of each condition, p = max average radial absolute pressure of each condition with the standard deviations. T(RR=4 m (13,1 ft), ambient) =* 6 ± 9 °C*; T(RR) =1.7 m (5.6 ft), ambient) = 15.5 ± 0* °C*. Vessel pressure at ignition = 82.73 kPa (~12 psia)*

Figure 101 shows the results comparison for 30.48 m (100 ft) long reactor without and with rock rubble. In these tests, the gas barrier located 22.86 m (75 ft) away from the closed end burst open when the flame front has travelled around 11 m (36.1 ft) away from the closed-end, while the water barrier burst open when the flame front was located 26 m (85 ft) away from the closed-end. Note that the flame front measurement for the empty reactor cases only available in the reactive zone. The timing and location of the flame front when these gas and water barriers opened vary with each test. However, it occurred roughly when the flame front is located at the same location for each test.

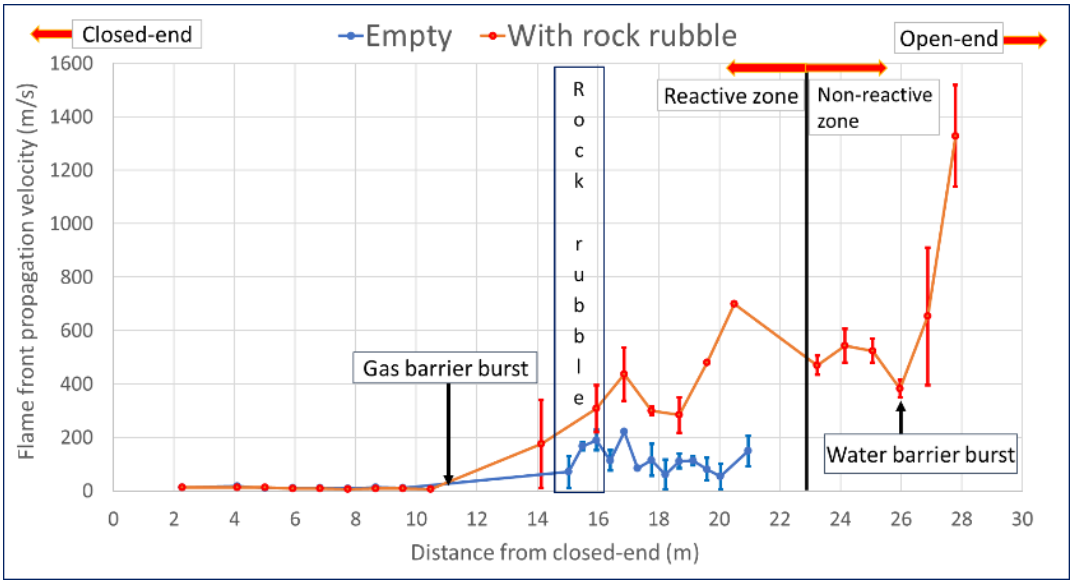


*Figure 101: Comparison of flame propagation speed with and without rock rubble in a 30.48 m (100 ft) reactor with a 22.86 m (75 ft) reactive zone.*

The results show similar trend for both cases up to the point when the gas barrier opened, and the flame encountered the rock rubble. The results with the rock rubble show a noticeable increase in flame speed and continue to accelerate until it the flame front get closer to the water barrier. The second notable acceleration occurred once the water barrier opened when the flame front was ~7 m (23 ft) away from the open-end, which resulted in the final flame front speed of around 1,400 m/s (4600 ft/s) before exiting the reactor. These results confirmed the trend reported in previous studies using smaller reactors. The rock rubble induce turbulence and help the flame transition faster to a fully turbulent high-speed deflagraion, shortening the required run up length for the flame to transition to detonation prior to exiting the reactor.

*Table 25: Summary of experiments conducted with rock rubble*

| Reactor Length (m (ft)) | Reactive Length (m (ft)) | $CH_4$ | Obstacles | Ignition location | Number of tests | Water Barrel |
|---|---|---|---|---|---|---|
| 15.24 m (50 ft) | 15.24 m (50 ft) | 7.50 % | RR (L=1.7 m (5.6 ft)) | closed end | 1 | no |
| 15.24 m (50 ft) | 15.24 m (50 ft) | 11.50 % | RR (L=1.7 m (5.6 ft)) | closed end | 1 | no |
| 15.24 m (50 ft) | 7.62 m (25 ft) | 7.50 % | RR (L=1.7 m (5.6 ft)) | closed end | 7 | no |
| 15.24 m (50 ft) | 7.62 m (25 ft) | 9.50 % | RR (L=1.7 m (5.6 ft)) | closed end | 3 | yes |
| 15.24 m (50 ft) | 7.62 m (25 ft) | 11.50 % | RR (L=1.7 m (5.6 ft)) | closed end | 4 | no |
| 30.48 m (100 ft) | 22.86 m (75 ft) | 7.50 % | RR (L=1.7 m (5.6 ft)) | closed end | 2 | yes |
| 30.48 m (100 ft) | 22.86 m (75 ft) | 7.50 % | RR (L=4 m (13.1 ft)) | closed end | 2 | yes |

Figure 102 and Figure 103 show the impact on the maximum flame front velocity of experiments in the 15.24 m (50 ft) reactor with rock rubble and methane concentrations of 7.5 vol.%, and 11.5 vol.% for different initial reactor pressures 103.4 kPa (15 psia) and 86.2 kPa (12.5 psia). The results in Figure 103 show that the flame velocity is approximately 57 m/s (187ft/s) higher with the increased initial vessel pressure. The impact in Figure 102 is less significant with a difference in the flame front propagation velocity of about 12 m/s (39.4 ft/s).

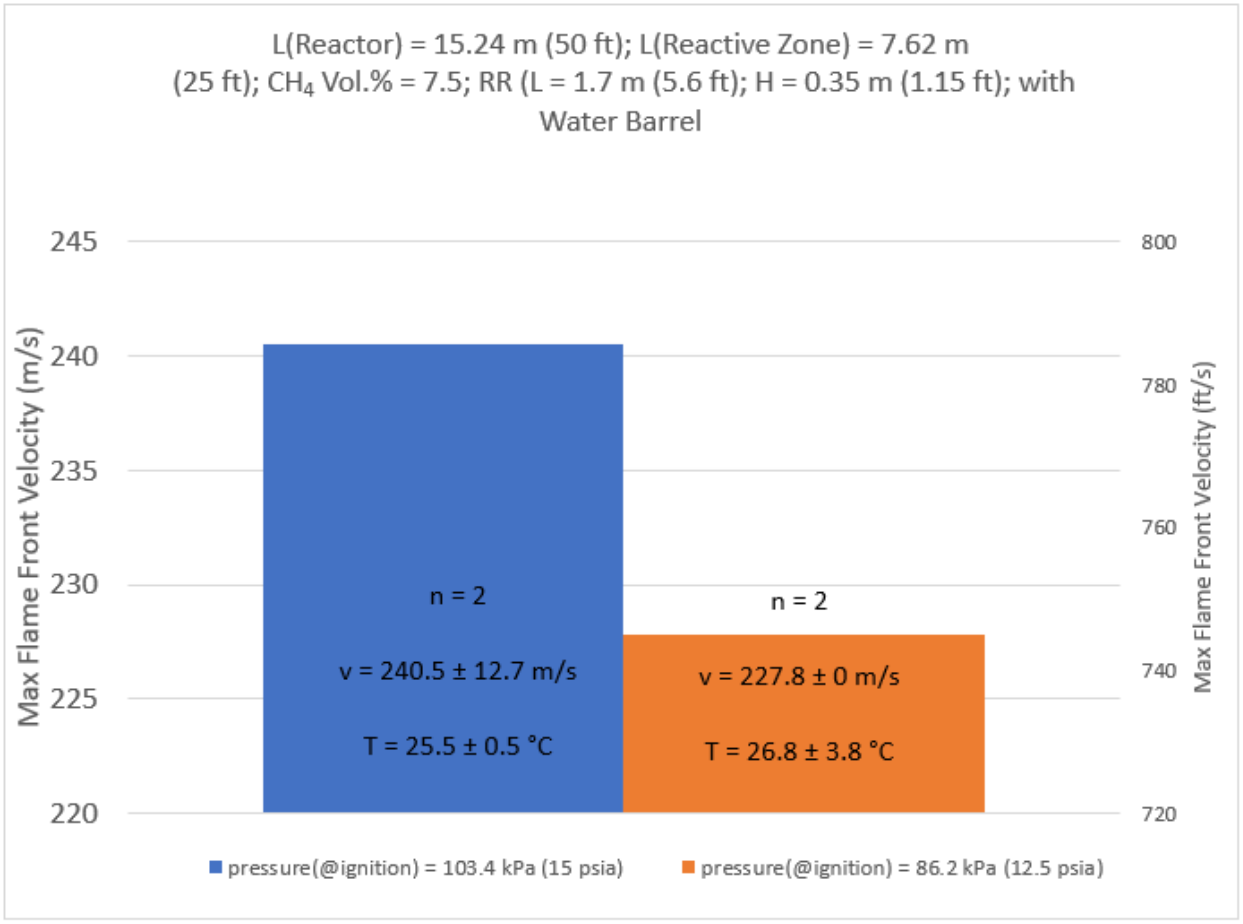


*Figure 102: Comparison of maximum flame propagation velocity with different initial absolute pressures. Methane concentration = 7.5 vol.% RR = rock rubble test. n = number of tests of each condition, v = max average flame front velocity of each condition with the standard deviation. T = average ambient temperature measured on the side at the time of ignition with the standard deviation*

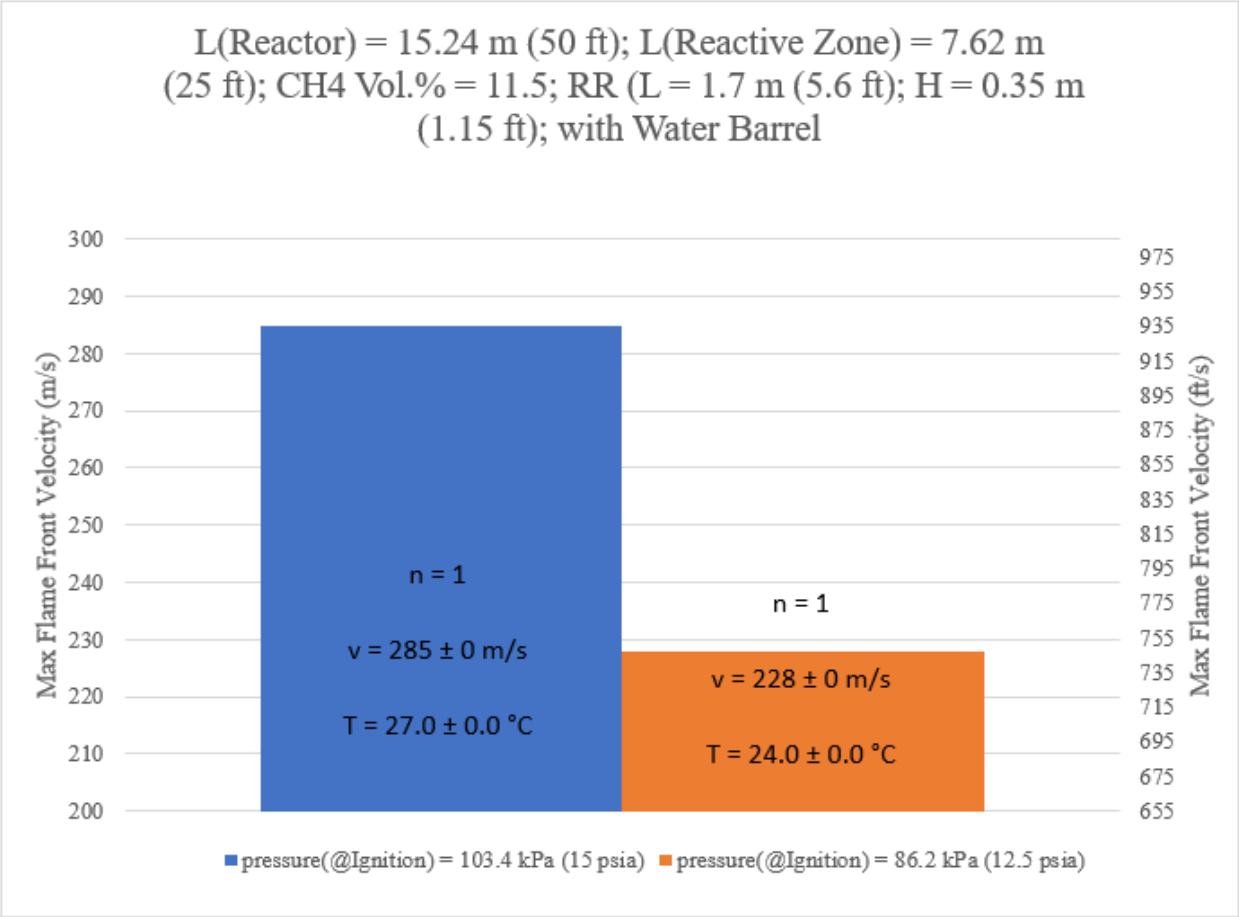


*Figure 103: Comparison of maximum flame propagation velocity with different initial absolute pressures. Methane concentration = 11.5 vol.%. RR = rock rubble test. n = number of tests of each condition, v = max average flame front velocity of each condition with the standard deviation. T = average ambient temperature measured on the side at the time of ignition with the standard deviation*

**Objective 2: Continue development, improvement and validation of the CSM high-speed turbulent deflagration combustion model using the new extended large-scale explosion reactor.**

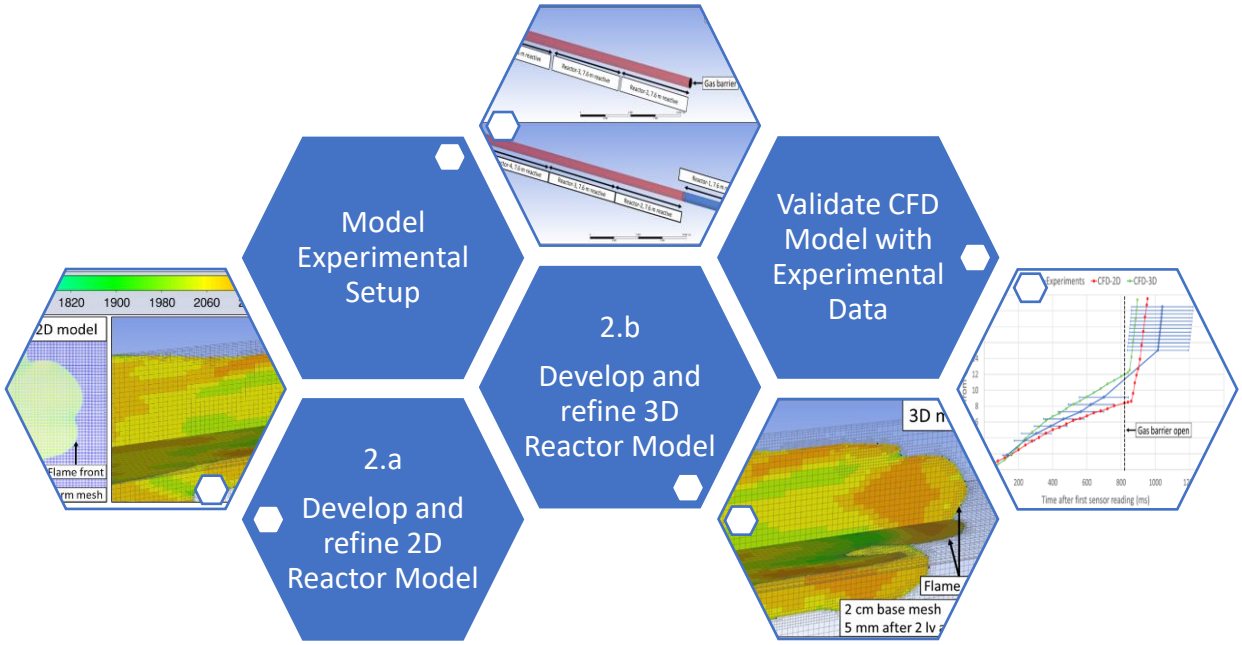


**Objective 2.1a: Initial modeling of the small and large-scale reactor using 2D models to investigate the relative impact of ignition location, rock rubble geometry, and the addition of other flammable gas species**

**Objective 2.1b: Information obtained from the 2D model will be used in the 3D models recently developed for the smaller-scale and will be used to validate the 3D models for the large-scale reactor for select cases to reduce computational effort**

The 2D model of an unobstructed 30.48 m (100 ft) reactor with a 22.86 m (75 ft) reactive zone took 5 days to simulate 960 ms of combustion event using 4 x 36 cores computational power. Similar to the event observed in the physical experiment, the gas barrier was opened at 820 ms after the ignition occurred. The 2D model predicts 56 kPa (8.1 psig) at 820 ms, just before the gas barrier is opened. This under predicts the explosion pressure at the moment of the gas barrier rupturing and is slightly below the tested strength of the gas barrier, as well as pressures recorded at that point during experiments.

The 2D and 3D CFD model show the same flame propagation trend with the experiments. The flame propagated slowly when the gas barrier still intact, and significantly increases once the barrier opened from time 820 ms onwards. Pressure comparison at 820 ms, just before the gas barrier open, show that the 3D CFD model (~113 kPa (16.4 psig)) is in good agreement with the experiment (~103 kPa (14.9 psig)). In comparison, the 2D CFD model (~56 kPa (8.1 psig)) significantly underpredicted the resulting explosion pressure. To better evaluate the accuracy of the CFD model, two important parameters are compared between the measurement from experiment and CFD model prediction. These two parameters are the flame front location at different time instances, and the flame front propagation speed. Figure 104 shows the comparison of flame front location over time between experiments and CFD models, while Figure 105 shows the comparison of flame front propagation speed over distance from ignition location between experiments and CFD models.

In terms of flame front location at different time instances, shown in Figure 104, both the 2D and 3D CFD models show good prediction. Experiment results show time ranges from ~860 – 1,200 ms for the flame front to propagate 21 m (68.9 ft) from the ignition location. This ~350 ms difference in time difference is most likely due to the inconsistency on the timing and opening condition of the gas barrier. In comparison, the 2D and 3D CFD model predict ~950 ms and ~895 ms respectively, which are still within the time ranges.

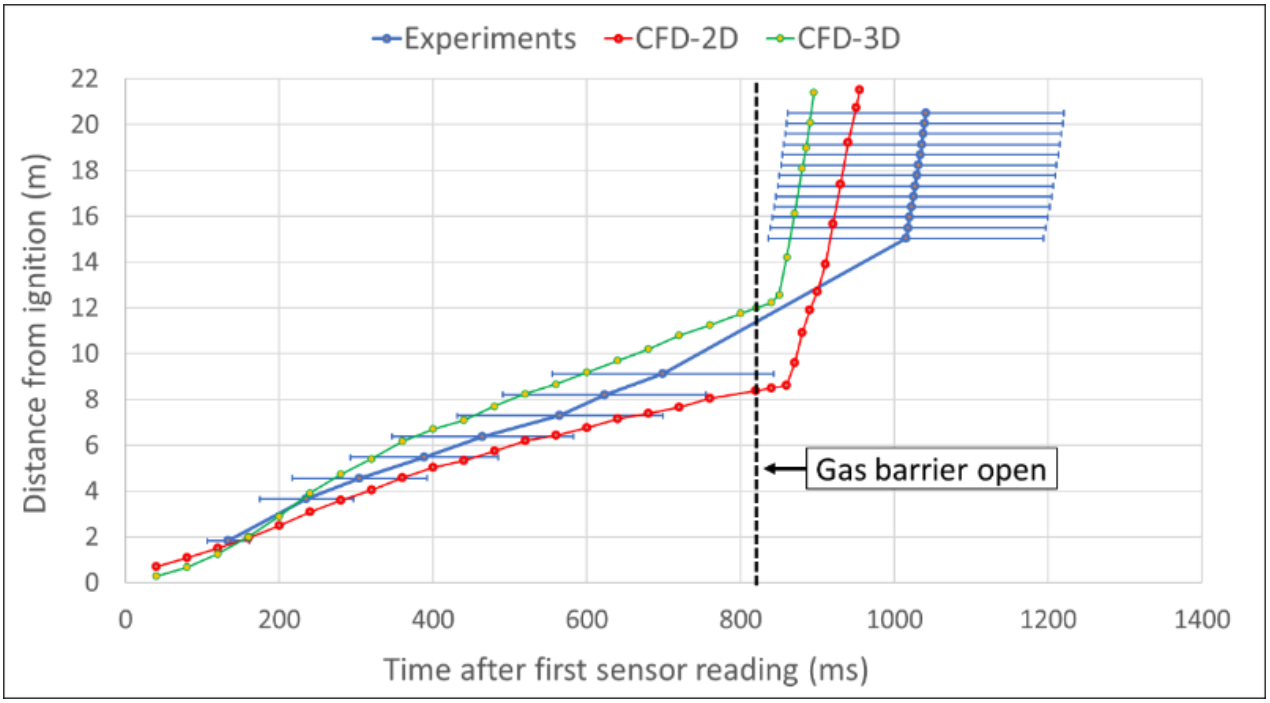


*Figure* 104*: Comparison of flame front location over time between experiments and CFD models for empty reactor case.*

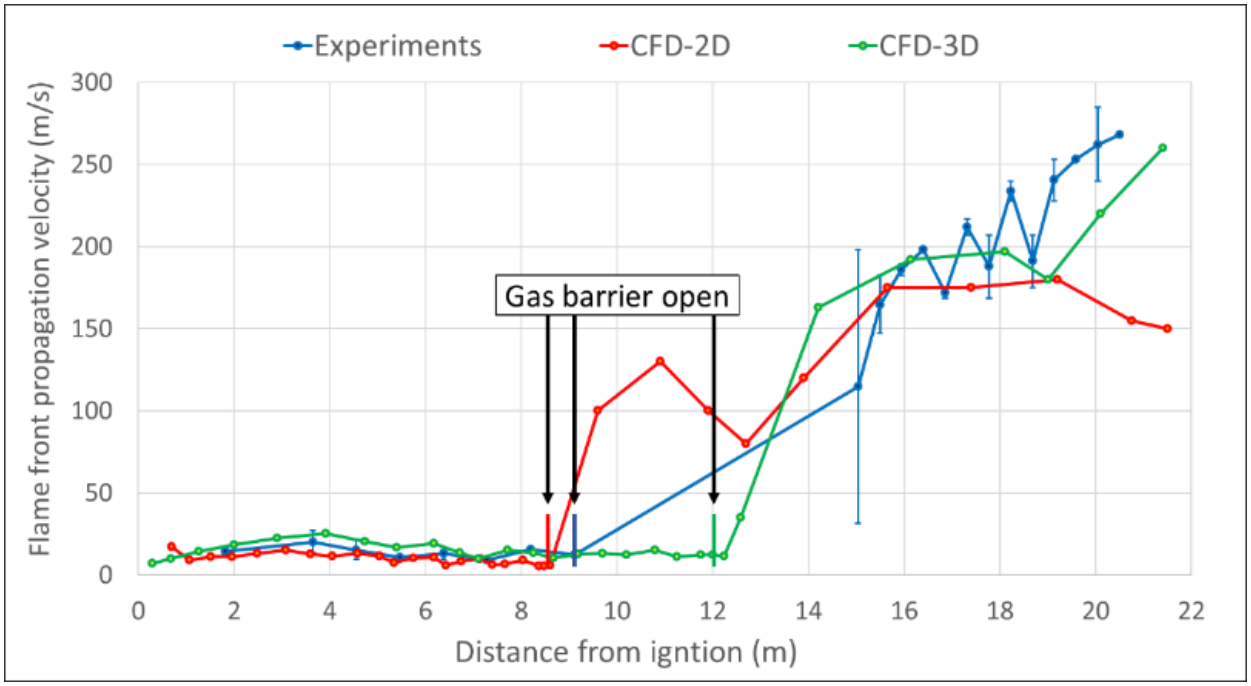


*Figure* 105*: Comparison of flame front propagation velocity over distance between experiments and CFD models for empty reactor case.*

Comparison of the changes in flame front propagation speed over distance, shown in Figure 105, show good agreement between experimental results and the 3D CFD models. The 2D CFD model shows a good prediction for the first 18 m (59.1 ft) flame propagation distance but start to deviate past 18 m (59.1 ft) as the 2D CFD model show a decrease in flame speed, while the experiment results still showing a continuous increase. Overall, the CFD models managed to capture the effect of the gas barrier opening as observed in the experiments. In the case of 2D CFD model, the flame front was located 8.1 m (26.6 ft) away from the ignition when the gas barrier opened at 820 ms, while in 3D CFD model case, the flame front already propagated 12 m (39.4 ft) away. Both models show significant increase in flame speed once the gas barrier opened.

**Objective 2.2: The initial full mine scale CFD model was substantially improved with the knowledge gained from the 2D and 3D models developed. This resulted in an improved model based on an experimentally validated framework that can to a variety of situations that are impractical to experimentally test.**

The development of the Full Mine Scale CFD Model was a groundbreaking advance in modeling gas explosions in underground coal mines. This is the first known published CFD model of its kind and a substantial improvement over the very preliminary pioneering efforts produced previously. The model was approached in stages. A mine wide ventilation model was used to generate a rough ventilation flow to the face. This was then improved with a high-fidelity ventilation model of the active longwall face, to produce the initial conditions for the explosion model. This model included the rotation of the shear and other details that can influence the localized gas flow. The Full Mine Scale CFD Model was then used to model several ignition scenarios on the longwall face, producing the first reliable numerical models of a gas explosion at the longwall face.

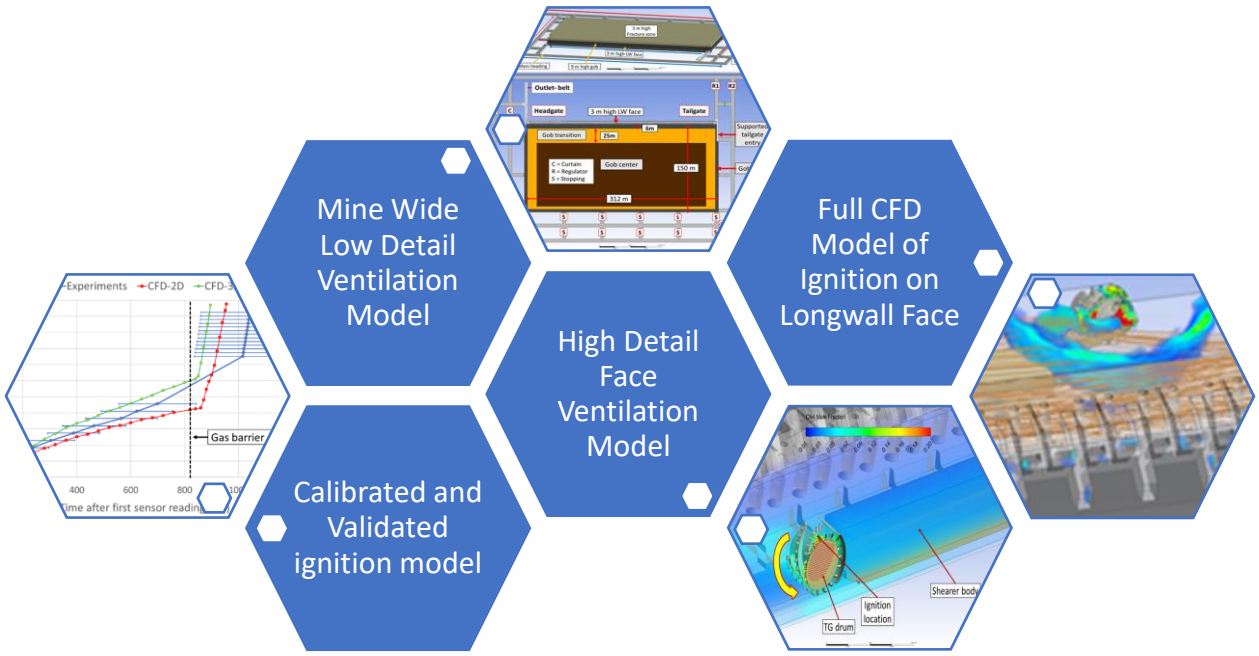

**Objective 2.2.a: The full mine scale CFD model was successfully used to model a face ignition near the shear drum, producing a high accuracy model of a long ignition and explosion.**

The 3D full-scale longwall explosion model is the result of an integration of the 3D cylindrical gas explosion model and the 3D full-scale longwall ventilation model, producing a model which successfully simulated methane-air ignition and explosion overpressures in an active longwall face area. The completed 3D full-scale longwall explosion model is capable of simulating a gas explosion on an active longwall face, as well as in the gob area near the shields; which allows various ignition and explosion scenarios to be investigated.

*Figure* 106 shows a volume rendering of the initial explosion temperatures and pressures from an ignition near the tailgate drum. The wave front from the explosion overpressure is expanding more quickly than the flame front. This is important because the pressure wave preheats the air ahead of the flame front, which will enhance the flame propagation velocity leading to a more violent explosion. In addition, these overpressure waves also have the potential of coalescing into a single shock wave. If this happens, the shock wave or waves may interact with each other or nearby surroundings and potentially transition the explosion from a deflagration to detonation which can be much more devastating to nearby mine equipment, structures, and miners [39].

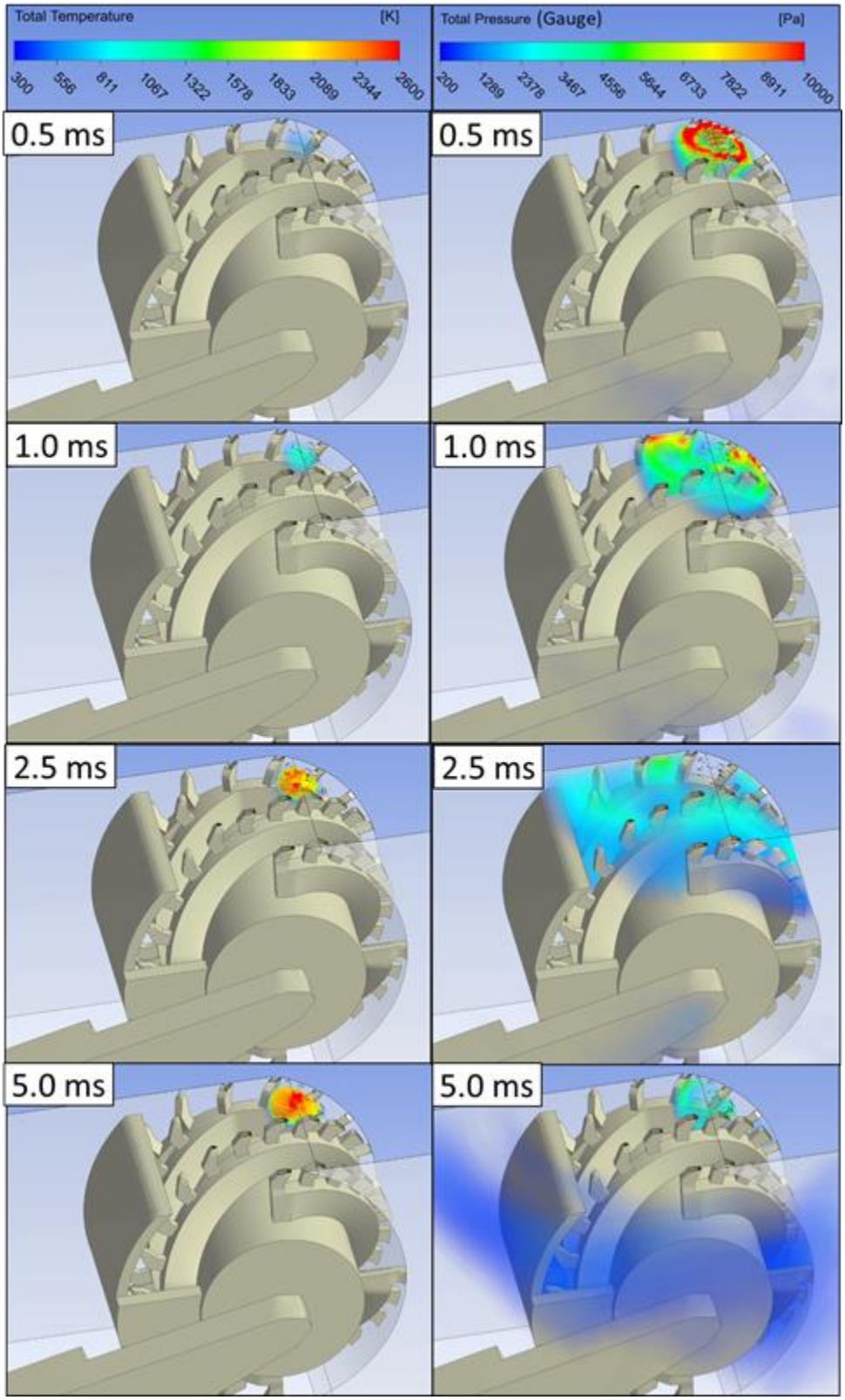


*Figure* 106*: Volume rendering of the temperature and overpressure showing the early stages of flame propagation.*

Figure 107 and Figure 108 show volume renderings of temperature and total gauge pressure at different time instances. The brown streamlines in Figure 108 represent the airflow streamlines in the longwall face.

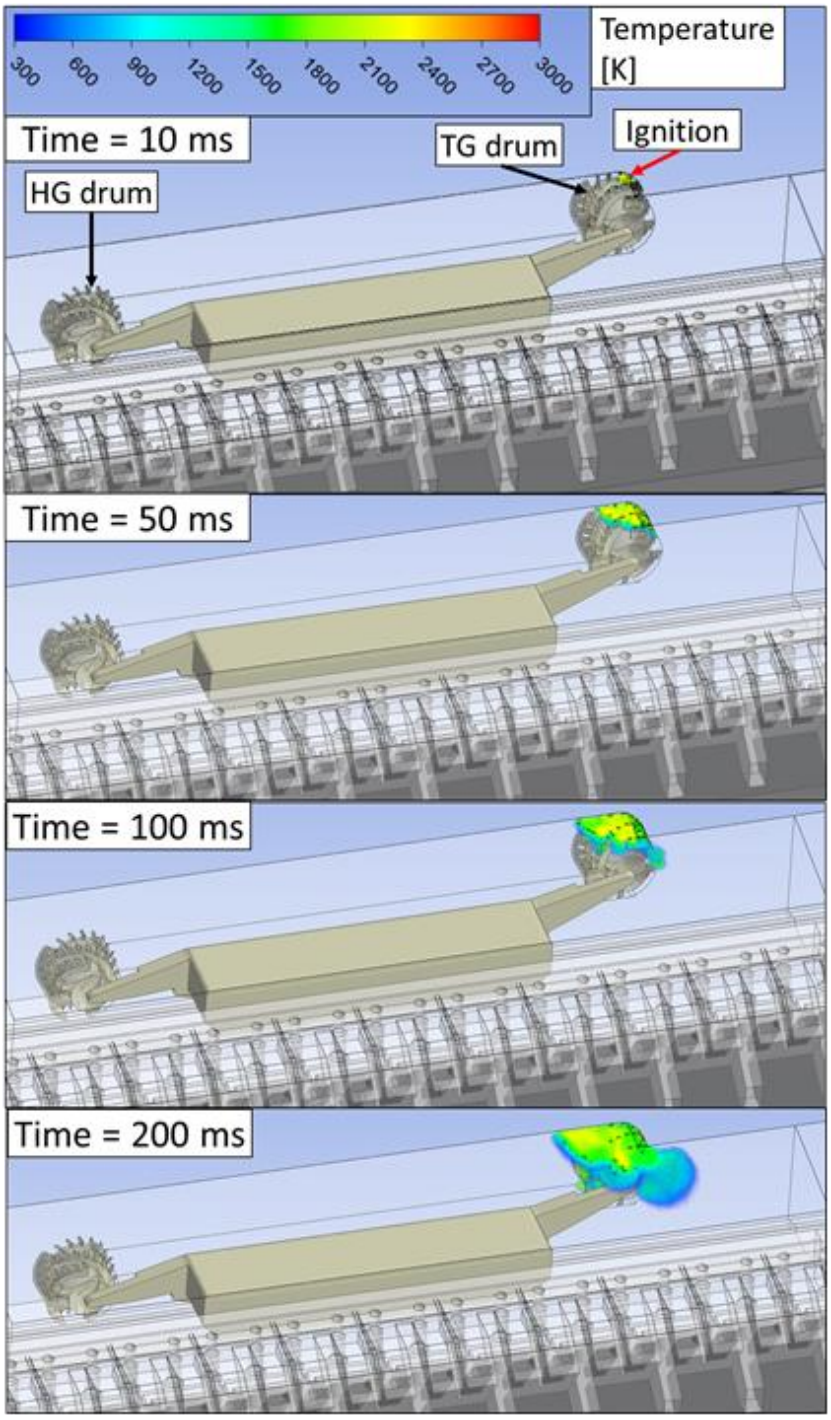


*Figure 107: Volume rendering of temperature showing flame propagation at different time instances.*

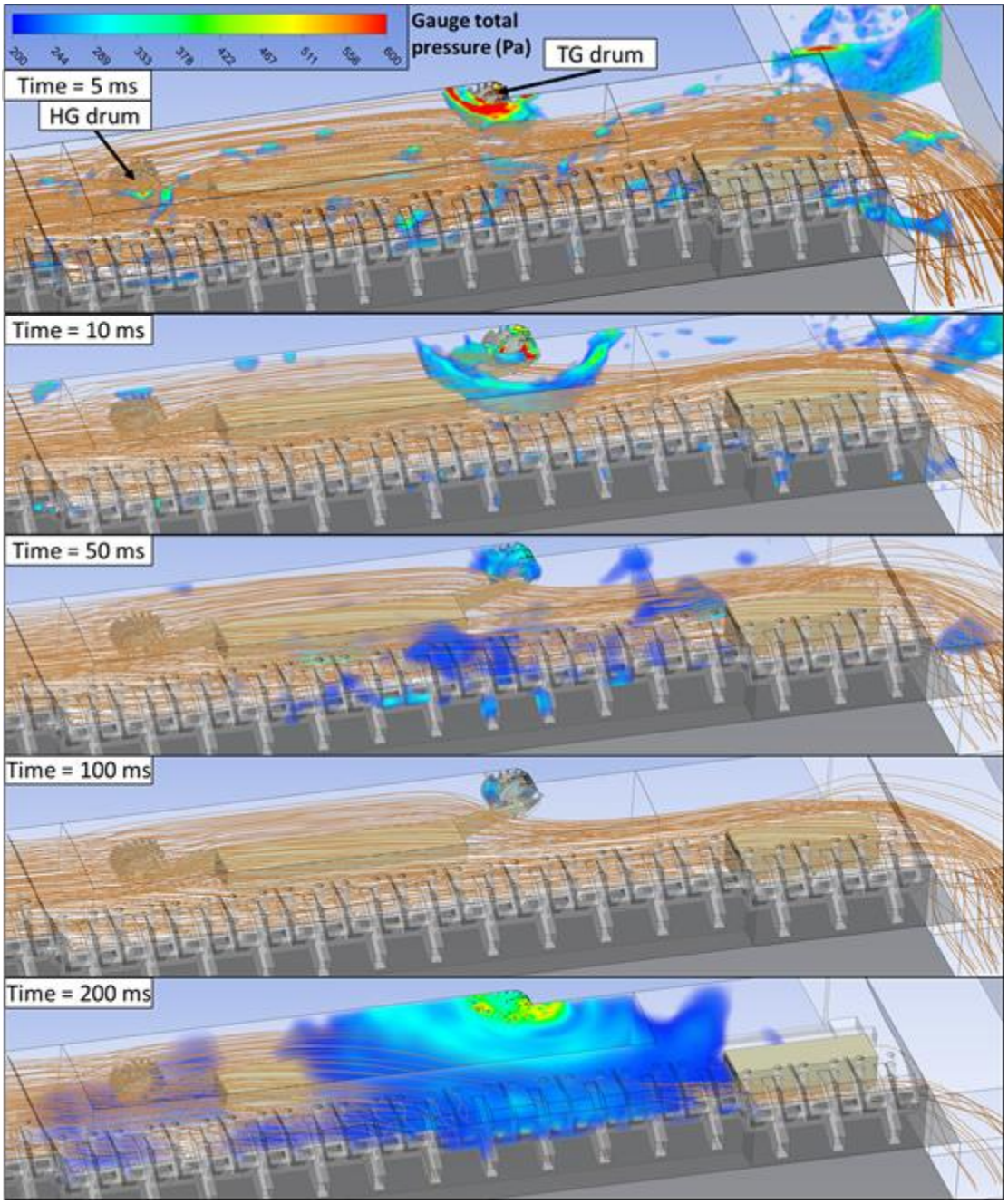


*Figure 108: Volume rendering of total gauge pressure showing ignition and explosion overpressure. Brown lines represent the streamlines of airflow in the longwall face.*

Results show that initially the flame expands in all directions, but at 100 ms the flame begins to expand preferentially towards the headgate side of the face. At this same time, the pressure waves are beginning to divert the airflow away from the face. The results show that the ignition produces multiple pressure waves. The snapshot at 200 ms clearly shows that the overpressure from the

explosion is sufficient to divert face airflow into the gob area where it can mix with the available methane, creating new or expanding explosive mixtures inside the gob area. In addition, diverting the flow from the shearer drums reduce the available fresh air to dilute the methane around the drums, potentially creating an environment which can lead to secondary or tertiary explosions. Figure 109 shows the flame front propagation velocity over time. To analyze the flame front propagation velocity, multiple lines are created using the ignition location as the base. Several parameters such as temperature gradient and kinetic rate of reaction are compared.

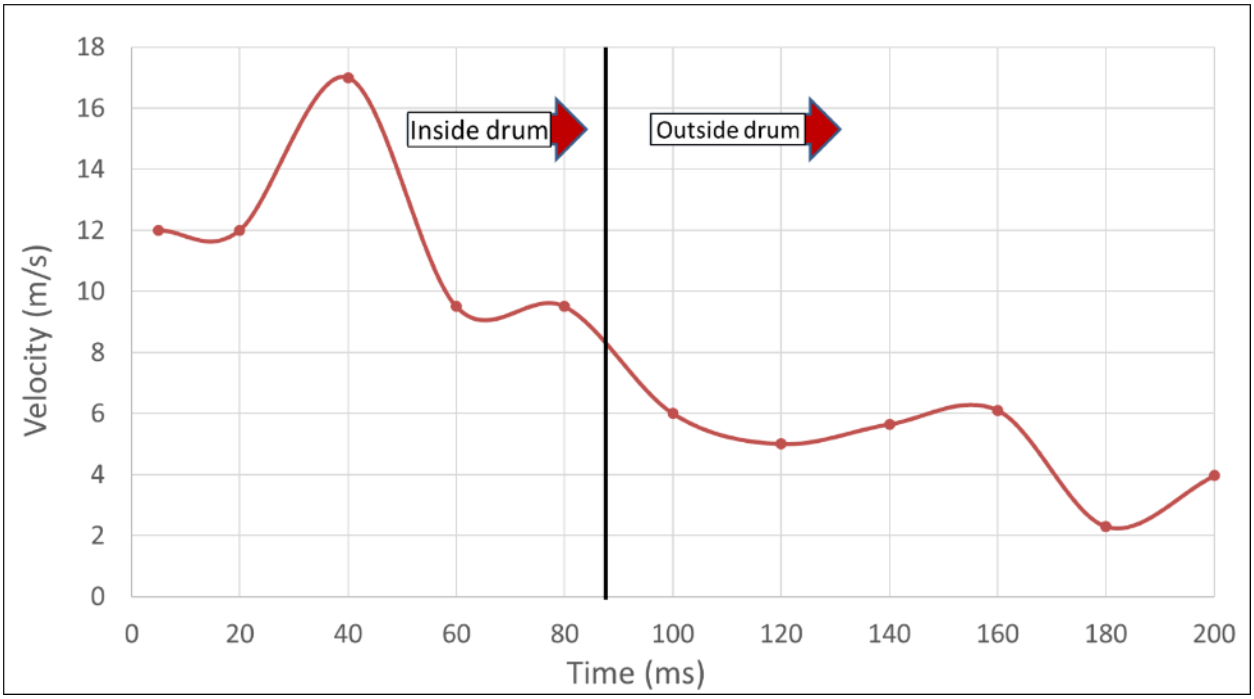


*Figure 109: Flame front propagation velocity over time based on kinetic rate of reaction*

Based on the result, high velocity and oscillation effect is observed when the flame propagating in the confined space between the picks, uncut coal, and shearer cowl, around the shearer tailgate drum area. After around 85 ms, the flame front exits the tailgate drum area to a more open space, and the speed decreased significantly to around 5 m/s (16.4 ft/s). This decrease in the flame speed may also be attributed to the flame propagating from the explosive mixture region close to the coal face, into the fuel-lean mixture region that is not adequate to sustain flame propagation, as shown in Figure 110. This would change if the volume was larger and if the explosive mixture extended out past the drum.

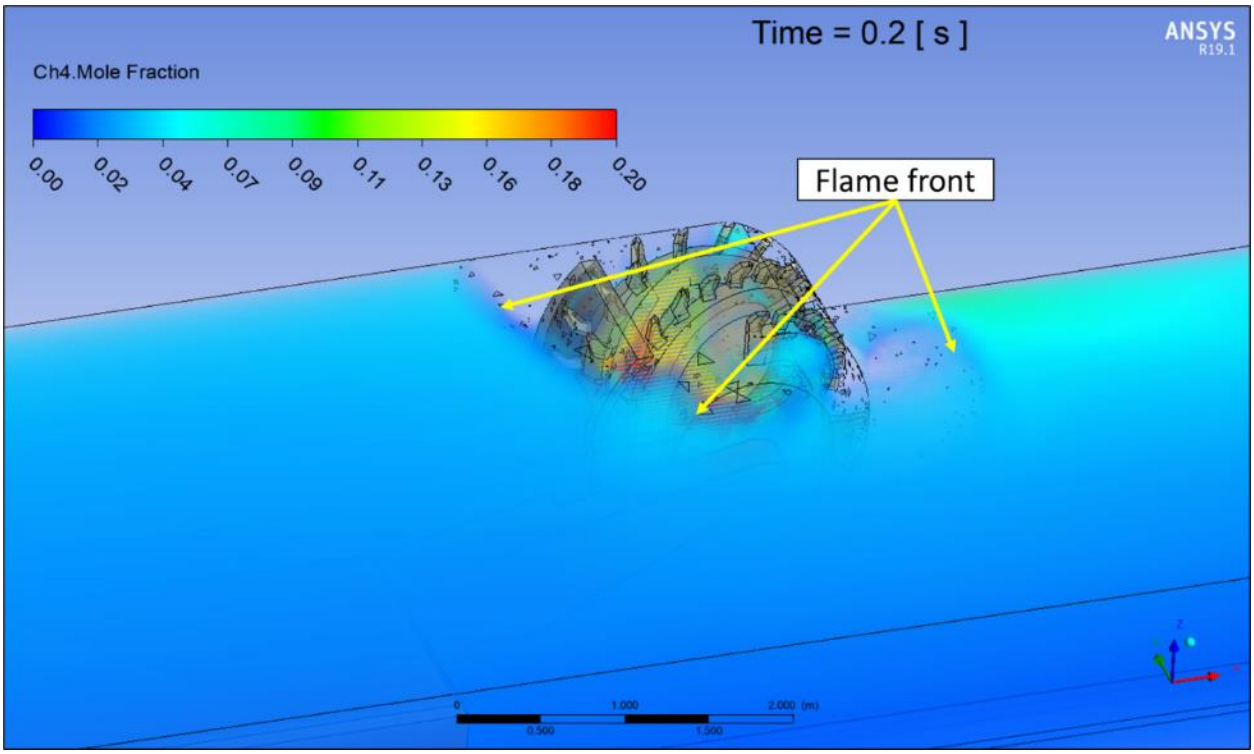


*Figure 110: Volume rendering of $CH_4$ mole fraction, showing flame propagating into fuel lean mixtures at 200 ms*

Based on the magnitude of the flame speed and the resulting overpressure, this case represents an early stage of a small face ignition during the shearer cutting operation. It is important to note that different ventilation scenario and methane distribution can significantly impact the resulting flame speed and overpressure. To test this, similar simulation was done using a second model with larger explosive gas zone (EGZ), as shown in Figure 111 and Figure 112. In the second case, the amount of methane inflow from the coal face is doubled, from 0.07 $m^3/s$ (2.47 $ft^3/s$) to 0.14 $m^3/s$ (4.94 $ft^3/s$), while maintaining the same amount of fresh air supplied from the headgate side of the longwall face. This second scenario represent the case when the sensors on the shearer and on the tailgate drive both fail to detect high concentration of methane.

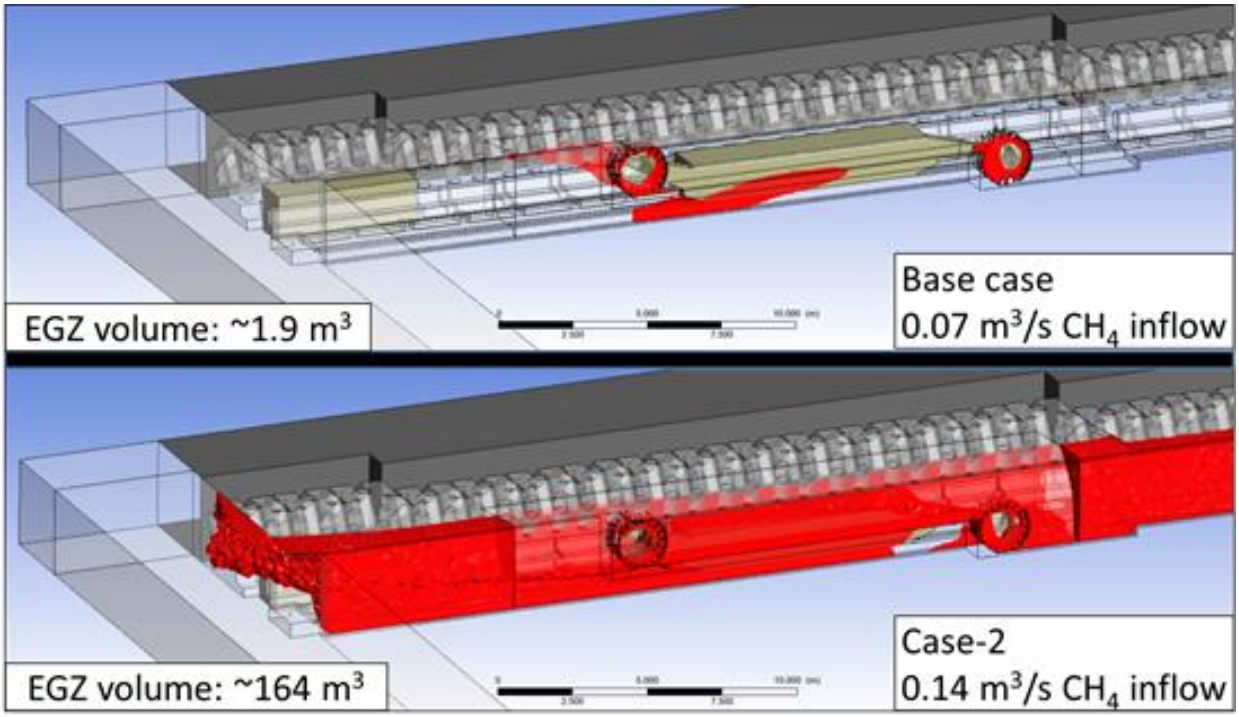


*Figure 111: Comparison of explosive gas zone volume for the two cases. The red colored cloud represents explosive gas mixtures with $CH_4$ mole fraction value between 5 % - 14 %.*

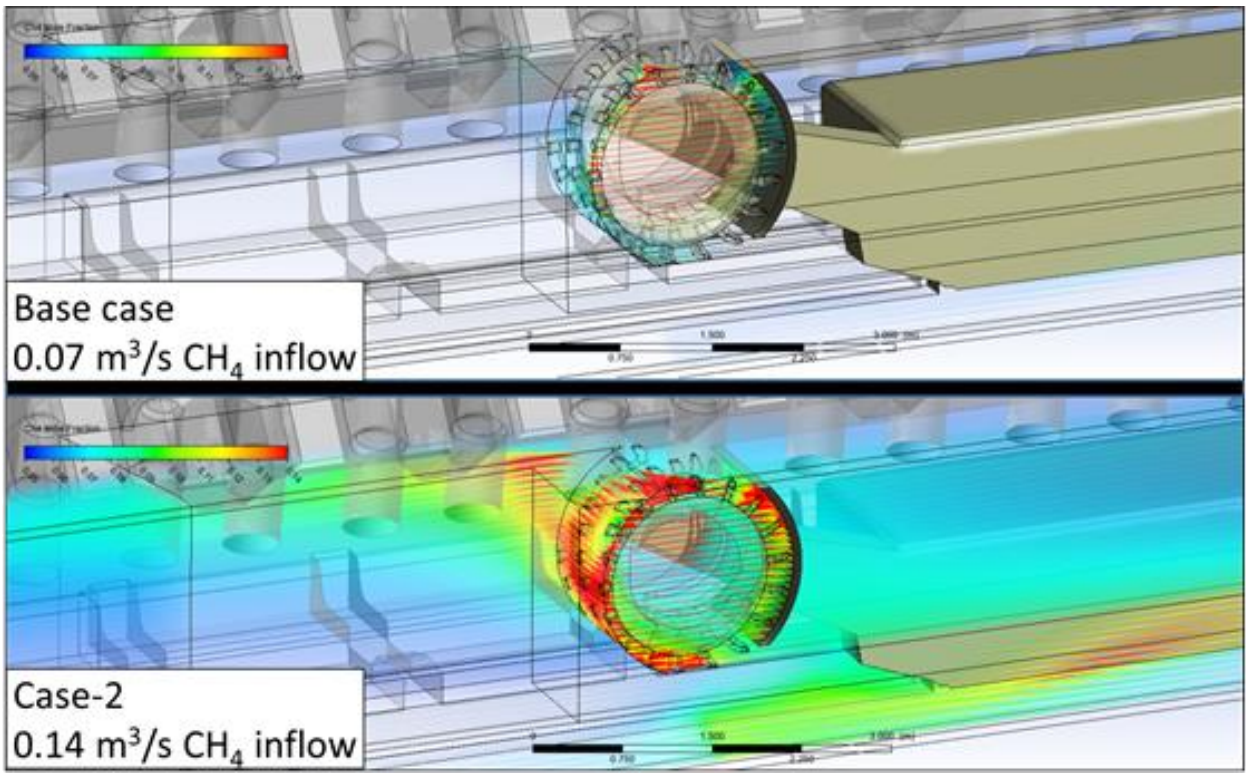


*Figure 112: Comparison of methane distribution around the tailgate shearer, showing volume rendering of $CH_4$ mole fraction.*

Figure 113, Figure 114, Figure 115, and Figure 116 show the comparison of flame propagation for the two cases. Note that the ignition location for case-2 is slightly offset to simulate the start of ignition where the methane concentration is 9.3 % by volume, similar starting condition with the base case.

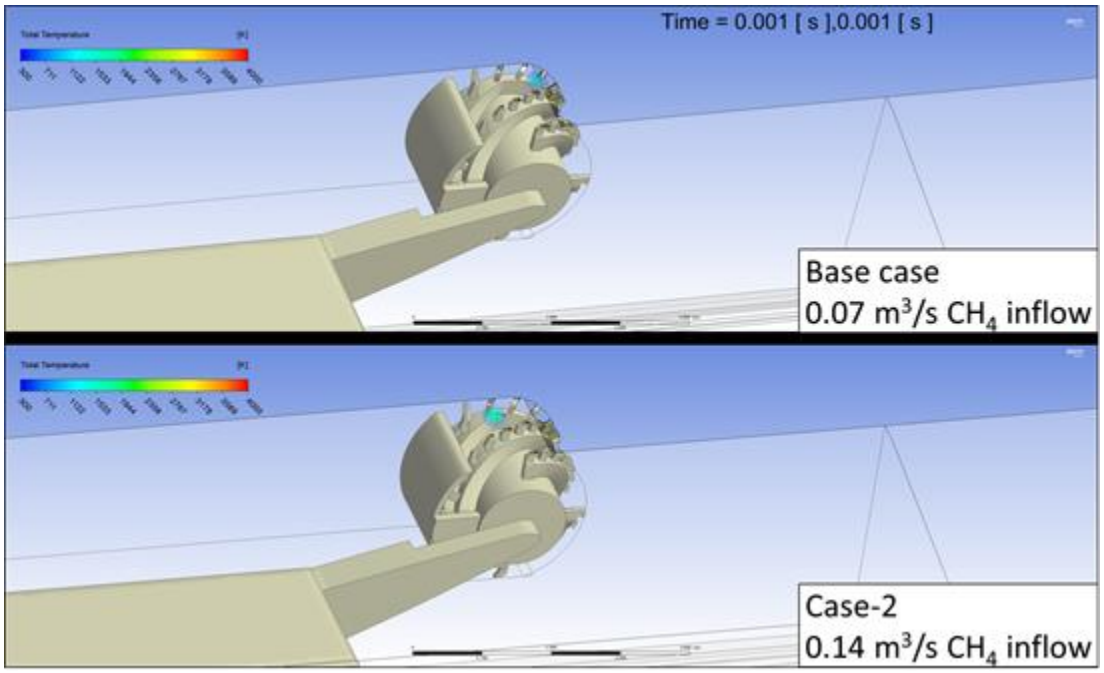


*Figure 113: Volume rendering of total temperature showing flame propagation at 1 ms.*

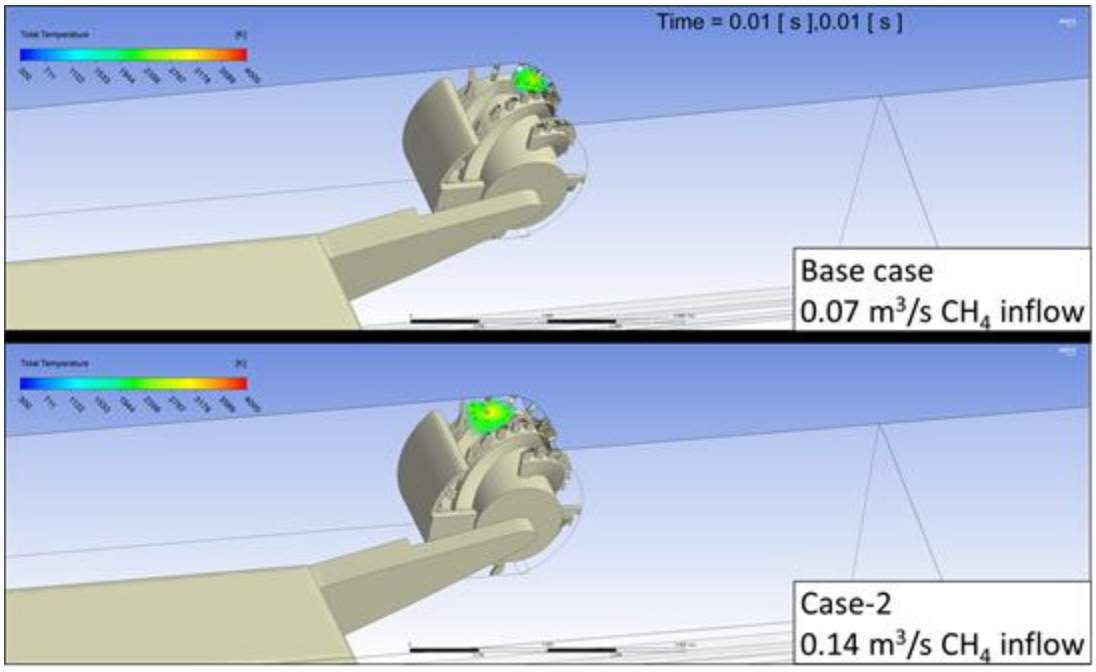


*Figure 114: Volume rendering of total temperature showing flame propagation at 10 ms*

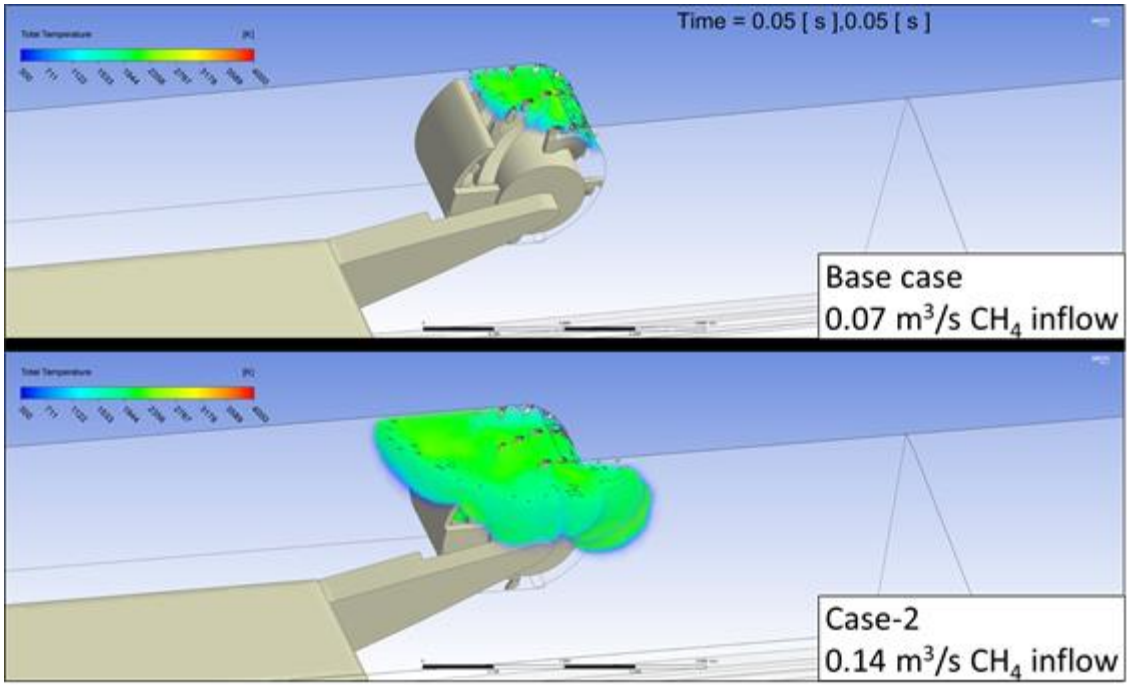


*Figure 115: Volume rendering of total temperature showing flame propagation at 50 ms*

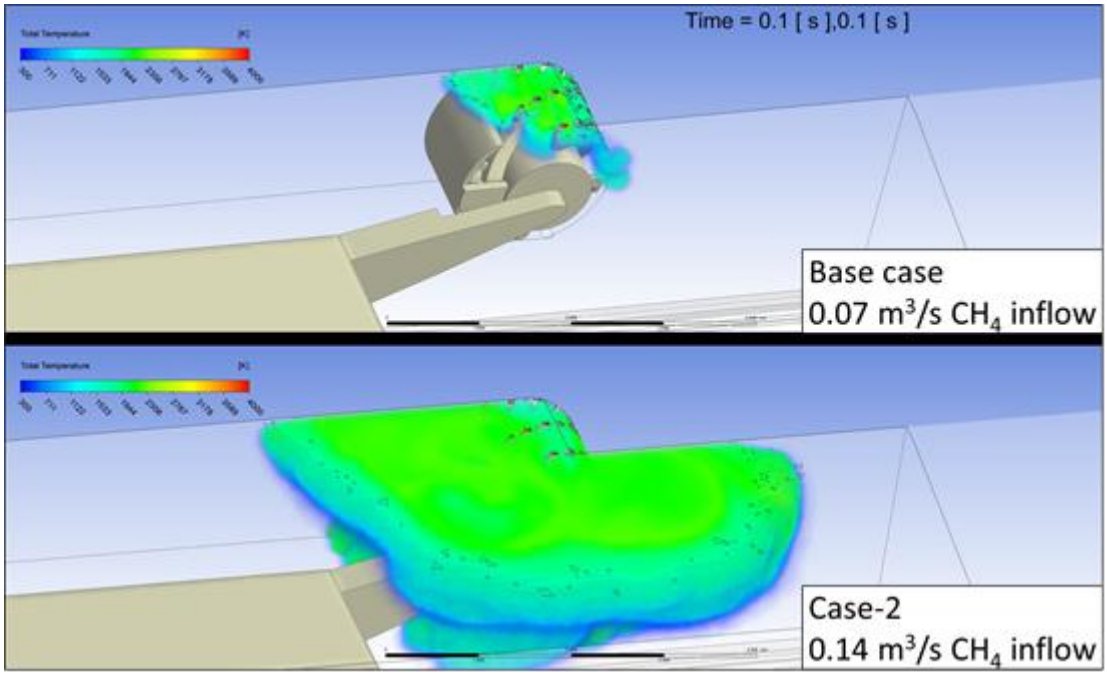


*Figure 116: Volume rendering of total temperature showing flame propagation at 100 ms*

Figure 117 shows comparison of the flame front propagation velocity over time.

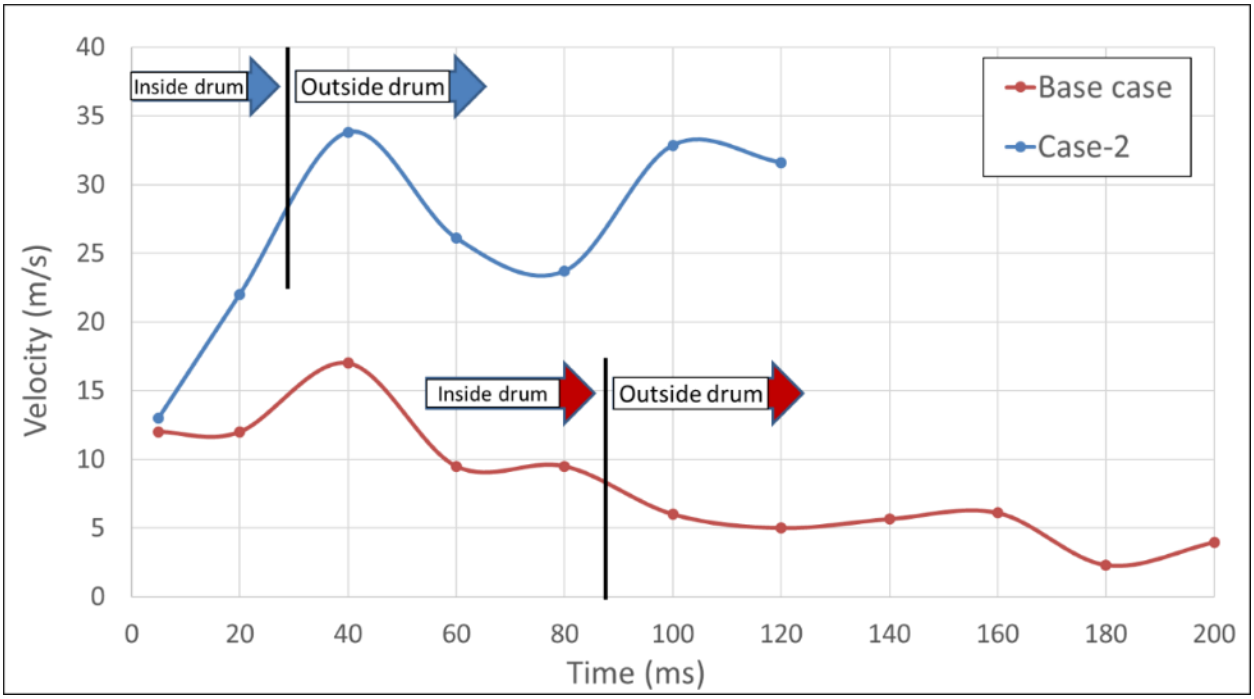


*Figure 117: Comparison of flame front propagation velocity over time based on kinetic rate of reaction*

The results comparison clearly shows the impact of the available explosive gas zones on the resulting flame propagation, with the second case shows significant increase propagation velocity and overpressure from less than 1,000 Pa (0.15 psig) to greater 6,000 Pa (0.87 psig) within the 120 ms time frame after the ignition.

## Objective 2.3 & 2.3.a: Investigate the impact of rock rubble on the acceleration and transition to Detonation and providing data to researchers at UMD and NRL for further validation of DDT models.

The geometry and dimensions of a rock rubble obstruction drive the behavior, shape, and dimensions of the turbulent flame regime. It was therefore hypothesized that increasing the length of the rock rubble obstruction would result in a greater increase in the flame speed. In the short rock rubble obstruction experiments, the rock rubble was contained in a 1.7 m (5.6 ft) long sled, centered on the reactor 2 to 3 joint and piled to 50 % of the total height. For the extended configuration, the sled was moved towards the gas barrier and fully into reactor 3 as labeled in Figure 118. Rock rubble was then stacked on the upstream side in reactor 2, resulting in a 4 m (13.1 ft) long rock rubble obstruction with a height of 50 % of the reactor diameter. The overall rock rubble length was increased by slightly over double, with the obstruction centered on the joint between reactors 2 and 3, as shown in Figure 118.

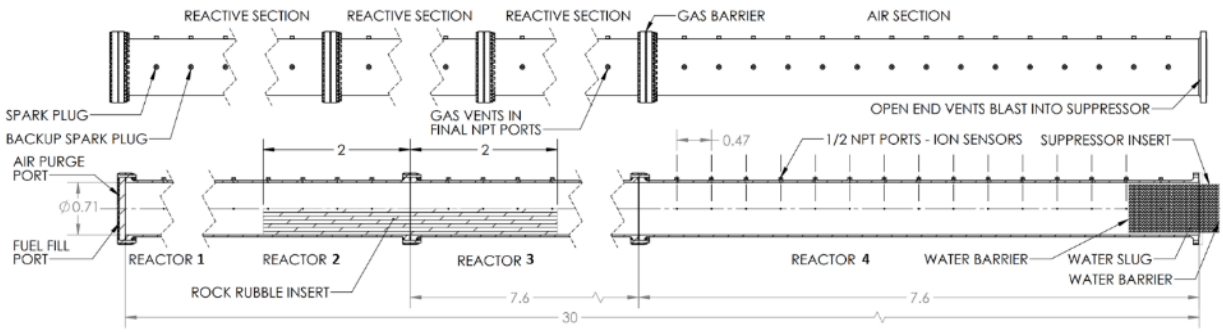


*Figure 118: Reactor configuration for 30.48 m (100 ft) experiment with a 22.86 m (75 ft) reactive zone, a water slug in the air filled section, and the extended rock rubble.*

A pair of extended rock rubble experiments were conducted with a 30.48 m (100 ft) reactor and 22.86 m (75 ft) reactive zone. As with the other 30.48 m (100 ft) experiments, these were conducted with a lean mixture, 7.5 %, in order to minimize the risk of flames exiting the reactor due to the extreme fire danger in Colorado at that time. Due to the potential for high flame propagation velocities, the reactor was configured with a water slug for all 30.48 m (100 ft) rock rubble and extended rock rubble experiments. While this will reduce the flame propagation velocity as demonstrated, it provides a uniform point of comparison and was necessary to operate responsibly in the prevailing extreme and unseasonal weather conditions.

As predicted by the longer turbulent zone, the extended rock rubble experiments produced substantially higher flame propagation velocities than any other experiments conducted to date. Instantaneous velocities between ion sensors measured as high as 2,000 m/s (6562 ft/s), indicating that instantaneous flame propagations speeds may be near or above the DDT at least in a small region near the exit of the reactor during the experiments. The flame front propagation velocities for an extended rock rubble experiment are shown in Figure 119, showing increased detail of the barrier rupture and high-speed flame propagation at the end of the reactor.

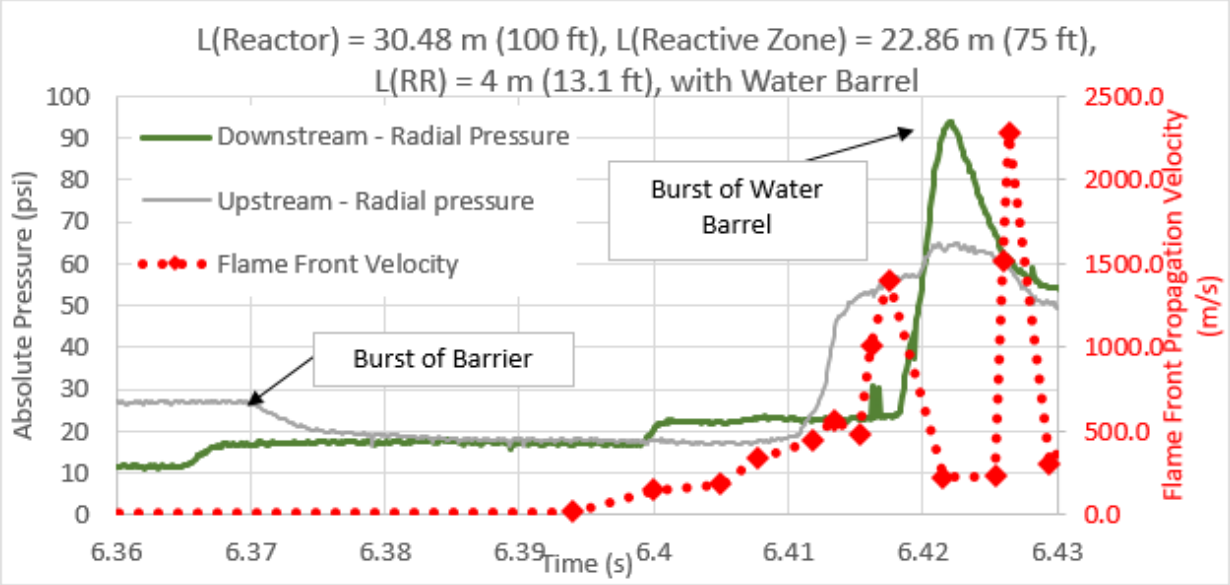


*Figure 119: Pressure and flame front propagation velocity plot with the extended rock rubble. Methane concentration = 7.5 vol.%. RR = rock rubble test. Vessel pressure at ignition = 82.73 kPa (~12 psia). T = 15.5 C*

The flame propagation velocities and pressures behave as expected when encountering a transient obstacle. Initially, the pressure rises at the sensors closer to the barrier. Once the barrier breaks, the pressure drops. The flame front propagates rapidly towards the low-pressure region, causing a spike in velocity. The upstream sensor, which is further separated from the water barrel does not detect a substantial change in pressure, while the closer sensors detect the associated pressure change. In

Figure 120, the flame front velocity is compared by position (ion sensor), and the two experiments have similar velocity trends.

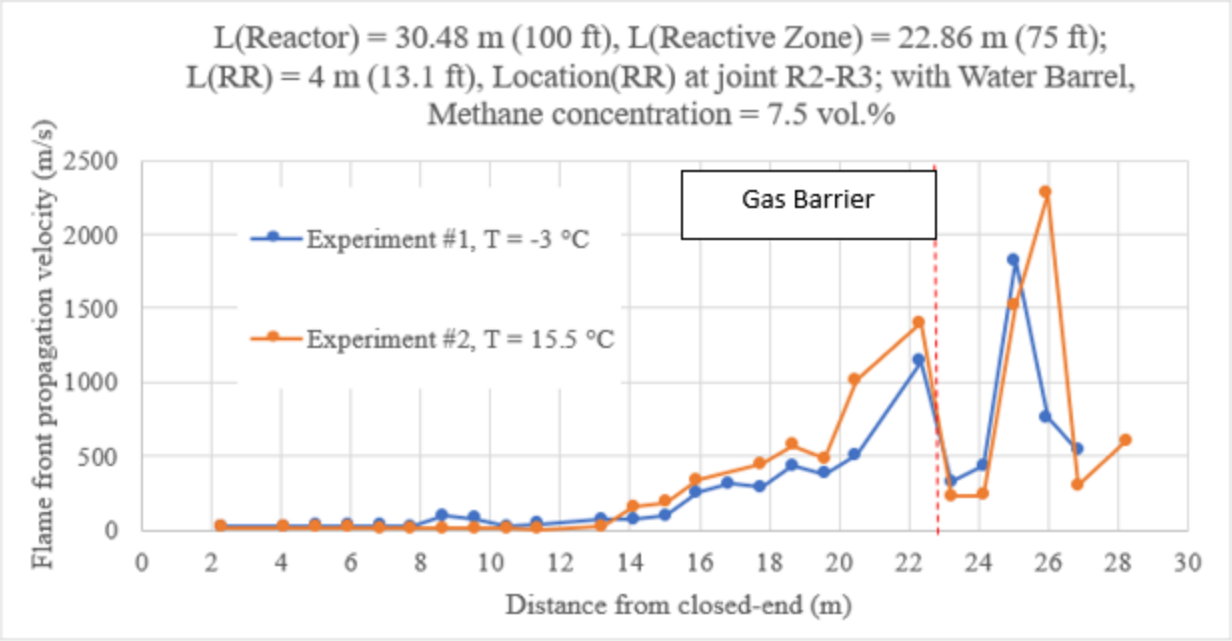


*Figure 120: Velocity comparison between the two experiments with the extended rock rubble. Methane concentration = 7.5 vol.%. RR = rock rubble test. Note the similarity in trends and flame propagation velocity. Vessel pressure at ignition = 82.73 kPa (~12 psia).*

## 5.0 Dissemination Efforts and Highlights

There are currently 4 journal articles in progress covering the primary research objectives of this work. One paper highlighting the full-scale longwall CFD accomplishments has already been accepted to Mining, Metallurgy, and Exploration on January 23rd with minor revisions. The remaining papers are all in the process of moving towards publication.

- **The Impact of Scaling and Rock Pile Location on the Propagation of Methane Flames in Experimental Flame Reactors**
    - **Status:** Final internal review, submission expected to Process Safety and Environmental Protection in 1-3 weeks.
    - Aditya Juganda[1], Matt Fig[1], Claire Strebinger[2], Erik Charrier[1], Patrick Maier[1], Gregory Bogin [1*], Jürgen Brune[1]
      *[1]Colorado School of Mines, United States*
      *[2]Seattle University, United States*

- **Investigation of the Impact of Rock Rubble on Methane-Air Explosions: High-speed Turbulent Deflagrations and Transition to Detonations**
    - **Status:** Internal draft, expected to be submitted in 4-6 weeks.
    - E. K. Charrier, A. Juganda, P. Maier, Z. Alspach, G. E. Bogin, Jr., J. F. Brune
      *Colorado School of Mines, Golden, United States*
      Y. Zhu
      *China University of Mining and Technology, Xuzhou, China*

- **Study of Methane Flame Interaction with Obstacles Using 30.5 m Long Reactor and CFD Model**
    - **Status:** Final internal review, expected to be submitted in 4-6 weeks.
    - Aditya Juganda[1], Erik Charrier[1], Patrick Maier[1], Jürgen Brune[1], and Gregory Bogin[1*]
      *[1]Colorado School of Mines, United States*

- **COMPUTATIONAL FLUID DYNAMICS MODELING OF A METHANE GAS EXPLOSION IN A FULL SCALE, UNDERGROUND LONGWALL COAL MINE**
    - **Status:** Accepted to Mining, Metallurgy, and Exploration on January 23rd with minor revisions
    - Aditya Juganda, Jürgen. F. Brune, *Gregory E. Bogin, Jr
      *Colorado School of Mines*
      *Golden, United States*

Claire Strebinger
*Seattle University*
*Seattle, United States*

GERF Explosion videos made available on YouTube for research and educational purposes

**SPARX Channel**

https://www.youtube.com/channel/UC7aVDgQPFAoSNjX5XO_H5gg

**Video 1**

**Research Area:** Large-scale Gas Explosions

**Facility**: Gas Explosion Research Facility (GERF)

**Title:** Methane-air (7% vol. CH4) Explosion Tests {15.2m long explosion vessel; outside view}

**Description:** Investigation of flame propagation and overpressures during a lean methane-air explosion test in a semi-confined vessel.

**Link:** https://youtu.be/gCK3vLSTBQc

**Video 2**

**Research Area:** Large-scale Gas Explosions

**Facility**: Gas Explosion Research Facility (GERF)

**Title:** Methane-air (9% vol. CH4) Explosion Tests {6.1m long explosion vessel; inside view}

**Description:** Investigation of flame propagation and overpressures during a stoichiometric methane-air explosion test in a semi-confined vessel.

**Link**: https://youtu.be/FzcPlM5P8RU

**Video 6**

**Research Area:** Large-scale Gas Explosions

**Facility**: Gas Explosion Research Facility (GERF)

**Title:** Methane-air (9% vol. CH4) Explosion Tests with Rock Rubble {6.1m long explosion vessel; inside view}

**Description:** Investigation of flame propagation and overpressures during a stoichiometric methane-air explosion test in a semi-confined vessel with rock rubble.

**Link:** https://youtu.be/WrRBb_BHmN0

## 6.0 Conclusions and Impact Assessment

The goal of this research is centered on the experimental and numerical investigation of the impact of rock rubble obstructions on flame front propagation velocity and overpressure of a semi-confined methane-air explosion which can occur in an underground longwall coal mine. Two are major groundbreaking outcomes of the current research. The first significant outcome is world-class research facility with one of the largest publicly available gas explosion reactor testing facilities in the world. This new explosion reactor is one of only 7 active gas explosion testing facilities capable of investigating gas explosions over 12K Liters (107 cu. ft.) found in the public literature, thus providing new and capabilities for large-scale explosion testing at a public university in the United States. The second major outcome is the development of a three-dimensional CFD full-scale underground longwall ventilation model with moving equipment and fully coupled with a transient 3D combustion model capable of simulating realistic methane-air explosions; as demonstrated with the ignition of an explosive gas zone at the coal face near the shearer drum.

**Technical Research Findings:**

This is a multi-disciplinary project that included building a new facility, designing and conducting a variety of gas explosion experiments in a large-scale explosion reactor, and extensive numerical modeling. The strong coupling of experimental and numerical work in the same research group allowed the reliable modeling of scenarios that would be impractical to investigate using a purely experimental process.

- Rock rubble blockages accelerated the flame propagation velocities in every combination tested at the GERF. It is clear that obstruction of a reactor with rock rubble can lead to a sustained increase in flame propagation velocity, which in turn leads to a reduction in the run-up length required for a deflagration to reach the DDT. This can lead to a detonation where the overall dimensions of a space would imply that there is not enough run-up length for the acceleration to occur. Obstructions, such as equipment, rock rubble, infrastructure, and other internal geometries can potentially increase flame front acceleration. It is highly recommended that follow-up research be conducted beyond the geometries considered in this work.

- Transient conditions that influence pressure buildup have a substantial impact on flame front behavior. Experiments conducted at the GERF show a detectable decrease in flame propagation velocity from transient backpressure caused by variations in the gas barrier strength and the water suppression system. This confirms the expected behavior of a flame front when encountering a pressure buildup and shows that even relatively weak and easily breached seals can have a substantial and detectable impact on deflagration behavior and alter the run-up distance required to reach the DDT. This implies that there is potential for non-structural and relatively weak objects to have a substantial impact on explosion behavior. Further research into the impact of transient and geometry is recommended both to investigate the potential of suppression mechanisms and to identify where this geometry may briefly cause turbulence that accelerates the flame front.
- The impact of transient obstructions on flame propagation and the pressure wave is readily apparent in the performance of the suppression system. The use of a water barrier disrupted the pressure wave, dampening the sound by 30 decibels. The backpressure from the suppressor reduced the maximum flame propagation velocity, though not to the extent that it reduced the noise from an experiment. The osciallations of the reflected pressure waves also had strong interactions with the flame front and causes an oscillatory behavior as obsevered in the cyclic increase and decrease of the flame propagation velocities prior to the water barrier bursting completely with the resulting flame accelerating towards the exit of the reactor.
- The phenomenon of partial obstructions accelerating flame front velocity was shown to scale over a wide range of experimental reactors. The geometric ratios tested were similar to the smaller reactor datasets. This allowed the comparison of the 0.4m, 0.8m, and 6.1m long reactor data sets, and shows that flame front behavior is similar. The data available shows a similar acceleration across all reactor scales tested. Additionally, the scaling of the phenomena and flame front behavior is evident in the qualitative shape of the flame across scales. This shows that experiments conducted at a smaller scale are indicative of behavior at a larger scale.
- The location of the ignition plays a substantial role in the behavior of the ensuing deflagration. The maximum flame front velocities were observed when the ignition location was next to the closed end of the reactor, correlating with the maximum run-up

distance. The experiments with a mid-reactor ignition produced a substantially lower flame propagation velocity. However, the pressure was found to be substantially higher, especially where the flame front was propagating towards the closed end of the reactor. This demonstrates that there is an interplay between the internal geometry and the ignition location and constructive and deconstructive interference of the pressure waves that can either increase or decrease the magnitude of the pressure wave depending on the relative ignition location relative to barriers; future work in varying the ignition location in addition to more complex geometries will provide further insight to the complex interaction of the pressure wave and reaction kinetics.

- The 2D and 3D CFD reactor models show good prediction of the flame behavior inside the empty reactor. Both models are able to capture the confinement effect of the gas barrier and the resulting flame acceleration after the gas barrier opened. The 3D reactor model shows better agreement with the experimental results compared to the 2D model. However, considering the computational time required to run the simulation, the 2D model is sufficient to simulate flame propagation in an empty reactor. In the case where rock rubble is included in the reactor, a 3D CFD model is required to simulate flame propagation, since the 2D model cannot capture the effect of flame propagating through small channel openings between the rock rubble.
- Successfully developed the first CFD model of a full-scale model of a methane explosion in a longwall coal mine. This capability is required to better understand the fundamental physics of an underground longwall coal mine explosion and the potential impact of the explosion.
- This modeling effort successfully demonstrates the viability of integrating methane combustion model into a full-scale, 3D longwall bleeder ventilation CFD model. From these results, researchers conclude that even small ignitions can initiate major explosions underground. The pressure from an explosion can divert airflow away from the face and tailgate, creating more explosive mixtures near the face or potentially transition into coal dust explosions, as was the case in The Upper Big Branch disaster in 2010.
- The model developed has the potential to better predict the following:
    - Expansion and impact of methane explosions for different ventilation scenarios and ignition locations.

    - Evaluation of explosion prevention and mitigation strategies, including explosion barriers.
    - Improvements in ventilation layout.
    - Structural design of ventilation control structures and mine seals.
- Balancing computational time and model accuracy remains a challenge when integrating combustion model into a full-scale longwall ventilation model. Current simulations take approximately 15 days to simulate the first 200 ms of a methane-air explosion using 4 x 36 cores of high-performance computational power. Combination of advance modeling techniques such as partial longwall sections replacement with profile boundaries and data interpolation, adaptive meshing, and adaptive time step are required to resolve this issue. However, further studies need to be done to test the viability and limitation of these techniques.

**Generalized findings for industry**:

These research findings can be generalized into several key points for industry. The prevention of explosions can be viewed as a pathway, with discrete steps representing a step in the sequence of events required for an explosion. Every step in the process has a range of conditions that must be met in order for an explosion to occur. For a generalized example, an explosion will require a potentially explosive gas source, ventilation and confinement conditions that allow the mixture to reach a fuel concentration where an ignition can occur, a spark, a volume of gas or dust where flame propagation can occur, and geometry that is amenable to propagations. In an idealized sense, safety can be achieved by interrupting the pathway to an explosion at any point. However, absolute control over and perfect information about all potentially relevant conditions in an operating mine is not feasible. For example, the complete removal of gas sources, such as strata gases in an underground coal mine is not possible. Instead, a ventilation plan is designed to remove strata gases from the working areas of the mine and prevent dangerous buildups. In this example, it is expected that the ventilation system will provide substantial benefit, but it cannot be expected to be perfectly effective in all places all of the time. Higher gas concentrations may occur in regions, such as the gob of a longwall mine, where it is not readily mitigated and the ventilation plan must mitigate gas buildup where it exits the gob into the workings. Safety is therefore dependent on understanding both the range of possible conditions, the potential pathways to an explosion from

those conditions, and what is sufficient mitigation. For example, uncertainty about the impact of various conditions on the run-up distance required for a deflagration to reach the DDT reduces the confidence in safety measures. This research quantified the behavior of flame fronts in a variety of conditions and proved that the independent variables tested can alter the run-up distance. The primary output to industry from this research is the identification of a set of conditions that may reduce the requirements for a catastrophic explosion to occur.

The generalized conclusions for industry are listed below. This work is intended to support a qualified professional in identifying hazards that have been previously. It in no way claims to be a substitute to professional experience and judgement, nor is the absence of a potential hazard in this research meant to imply that is not a hazard. In general, this research shows experimental and numerical evidence that some situations may present a greater hazard than previously understood.

- Gas explosion characteristics are heavily influenced by the confining geometry. Obstructions that generate turbulence in a propagating flame have been proven to accelerate the flame front. In practical terms, it means that objects partially obstructing a mine working or other confined space with an explosive atmosphere can turn a deflagration into a detonation. There is a run-up distance required for a flame front to hit a sufficiently high speed to transition into a much more damaging detonation. Accelerating the flame front with obstructions reduces the run-up distance, which may result in a detonation where the outside dimensions of the space would imply that a detonation would not be possible.
- The point of ignition within a given volume can have a substantial impact on the characteristics of the resulting explosion. Experiments showed that moving the ignition point from the closed end to the center of an open-ended reactor resulted in substantially lower flame propagation velocities and higher pressures in the closed end. It cannot be assumed that otherwise similar gas explosions will have similar behaviors and overpressures if the ignition occurs in a different point.
- Gas parameters, such as the pressure and the fuel concentration have a substantial impact on the behavior of the resulting explosion. For example, higher pressures in the explosion reactor correlated with a higher flame front velocity. As expected, stoichiometric mixtures were found to produce higher velocities than either lean or rich mixtures. It should be noted that the gas properties in a mine may be transient and that this may alter other factors, such as the run-up distance to the DDT.

- The impact of transient condition should not be ignored. Factors ranging from a partial collapse to equipment movement creates an altered internal geometry, which may impact flame front propagation. Assumptions about the designed geometry of a space may not accurately reflect the existing conditions. As a more extreme example, a partial collapse may result in both altered ventilation and similar obstruction geometry to the extended rock rubble experiments presented in this research. That implies that a substantial change in both the explosive gas concentration and a reduction in the run-up distance could occur from a single incident.
- Transient variations in ventilation can be caused by a variety of factors, including explosions within the gob. During normal operation, methane concentrations on the longwall face may be within the targeted range. However, the resulting gas movement within the gob may rapidly expel a plume of air with a methane concentration in the explosive range, creating a transient explosion hazard. Transient hazards caused by an unexpected and undetected elevated methane concentration may occur repeatedly without detection.

The project has met the expected research outcomes: The replacement of the 6.0 m (20 ft) reactor with the GERF provided a sophisticated 30.5 m (100 ft) long explosion reactor that is capable of safely conducting experiments with flame propagation velocities approaching or reaching the DDT. This has, as expected, provided additional insight into the complex interaction of high-speed turbulent deflagrations and detonations with a simulated gob (i.e. rock rubble). This data was used to validate and extend CSM's high-speed deflagration combustion model. Once the CSM combustion CFD models were calibrated and validated, the models were scaled up to full size mine workings. This allowed researchers to study the impact of mine explosions and identify the mechanisms, and therefore conditions, which must be met to prevent such explosions through measures including ventilation system design, early detection, and appropriate emergency response. This development provides engineers and researchers with an unprecedented toolkit for identifying and characterizing key mechanisms, quantifying potential hazards, and improving mine safety.

## 7.0 Recommendations for Future Work

The numerical modeling work and the experimental foundations have provided substantial new insights into gas explosions in coal mines, the role of rock rubble in increasing the flame propagation velocity and opened up a new numerical modeling toolset for engineers and researchers. As a consequence, there are a variety of new situations that can now be evaluated. Additionally, the confirmation of the impact of obstructions and the demonstrated impact of transient obstructions opens new avenues of investigation.

- The turbulent flow over the rock rubble obstruction should be experimentally and numerically studied to further characterize the mechanism of flame acceleration and it's interaction with the obstruction geometry. Rock rubble was an excellent starting point, but there are many other geometries present in a mine. It would be valuable to safety planning to characterize the impact of a wider array of relevant geometries on flame propagation that may intensify the explosion hazard. Geometries to consider:
    - Equipment, such as shields, pillars, or a road header.
        - Some of this initial work is currently underway by CSM at a $1/40^{th}$ scale, however, scaling this up to larger scale similar to GERF is a crucial next step
    - Piled supplies, clutter, or other items
    - Utilities and other underground infrastructure
- Full scale detonation experiments should be conducted to further characterize the process. Additionally, running experiments at detonation would provide a data set of detonation pressures and allow an improved assessment of the impact of overpressure on equipment and the structure of the mine.
- Investigation of impact of mine geometry on ventilation and explosion hazard via CFD modeling should be conducted. Especially to investigate the impact of transient events, such a disruptions caused by equipment movement, operations, or accidents.
- Coupling structural mechanics with full scale combustion CFD model to capture the impact of the explosion on mine equipment and workings. This would allow for the estimation of the potential forces on a variety of structures, and assist with the design of explosion resistant components.

- Experimental investigation into the transient impact of relatively weak obstacles on flame front propagation and potential hazards that occur as a result of this or safety systems that could utilize these effects.

# 8.0 References


[1] R. P. J. U. C. S. W. D. JW Rutherford, "Report of investigation, underground coal mine explosion, Blacksville No. 1 mine – I.D. No. 46-01867, Consolidation Coal Company, Blacksville West Virginia," Mine Safety and Health Administration, Arlington, VA, 1992.

[2] G. RA, P. RL, U. JE and e. al., "Report of Investigation, Fatal Underground Coal Mine Explosion, January 2, 2006, Sago Mine, Wolf Run Mining Company, Tallmansville, Upshur County, West Virginia, ID No. 46-08791," Mine Safety and Health Administration, Arlington VA, 2006.

[3] N. Page, S. Caudill, J.F. Godsey, S. A.D. Moore, D. Phillipson, R. Steffey and e. a. Stoltz, "Report of Investigation Fatal Underground Mine Explosion, April 5, 2010, Upper Big Branch Mine-South, Performance Coal Company. ID No. 46-08436.," U.S. Department of Labor, MSHA, 2011.

[4] N. 1. Page, T. Watkins, S. Caudill, D. Cripps, J. Godsey, C. Maggard, A. Moore, T. Morley, S. Phillipson, H. Sherer, D. Steffey, C. Stephan, R. Stoltz, J. Vance and A. and Brown, "Report of Investigation, Fatal Underground Mine Explosion, April 5, 2010, Upper Big Branch Mine-South. Performance Coal Company, Montcoal, Raleigh County, West Virginia. ID No. 46-08436.," Mine Safety and Health Administration, Arlington, VA, 2011.

[5] *2. U.S. Code of Federal Regulations. Title 30–Mandatory Safety Standards-Underground Coal Mines, Part 75.*.

[6] S. 3. Davis, D. Engel and K. v. Wingerden, "Complex Explosion Development in Mines: Case Study 2010 Upper Big Branch Mine Explosion," *Process Safety Progress,* vol. 34, pp. 286-303, 2015.

[7] H. F. Coward and G. W. & Jones, "Limits of Flammability of Gases and Vapors.," US Government Printing Office, 1952.

[8] S. Kundu, J. Zanganeh and B. Moghtaderi, "A review on understanding explosions from methane-air mixture," *Journal of Loss Prevention in the Process Industries,* vol. 40, pp. 507-523, 2016.

[9] S. a. C. H. Peng, "Air velocity distribution measurements on four mechanized longwall coal faces.," *International Journal of Mining and Geological Engineering,* pp. 235-246, 1986.

[10] P. Thakur, "Optimum widths of longwall panels in highly gassy mines," in *11th U.S. Mine Ventilation Symposium*, 7. ennsylvania State University, PA, 2006.

[11] R. Krog, S. Schatzel and H. Dougherty, "Methane emissions and airflow patterns along longwall faces and through bleeder ventilation systems," *International Journal of Mining and Mineral Engineering,* vol. 5, pp. 328-349, 2014.

[12] V. Gangrade, S. Harteis and J. and Addis, "Development and Applications of a scaled aerodynamic model for simulations of airflows in a longwall panel," in *Proceedings of the Sixteen North American Mine Ventilation Symposium*, Golden, CO, 2017.

[13] V. Gangrade, S. Schatzel, S. Harteis and J. and Addis, "Investigating the Impact of Caving on Longwall Mine Ventilation Using Scaled Physical Modeling," *Mining, Metallurgy & Exploration,* 2019.

[14] J. Brune and M. and Sapko, "11. A modeling study on longwall tailgate ventilation," in *Proceedings of the 14th Annual North American Ventilation Conference*, University of Utah, Salt Lake City, UT., 2012.

[15] A. Juganda, J. Brune, J. G. Bogin, J. Grubb and S. and Lolon, "CFD Modeling of Longwall Tailgate Ventilation Condition," in *SME Annual Conference and Exhibit 2017*, Denver, CO, 2017.

[16] W. Diamond, F. Garcia, G. Aul and R. and Ray, "Analysis and prediction of longwall methane emissions: a case study in the Pocahontas No. 3 Coalbed, VA.," NIOSH Report of Investigations, RI 9649.

[17] F. (. Kissell, in *Handbook for Methane Control in Mining.*, Pittsburgh, PA:, U.S. Department of Health and Human Services, Public Health Service, Centers for Disease Control and Prevention, National Institute for Occupational Safety and Health (NIOSH)., 2006.

[18] S. Schatzel, R. Krog, F. Garcia, J. Marshall and J. Trackemas, "Prediction of longwall methane emissions and the associated consequences of increasing longwall face lengths: a case study in the Pittsburgh coalbed.," in *Proceedings of 11th US/North American Mine Ventilation Symposium.*, Pennsylvania State University, PA, 2006.

[19] S. Schatzel, R. Krog and H. and Dougherty, "Methane emissions and airflow patterns on a longwall face," in *SME Annual Meeting (preprint)*, 2012.

[20] T. Ren and Z. and Wang, "Computational fluid dynamics modelling of respirable dust and gas behavior on a longwall face," in *Australian Mine Ventilation Conference*, 2013.

[21] Z. Wang, T. Ren, L. Ma and J. and Zhang, "Investigations of Ventilation Airflow Characteristics on a Longwall Face—A Computational Approach," *Energies,* vol. 11, no. 11, 2018.

[22] Z. Wang, T. Ren, L. Ma and J. and Zhang, "Investigations of Ventilation Airflow Characteristics on a Longwall Face—A Computational Approach," *Energies,* vol. 11, no. 11, 2018.

[23] J. Brune, H. Düzgün, B. J. G.E., A. Juganda, C. Strebinger, T. E. Nguyen and a. C. D. Isleyen, "Proximity Detection of Explosive Methane Clouds in Longwall Mines," in *39th Application of Computers and Operations Research In The Mineral Industry*, 19. Wroclaw, Poland, 2019.

[24] A. Juganda, Evaluation of Point-Based Methane Monitoring and Proximity Detection for Methane Explosive Zones in Longwall Faces of Underground Coal Mines, Golden, CO: Colorado School of Mines, 2020.

[25] J. Marts, R. Gilmore, J. Brune, G. Bogin Jr., J. Grubb and S. Saki, "Dynamic Gob Response and Reservoir Properties for Active Longwall Coal Mines.," *Transactions of the Society for Mining, Metallurgy and Exploration,* vol. 336, pp. 129-136, 2015.

[26] R. Gilmore, J. Marts, J. Brune, G. J. Bogin, J. Grubb and S. & Saki, "CFD Modeling Explosion Hazards - Bleeder vs. Progressively Sealed Gobs," in *10th International Mine Ventilation Congress*, Sun City, South Africa, 2014.

[27] J. Brune, J. Grubb, B. J. G.E., J. Marts, R. Gilmore and S. and Saki, "Lessons learned from research about methane explosive gas zones in coal mine gobs.," *Journal of Mining and Mineral Engineering,* vol. 7, no. 2, pp. 155-169, 2015.

[28] S. Saki, J. Brune, R. Gilmore, G. Bogin Jr, J. Grubb and J. and Marts, "CFD Study of Face Ventilation Effect on CH4 in Returns and EGZs in Progressively Sealed Longwall Gobs," *Journal of the South African Institute for Mining and Metallurgy (SAIMM),* vol. 117, pp. 257-262, 2017.

[29] A. Juganda, J. Brune and J. G. Bogin, "Incorporating Ventilation Network Simulation into CFD Modeling to Analyze Airflow Distribution Around Longwall Panels," in *Proceedings the 11th International Mine Ventilation Congress.* , 2018.

[30] K. Tanguturi and a. B. R.S., "Computational fluid dynamics simulations for investigation of parameters affecting goaf gas distribution," *Journal of Mining and Environment,* vol. 9, no. 3, pp. 547-557, 2018.

[31] S. Lolon, J. Brune, G. Bogin Jr and A. Juganda, "Study of methane outgassing and mitigation in longwall coal mines," *Mining, Metallurgy & Exploration,* vol. 37, pp. 1437-1449, 2020.

[32] A. Juganda, H. Pinheiro, F. Wilson, N. Sandoval, G. Bogin Jr and J. and Brune, "Investigation of explosion hazard in longwall coal mines by combining CFD with 1/40th scaled physical modeling," in *Proceedings of the 18th North American Mine Ventilation Symposium*, Virtual Event, 2021.

[33] H. Pinheiro, A. Juganda, N. Sandoval, F. Wilson, K. Gallagher, G. Bogin Jr and J. and Brune, "Scaling and flow similarity considerations to develop a 1/40th scaled aerodynamic model of a longwall coal mine for methane hazards investigation," in *Proceedings of the 18th North American Mine Ventilation Symposium*, Virtual Event, 2021.

[34] G. 30. Esterhuizen and C. and Karacan, "A methodology for determining gob permeability distributions and its application to reservoir modeling of coal mine longwalls," in *Preprint of the Society for Mining, Metallurgy and Exploration Annual Meeting*, Denver, CO, 2007.

[35] L. Yuan, A. Smith and J. Brune, "Computational fluid dynamics study on the ventilation flow paths in longwall gobs," in *Proceedings of the 11th U.S./North American Mine Ventilation Symposium*, University Park, PA., 2012.

[36] Wachel and E. W., *Establishing longwall gob porosity from compaction in western coal mines.,* Colorado School of Mines.

[37] R. Blickensderfer, D. Deadorff and J. and Kelley, "Incendivity of some coal-cutter materials by impact-abrasion in air-methane," Bureau of Mines, 1974.

[38] G. Andrews and D. & Bradley, "The Burning Velocity of Methane-Air Mixtures," *Combustion and Flame,* vol. 19, pp. 275-288, 1972.

[39] M. Fig, C. Strebinger, G. Bogin Jr. and J. Brune, "Gob Location and the Propagation of Methane Flames in Simulated and Experimental Flame Reactors," in *SME Annual Conference and Exhibit*, Denver, CO, 2019.

[40] C. Strebinger, J. G. Bogin and J. and Brune, "CFD Modeling of Methane Flame Interaction with a Simulated Longwall Coal Mine Gob," in *Proceedings of the 17th North American Mine Ventilation Symposium*, Montreal, Canada, 2019.

[41] F. Dryer and I. & Glassman, "38. High-temprature oxidation of CO and CH4," in *International Symposium on Combustion*, 1973.

[42] M. K. Fig, The Impact of Environmental Conditions on Methane-Air Explosion Development and Propagation Through Rock Rubble in Confined Spaces., 2018.

[43] C. Strebinger, Modeling Large-Scale High-Speed Methane Gas Deflagrations in Confined Spaces: Applications for Longwall Coal Mines, 2019.

[44] A. Juganda, "Evaluation of Point-Based Methane Monitoring and Proximity Detection for Methane Explosive Zones in Longwall Faces of Underground Coal Mines," 2020.

[45] M. J. Ajrash, J. Zanganeh and B. Moghtaderi, "Deflagration of premixed methane–air in a large scale detonation tube," *Process Safety and Environmental Protection,* pp. 374-386, 2017.

[46] H. Barnett and R. & Hibbard, "Basic Considerations in the Combustion of Hydrocarbon Fuels with Air," 1959.